2003-09

Performance evaluation of the AN USQ / 146 Jammer over uncoded slow FH/MFSK military communication systems and the IEEE 802.1 1a wireless LAN commecial communication standard

Dalakos, Aristeidis

Monterey, California: Naval Postgraduate School.

NAVAL
POSTGRADUATE
SCHOOL

MONTEREY, CALIFORNIA

THESIS

PERFORMANCE EVALUATION OF THE *AN / USQ* – 146 JAMMER OVER UNCODED SLOW FH/MFSK MILITARY COMMUNICATION SYSTEMS AND THE IEEE 802.11*a* WIRELESS LAN COMMERCIAL COMMUNICATION STANDARD

by

Aristeidis Dalakos

September 2003

Thesis Advisor: Tri T. Ha
Second Reader: David C. Jenn

Approved for public release; distribution is unlimited

THIS PAGE INTENTIONALLY LEFT BLANK

REPORT DOCUMENTATION PAGE			Form Approved OMB No. 0704-0188
Public reporting burden for this collection of information is estimated to average 1 hour per response, including the time for reviewing instruction, searching existing data sources, gathering and maintaining the data needed, and completing and reviewing the collection of information. Send comments regarding this burden estimate or any other aspect of this collection of information, including suggestions for reducing this burden, to Washington headquarters Services, Directorate for Information Operations and Reports, 1215 Jefferson Davis Highway, Suite 1204, Arlington, VA 22202-4302, and to the Office of Management and Budget, Paperwork Reduction Project (0704-0188) Washington DC 20503.			
1. AGENCY USE ONLY *(Leave blank)*	**2. REPORT DATE** September 2003	**3. REPORT TYPE AND DATES COVERED** Master's Thesis	
4. TITLE AND SUBTITLE: Performance Evaluation of the *AN/USQ - 146* Jammer over Uncoded Slow FH/MFSK Military Communication Systems and the IEEE 802.11*a* Wireless LAN Commercial Communication Standard			**5. FUNDING NUMBERS**
6. AUTHOR(S) Aristeidis Dalakos			
7. PERFORMING ORGANIZATION NAME(S) AND ADDRESS(ES) Naval Postgraduate School Monterey, CA 93943-5000			**8. PERFORMING ORGANIZATION REPORT NUMBER**
9. SPONSORING /MONITORING AGENCY NAME(S) AND ADDRESS(ES) N/A			**10. SPONSORING/MONITORING AGENCY REPORT NUMBER**
11. SUPPLEMENTARY NOTES The views expressed in this thesis are those of the author and do not reflect the official policy or position of the Department of Defense or the U.S. Government.			
12a. DISTRIBUTION / AVAILABILITY STATEMENT Approved for public release; distribution is unlimited.			**12b. DISTRIBUTION CODE**

13. ABSTRACT ***(maximum 200 words)***

On the modern battlefield communication is critical. Individual units require a steady flow of accurate information between headquarters and field units to remain effective. Just as important, denying the enemy the same needs of communicating with the help of *electronic countermeasures* (ECM), is essential to success. Communications jamming and surveillance are critical to achieve information superiority.

This thesis evaluates the performance and capabilities of one of the most advanced devices that detects, analyzes and denies enemy signals: the Rockwell Colins *AN/USQ - 146* transportable communication jammer. The jammer's best strategy varies with respect to the modulation technique that the hostile communication system uses. As the theoretical analysis and the simulation results indicated, the *AN/USQ - 146* jammer achieves its best performance over a FH/MFSK system when it selects the repeat multitone jamming strategy. However, when the hostile communication system is the IEEE 802.11*a* *wireless local area network* (WLAN) system, the *AN/USQ - 146* (Rubicon II) jammer must select the partial-band jamming strategy with $\rho = 0.1$.

The results of the theoretical analysis and the simulation modeling of the specific jammer for all types of jamming in manual spot and repeat modes over FH/MFSK military communication systems and new advanced wireless standards such as the IEEE 802.11*a* can be used as guidelines to select the most effective jamming strategy for the specific type of hostile waveform encountered.

14. SUBJECT TERMS *AN/USQ - 146* jammer, FH/MFSK, SINCGARS, probability of bit error, manual spot mode, repeat mode, barrage jamming, partial-band jamming, multitone jamming, Operational limitations, IEEE 802.11*a* , SystemView, Simulation Model	**15. NUMBER OF PAGES** 191
	16. PRICE CODE

17. SECURITY CLASSIFICATION OF REPORT	**18. SECURITY CLASSIFICATION OF THIS PAGE**	**19. SECURITY CLASSIFICATION OF ABSTRACT**	**20. LIMITATION OF ABSTRACT**
Unclassified	Unclassified	Unclassified	UL

NSN 7540-01-280-5500 Standard Form 298 (Rev. 2-89)
Prescribed by ANSI Std. 239-18

THIS PAGE INTENTIONALLY LEFT BLANK

Approved for public release; distribution is unlimited

PERFORMANCE EVALUATION OF THE *AN/USQ-146* JAMMER OVER UNCODED SLOW FH/MFSK MILITARY COMMUNICATION SYSTEMS AND THE IEEE 802.11*a* WIRELESS LAN COMMERCIAL COMMUNICATION STANDARD

Aristeidis Dalakos
Lieutenant, Hellenic Navy
Bachelor of Engineering, Hellenic Naval Academy, 1995

Submitted in partial fulfillment of the
requirements for the degree of

MASTER OF SCIENCE IN ELECTRICAL ENGINEERING
AND
MASTER OF SCIENCE IN SYSTEMS ENGINEERING

from the

NAVAL POSTGRADUATE SCHOOL
September 2003

Author: Aristeidis Dalakos

Approved by: Tri T Ha
Thesis Advisor

David C. Jenn
Second Reader

John P. Powers
Chairman, Department of Electrical and Computer Engineering

Dan C. Boger
Chairman, Department of Information Sciences

THIS PAGE INTENTIONALLY LEFT BLANK

ABSTRACT

On the modern battlefield communication is critical. Individual units require a steady flow of accurate information between headquarters and field units to remain effective. Just as important, denying the enemy the same needs of communicating with the help of *electronic countermeasures* (ECM), is essential to success. Communications jamming and surveillance are critical to achieve information superiority.

This thesis evaluates the performance and capabilities of one of the most advanced devices that detects, analyzes and denies enemy signals: the Rockwell Collins $AN/USQ-146$ transportable communication jammer. The jammer's best strategy varies with respect to the modulation technique that the hostile communication system uses. As the theoretical analysis and the simulation results indicated, the $AN/USQ-146$ jammer achieves its best performance over a FH/MFSK system when it selects the repeat multitone jamming strategy. However, when the hostile communication system is the 802.11*a* *wireless local area network* (WLAN) system, the $AN/USQ-146$ (Rubicon II) must select the partial-band jamming strategy with $\rho = 0.1$.

The results of the theoretical analysis and the simulation modeling of the specific jammer for all types of jamming in manual spot and repeat modes over FH/MFSK military communication systems and new advanced commercial wireless standards such as the IEEE 802.11*a*, can be used as guidelines to select the most effective jamming strategy for the specific type of hostile waveform encountered.

THIS PAGE INTENTIONALLY LEFT BLANK

TABLE OF CONTENTS

LIST OF FIGURES

LIST OF TABLES

THIS PAGE INTENTIONALLY LEFT BLANK

ACKNOWLEDGMENTS

This thesis is dedicated to my loving wife Olga for enduring my stress and absence during my research here at the Naval Postgraduate School. I am forever indebted to her for her love, consideration, and unrelenting support that continually inspired me to visualize reality from a different perspective.

I also wish to dedicate this thesis to my thoughtful and supportive parents, and especially to the memory of my father who taught me the values of education, diligence and conscientiousness.

I would like to express my sincere appreciation to my advisors Professor Tri Ha Professor David C. Jenn and Professor Clark Robertson. Without their support coupled with clear explanations and supervision, this thesis would not have been possible.

Thanks go out as well to Ron Russell for his help in editing my thesis.

Lastly, I must thank the Hellenic Navy, for providing an opportunity for me to pursue my postgraduate study here in the Naval Postgraduate School.

THIS PAGE INTENTIONALLY LEFT BLANK

EXECUTIVE SUMMARY

The $AN/USQ-146$ jammer of Rockwell Collins is employed by the United States Navy for shipboard applications and by the United States Marine Corps for tactical ground mobile applications. Evaluating the performance of the specific jammer and investigating the most effective jamming strategies based on its capabilities are critical for digital battlespace dominance.

In this thesis both the theoretical analysis and the simulation models of the $AN/USQ-146$ jammer were developed. Based on the specifications and the operational modes of the jammer, the theoretical analysis investigated the reliability and the performance of the jammer in slow FH/MFSK military communication systems and the IEEE $802.11a$ wireless LAN commercial standard.

Firstly, the performance of the $AN/USQ-146$ jammer in the manual spot mode versus the SINCGARS, FH/MFSK military communication system is presented. The jamming techniques that were analyzed are barrage noise jamming, partial band noise jamming and multitone jamming. The theoretical analysis showed that the interference of the first two types of jamming cannot be considered efficient enough on the modern battlefield, since the effect of the jamming signal on the BER becomes significant when the signal-to-interference noise ratio is equal to -30 dB. On the other hand, the manual spot multitone jamming technique proved to be the most effective type of manual spot jamming with a capability of inflicting severe damage on a SINCGARS system for $E_b/N_I = 0$ dB.

Secondly, the fundamental limitations of the $AN/USQ-146$ jammer in reactive mode and the link budget considerations between the transmitter-jammer and the jammer-receiver were analyzed. It was shown that the $AN/USQ-146$ is capable of operating in the reactive mode with no practical limitations. On the other hand, the link budget analysis revealed that the receive sensitivity and the output transmitted power of the jammer are the basic factors that determine its optimum position relative to the hostile communication system.

Next, the performance of the $AN/USQ-146$ jammer in repeat mode against the SINCGARS communication system is presented. In this mode of operation the jammer can select the following three strategies: (1) noise repeat jamming, (2) the repeat partial-band jamming, or (3) follower multitone jamming. All three reactive jamming strategies of the $AN/USQ-146$ jammer proved to be efficient enough over the SINCGARS system with the follower multitone jamming technique to be the most effective. Consequently, the probabilistic comparison of all types of jamming in manual spot and repeat mode showed that the most effective jamming strategy over an uncoded slow FH/MFSK system is the follower multitone jamming.

Lastly, the simulation models of the $AN/USQ-146$ jammer over two communication systems were developed with the use of the SystemView software by Elanix. First, the simulation models of the $AN/USQ-146$ jammer in all types of jamming over the SINCGARS systems were implemented. In all cases the simulation results verified the conclusions that were derived from the theoretical analyses in Chapters IV and VII. Then the performance of the new version of the $AN/USQ-146$ jammer (Rubicon II) over the IEEE 802.11a, $64-$QAM ($R_c = 3/4$) with soft decision decoding WLAN commercial system was investigated. The simulation results indicated that the $AN/USQ-146$ (Rubicon II) jammer must select the partial-band jamming technique with $\rho = 0.1$.

I. INTRODUCTION

On the modern battlefield communication is critical. Individual units require a steady flow of accurate information between headquarters and field units to remain effective. Just as important, denying the enemy the same needs of communicating, with the help of *electronic countermeasures* (ECM) is essential to success. Communications *jamming and surveillance* are critical to achieve information superiority. One of the most advanced devices that detects, locates and analyzes enemy signals is the Rockwell Collins $AN/USQ-146$ transportable communication jammer, which the United States Navy employs for shipboard applications, and which the United States Marine Corps employs for tactical ground mobile applications.

A. PURPOSE OF ECM

Electronic combat in the area of *command, control* and *communications* (C^3), ECM and *electronic counter-countermeasures* (ECCM) involves strategic planning, high technology equipment and operational experience. Although fixed frequency C^3 nets are vulnerable to relatively unsophisticated ECM, spread spectrum ECCM severely challenges the ECM system design by reducing its ability to select its targets.

Applying ECM against target C^3 signals may have one or more of the following basic purposes: detecting target activity, monitoring target signals, jamming target nets, and imitating target messages to deceive the operators. The ECM will normally be applied selectively and covertly, if possible, to avoid a defensive response by the target. Since a jamming transmitter may be vulnerable to lethal countermeasures, prudent ECM operational procedures require detection and identification of a target signal and perhaps an estimate of the potential jamming effectiveness before a jamming signal is transmitted. In addition, the ECM system may record target traffic on a long-term basis, determine the bearing or location of the various targets, and identify specific emitters.

B. SCOPE OF THESIS

Fixed-frequency communication channels are vulnerable to electronic countermeasures since an adversary has sufficient time to identify the operating frequency. To decrease this vulnerability, several modes of ECCM have been developed. These modes spread the transmitted signal over a large bandwidth in order to reduce the probability of detection and jamming. The two principal forms of ECCM are frequency-hopping spread spectrum (FHSS or FH) and Direct Sequence Spread Spectrum (DSSS or DS).

Each of these ECCM techniques possesses advantages and disadvantages for various operational situations. The objective of this thesis was to evaluate the performance of the $AN/USQ-146$ jammer in military communication nets for both fixed-frequency and frequency-hopped channels in order to determine the system's capabilities and limitations. Based on the technical characteristics of the device, the performance of the specific jammer was investigated for a non-coherent frequency-hopped M-ary frequency-shift keying (FH/MFSK) communication system under an additive zero-mean Gaussian noise (AWGN) environment for various kinds of jamming. Based on the operational modes of the $AN/USQ-146$ jammer, the types of jamming are separated into two categories, jamming methods in a *manual spot jamming* mode and jamming methods in a *reactive or follower jamming* mode.

The thesis is organized as follows. Chapter II analyzes the characteristics and the mode of operations of $AN/USQ-146$. Chapter III explores the importance of spread spectrum communication systems. Chapter IV presents the performance of the jammer in various methods of manual-spot jamming in frequency-hopped communication systems. Chapter V discusses the configuration of the jammer and its geometric and physical restrictions in reactive or follower jamming mode. Chapter VI describes the performance of $AN/USQ-146$ to determine which frequency range to jam when it operates in the reactive jamming mode. Chapter VII analyzes the performance of the jammer for FH/MFSK systems using various types of jamming in reactive or follower jamming mode. In the first part of Chapter VIII, the simulation models that correspond to the theoretical analysis of Chapters IV and VII are presented together with a comparison of the theoretical and simulation results. The second part presents the simulation models and the corre-

sponding results of the performance of the $AN/USQ-146$ over the IEEE 802.11*a* Wireless LAN commercial standard. Chapter IX presents a summary with conclusions and proposes prospective developmental work in this area.

THIS PAGE INTENTIONALLY LEFT BLANK

II. TECHNICAL DESCRIPTION AND MODES OF OPERATION OF THE AN/USQ-146 JAMMER

This chapter analyzes the technical characteristics of the $AN/USQ-146$ jammer, its capabilities, and its modes of operation. This chapter contains the information used for the theoretical analysis and the simulation models that are presented in the following chapters.

A. SYSTEM OVERVIEW

1. Description

The $AN/USQ-146$ jamming device combines fixed-frequency communications, *electronic support* (ES) and *electronic attack* (EA) functions within the frequency range of 1.5 MHz to 2500 MHz. In all ES and EA modes, the system provides communications monitoring or jamming capability against single-channel fixed frequency and frequency hopping communications in the high frequency (HF), very high frequency (VHF), ultra high frequency (UHF), and super high frequency (SHF) bands. When not used for *command and control warfare* (CCW), the system can be operated as a standard radio for conventional AM/FM/SSB communications within its frequency range.

2. Architecture

The $AN/USQ-146$ CCW system is supplied with dual receiver-transmitter (RT) and dual base band cards. Using two RTs for CCW functions reduces scan time and permits simultaneous scan and jamming activities.

The major components of the system are the control computer, splitter/limiter, receiver, signal processor, audio interface, waveform generator, exciter, amplifier interface, and power amplifier. The system contains several other components that are not considered important for the analysis and the scope of this thesis.

3. System Components

The following sections describe the functions provided by the system blocks in Figure 1.

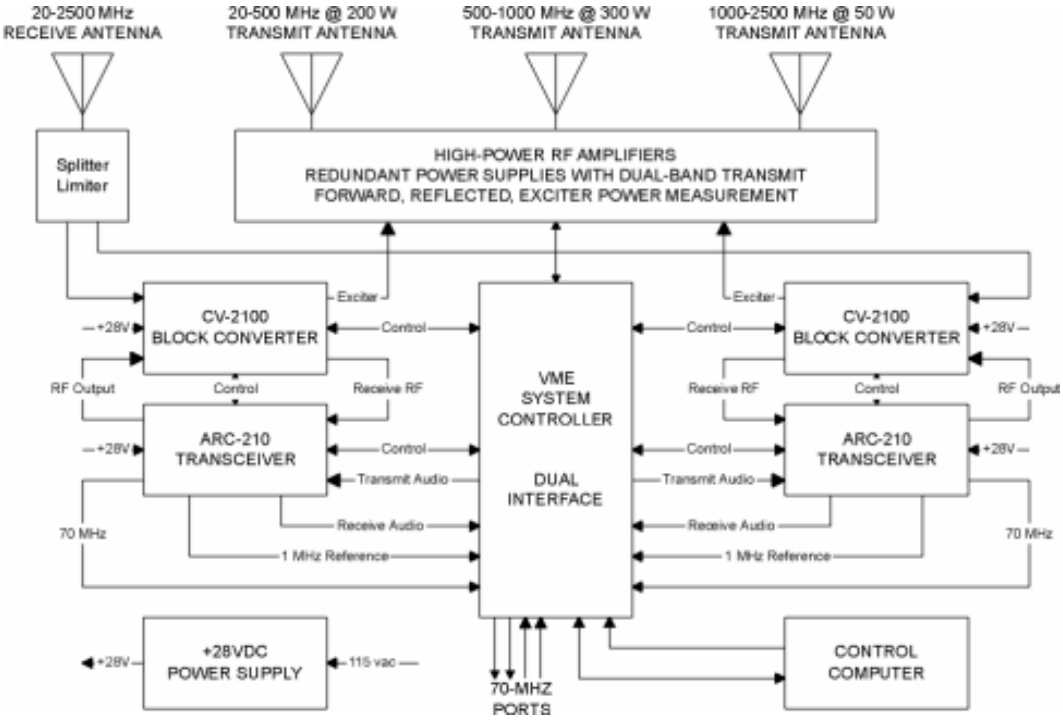

Figure 1. System Functional Block Diagram [From Ref. 1]

a. Control Computer

The system is initialized and managed through use of a laptop control computer. The CCW system is entirely operable by one operator using only the controls and displays of the control computer. The computer provides a digital audio interface that allows recording and playback of audio files.

b. System Controller

The system contains a processor that communicates with the laptop computer and controls all other equipment of the device.

c. Splitter/Limiter

The splitter/limiter connects multiple receiver units to a single receive antenna. It also provides a limiter that protects the receiver unit from being damaged by input RF power levels.

d. Receiver Unit

The receiver unit seen in Figure 2 provides the RF signal selection and signal demodulation functions. The receiver supports narrowband and wideband filtering and can provide a 70-MHz IF output.

Figure 2. Radio Receiver-Transmitter RT-1747 [From Ref. 1]

e. Receive Signal Processor

The receive signal processor provides signal processing of a receiver signal to measure energy and, based on this measurement, in turn measures the frequency offset from the tuned frequency. The signal processor provides signal digitization and demodulation to store digital signal information during reception.

f. Waveform Generator

The waveform generator drives the RF exciter. The generator can select from the following input sources: microphone, analog line, input including internal analog tone generators, digitized FSK/PSK data stream from a data port, digitized I/Q quadrature data stream from a data port, and an internally available coded-synthesis algorithm.

g. RF Exciter Unit

The RF exciter unit accepts a wideband 70-MHz IF signal output from a waveform generator and translates the signal to the tuned RF frequency to drive a high power amplifier. The RF exciter also accepts narrowband signals and processes the signals as indicated previously.

h. Amplifier Interface

The amplifier interface provides the necessary interfaces and control logic for the RF *high power amplifiers* (HPA). The interface accepts the exciter signal from the exciters and provides appropriate RF switching that allows an exciter output to be connected to any of the HPA bands.

i. High Power Amplifiers

The RF high power amplifiers amplify the exciter RF output to obtain a high power RF output to an appropriate antenna. Each amplifier output gain is adjustable and provides power feedback that can measure the power level and display it to the operator.

B. INTEGRATED SYSTEM

The $AN/USQ-146$ jammer has three operating modes: normal communications, electronic support, and electronic attack. All of the modes of operation cooperate with the waveform generator in order to produce the necessary signals for every kind of operation.

1. Communication Mode

The system functions as a half-duplex communications transceiver or as a wideband transceiver in the 1.5-MHz to 2500-MHz frequency ranges. It supports AM and FM modulation/demodulation in VHF/UHF/SHF and AM SSB demodulation in HF, using a baseband analog audio. The system provides the option for an externally modulated 70-MHz IF signal as an input to the RF transmit frequency, the HPA selection and the

system key state. The carrier frequency of the transmitted signal has an accuracy of 1 part in 10^7.

2. Electronic Support (ES) Modes

The system behaves as an ES system by searching the desired frequency range or channels for signal activity. It provides a preset channel mode in which the acquisition time is less than 750 μs per preset channel frequency plus 1.05 times the sum of the sample time of the active signals plus the delay associated with the selected IF bandwidth.

The system can also perform a logging mode for all signals detected within the selected frequency range and resolution. The scan rate of the log mode is 500 kHz/ms with a resolution of 25 kHz.

3. Electronic Attack (EA) Modes

The system performs as an EA mode by searching the desired frequency range or channels for signal activity and jamming detected target frequencies. The system has two modes of operations in EA, (1) spot and (2) reactive communications jamming. *Manual spot jamming* is defined as jamming on a single frequency for a duration determined by the operator. This focuses the jammer's entire power output on a single target. This technique seems to be inefficient against frequency hopping systems, but a skilful operator can use it against FH systems with the proper use of the waveform generator, as explained in Chapter IV.

In *Reactive jamming or follower jamming,* the jammer detects energy above a preselected signal threshold and automatically jams upon detection. It ceases jamming when the signal is no longer above the set threshold. This technique focuses the jammer's power output on a single frequency and is highly energy efficient but does not reduce the potential for electronic fratricide. The tuning frequency accuracy of the transmit signal with respect to the tuning frequency of the received signal is equal to or better than 500 Hz. The *reactive jamming* mode of operation can detect, track, and jam frequency hoping systems with the jammer's receiver and processing means. The effectiveness of

this mode of operation, discussed in Chapter V, is determined by the physical geometry, the target hopping rate, the percent of each target's signal dwell required to be interfered with, and the jammer speed.

The response time of the system, as defined by the time from signal detection to signal jamming, is less than $500\ \mu s$. The response time does not include the acquisition time and the tuning time.

The system provides a look-through capability to determine if the signal has ceased transmission. The look-through interval is adjustable from 5 to 9999 ms, and the look-through time does not exceed 1 ms.

A basic capability of $AN/USQ-146$ is the insertion of time holes in the transmit waveform. The interval between time holes is adjustable from 0 to 9999 ms, and the duration of the time hole is adjustable from 0 to 2000 ms.

4. Waveform Generation

The system provides RF modulation modes of AM, FM, CW, and external. The system is capable of producing MFSK modulation for $M = 2, 4, 8$. The symbol rate (R_s) is programmable between 25 Hz and 25 kHz with a resolution of 1 Hz. With the same specification, the system can also generate an MPSK modulation for $M = 2, 4$.

C. SUBSYSTEM SPECIFICATIONS

1. Receiver Subsystem

The receiver subsystem provides the RF-to-IF conversion for signal detection and wideband receive modes, and provides RF to baseband conversions for all other modes of operation. The tuning resolution is 1 Hz in less than $500\ \mu s$, and the noise figure is 3 dB for VHF and 6 dB for HF. This specification is based on the use of a low-noise amplifier (LNA) in the RF receive path and does not include losses due to RF cables and the slitter/limiter.

The receiver can detect signal energy from −97 dBm to 50 dBm in a 3.2 kHz bandwidth for HF, and −120 dBm to −75 dBm in 16-kHz bandwidth, with an LNA pre-amplifier, in all other bands. The accuracy of the detecting signal is within ±3 dB. The receiver can provide two analog selectable bandwidths for the reception of narrowband, nominal 16-kHz BW and wideband, nominal 110-kHz BW signals. The receiver can also provide digital filter bandwidths from 3.2 kHz to 100 kHz in octave steps. The digital filters have a passband ripple of 1 dB, a bandwidth accuracy of 10%, and a stopband attenuation of 60 dB.

The receiver subsystem provides a wideband 70-MHz intermediate frequency interface. The bandwidth of the receive wideband interface is shown in Table 1.

Frequency Range	Bandwidth
1.5 MHz – 30 MHz	10% of tuned frequency
20 MHz – 30 MHz	2 MHz
30 MHz – 50 MHz	4 MHz
50 MHz – 2500 MHz	6 MHz

Table 1. Bandwidth of the Receive Wideband Interface

2. Waveform Generator

The waveform generator can mix the audio from a microphone, external audio and internal tone generators. It provides two simultaneous output signals. Each output is routed to an independent RF exciter. Waveform generators are capable of independently selecting any of the modulation sources. This includes analog and digital sources, such as pre-recorder WAV files and digital data streams. The modulation formats are described as follows:

a. Voice Modulation

The waveform generator provides AM and FM modulation from the base-band analog audio.

b. Digital Modulation

The waveform generator produces M-ary FSK with $M = 2, 4, 8$ and MPSK with $M = 2, 4$.

c. On-Off Keying (OOK) Capability

OOK modulation can be provided from the waveform generator with a programmable on-off duty cycle and frequency. The OOK modulation can operate in conjunction with any of the supported modulation, and is programmable to generate time holes from 100 to 2000 ms with a resolution of 20 ms with an accuracy of 10 ms.

d. Continuous Wave (CW) Tone Frequency

A CW tone that can be adjusted from 2 Hz to 12.5 kHz with 1% accuracy is generated by the waveform generator.

e. Random Tone Frequency

The waveform generator provides a modulation that consists of multiple tone frequencies that are adjustable in both frequency range and duration. A *pseudo-random number* generator (PN sequence) determines the selected frequencies and their duration.

f. Random Data Stream

A pseudo-random data stream of bits generated from a feedback shift register with 8 stages, as shown in Figure 3, is available in the waveform generator.

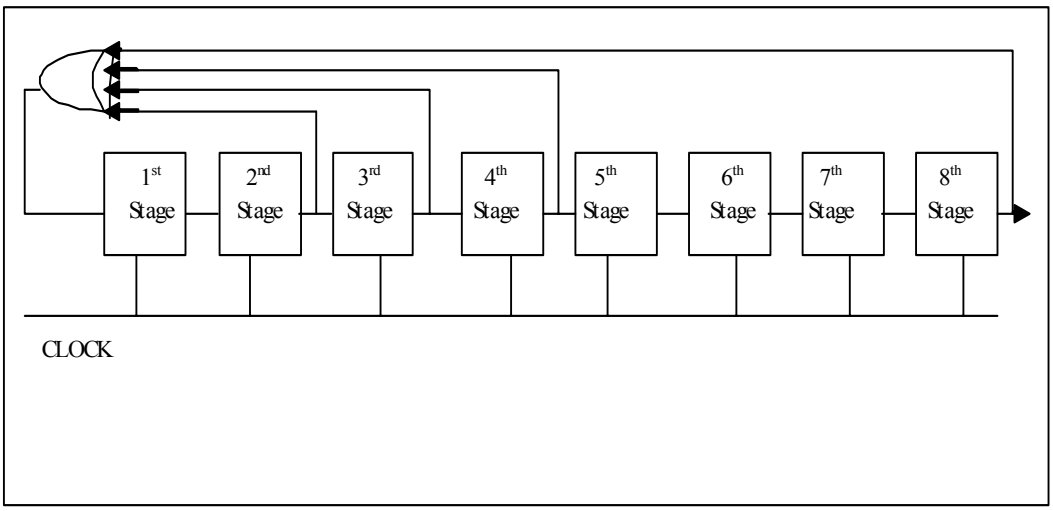

Figure 3. Linear Feedback Shift Register with 8 Stages

g. Keystream

The waveform generator can provide an FM modulation form consisting of a 300 Hz square, followed by 500 Hz tone, followed by 700 Hz tone, followed by no tone. This keystream sequence has programmable intervals for each sequence step between 1 ms and 2000 ms in 1 ms steps. An example of such a keystream is shown in Figure 4.

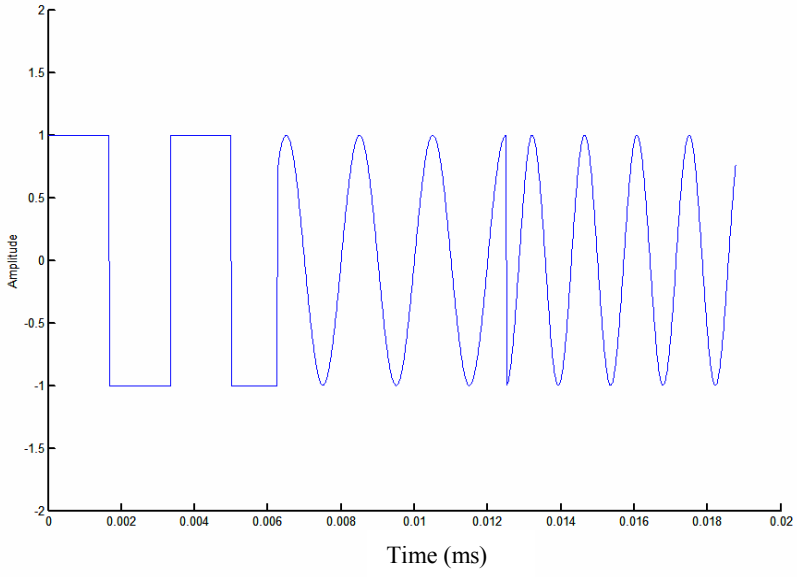

Figure 4. Keystream Produced by the Waveform Generator

h. FDMA Generator

The waveform generator can produce a composite baseband signal consisting of a programmable number from 1 to 24 contiguous channels with the same information in each channel. The channel spacing is variable from 4 kHz to 200 kHz with a resolution equal to 20 Hz. The number of contiguous channels is restricted by the available exciter IF bandwidth.

3. Amplifier Subsystem

The transmitter is capable of sustaining a continuous output when operated within the limits of the environmental conditions.

The amplifiers provide a RF output power depending on the frequency range. Table 2 specifies the minimum output power of the amplifiers for each frequency range.

Frequency Range	Output Power (Watts)
1.5 MHz – 30 MHz	1000
20 MHz – 30 MHz	200
30 MHz – 50 MHz	300
50 MHz – 2500 MHz	50

Table 2. RF Output Power from Amplifiers

4. Signal Detection

The system can measure the frequency of a single signal within the selected received passband to within 1 part in 10^7. The frequency accuracy for a single carrier signal is shown on Table 3.

Measurement Accuracy (±)	Measurement Time
1 Hz	1s
10 Hz	100 ms
100 Hz	10 ms
200 Hz	5 ms
1000 Hz	1 ms
10 kHz	100 μs
100 kHz	10 μs

Table 3. Frequency Measurement Accuracy of Signal Detector

The system has variable filter bandwidths that can suppress signals 60 dB with a separation of 16 kHz in the 20 to 2500-MHz band and 3.2 kHz in the 1.5 to 30-MHz HF range.

5. Operator Control Unit (OCU)

The (OCU) provides the primary interface through which the system is controlled. The OCU is implemented as a *Windows* application running on an IBM compatible lap-top computer. Figure 5 shows the standard model that Rockwell Collins uses for the CCW systems.

Figure 5. Rockwell's Standard Control Computer for CCW Systems

The interface to the control computer can update the target-table status 10 times/s, and the time interval between the selection of a system mode and the activation of the mode does not exceed 1 second.

The laptop display-activity screen shows the operating modes, selected parameters, EA activity, target tables, and all other system information. The control screen allows a user to select any of the following CCW modes:

- Reactive Mode
- Blind Mode
- Scan Mode
- Log Mode.

The *reactive, blind,* and *scan* modes are exclusive modes, and selecting any mode automatically deselects the other two modes. The display-activity screen also has the capability of enabling fixed–frequency communications, jamming, monitoring, or recording modes of operation.

As seen in Figure 6, the main control screen consists of three informational and control areas. The *target table*, the *communication screen*, and the *jammer techniques screen*.

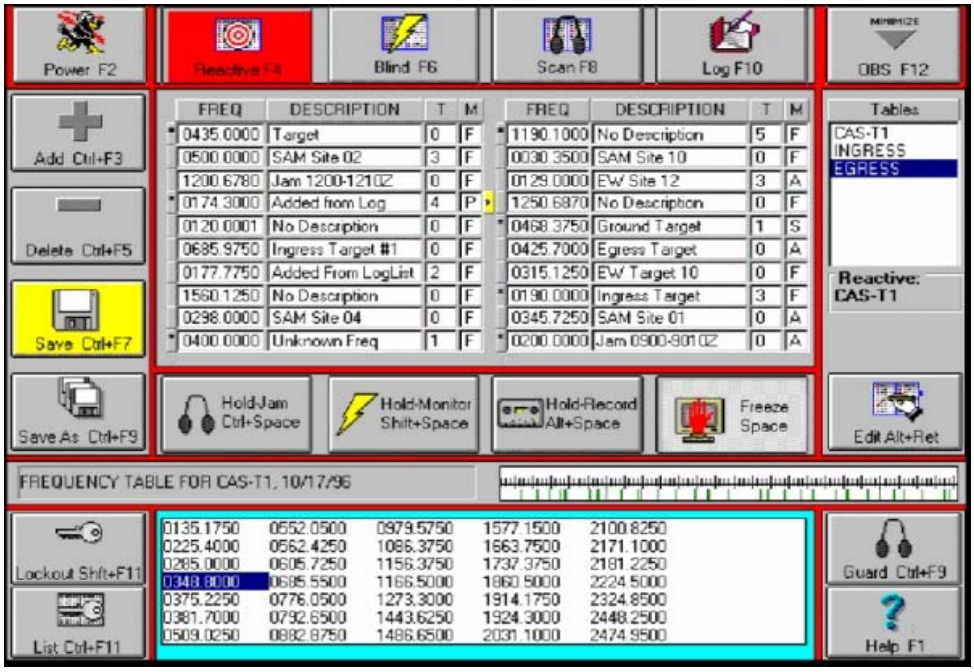

Figure 6. Control Screen for the $AN/USQ-146$

a. Target Table

The target table displays a minimum of 20 target frequencies, with each entry containing the following fields:

- Center frequency
- Description
- Technique number
- Priority number.

A separate table displays the list of the frequencies that are not to be jammed.

b. Communication Screen

The communication screen allows either or both of the transceivers to be employed for fixed-frequency communication modes. Each transceiver constantly measures and displays the following parameters in addition to the status of the controlled parameters:

- Signal level
- Measured frequency
- Forward-output power
- Reflected-output power
- Scan speeds
- Frequency-dependent threshold settings
- Bin resolution
- Receive and scanning bandwidths.

If the parameter measurement cannot occur for the selected mode, then the measurement and display occurs only when the transceiver frequency is changed.

c. Jamming Techniques Screen

The jamming techniques screen basically contains the description of the technique that is used with its parameters, such as the jamming modulation, the frequency offset from the received frequency, the detection threshold, the channel width and some other modulation parameters that help the operator control the jamming signal.

D. SUMMARY

This completes the technical description of the $AN/USQ-146$ jammer and its modes of operation. All the above unclassified information is the basic material used in this thesis to develop the theoretical models in Chapters III through VII and for the simulations models used to verify the theoretical results in Chapter VIII.

The next chapter discusses the performance of the $AN/USQ-146$ jammer in the case of a fixed-frequency communication signal. The results verify the theory that the fixed-frequency communication systems are vulnerable in simple jamming techniques and that the only apparent solution for less interfered systems are the frequency-hopping systems that are analyzed in Chapter IV.

III. IMPORTANCE OF EFFECTIVE ECM IN FHSS SYSTEMS

The main idea of frequency-hopping spread-spectrum communications is to protect against a hostile jammer by greatly increasing the transmission bandwidth far beyond the minimum required for the signal information. By increasing the frequency range over which a system effectively operates, the jammer is forced to spread its power over a wider frequency band and thus be less effective from a "per-frequency" signal corruption capability point of view.

A. BACKGROUND IN FREQUENCY HOPPING SYSTEMS

The FH waveform consists of short segments of the signal being transmitted on a set of many different frequencies spread across a large frequency band, with the frequency sequence of the hops being determined by a (PN) code. The multiplication of the signal prior to transmission by the output of the pseudorandom sequence generates an intermediate frequency of the form

$$f_i = f_1 + (i-1)\cdot \Delta f_{fh},\ i = 1,2,...,N, \tag{3.1}$$

where N is the maximum number of possible frequency hop bins, Δf_{fh} is the separation between the carrier frequencies of adjacent bins, and i changes pseudorandomly every T_h seconds. By so doing, the entire spectrum of the signal transmitted is shifted from its carrier frequency f_c to the new carrier frequencies

$$f_{c_i} = f_c + f_1 + (i-1)\cdot \Delta f_{fh}. \tag{3.2}$$

The result is that the new data modulated carrier that is shifted from one frequency to the next is created as Figure 7 shows. In Equation (3.2), there are N different frequency hop bins, each of bandwidth Δf_{fh}. The value of i and thus f_{c_i} is changed periodically according to some predetermined (but apparently random to a third-party observer) noiselike spreading code called a pseudorandom or pseudonoise sequence.

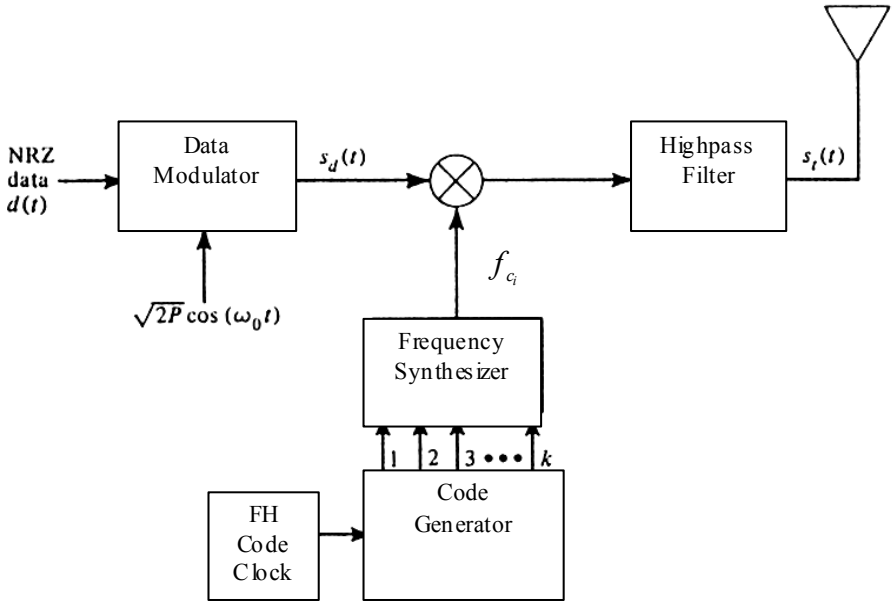

Figure 7. Transmitter of a FH/MFSK System

Generally, frequency hopping is used with noncoherent modulation formats such as noncoherent MFSK. Such a signal is described by

$$s(t) = \sqrt{2}A_c \cos\left[2\pi(f_s + (m-1)\cdot\Delta f)t + \theta_i\right], \tag{3.3}$$

where $m = 1, 2, ..., M$, θ_i is the i^{th} symbol phase, and Δf is the frequency separation between each of the *M* signaling tones. Multiplying this signal by a signal at the intermediate frequency in (3.1) we get:

$$\begin{aligned} s'(t) &= 2\sqrt{2}A_c \cos\left\{2\pi\left[f_s + (m-1)\Delta f\right]t + \theta_i\right\}\cos(2\pi f_i) \\ &= \sqrt{2}A_c \cos\left\{2\pi\left[f_i + f_s + (m-1)\Delta f\right]t + \theta_i\right\} + \sqrt{2}A_c \cos\left\{2\pi\left[f_i - f_s - (m-1)\Delta f\right]t - \theta_i\right\}. \end{aligned} \tag{3.4}$$

The carrier frequencies of the first term are

$$f_i + f_s + (m-1)\Delta f = f_1 + (i-1)\Delta f_{fh} + f_s + (m-1)\Delta f, \tag{3.5}$$

which is smallest for $i = 1$ and $m = 1$. In this case the carrier frequency becomes $f_s + f_1$. The carrier frequencies for the second term are

$$f_i - f_s - (m-1)\Delta f = f_1 + (i-1)\Delta f_{fh} - f_s - (m-1)\Delta f, \tag{3.6}$$

which is largest for $i = N$ and $m = 1$. In this case the carrier frequency becomes $f_1 + (N-1)\Delta f_{fh} - f_s$.

If the smallest frequency of the first term is greater than the largest frequency of the second term, then

$$f_s > f_1 + B + \frac{(N-1)}{2}\Delta f_{fh}, \tag{3.7}$$

where *B* is the required guardband above and below the high and the low frequency signaling tones, respectively. In this case, a high-passed filter is used to remove the frequency difference contribution, and the frequency-hopped signal becomes

$$s_T(t) = \sqrt{2}A_c \cos\left\{2\pi\left[f_i + f_s + (m-1)\Delta f\right]t + \theta_i\right\}. \tag{3.8}$$

One obvious advantage is that a hostile jammer needs to know the pseudonoise sequence of the communicator's transmitter in order to jam the specific hop bin where the transmitter operates at each time instant. To overcome a follower jammer, the signal must hop to a new carrier frequency before the jammer can complete its tracking process. In Chapter V, the fundamental limitations of a repeat jammer are analyzed and the specific parameters that influence the capabilities of the $AN/USQ-146$ jammer are described.

Another advantage of a FH system is due to the fact that the power spectral density of the frequency-hopped signal is identical to that of the conventional signal in a specific hop bin as can also be seen in Figure 7. However, since the signal hops from bin to bin, and assuming that the probability that any bin is occupied is equal to $1/N$, the average power spectral density is

$$PSD_{FH/FSK} = \frac{1}{N} \cdot \sum_{i=1}^{N} S_{FSK}(f \,|\, f_c = f_{c_i}). \tag{3.9}$$

Hence, the signal power spectral density is lower by a factor of *N* on average.

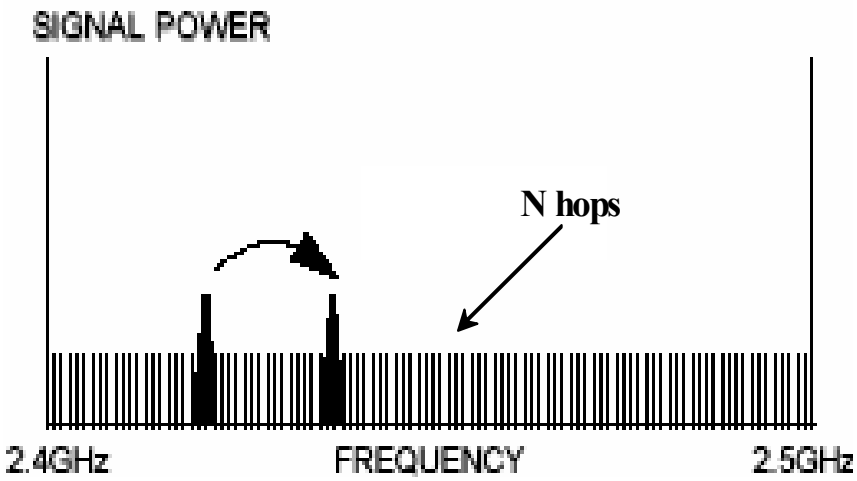

Figure 8. Frequency-Hopped Signal

B. SUMMARY

The above advantages have characterized the FH systems as being the most resistive to jamming when compared to other communication systems. As a result, most of the military communication systems use this technique to secure communication and to avoid interference. However, this thesis attempts to identify and to classify the strengths and the weaknesses of these ECCM techniques in order to define the physical limitations and parameters of an optimum advanced transponder ECM system.

In the next chapters, the capabilities of a technologically advanced, $AN/USQ-146$ jammer are investigated in the worst environment, from the jammer's point of view, such as FH/MFSK systems. Specifically, Chapter IV analyzes the performance of the jammer when it operates in manual spot jamming against an uncoded slow FH/MFSK communication system with barrage, partial-band, and multitone jamming strategies.

IV. PERFORMANCE OF THE AN/USQ-146 JAMMER IN VARIOUS METHODS OF MANUAL SPOT JAMMING

The purpose of this chapter is to predict the message error probability that the $AN/USQ-146$ produces in an uncoded slow frequency hopped MFSK communication system in manual spot jamming. Before examining each jamming strategy, describing the basic characteristics of a FH/MFSK system, the channel model, and the symbology used is important.

A. FH/MFSK SYSTEM, CHANNEL MODEL, AND SYMBOLOGY USED

The FH/MFSK communication system is assumed to have N non-overlapping FH bins. The bandwidth of each bin is B_{nn} Hz, where B_{nn} is the bandwidth of the non-hopped MFSK signal. So the total frequency hopped bandwidth is augmented to be greater than or equal to $B_{nn}N$. In the analysis, M expresses the modulation order where

$$M = 2^k, \tag{4.1}$$

and k is the number of bits per M -ary symbol. Since the number of signal tones within a hop bin is M and the total number of bins is N, the result is a total of $M \cdot N$ possible signal tone locations.

The symbol duration T_s is related to the hop duration T_h by:

$$T_h = K \cdot T_s, \tag{4.2}$$

where $K = 1, 2, \ldots$. The symbol and hop rates are the reciprocal of the corresponding durations, so

$$R_s = \frac{1}{T_s}, \tag{4.3}$$

and

$$R_h = \frac{1}{T_h}. \tag{4.4}$$

The symbol rate is related to the hop rate by

$$R_s = K \cdot R_h. \tag{4.5}$$

Using the frequency-hopped signal from Equation (3.8), it is assumed that the M symbols possess an equal probability of occurring, so both f_i and f_s are taken to be integer multiples of the symbol rate R_s, and the frequency difference between signal tones Δf is taken to be an integer multiplier of the symbol rate. Hence,

$$\Delta f = p \cdot R_s. \tag{4.6}$$

The channel that the FH/MFSK operates on is considered to be *Additive White Gaussian Noise*, and σ^2 is the power of the AWGN. The transmitter and receiver are assumed to function in perfect synchronization. The receiver (seen in Figure 9), after dehopping the signal, uses a bank of M quadrature detectors, where the integrator time constants are normalized to the symbol duration for notational convenience. The existing noise interference is expressed as AWGN with a flat average power spectral density defined as $N_0/2$.

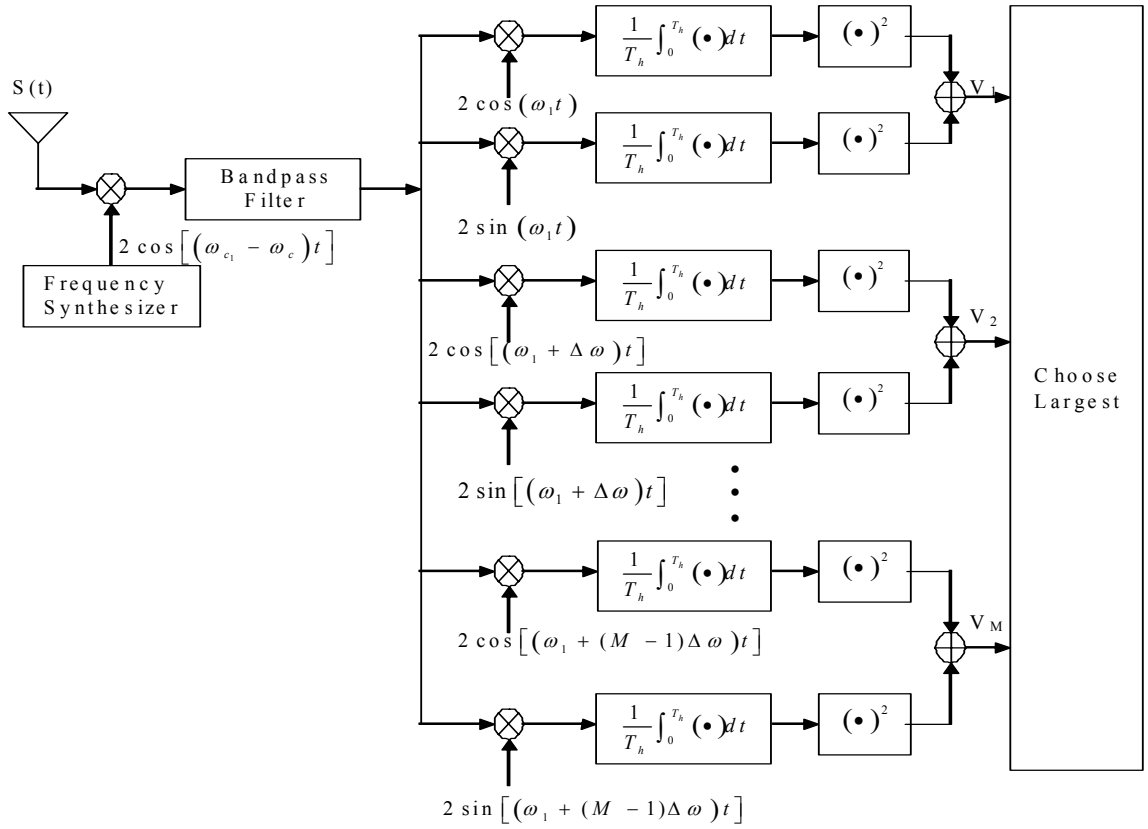

Figure 9. Non-coherent FH/MFSK Receiver

B. PERFORMANCE OF THE AN/USQ-146 JAMMER IN MANUAL SPOT JAMMING MODE

This section analyzes the performance of the $AN/USQ-146$ jammer in manual spot jamming. In this mode of operation, the jammer has no information about the transmitting frequency of the hostile signal. Considering that the signal is transmitted in the bandwidth that the $AN/USQ-146$ covers, the methods that the operator can use are *barrage noise jamming, partial-band noise jamming, and multitone noise jamming*.

Before analyzing all of the above methods, it is necessary to show the performance of the system without any interference other than the existence of AWGN. This is important because many of the following results are based on the performance of the slow FH/MFSK system in AWGN.

1. Performance of FH/MFSK in AWGN

When AWGN is present, the total received signal in the receiver of the FH/MFSK is the transmitted signal (3.8) plus the AWGN $n(t)$ with PSD $N_0/2$. So

$$s_T(t) = \sqrt{2}A_c \cos\left\{2\pi\left[f_i + f_s + (m-1)\Delta_f\right]t + \theta_i\right\} + n(t). \tag{4.7}$$

The process of dehopping does not affect AWGN. Hence, considering perfect synchronization and timing, the performance of the FH/MFSK is the same as when no frequency hopping existed. Based on the analysis of Reference [2], the probability of the symbol error of a noncoherent MFSK signal is

$$P_s = \sum_{n=1}^{M-1}\binom{M-1}{n}(-1)^{n+1}\frac{1}{n+1}e^{\frac{-n\log M}{n+1}\cdot\frac{E_b}{N_o}}, \tag{4.8}$$

where E_b is the bit energy and the fraction of E_b/N_0 is the signal-to-noise ratio.

For orthogonal signaling, when a symbol error occurs, all $M-1$ wrong symbols have an equal probability of occurring. Since the probability of symbol error is independent of the symbol transmitted, for the following analysis any symbol can be chosen to be analyzed. Suppose the signal corresponding to the all-zero symbol is transmitted. In this

case, the average number of 1's corresponds to the average number of bit errors. Based on Reference [3] the total number of 1's in an M-ary symbol set is

$$T_1 = \frac{1}{2} kM. \tag{4.9}$$

When the signal corresponding to the all-zero symbol is transmitted, Equation (4.9) represents the total number of possible wrong bits in all of the incorrect symbols. Since there are $M-1$ incorrect symbols, the average number of wrong bits per incorrect symbol is $\frac{T_1}{M-1} = \frac{kM}{2(M-1)}$.

Therefore, given that a symbol error has occurred, the average probability of bit error can be related using the following equation

$$z = \frac{\text{average number of wrong bits}}{\text{number of } \dfrac{\text{bits}}{\text{symbol}}}$$

$$= \frac{kM}{2(M-1)} \frac{1}{k} = \frac{M}{2(M-1)}. \tag{4.10}$$

As Reference [2] indicates, the combination of Equations (4.8) and (4.10) results in the probability of bit error for the non-coherent FH/MFSK system in AWGN. So $P_b = z \cdot P_s$, or

$$P_b = \frac{M}{2(M-1)} \sum_{n=1}^{M-1} \binom{M-1}{n} (-1)^{n+1} \frac{1}{n+1} e^{\frac{-n \log_2 M}{n+1} \frac{E_b}{N_0}}. \tag{4.11}$$

Figure 10 is the plot of (4.11) for the cases of FH/BFSK, FH/4FSK, and FH/8FSK, which are the three FH systems that are compared for all methods of jamming.

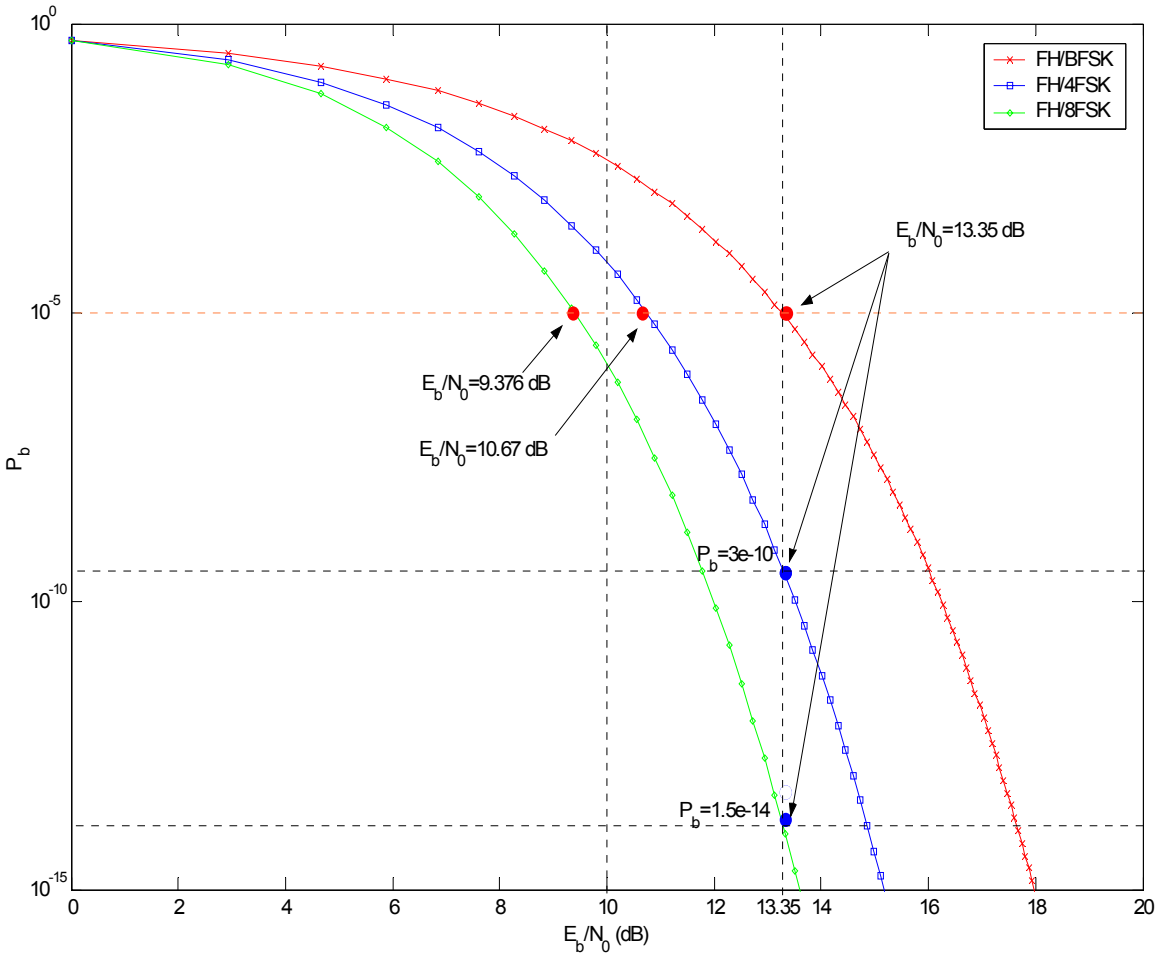

Figure 10. Performance of FH/MFSK in AWGN for $M = 2, 4, 8$

In Figure 10, the values of the three curves for $E_b/N_0 = 13.35$ dB have been marked. This is the value of the signal-to-noise ratio that is considered for the future theoretical and simulation models.

2. Performance of the AN/USQ-146 Jammer Using the Barrage Noise Jamming Technique over a FH/MFSK Communication System

Let the frequency hopping system consist of N non-overlapping bins, each B_{nn} Hz wide, where B_{nn} is the null to null transmission bandwidth for the conventional MFSK signal. Hence the bandwidth of the FH system is

$$W = NB_{nn} \Rightarrow N = \frac{W}{B_{nn}}. \tag{4.12}$$

In order for the jammer to perform barrage noise jamming (BNJ) in this communication system, it creates a bandlimited noise-like signal $n_I'(t)$ with PSD $S_{n_I'}(f)$. Since $n_I'(t)$ and the PSD of the AWGN of the channel $n(t)$ are independent random processes, the total PSD is

$$N_T = \frac{N_0}{2} + S_{n_I'}(f). \tag{4.13}$$

As mentioned in Chapter II, for manual spot jamming, the $AN/USQ-146$ jammer has no efficient way of knowing in which bandwidth the communication system operates. However based on its ability to observe specific portions of bandwidths over a long period of time, the $AN/USQ-146$ jammer can make an estimate and decide to transmit barrage noise jamming in the hypothetical bandwidth W, as can seen in Figure 11.

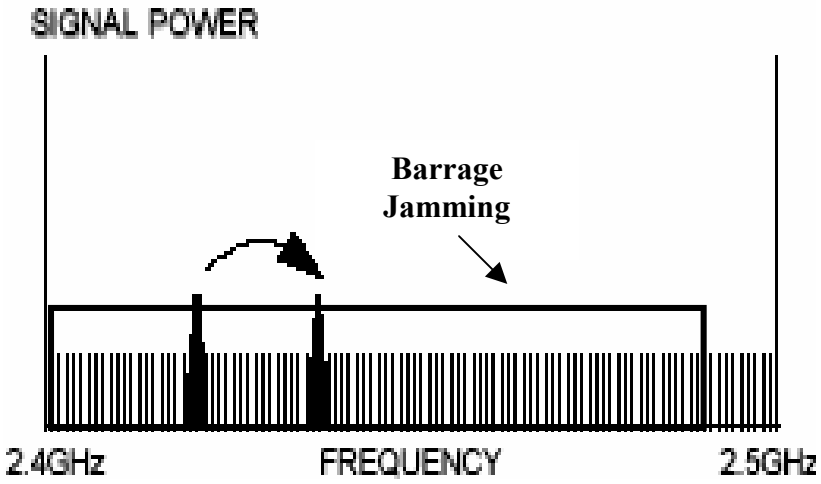

Figure 11. Barrage Noise Jamming

Suppose $S_{n_I'}(f)$ is $N_I'/2$ across the entire frequency bandwidth. Since the barrage noise that the jammer has created is flat across the bandwidth of the receiver, it affects the receiver just as if it were AWGN and

. $$N_T = \frac{N_0}{2} + \frac{N_I'}{2}. \tag{4.14}$$

Based on Reference [2], by replacing the noise power N_o from Equation (4.11) with the total noise power N_T from Equation (4.14), the performance of the jammer in the case of barrage noise jamming can be calculated.

$$P_b = \frac{M}{2(M-1)} \sum_{n=1}^{M-1} \binom{M-1}{n} (-1)^{n+1} \frac{1}{n+1} e^{\frac{-n\log_2 M}{n+1} \left(\frac{1}{\left(\frac{E_b}{N_0}\right)^{-1} + \left(\frac{E_b}{N_I'}\right)^{-1}} \right)}. \tag{4.15}$$

The jammer has no information in this mode of operation whether the system it is trying to jam is a FH or not, so the overall jamming power is the same as if the system were a conventional MFSK. The interference power with barrage noise jamming for conventional MFSK is

$$P_I = B_{nn}\left(\frac{N_I}{2} + \frac{N_I}{2}\right) = B_{nn} N_I . \tag{4.16}$$

The interference power with barrage noise jamming for FH/MFSK is

$$P_I' = W\left(\frac{N_I'}{2} + \frac{N_I'}{2}\right) = NB_{nn} N_I'. \tag{4.17}$$

Since the amount of power that the jammer spends is specific, Equations (4.16) and (4.17) are equals, so

$$WN_I' = B_{nn} N_I ,$$

$$N_I' = \frac{N_I}{N}. \tag{4.18}$$

Replacing N_I' in Equation (4.15) with the result in Equation (4.18) reveals that the influence of $AN/USQ-146$ jammer in a FH/MFSK system in BNJ is

$$P_b = \frac{M}{2(M-1)} \sum_{n=1}^{M-1} \binom{M-1}{n} (-1)^{n+1} \frac{1}{n+1} e^{\frac{-n\log_2 M}{n+1} \left(\frac{1}{\left(\frac{E_b}{N_o}\right)^{-1} + \left(\frac{E_b}{N_I}\right)^{-1} \frac{1}{N}} \right)}. \tag{4.19}$$

When AWGN is not considered negligible, a common value for the signal-to-noise ratio, E_b/N_0, is the 13.35 dB. The number of channels N that the FH system has is a parameter that the jammer in this mode of operation cannot estimate. The signal-to-

interference power, E_b/N_I, is the basic variable that the jammer can dynamically control. The two other parameters that Equation (4.19) depends on is the modulation order M and the number of channels N. In Figure 12, the performance of FH/MFSK for $M = 2, 4, 8$ has been plotted, keeping the number of the channels as a parameter in order to observe how N influences the performance of the jammer.

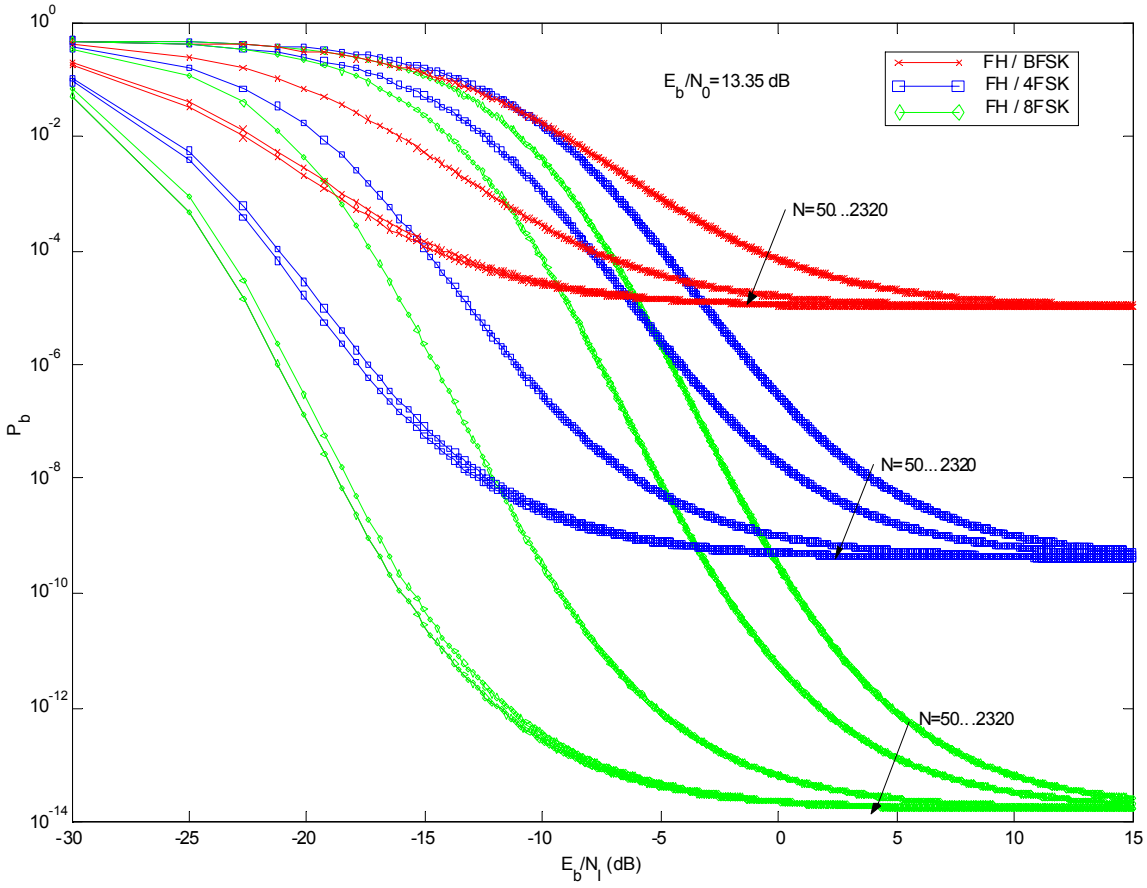

Figure 12. Effect of the $AN/USQ-146$ jammer in Manual Spot Barrage Noise Jamming on the Performance of a FH/ MFSK System in AWGN for Various Number of Hop Bins

Figure 12 clearly shows that as the number of channels in the FH system increases, the performance of the jammer decreases. The performance of the jammer is also influenced by the order of the FH/MFSK modulation. As M increases, the ability of the jammer to jam the signal decreases. It is characteristic of the fact that in order for the

jammer to cause a probability of bit error in the range of $P_b = 0.5,$ it has to achieve a signal-to-interference noise power equal to -30 dB.

Comparing Figure 10 with Figure 12, it is clear that for the whole range of positive values E_b/N_I the barrage noise jamming negligibly increases the probability of error in the FH/MFSK system when the number of channels is increased to 2320. The number 2320 is the number of channels that is used in the rest of the thesis, since the most advanced airborne system, which is called SINCGARS, has $N = 2320$ hop bins with a hopping rate $R_h = 100$ hops/s. Focusing on the case in which the $AN/USQ-146$ jammer's purpose is to jam a SINCGARS system, the performance of the jammer is described by Equation (4.19) with the parameter $N = 2320.$

In order to understand the jammer's influence on a FH/MFSK signal when it operates using barrage noise jamming in the manual spot mode, one can examine Figure 13, which compares the case of a FH/MFSK system, like SINCGARS ($N = 2320$), in BNJ and in AWGN. In Figure 13, the dash lines indicate the probability of error for each case of modulation order, in AWGN for $E_b/N_0 = 13.35$ dB.

The conclusions that arise from the Figure 13 is that the barrage noise jamming technique has a basic disadvantage. It lacks any information about the instantaneous frequency of the transmitted signal. This forces the jammer to spread its power equally on the whole transmitted bandwidth. As the number of channels M of the FH signal increases, the width of the area that the jamming power must cover also increases, which reduces the PSD of P_J. This is the reason that the jammer needs an output power 1000 times greater that the signals power in order to achieve a probability of bit error between 0.1 and 0.5.

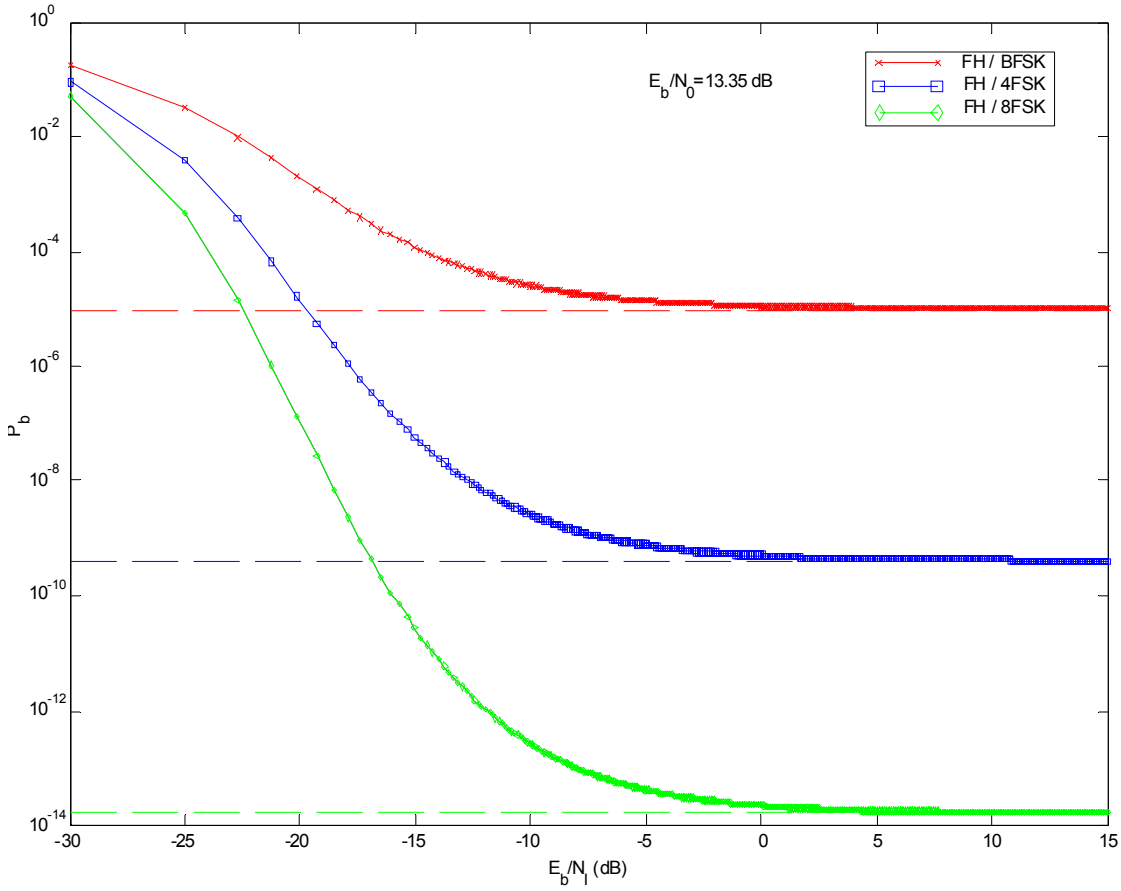

Figure 13. Performance of the $AN/USQ-146$ in Barrage Noise Jamming for $N=2320$ in FH/MFSK

Figure 13 reflects the performance of the jammer in BNJ and emphasizes the fact that the jammer does not influence the communication system for all the positive values of E_b/N_I, since the probability of error of the signal is at the same level as if the system were experiencing only the noise of the channel. Only when the jamming power becomes large enough in relation with the signal power does the communication system begin to be affected by the barrage noise jamming.

The performance of the $AN/USQ-146$ jammer in a manual spot jamming using the BNJ technique cannot be considered efficient enough, especially on the modern battlefield. It does not degrade the system's performance enough, is not power efficient, and its success depends to a great extent on the experience of the operator. These disadvantages lead to the investigation of other more advanced ways of jamming, such as the partial-band jamming with the $AN/USQ-146$ jammer in manual spot jamming.

3. Performance of the AN/USQ-146 Jammer Using the Manual Spot Partial-band Noise Jamming Technique over a FH/MFSK Communication System

In partial-band noise jamming (PBJ), the jammer spreads the noise interference over a portion of the entire spread spectrum bandwidth. Because of the smaller bandwidth, the partial-band noise jammer is considerably more effective than the barrage noise jammer.

The $AN/USQ-146$ jammer, as described in Chapter II, can produce, with the help of the waveform generator, pulses containing noise with variable bandwidth. Practically and analytically, this is identical to creating pulse noise jamming.

In the following analysis, the jammer transmission bandwidth is denoted as W_j. Considering that that the spread spectrum bandwidth is W, the fraction of the communication bandwidth that is jammed is denoted as

$$\rho = \frac{W_j}{W}, \tag{4.20}$$

with

$$0 < \rho \leq 1. \tag{4.21}$$

Based on the information that the control screen of the $AN/USQ-146$ jammer provides to the operator, it is logical to assume that an integral part of the frequency hop bins will be jammed, as seen in Figure 14.

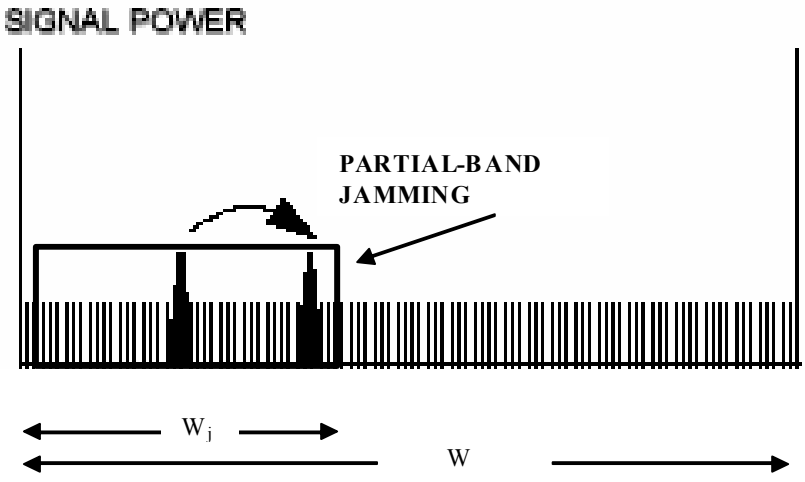

Figure 14. Partial-band Noise Jamming

The jammer is transmitting a noise-like signal with PSD

$$S''_{n_I}(f) = \frac{N''_I}{2}, \tag{4.22}$$

in the W_j bandwidth and zero elsewhere. The overall output power of the $AN/USQ-146$ jammer is the same whether it is using a barrage or a partial-band jamming technique. The interference power with partial-band noise jamming P''_I is equal to the interference power in barrage noise jamming P'_I, which equals the interference power P_I for the conventional MFSK.

$$P_I = P'_I = P''_I . \tag{4.23}$$

The interference power with partial-band noise jamming for the FH/MFSK is

$$P''_I = 2W\left[\frac{\rho N''_I}{2} + (1-\rho)\cdot 0\right] = W\rho N''_I = NB_{nn}\rho N''_I . \tag{4.24}$$

Rearranging the terms in (4.16), (4.17), (4.23) and (4.24), the result is

$$N''_I = \frac{N'_I}{\rho} = \frac{N_I}{N\rho} . \tag{4.25}$$

From (4.25) it becomes clear that the main effect of the partial-band noise jamming is the increase of the PSD by $1/\rho \geq 1$ in the bins that are affected. As ρ becomes smaller, the PSD of the noise-like signal increases and the jammer affects the communication system even more.

As Reference $[3]$ indicates, the practical limitation is that the jammer may not be able to transmit the peak power $P_I/(N\rho)$ when ρ is too small. One other limitation is that the jammer cannot jam less than one frequency hopping bin. This observation results in a lower limit in ρ, and (4.21) becomes

$$\frac{1}{N} < \rho \leq 1 . \tag{4.26}$$

Keeping in mind the two above limitations, the analysis of how the partial-band jamming technique performs continues by using the result obtained in the barrage noise

jamming (4.15). Replacing N_I' in Equation (4.15) with N'', and using the result of (4.25) shows that the probability of error when a frequency hop is jammed is

$$P_b(\text{hop is jammed}) = \frac{M}{2(M-1)} \sum_{n=1}^{M-1} \binom{M-1}{n} (-1)^{n+1} \frac{1}{n+1} e^{\frac{-n\log_2 M}{n+1}\left(\frac{1}{\left(\frac{E_b}{N_0}\right)^{-1} + \left(\frac{E_b}{N_I}\right)^{-1} \frac{1}{N\rho}}\right)}. \quad (4.27)$$

The probability that a bin is jammed $\Pr(\text{bin is jammed})$ is equal to ρ. On the other hand, the probability that the bin is not jammed $\Pr(\text{bin not jammed})$ is equal to $1-\rho$. When the signal is not jammed, only the AWGN that exists in the channel influences it. Therefore the general form of the probability of error of the FH/MFSK system under the influence of the $AN/USQ-146$ jammer in manual spot mode using the partial-band jamming technique is

$$P_b = \Pr(\text{bin jammed}) \cdot P_b(\text{hop is jammed}) + \Pr(\text{bin not jammed}) \cdot P_b(\text{hop is not jammed}),$$

$$\begin{aligned} P_b = {} & \rho \frac{M}{2(M-1)} \sum_{n=1}^{M-1} \binom{M-1}{n} (-1)^{n+1} \frac{1}{n+1} e^{\frac{-n\log_2 M}{n+1}\left(\frac{1}{\left(\frac{E_b}{N_0}\right)^{-1} + \left(\frac{E_b}{N_I}\right)^{-1} \frac{1}{N\rho}}\right)} \\ & + (1-\rho) \frac{M}{2(M-1)} \sum_{n=1}^{M-1} \binom{M-1}{n} (-1)^{n+1} \frac{1}{n+1} e^{\frac{-n\log_2 M}{n+1}\left(\frac{E_b}{N_0}\right)}. \end{aligned} \quad (4.28)$$

Figure 15 illustrates the plot of (4.28) for $E_b/N_0 = 13.35$ dB with ρ as a parameter. This clearly shows that as ρ becomes smaller, the performance of the jammer improves.

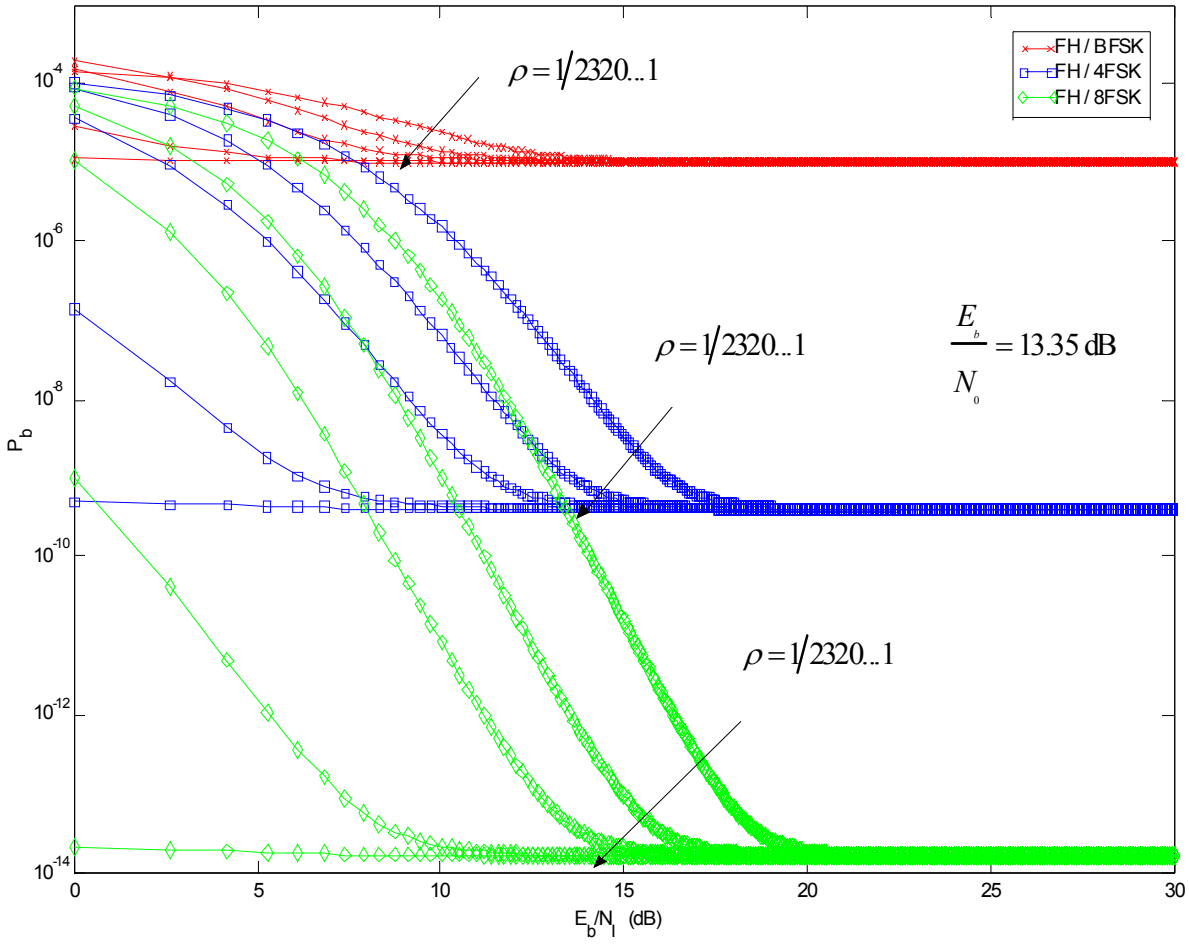

Figure 15. Effect of the $AN/USQ-146$ jammer in Manual Spot Partial-Band Noise Jamming on the Performance of a FH/ MFSK $(N=2320)$ System in AWGN for Various ρ

As mentioned previously $E_b/N_0 = 13.35$ dB, which means $E_b/N_0 \gg 1$. Also it is correct to consider that the PSD N_I'' of the partial-band jamming is much larger than the PSD N_0 of the AWGN. The first assumption allows an analyst to neglect the second term in (4.28). By taking into account the second assumption, the E_b/N_0 term can also be neglected. Therefore (4.28) becomes

$$P_b = \rho \frac{M}{2(M-1)} \sum_{n=1}^{M-1} \binom{M-1}{n} (-1)^{n+1} \frac{1}{n+1} e^{\frac{-n\log_2 M}{n+1}\left(\frac{E_b N \rho}{N_I}\right)}. \qquad (4.29)$$

Since the jammer wishes to maximize P_b, it must find the appropriate ρ that will cause the maximum error. Taking the first derivative of (4.29) with respect to ρ, the result is

$$\frac{\partial P_b}{\partial \rho} = \rho \frac{M}{2(M-1)} \sum_{n=1}^{M-1} \binom{M-1}{n} (-1)^{n+1} \frac{1}{n+1} e^{\frac{-n\log_2 M}{n+1}\left(\frac{E_b N \rho}{N_I}\right)} \cdot \frac{-n\log_2 M}{n+1} \cdot \frac{E_b N}{N_I}$$
$$+ \frac{M}{2(M-1)} \sum_{n=1}^{M-1} \binom{M-1}{n} (-1)^{n+1} \frac{1}{n+1} e^{\frac{-n\log_2 M}{n+1}\left(\frac{E_b N \rho}{N_I}\right)}. \tag{4.30}$$

In order to find the most appropriate ρ, which will cause the worst performance in the FH/MFSK system, (4.30) must be set equal to zero. For convenience, in the following analysis, the quantity $E_b N \rho / N_I$ is set equal to y. Then,

$$y = \frac{\sum_{n=1}^{M-1} \binom{M-1}{n} (-1)^{n+1} \frac{1}{n+1} e^{\frac{-n\log_2 M}{n+1} \cdot y}}{\sum_{n=1}^{M-1} \binom{M-1}{n} (-1)^{n+1} \frac{1}{n+1} e^{\frac{-n\log_2 M}{n+1} \cdot y} \frac{n\log_2 M}{n+1}}. \tag{4.31}$$

As Reference $[2]$ reveals, the numerical solutions y_0 of the above equation, for $M = 2, 4, 8$, are given in Table 4.

M	**y_0**
2	2
4	2.38
8	2.78

Table 4. Solution of (4.31) as a Function of M

The worst case fraction of jammed bandwidth (ρ_{wc}), which depends on the type of modulation and the signal-to-interference noise ratio is

$$\rho_{wc} = \frac{y_0}{\frac{E_b}{N_I} N}. \tag{4.32}$$

Then based on (4.26)

$$N_I > \frac{A_c^2 T_b}{y_0}. \tag{4.33}$$

By replacing in (4.16) the result of (4.33) follows

$$P_I > B_{nn} N_I ,$$

$$P_I > \frac{B_{nn} A_c^2 T_b}{y_0}. \tag{4.34}$$

The null-to-null transmission bandwidth of an MFSK system is

$$B_{nn} = (M-1)\Delta f + 2R_s . \tag{4.35}$$

For orthogonal noncoherent MFSK, (4.35) becomes

$$B_{nn} = (M-1)R_s + 2R_s = \frac{(2^k+1)R_b}{k} . \tag{4.36}$$

The combination of (4.34) and (4.36) gives

$$\frac{P_I}{P_c} > \frac{\left(2^k+1\right)}{k y_0} A_c^2 ,$$

$$P_I > \frac{\left(2^k+1\right)R_b}{k y_0} A_c^2 T_b ,$$

$$P_I > \frac{\left(2^k+1\right)}{k y_0} P_c ,$$

$$\frac{P_I}{P_c} > \frac{\left(2^k+1\right)}{k y_0} . \tag{4.37}$$

The numerical replacement of k and y_0 in (4.37) give the results in Table 5.

M	$\left[\frac{P_I}{P_c}\right]_{dB} >$
2	1.76 dB
4	0.213 dB
8	0.33 dB

Table 5. Lower Limits of P_I/P_c for Worst Case Partial-Band Jamming

The values in Table 5 show the output power that the jammer must produce in order to be effective in the worst case partial-band jamming technique.

The result of the replacement of (4.32) in (4.29) gives

$$P_b = \frac{y_0}{\frac{E_b}{N_I} N} \frac{M}{2(M-1)} \sum_{n=1}^{M-1} \binom{M-1}{n} (-1)^{n+1} \frac{1}{n+1} e^{\frac{-n \log_2 M}{n+1} \cdot y_0} . \qquad (4.38)$$

The above equation has as a variable the signal-to-interference noise ratio E_b/N_I, and two basic parameters: M and N. Setting $N = 2320,$ the only parameter is the modulation order $M,$ which also specifies the value of y_0 from Table 4.

For comparison reasons, Figure 16 gives the performance of the $AN/USQ-146$ jammer in the manual spot mode using the partial-band jamming technique based on Equation (4.38) for two values of N. It is obvious from the figure that the increase in the number of hop bins (N) negatively influences the performance of the jammer. The jammer for the case of the SINCGARS system $(N = 2320)$ can achieve a probability of bit error equal to 0.5 when $E_b/N_I = -35$ dB. On the other hand for $N = 50,$ the necessary signal-to-interference noise ratio is close to -20 dB.

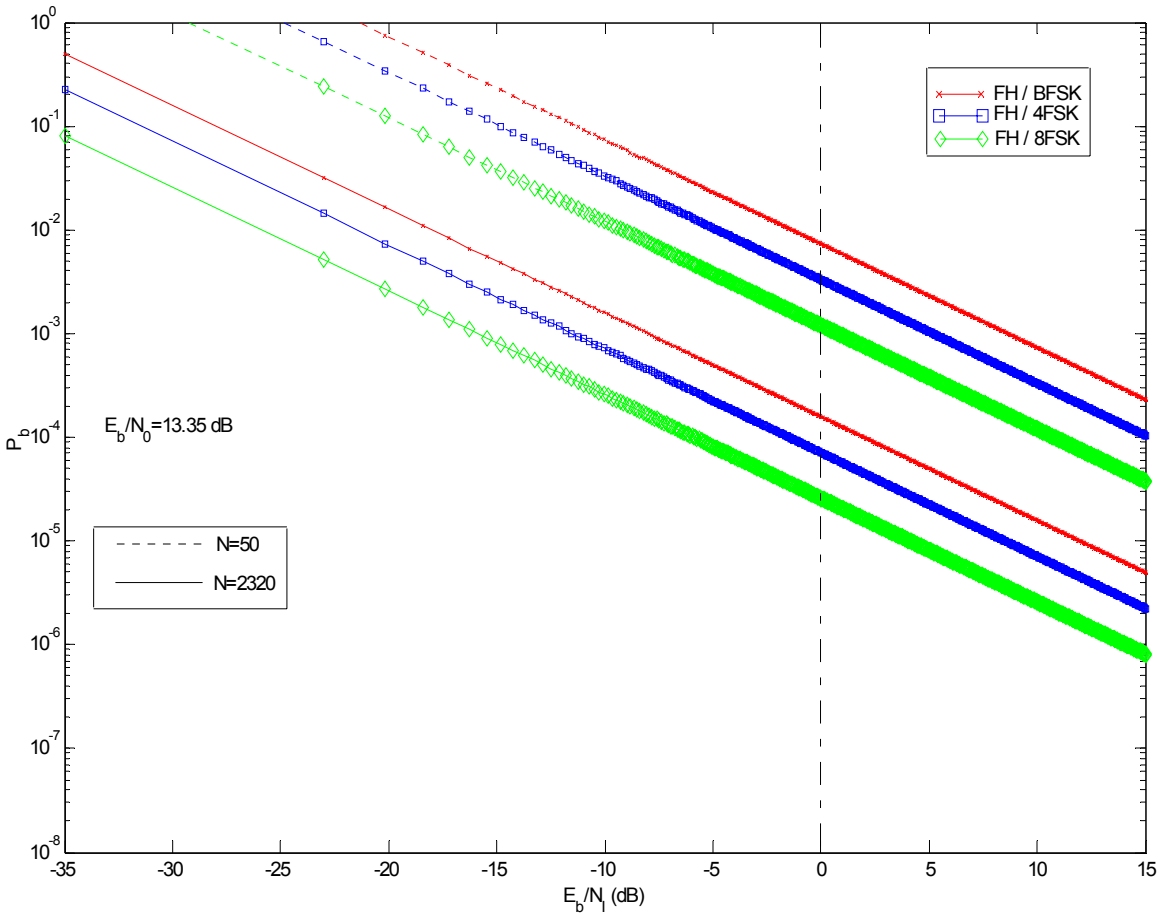

Figure 16. Effect of the $AN/USQ-146$ Jammer in Worst Case Partial-Band Noise Jamming on the Performance of a FH/ MFSK System in AWGN for $N=2320$ and $N=50$

By comparing Figure 15 to Figure 16, it becomes clear that the effect of the worst case partial-band noise jamming is to change the dependence of P_b on E_b/N_I from an exponential one to an inverse one. The result improves the performance of the jammer, especially for the case of the FH/4FSK and FH/8FSK. The problem for the jammer in the worst case PBJ is that as E_b/N_I increases, the jammer requires higher peak power and covers fewer and fewer frequency hop bins, since ρ_{wc} becomes smaller.

By knowing that the $AN/USQ-146$ jammer has specific output power that depends on the range of the bandwidth that it will jam, it can be concluded that even though partial-band noise jamming is always possible from the jammer, the worst case may not.

The worst case will be possible only when the output power of the jammer (P_I) divided by the power of the signal (P_c) is greater than the limits of Table 4.

The operation of the jammer in manual spot mode, using the partial-band jamming technique, can seriously damage the communication system if it is working with the worst case fraction of jammed bandwidth ρ_{wc}. In the case when the power of the signal is so large that the jammer cannot transmit the appropriate output power that Table 4 indicates, then the partial-band jamming causes a smaller degradation in the performance of the communication system. This degradation cannot be considered efficient enough on the modern battlefield.

4. Performance of the AN/USQ-146 Jammer Using the Manual Spot Multiple-Tone Jamming Technique over a FH/MFSK Communication System

The $AN/USQ-146$ jammer operating in manual spot mode can transmit equal power jamming tones, randomly distributed across the entire frequency-hopped bandwidth. The particular jammer also has the capability to observe the transmitted frequencies and their history in order to understand the structure of the signal. If the jammer cannot verify the structure of the system, then this mode of operation is worthless in a FH system. This type of multiple-tone jamming is called *independent multitone interference*.

Based on Reference $[3]$ for the FH/MFSK, in this mode of operation, there are two possible cases concerning the signal and jammer tones within a specific frequency-hop bin. In the first case, there is no interference at all in the bin (the jammer tones are elsewhere), and the probability of error is the same as for the conventional MFSK in the AWGN. In the second case, there is jammer interference in the bin.

This section considers the general case of a jammer using q jamming tones within the N frequency hop bins, even though Chapter II revealed that the $AN/USQ-146$ jammer can transmit two tones simultaneously. The replacement of $q=2$ will be done at the end of the analysis.

It is obvious that the number of interfering tones (q) is less than or equal the possible signaling frequencies (M),

$$1 \le q \le M \ . \tag{4.39}$$

Since, the jammer is transmitting q tones for each hop, the power of each tone is

$$P_I = \frac{P_{I_T}}{q}, \tag{4.40}$$

and they are spaced in frequency, at least, by B_{nn} Hertz. The jammer's total power is P_{I_T}. This is the most suited assumption, since the $AN/USQ-146$ jammer in this mode of operation cannot specify the bandwidth of the FH system and cannot send the jamming tones in the same frequency hop bin.

When $P_I < P_c$ the jammer cannot cause any damage to the communication system and the probability of error ensues from the AWGN only. When $P_I > P_c$, a symbol error is made if the jamming tone is within the FH band but not in the same energy detector filter bandwidth as the desired signaling tone. When $P_I = P_c$ a symbol error occurs with a probability 0.5 under the conditions described for $P_I > P_c$.

Based on Reference $[2]$, the jammer can therefore jam the most FH bands if $P_I = P_c + \varepsilon$ where $\varepsilon \ll P_c$, and the number of jammer tones is approximately given by

$$q \approx \left\lfloor \frac{P_I}{P_c} \right\rfloor, \tag{4.41}$$

where $\lfloor \bullet \rfloor$ denotes the largest integer less than or equal to P_I/P_c. Of course there must be at least one jammer tone so that $q_{\min} = 1$ and $q_{\max}$ is limited by the total number of FH bands or $q_{\max} = N$. When $q \approx \lfloor P_I/P_c \rfloor \le 1$, no errors will be made since there is insufficient jammer power to jam even a single FH band. Equation (4.41) is approximate only because ε has been set to zero. This value of q is optimum since a larger q results in $P_c > P_{I_T}$ and no errors, and since a smaller q results in fewer bands being jammed but no larger error probability for any one band.

The probability that any of the N FH bins is jammed is

$$\Pr(\text{bin jammed}) = \frac{q}{N}. \tag{4.42}$$

The probability that the hop is not jammed is

$$\Pr(\text{bin not jammed}) = 1 - \frac{q}{N}. \tag{4.43}$$

When a FH band is jammed and q is chosen using (4.41), the symbol error probability is the probability that the jammer and the signal are not in the same band. This probability is $\frac{M-1}{M}$ and the total symbol error probability P_s is

$$P_s = \begin{cases} \dfrac{M-1}{M} & N < \left\lfloor \dfrac{P_J}{P_c} \right\rfloor \\ \dfrac{M-1}{M}\dfrac{q}{N} + \left(1 - \dfrac{q}{N}\right) P_s\left(q=0\right) & 1 \le \left\lfloor \dfrac{P_J}{P_c} \right\rfloor \le N \\ 0 & \left\lfloor \dfrac{P_J}{P_c} \right\rfloor < 1. \end{cases} \tag{4.44}$$

The symbol error probability is related to the bit error probability by $P_b = \frac{M}{2(M-1)} P_s$ for orthogonal signals. Inserting (4.41) into (4.44) gives the following expression for the bit error probability for q tone jamming

$$P_b = \begin{cases} \dfrac{1}{2} & N < \left\lfloor \dfrac{P_J}{P_c} \right\rfloor \\ \dfrac{q}{2N} + \left(1 - \dfrac{q}{N}\right) P_b\left(q=0\right) & 1 \le \left\lfloor \dfrac{P_J}{P_c} \right\rfloor \le N \\ 0 & \left\lfloor \dfrac{P_J}{P_c} \right\rfloor < 1. \end{cases} \tag{4.45}$$

where $P_b(q=0)$ represents the probability of bit error for the FH/MFSK system, and is given by (4.11). Based on (4.41) the above equation can be expressed as a function of q or a function of P_J/P_c. In both cases, the results are exactly the same. For compatibility with the previous cases q is replaced and (4.45) becomes

$$P_b = \begin{cases} \dfrac{1}{2} & N < \left\lfloor \dfrac{P_I}{P_c} \right\rfloor \\ \dfrac{P_I}{2NP_c}\dfrac{q}{N} + \left(1 - \dfrac{P_I}{NP_c}\right)\dfrac{M}{2(M-1)}\displaystyle\sum_{n=1}^{M-1}\binom{M-1}{n}(-1)^{n+1}\frac{1}{n+1}e^{\frac{-n\log_2 M}{n+1}\frac{E_b}{N_0}} & 1 \le \left\lfloor \dfrac{P_I}{P_c} \right\rfloor \le N \\ 0 & \left\lfloor \dfrac{P_I}{P_c} \right\rfloor < 1. \end{cases} \quad (4.46)$$

By examining the above equation, it is apparent that the probability of bit error in multitone jamming depends on the fraction P_I/P_c, the number of hop bins N, and the modulation order M. It is also obvious that since the first part of the summation is much larger than the second part, the modulation order M will influence the above equation slightly. The graphical presentation of Equation (4.46) is shown in Figure 17 for various values of N.

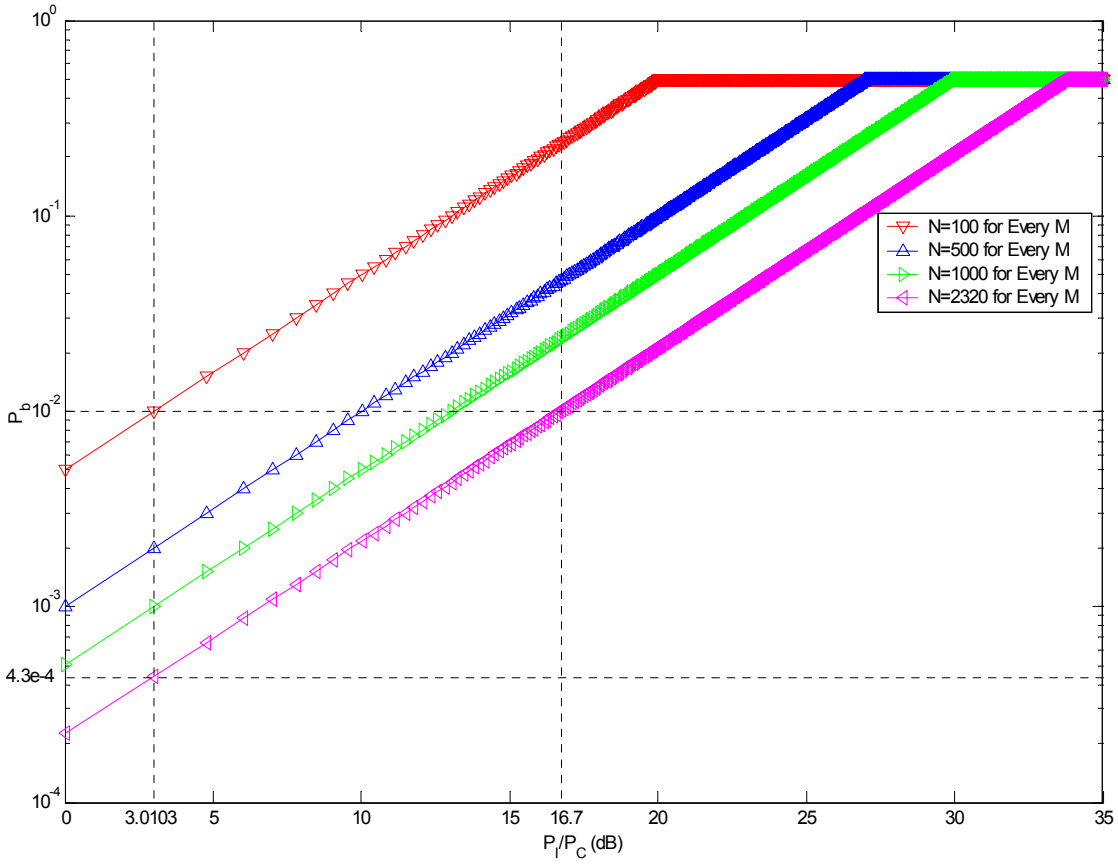

Figure 17. Performance of the $AN/USQ-146$ in Manual Spot Multitone Jamming Versus the Ratio of the Jamming Power (P_I) to the Signal Power (P_c) for Various N

Figure 17 illustrates that similar to the case of the worst case partial-band jamming, the FH system can increase the number of hop bins in order to decrease the performance of the jammer. It is also obvious that as the power of the jammer becomes larger, the available number of jamming tones increases and the performance of the interferer becomes greater.

As noted in the beginning of this section, the $AN/USQ-146$ jammer has the capability of transmitting two jamming tones with power $P_I/2$. In Figure 17, for $q=2,$ the probability of error of a FH system with $N=2320$ is $4.3\times10^{-4}.$ The maximum probability of bit error in this case is 0.5 and can be achieved when the number of jammer tones is equal to the number of FH bins.

As can be concluded from Figure 17, it would be useless for the jammer to consume power in order to transmit more than two tones since its performance does not improve dramatically. Moreover, since the output power of the jammer is constant, if the jammer were able to transmit more tones, for example $K,$ with the same power as before, it would have to increase its power by $K/2$. For example, Figure 17 indicates that if the jammer wants to cause the same probability of error in the SINCGARS system as it causes in a system with $N=100$, it has to produce 47 tones instead of $2.$ This increases the output power of the jammer by $23.5.$ For a comparison, Equation (4.46) can be rearranged in order to be a function of E_b/N_I. Knowing that

$$\frac{P_I}{P_c}=\frac{B_{nn}NN_I}{qE_bR_b}=\frac{\left(\frac{2^k+1}{k}\right)}{q\frac{E_b}{N_I}}=\left(\frac{2^k+1}{qk}\right)\left(\frac{E_b}{N_I}\right)^{-1}N\,, \tag{4.47}$$

Equation (4.46) becomes

$$P_b=\begin{cases}\dfrac{1}{2} & \dfrac{2^k+1}{qk}\left(\dfrac{E_b}{N_I}\right)^{-1}>1\\[2ex] \dfrac{2^k+1}{2qk}\left(\dfrac{E_b}{N_I}\right)^{-1}+\left(1-\dfrac{2^k+1}{qk}\left(\dfrac{E_b}{N_I}\right)^{-1}\right)\displaystyle\sum_{n=1}^{M-1}\binom{M-1}{n}(-1)^{n+1}\frac{1}{n+1}e^{-\frac{n\log(M)}{n+1}\frac{1}{\left(\frac{E_b}{N_0}\right)^{-1}}} & \dfrac{1}{N}\le\dfrac{2^k+1}{qk}\left(\dfrac{E_b}{N_I}\right)^{-1}<1\\[2ex] 0 & \dfrac{2^k+1}{qk}\left(\dfrac{E_b}{N_I}\right)^{-1}<\dfrac{1}{N}.\end{cases} \tag{4.48}$$

The plot of (4.48) in Figure 18 illustrates the probability of bit error that the $AN/USQ-146$ causes in a FH/MFSK system as the E_b/N_I increases for two values of N.

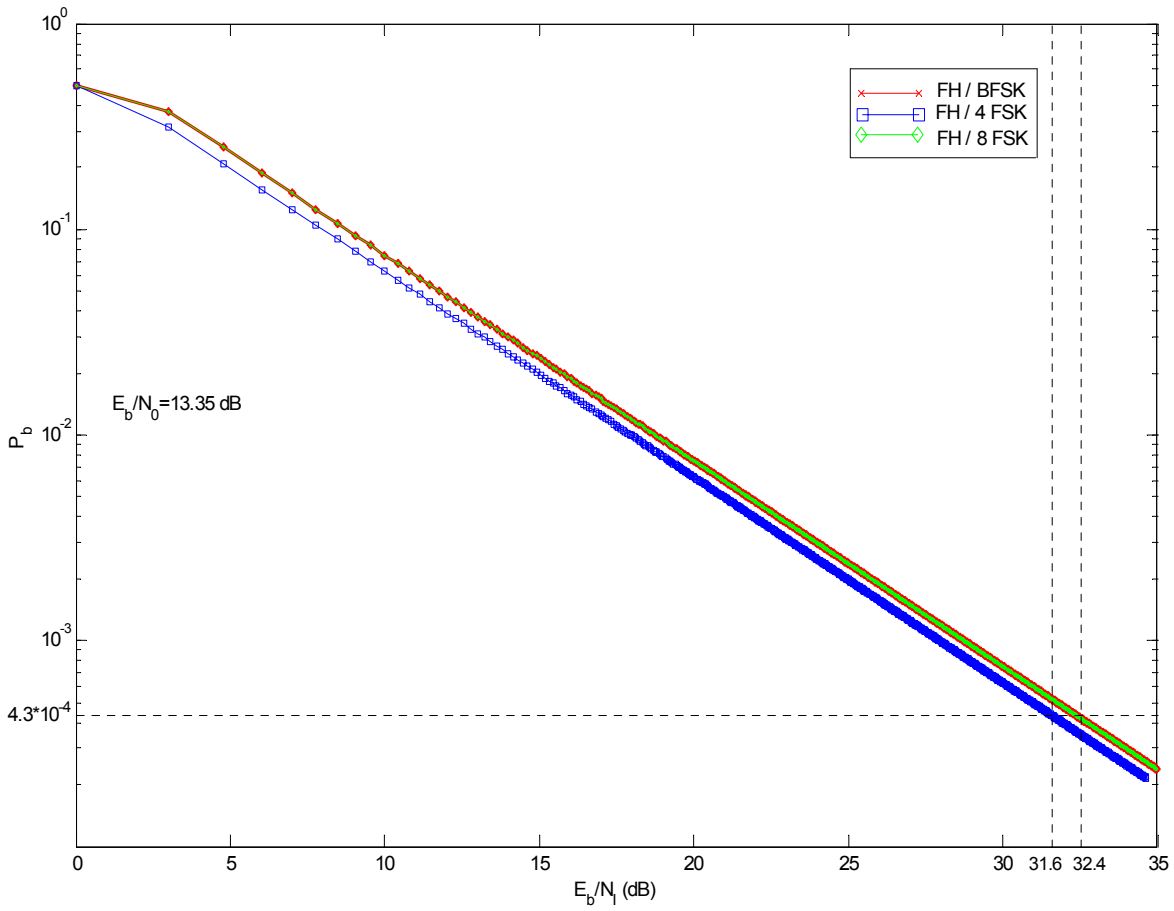

Figure 18. Effect of the $AN/USQ-146$ Jammer in Manual Spot Tone Noise Jamming on the Performance of a FH/ MFSK System in AWGN for $N=2320$ and $N=50$

Figure 18 verifies that the modulation order (M) and the number of hop bins (N) only slightly influence the performance of the jammer in multitone jamming, since for all cases the lines are quite close to each other. In addition to that, for a relatively large number of hop bins, as M increases, the performance of the system become worse. This phenomenon can be observed in the above figure, where the SINCGARS system with $M=8$ behaves worse than the case of $M=4$.

The two output tones of the $AN/USQ-146$ jammer produce a signal-to-interference jamming ratio that depends on the modulation order M. A rearrangement of the terms in Equation (4.47) gives

$$\frac{P_I}{P_c} = q = \left(\frac{2^k+1}{qk}\right)\left(\frac{E_b}{N_I}\right)^{-1} N,$$

$$\frac{E_b}{N_I} = \left(\frac{2^k+1}{q^2 k}\right) N. \tag{4.49}$$

By setting $N = 2320$ and $q = 2$, Table 6 gives the values of E_b/N_I for all the cases of M.

$M = 2^k$	$\frac{E_b}{N_I}(\text{dB})$
2	32.4
4	31.66
8	32.4

Table 6. E_b/N_I of the $AN/USQ-146$ Jammer in the Multitone Jamming Technique

As Figure 18 indicates, the $AN/USQ-146$ jammer achieved a probability of bit error near to 4.3×10^{-4} for the values of Table 6. For the same values of E_b/N_I in PBJ, as can be observed in Figure 19, the probability of bit error is between 10^{-7} and 10^{-8}. That is, the multitone jamming technique improves in the jammer performance to nearly 40 dB.

Generally the operation of the $AN/USQ-146$ in manual spot mode, using the multitone jamming technique is considered to be a successful strategy. The jammer with no capability of detecting the transmitting frequency of the FH signal manages to cause a probability of bit error of nearly 10^{-3} in a very advanced combat radio system, with the transmission of two jamming tones at each instance. As the jammer increases the power of the output tones it can causes even greater degradation. Specifically, when the total

output jamming power becomes equal to the signal power, the probability of bit error is close to 0.5.

The above result is highly important since it states that in all the cases examined in this chapter, that is, barrage noise jamming, partial-band noise jamming, and multitone jamming, the most advanced is the multitone jamming. This result is also verified in Figure 19 in which results from all the jamming types are plotted together.

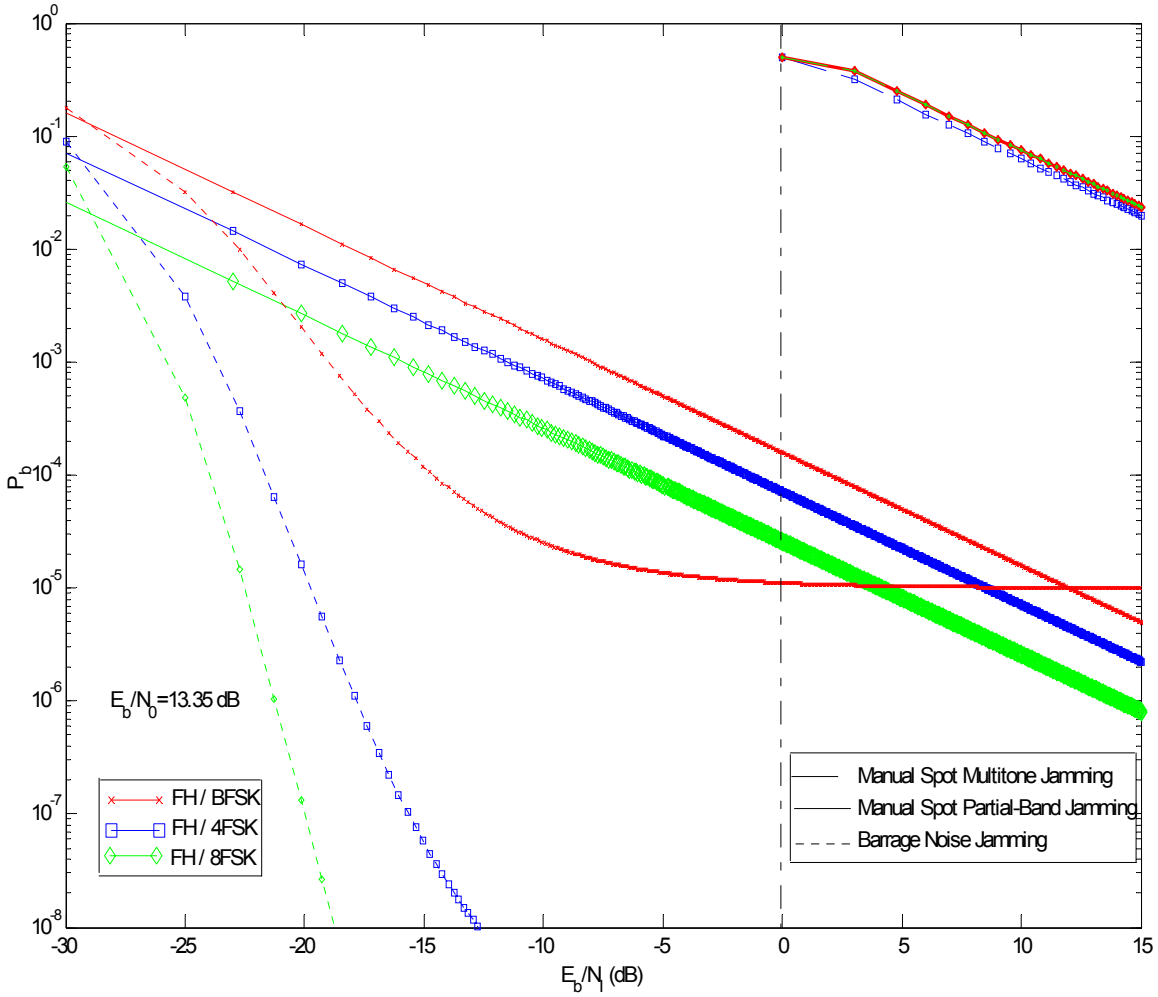

Figure 19. Comparison of Effect of the $AN/USQ-146$ Jammer in Manual Spot Barrage, Partial-Band and Multitone Jamming on the Performance of a SINCGARS System in AWGN

C. SUMMARY

In this chapter the performance of the $AN/USQ-146$ jammer in barrage, worst case partial-band and multitone jamming in manual spot mode was examined. The analysis of the results indicates that the performance of the jammer is influenced by the modulation order of the hostile FH/MFSK system and the number of hop bins. As Figure 19 shows, for the same number of hop bins $(N = 2320)$ and signal-to-noise ratio $E_b/N_0 = 13.35$ dB, the most advanced technique that the $AN/USQ-146$ jammer can use is the multitone jamming. In this way, independent of M, the jammer can greatly degrade the performance of the system, and can be compared to some more advanced jamming techniques, such as those that the $AN/USQ-146$ uses in a reactive mode. Characteristically, the multitone jamming technique can cause a probability of bit error in the range of 0.5 to 0.1 with $E_b/N_I = 0$ dB. On the other hand the partial-band and the barrage noise jamming methods need a jamming power 1000 times greater than the signal power $(E_b/N_I = -30$ dB$)$ in order to succeed a $P_b = 0.5$.

As mentioned in the beginning of this section, the disadvantage of the multitone jamming method is that the jammer must know the signal's full structure before starting to interfere in the system. Only then is it capable of selecting jamming frequencies so that no more than one tone appears in each FH bin. When the jammer has no complete knowledge of the communication scheme, this mode does not offer any remarkable degradation in the system's performance.

The reactive mode of operation is the next and most important capability of the $AN/USQ-146$ jammer. In the next chapter, before investigating the various jamming techniques in the reactive mode, some basic geometric and physical restrictions that the reactive or follower jamming mode possesses will be presented. The next chapter is crucial because it analyzes when and where the $AN/USQ-146$ jammer can perform in a reactive mode and which parameters influence its ability to first detect and then to jam each hop frequency that the system is using.

THIS PAGE INTENTIONALLY LEFT BLANK

V. FUNDAMENTAL LIMITATIONS OF THE AN/USQ-146 JAMMER ON REPEATING JAMMING OPERATION MODE

In this chapter, the fundamental limitations on the effectiveness of the $AN/USQ-146$ jammer in the follower jamming mode are derived. These limitations arise because of the geometry and the need for a frequency estimation.

As analyzed in Chapter II, frequency-hopping spread-spectrum is particularly useful for combat primarily because it is relatively easy to operate over very large spread bands and allows communicators to hop out of frequency channels with interference. The benefits of FH are potentially neutralized by a repeater jammer, also known as a follower jammer, which is the most important characteristic of the $AN/USQ-146$. This mode of operation is the reason this particular jammer is considered to be one of the most efficient jamming devices.

In the reactive mode, the jammer intercepts the transmit signal, tries to determine the frequency of the hop, and then generates jamming in a narrow range around this frequency. To be effective against a FH system, the jamming energy must reach the victim's receiver before it hops to a new set of frequency channels. Thus, the greater the hopping rate R_h of the FH system, the more difficult it is for the repeat jammer to perform effectively.

A. AN/USQ-146 JAMMER CONFIGURATION AND GEOMETRICAL RESTRICTIONS IN REPEAT MODE OF OPERATION

The geometry of the $AN/USQ-146$ jammer in repeat mode is illustrated in Figure 20. The transmitter to receiver distance is D_1, the transmitter to jammer distance is D_2, and the jammer to receiver distance is D_3. As Reference $[4]$ points out, for the repeater jamming to be effective, the arrival-time delay of the jamming relative to the desired signal at the receiver must not exceed a certain fraction of the dwell time of the signal. That means,

$$\frac{D_2 + D_3}{c} + T_{pr} \le \frac{D_1}{c} + \eta T_d , \tag{5.1}$$

where c is the speed of the electromagnetic wave, T_{pr} is the processing time required by the jammer, η is a fraction, and T_d is the dwell time of the transmitted pulse. A rearrangement of (5.1) yields

$$D_2 + D_3 \le \left(\eta T_d - T_{pr}\right)c + D_1 . \tag{5.2}$$

If the right-hand side of the inequality is regarded as a constant, then equating the two sides defines an ellipse with the transmitter and the receiver at the two foci. If the repeater $AN/USQ-146$ jammer is outside this ellipse, the jamming cannot be effective.

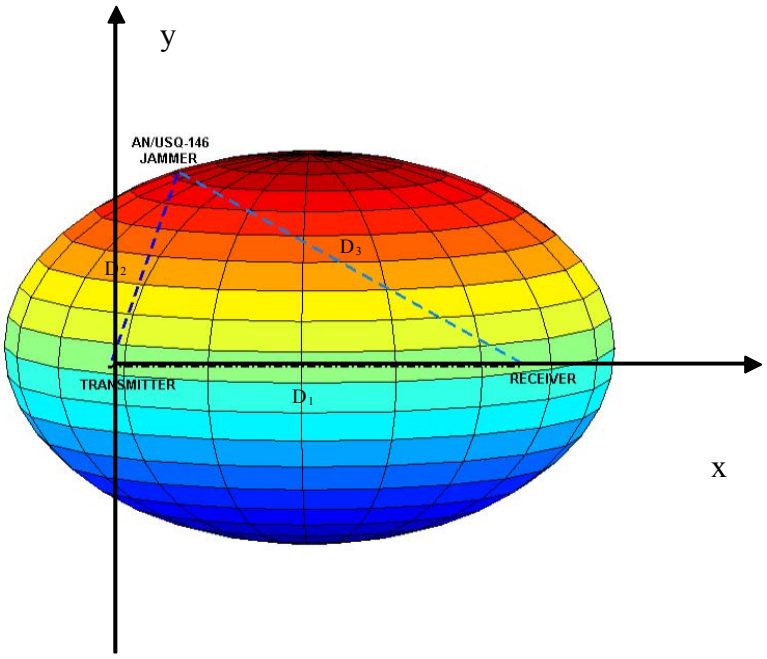

Figure 20. Geometrical Configuration of Communicators and the $AN/USQ-146$ Jammer

Considering that the transmitter, receiver, and jammer are in the same plane, the equation that gives the jammer location is

$$\frac{4\left(x-\frac{D_1}{2}\right)^2}{\left(D_1 + c\cdot\left(\eta T_d - T_{pr}\right)\right)^2} + \frac{4y^2}{\left(D_1 + c\cdot\left(\eta T_d - T_{pr}\right)\right)^2 - D_1^2} = 1 , \tag{5.3}$$

where the x and y axis are centered on the transmit antenna, as illustrated in Figure 20. Based on Reference $[4]$, the quantity $\left(\eta T_d - T_{pr}\right)$ can be considered equal to the hop duration T_h, so Equation (5.3) can be rewritten as

$$\frac{4\left(x-\frac{D_1}{2}\right)^2}{\left(D_1+c\cdot T_h\right)^2}+\frac{4y^2}{\left(D_1+c\cdot T_h\right)^2-D_1^2}=1. \tag{5.4}$$

Since the hop rate $\left(R_h\right)$ is equal to the inverse of the hop duration $\left(T_h\right)$, it is obvious that as the hop rate increases, the boundary distance that the $AN/USQ-146$ jammer can perform grows smaller. That is, the vehicle that the jammer is on must move closer to the area of interest. For example, by setting the distance between the transmitter and receiver $D_1 = 40$ km, the boundary ellipse in which the $AN/USQ-146$ jammer can operate in repeat mode varies. This is based on the value of the R_h of the system, as Figure 21 shows.

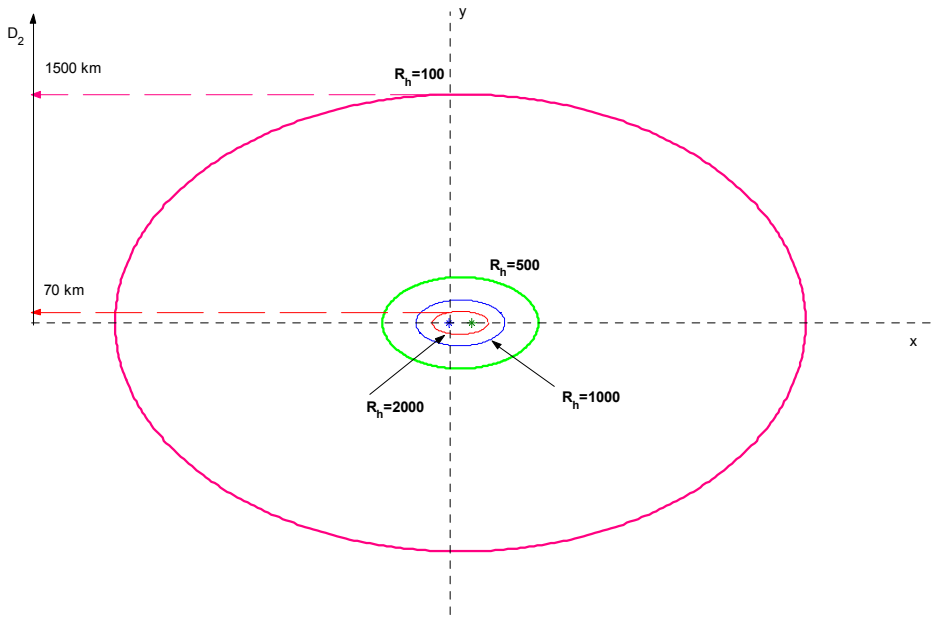

Figure 21. Boundary Ellipses for Operation of the $AN/USQ-146$ Jammer in Repeat Mode for Various R_h

Figure 21 clearly shows that the hop rate of the communication system is an important factor for the performance of the follower jammer. In the above example, if one considers that the jammer is on the *y* axis, then the distance D_2 between the jammer and transmitter in the case of $R_h = 2000$ hops/s is $D_2 = 70$ km. On the other hand, in the case for which $R_h = 100$ hops/s, $D_2 = 1500$ km.

Consequently, the first fundamental limitation of the $AN/USQ-146$ jammer is that its distance from the area of interest depends on the hop rate of the communication system. For the SINCGARS system, since its hop rate is $R_h = 100$ hops/s, the boundary limit of the $AN/USQ-146$ is an ellipse with a semi-major axis

$$a = 1.5\times 10^6 + \frac{D_1}{2}, \tag{5.5}$$

and semi-minor axis

$$b = \sqrt{1.5\times 10^6 D_1 + 2.25\times 10^{12}}\ . \tag{5.6}$$

As can be concluded from the value of D_2 for the SINCGARS case, the jammer has no practical boundary since the distance of 1500 km is far from any possible position of the jammer in a battlefield.

B. LIMITATIONS IN PROCESSING TIME OF THE AN/USQ-146 JAMMER IN REPEAT MODE OF OPERATION

Because of the repeater's processing time T_{pr} and the geometry, the jamming signal is not present in the victim's receiver during a certain portion of each frequency-hopping pulse. Based on Figure 21 and Reference [5], the duration of this portion is

$$T_{nj} = \min\left\{T_{pr} + \frac{D_2 + D_3 - D_1}{c},\ T_d\right\}. \tag{5.7}$$

Consider the repeater jamming of the FH/MFSK system for which a suitable performance measure is the average probability of an error in a channel symbol P_s. Let P_j denote the probability that a symbol is jammed given that the processing time and geome-

try are favorable for jamming the symbol. Among the reasons that P_j may be less than unity are

- The receiver of $AN/USQ-146$ jammer fails to monitor some of the frequency channels used by the communicators.
- The $AN/USQ-146$ jammer lacks the power to jam all the intercepted FH communications and so ignores some of the intercepted pulses.
- The interception receiver fails to detect some of the pulses.

If there are many symbols per pulse, then the fraction of the symbols that are geometrically susceptible to jamming is well approximated by $\left(T_d - T_{nj}\right)/T_d$. Among the susceptible symbols, the symbol error probability is

$$P_s = P_j F_j + \left(1 - P_j\right) F_{nj}, \tag{5.8}$$

where F_j is the conditional symbol error probability that a symbol is jammed, and F_{nj} is the conditional symbol error probability that a symbol is not jammed. Among the symbols that are not geometrically susceptible to jamming, which constitute the fraction T_{nj}/T_d of total symbols, the symbol error probability is F_{nj}. Thus, after regrouping the terms, the average symbol probability is given by

$$\overline{P_s} = \frac{T_d - T_{nj}}{T_d} P_j F_j + \frac{T_{nj}}{T_d} F_{nj}. \tag{5.9}$$

If the measured signal-to-jamming noise ratio in the passband of the victim's receiver were deterministic, then F_j would be a function of E_b/N_I . That is, $F_j \equiv F_j\left(E_b/N_I\right)$. However, the $AN/USQ-146$'s receiver must estimate the carrier frequency of each pulse and then transmit a jamming waveform with the same carrier frequency. If the estimate is inaccurate, less jamming power will be transmitted in the receiver passband. As Reference $[5]$ indicates, E_b/N_I is a random variable and

$$F_j = \int_0^{\left(\frac{E_b}{N_I}\right)_{\max}} F_j\left(\frac{E_b}{N_I}\right) f\left(\frac{E_b}{N_I}\right) d\left(\frac{E_b}{N_I}\right), \tag{5.10}$$

where $f(E_b/N_I)$ is the probability density of E_b/N_I, and $(E_b/N_I)_{\max}$ is the maximum value of E_b/N_I, which is realized when the frequency estimator is perfect and any other sources of random variation are negligible.

To disable the FH/MFSK system, $\overline{P_s} \geq P_{s_o}$ is necessary. Assuming that $F_j \geq P_{s_o} > F_{nj}$ since $\overline{P_s} > F_j$ cannot be achieved by any repeat jammer, and $\overline{P_s} = F_{nj}$ in the absence of $AN/USQ-146$. Therefore, $\overline{P_s} \geq P_{s_o}$ requires that $T_{nj} < T_d$. Equations (5.7) and (5.9) then imply that the processing time must satisfy

$$0 < T_{pr} \leq T_d - \frac{T_d(P_{s_o} - F_{nj})}{P_j(F_j - F_{nj})} - \frac{D_2 + D_3 - D_1}{c}. \tag{5.11}$$

This inequality provides a fundamental upper bound on the processing time for the repeat mode of the $AN/USQ-146$ jammer, which is to respond rapidly enough to disable a victim's receiver.

Chapter II revealed that the processing time of the $AN/USQ-146$ jammer is $500\ \mu s$. Since it is preferable for a jammer to use the largest amount of processing time available, the upper bound of Equation (5.11) is equal to $500\ \mu s$. Therefore

$$T_d\left(1 - \frac{P_{s_o} - F_{nj}}{P_j(F_j - F_{nj})}\right) = 5 \cdot 10^{-4} + \frac{D_2 + D_3 - D_1}{c}. \tag{5.12}$$

Based on Reference [5], the parenthesis on the left-hand side of the above equation is the fraction η. That is,

$$\eta = 1 - \frac{P_{s_o} - F_{nj}}{P_j(F_j - F_{nj})}, \tag{5.13}$$

so that

$$T_d \cdot \eta = 5 \cdot 10^{-4} + \frac{D_2 + D_3 - D_1}{c}. \tag{5.14}$$

Considering that the thermal noise in the victim's receiver is negligible $(F_{nj} = 0)$, and the probability that the symbol is jammed is $P_j = 1$, the above equation becomes

$$\eta = 1 - \frac{P_{s_o}}{F_j}. \tag{5.15}$$

Following the example in Section A, the numerical value of the right-hand side of (5.14) is

$$5\cdot 10^{-4}+\frac{D_2+D_3-D_1}{c}=5\cdot 10^{-4}+\frac{1500\text{ km}+1503.33\text{ km}-40\text{ km}}{3\cdot 10^5\text{ km}/s}=10.37\text{ ms.}$$

Thus, replacing the numerical result in (5.14) produces

$$T_d\cdot\eta=10.37\cdot 10^{-3}. \tag{5.16}$$

The result of (5.16) means that when the $AN/USQ-146$ jammer's purpose is to jam a SINCGARS system, with the specifications of the previous example and operates on the boundary ellipse, it can send the jamming signal in the right hop bin of the FH system, only when a specific fraction of the dwell time of the signal is equal to 10.37×10^{-3}. Based on (5.15), this specific fraction η depends on the lower probability of symbol error that the jammer must achieve in the system $\left(P_{s_o}\right)$ and the conditional symbol error probability given that the symbol is jammed $\left(F_j\right)$.

Combining Equation (5.15) and (5.16) and rearranging the terms results in

$$F_j=\frac{P_{s_o}}{1-\dfrac{10.37\cdot 10^{-3}}{T_d}}. \tag{5.17}$$

The conditional probability $\left(F_j\right)$ must always take values between 0 and 1. This implies

$$1-\frac{10.37\cdot 10^{-3}}{T_d}>0\,. \tag{5.18}$$

Solving (5.18) to obtain the dwell time of the signal, the inequality gives

$$T_d>10.37\text{ ms}\,. \tag{5.19}$$

The above result is very important for the effective operation of the $AN/USQ-146$ jammer in repeat mode because this result gives a second limitation of the jammer in the follower-on jamming. The jammer not only must work within the boundary ellipse, but the dwell time of the signal pulse must also be greater than a specific time. For the above example, this time is 10.37 ms.

In conclusion, obviously if the dwell time of the FH signal that the jammer is interested in does not satisfy the general inequality (5.11), then the $AN/USQ-146$ jammer cannot jam the signal at the proper time. Combining this fact with the result in Section A one can safely say that the effectiveness of the $AN/USQ-146$ jammer in the repeat mode depends on the hop rate and the dwell time of the targeted communication system. Both R_h and T_d are variable factors that the jammer cannot control. However, most of the standard FH communication systems have a specific value for the dwell time and restrictions in the maximum value of the hop rate. In the next section, the limitations on the hopping rate are analyzed in order to illustrate which factors influence the maximum value of R_h that a FH system can operate.

C. LIMITATIONS ON THE HOPPING RATE OF THE FH COMMUNICATION SYSTEM

One of the most common responses that a FH system makes to the threat of repeater jamming is to increase the hopping rate. However the following major problems arise as the hopping rate increases:

- The cost of the frequency synthesizer increases and its reliability decreases.
- Synchronization becomes more difficult.
- Limitations on the switching time become an obstacle.

The last problem, which usually poses the most fundamental limitation on the hopping rate, is analyzed in this section.

The various time durations associated with each pulse in a frequency hopping signal are illustrated in Figure 22 .

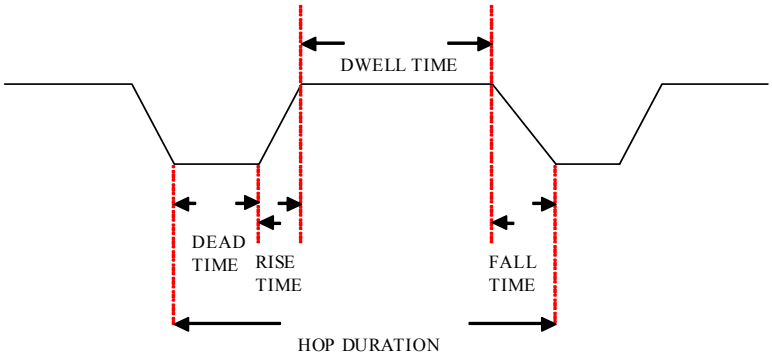

Figure 22. Time Duration Associated with a Pulse [After Ref. 5]

The hop duration is the duration of the time interval between changes in frequency, which is called the hop interval. The dead time is the duration of the part of the hop interval during which the frequency synthesizer produces no output. The switching time is the dead time plus the rise time and the fall time of the pulse. The non-zero switching time decreases the duration of the transmitted symbols, which in turn affects the transmitted spectrum.

The dwell time of a pulse is the duration of the dwell interval at which the pulse has its full amplitude and the channel symbols are transmitted. A buffer circuit is required to store code or data symbols during the switching time. The contents of the buffer are extracted and transmitted during the dwell time.

The switching time T_{sw}, plus the dwell time T_{dw}, is equal to the hop duration T_h. That is,

$$T_h = T_{dw} + T_{sw}. \tag{5.20}$$

The rise time (T_r), plus the fall time (T_f), plus the dead time (T_{de}), is equal to T_{sw}.

$$T_{sw} = T_r + T_f + T_{de}. \tag{5.21}$$

Let γ denote the required transmission rate of channel symbols. The number of symbols that must be transmitted during a hop interval is $\gamma \cdot T_h$, and if this number is constant from hop to hop, then

$$T_{dw} = \gamma T_h T_s , \tag{5.22}$$

where T_s denotes the duration of a channel symbol transmitted during the dwell time. Combining (5.20) through (5.22) results in

$$T_h(1 - \gamma T_s) = T_r + T_f + T_{de} . \tag{5.23}$$

This equation indicates that $\gamma \leq 1/T_s$, or $\gamma \leq R_s$, which is obvious from the definitions.

The switching time usually cannot be arbitrarily decreased for the following reasons:

- To limit the transmission of spurious frequencies when an indirect frequency synthesizer is used, it may be necessary to inhibit the transmitter output during frequency transitions.
- If a pulse rises too abruptly, ringing in the output of the receiver's intermediate-frequency (IF), filter may seriously degrade the first symbol of the dwell interval.
- Time may be needed for the IF filter to recover from one pulse before the next one is received.
- Spectral splatter, which is the spectral overlap in extraneous frequency channels produced by a time-limited transmitted pulse, increases as the rise and the fall time decreases.

The first symbol of the dwell interval may be seriously degraded by the phase discontinuities in the dehopped signal. A phase discontinuity may be caused by a Doppler shift, by frequency selective fading, by a non-zero dead time, or by imperfect synchronization in the receiver.

For combat net radios, the most serious limitation on the switching time is often due to the spectral splatter. The spectral splatter from one frequency-hopping signal can cause errors in the reception of another frequency-hopping signal even though the two signals have widely separated instantaneous carrier frequencies [5]. To reduce the amount of splatter into the nearby nets and to limit the other deleterious effects of a small switching time, it is necessary that neither T_r nor T_f be much less than T_s, which is itself

largely determined by the bandwidth of a single frequency channel and the need to limit the splatter. Thus, the following inequality is required

$$\min\left(T_r, T_f\right) > aT_s, \tag{5.24}$$

where a is a constant that typically satisfies $1 \le a \le 4$. The exact value of a is a function of the shape of the pulse edges.

Based on (5.24), Equation (5.23) becomes

$$\frac{1}{T_h} < \frac{\frac{1}{T_s} - \gamma}{2a + \frac{1}{T_s} T_{de}},$$

$$R_h < \frac{R_s - \gamma}{2a + R_s T_{de}}. \tag{5.25}$$

The above inequality must be satisfied if the spectral splatter and possibly the other problems arising from a short switching time are to be accommodated.

As an example of the application of (5.25), consider the SINCGARS system with $\gamma = 16$ kbits/s, which is the standard rate for combat net radios. Let $T_{de} = 0$, $R_s = 20$ kbits/s, and $a = 1$. Inequality (5.25) then yields $R_h < 2000$ hops/s. The fraction of the time that the symbols are transmitted is $\frac{T_{dw}}{T_h} = \gamma T_s = \frac{\gamma}{R_s} = 0.8$. If $a = 2$, then $R_h < 1000$ hops/s.

From these results, it appears that combat net radios cannot have hopping rates greater than 1 or 2 khops/s unless either serious spectral splatter is tolerated, or γ is lowered, or R_s is raised.

D. SUMMARY

To summarize the results of this chapter, it is obvious that the limitations of the $AN/USQ-146$ jammer in repeat mode are based on the geometry and the need for a frequency estimation of the instantaneous frequency of the FH signal. These two fundamental limitations are controlled by two basic characteristics of the FH system: (1) the

hopping rate of the signal, and (2) the dwell time of the pulse. The limitations in the range of R_h for each FH communication system and the characteristically small processing time of the $AN/USQ-146$ jammer are the elements that this specific device exploits in order to successfully operate as a follower jammer.

The primary purpose of any communication system is to neutralize the potential benefit of the repeat jammer. This benefit is the determination of the instantaneous frequency that the signal is transmitting. Most communication systems cope with this threat by increasing the hopping rate. The next chapter analyzes mathematically how the determinator of the $AN/USQ-146$ jammer works and estimates the probability of correctly determining the transmitting frequency. The result of the above estimation shows how the hopping rate influences the jammer's ability to find the correct transmitting frequency of the signal.

VI. PERFORMANCE OF THE AN/USQ-146 JAMMER'S DETERMINATOR IN REPEAT MODE-LINK BUDGET CONSIDERATIONS

This chapter studies the methods and the performance of the $AN/USQ-146$ jammer in determining which frequency range to jam. The jammer circuit for the frequency determination is not really a detector. Neither is it an estimator. It is most similar to a demodulator for M-ary NCFSK, but with some differences. This circuit is called a "determinator" and the next two sections describe and investigate its performance. In the third section of this chapter, the link budget considerations that arise from the conclusions of section two and the power limitations of the jammer are presented.

A. DESCRIPTION OF A DETERMINATOR

In repeat mode, the determinator of the $AN/USQ-146$ divides the received spread band, W_{ss}, into N_b segments, each of width

$$W = \frac{W_{ss}}{N_b}. \tag{6.1}$$

The jammer would like to determine which segment contains the frequency hop. In most repeat jammers, the classical energy detector is used for each segment which consists of a band-pass filter of width W, a square-law device and an integrator that integrated over a time T. Generally $T = T_h/2$, which meant that half a hop period was used just to determine the frequency. As a result, the geometrical restriction is extended so that the equivalent hop period that the communication system needs for anti-jam protection must entail replacing T_h to $T_h/2$.

The general problem for all jammers is how to determine the hop bin in a time that is considered small when compared to T_h. In contrast, the authorized receiver has the luxury of match filtering, which involves integration over the whole hop period. As discussed in [6] and based on the analysis in [4], for detectors, when $TW \approx 1$, which is the condition pertaining here, then the "integration" just takes a single sample. The analysis

cannot use the Gaussian approximations typically used in energy detectors, which usually have $TW \gg 1$. Since only a single sample is taken, the jammer will take it as soon as possible after the hop starts. For a realizable filter of width W, the output due to a pulse will rise to its maximum at a time of about $1/W_f$ after the leading edge of the input pulse. The determinator of the $AN/USQ-146$ jammer chooses to sample at about this period:

$$T_w = \frac{1}{W}. \tag{6.2}$$

The determinator circuit has a form such as that shown in Figure 23. It is assumed that the band-pass filters of width W_f are ideal brick-wall filters. The unclassified description of the $AN/USQ-146$ does not specify if the circuit of the determinator uses a square law or a true envelope detector. As pointed out in [6], both detectors have the same performance analysis. Therefore, since directly applicable analysis can be taken from the literature an assumption is made and a true envelope detector is selected.

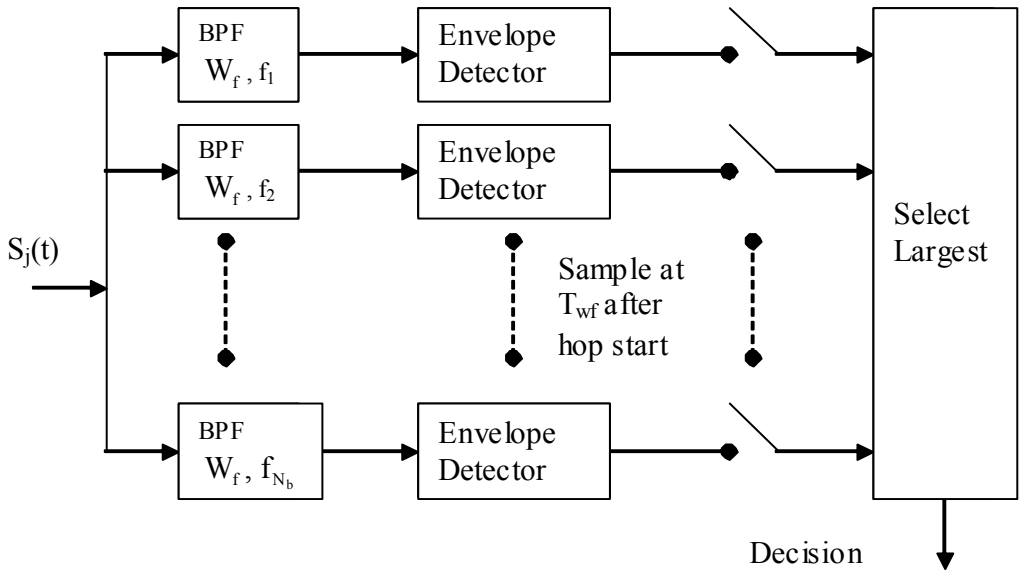

Figure 23. Block Diagram of the $AN/USQ-146$ Jammer's Frequency Bin Determinator Circuit

Based on the above figure, the next section analyzes the steps that the received signal follows in the $AN/USQ-146$ jammer. The primary purpose of this analysis is es-

timating the probability of correctly determining which of the N_b branches contains the hop.

B. PERFORMANCE ANALYSIS OF DETERMINATOR

The problem is similar to analyzing the demodulation of M -ary non-coherent FSK. The derivation in [7] will be followed. First the results of [7] are presented. Then these results are recast to fit the circuit of Figure 23.

Based on Equation (4.7), the received signal at the $AN/USQ-146$ jammer is

$$s_T(t) = \sqrt{2}A_h \cos\left\{2\pi\left[f_i + f_s + (m-1)\Delta_f\right]t + \theta_i\right\} + n(t), \tag{6.3}$$

where $i = 1, 2, ..., N_b$, and $0 \le t \le T_h$. The energy E_{hf} per symbol received at the jammer is

$$E_{hf} = A_h{}^2 T_h. \tag{6.4}$$

The combination of (6.3) and (6.4), results in

$$s_T(t) = \sqrt{2\frac{E_{hf}}{T_h}} \cos\left\{2\pi\left[f_i + f_s + (m-1)\Delta_f\right]t + \theta_i\right\} + n(t). \tag{6.5}$$

The demodulator discussed in [7] uses a bank of N_b matched filters and envelope detectors. The i^{th} branch is implemented by first performing I and Q down conversion by multiplying the signal by $\sqrt{2/T_h}\cos(2\pi f_i t)$ and $\sqrt{2/T_h}\sin(2\pi f_i t)$, respectively. The result is integrated over the interval T_h, and each of the I and Q integrator outputs are sampled at T_h, and the envelope is calculated. The largest is declared to be the bin in which the signal was sent. The probability of making a correct decision regarding which of the N_b branches actually contains the transmitted signal is given by [7]

$$P_c = \int_0^\infty \left(1 - e^{-\frac{r^2}{2}}\right)^{N_b - 1} \cdot r \cdot e^{-\frac{r^2 + 2\frac{E_h}{N_o}}{2}} \cdot I_0\left(r\sqrt{\frac{2E_h}{N_o}}\right) dr. \tag{6.6}$$

The steps in the above derivation for M -ary NCMFSK are now recast to fit the $AN/USQ-146$ jammer's determinator. First the values of the signal squared at the bin containing the signal and the noise variance at all bins, as seen at the sampler at the sam-

pling instant (T_h for the demodulator and T_w for the determinator), were found for both systems and are listed in Table 6. Then the corresponding output SNR for the determinator in Figure 23 is found to be $E_s/(2WT_hN_0)$, which is somewhat less than the SNR obtained in the corresponding demodulator.

	DEMODULATOR	**DETERMINATOR**
SIGNAL SQUARED	E_s	$\frac{E_s}{T_h}$
NOISE VARIANCE	$\frac{N_0}{2}$	$\frac{2N_0W}{T_h}$
OUTPUT SNR	$\frac{2E_s}{N_0}$	$\frac{E_s}{2WT_hN_0}$

Table 7. Signal-Noise-Ratio Components for the Demodulator and Determinator

The probability of correctly determining of which of the N_b branches contains the hop (P_{hc}) is then found by appropriate modification of (6.6) to get

$$P_{hc} = \int_0^\infty \left(1 - e^{-\frac{r^2}{2}}\right)^{N_b - 1} \cdot r \cdot e^{-\frac{r^2 + \frac{E_{hf}}{2WT_hN_o}}{2}} \cdot I_0\left(r\sqrt{\frac{E_{hf}}{2WT_hN_o}}\right) dr \,. \tag{6.7}$$

This probability depends upon the input SNR, W, T_h, and N_b. However, W and N_b are related by (6.1). It is useful to define a form of normalized SNR as

$$g = \frac{E_{hf}}{WT_hN_0}, \tag{6.8}$$

so that (6.7) becomes

$$P_{hc} = \int_0^\infty \left(1 - e^{-\frac{r^2}{2}}\right)^{N_b - 1} \cdot r \cdot e^{-\frac{r^2 + \frac{g}{2}}{2}} \cdot I_0\left(r\sqrt{\frac{g}{2}}\right) dr \,. \tag{6.9}$$

The values of P_{hc} were computed numerically as a function of g for the above three values of N_b. Figure 24 shows that the curves follow the "S" shape of the classical energy detectors with low values of $P_{hc} \approx 1/N_b$ for small g value, close to 1 for large g, and a fairly rapid transition region between these two extremes. The relative effects of increasing g and N_b are seen. The improvement in detectability by increasing g is offset slightly by the upward shift of the curves in Figure 24 as N_b increases. As an example, for an increase of N_b from 100 to 1000 (10 dB increase), the curves at $P_{hc} = 0.5$ shift to the right by almost 2 dB. Since an increase of N_b by 10 dB also corresponds to an increase of g by 10 dB, the overall advantage to the determinator is almost 8 dB.

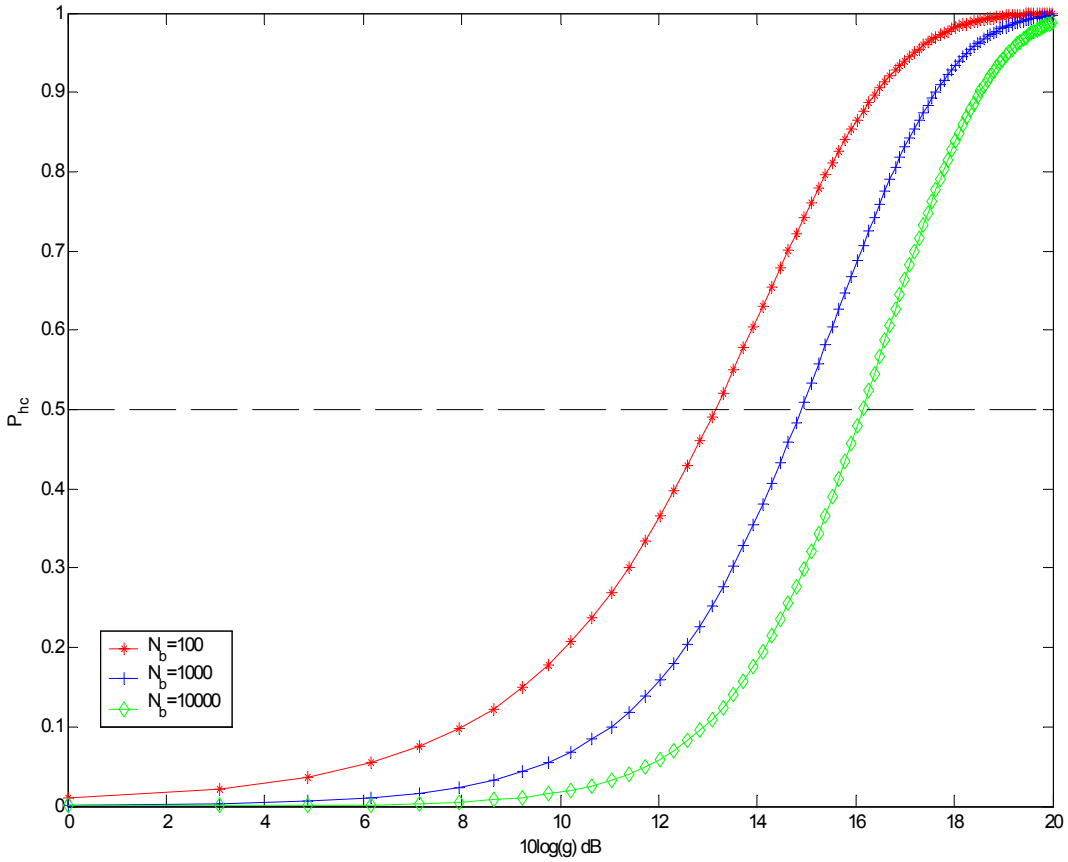

Figure 24. P_{hc} as a Function of g for Three Values of N_b

For effective follower jamming, a high value of P_{hc} is needed. Since the transition region from very poor to very good determinability is relatively small, the middle of the transition is taken as a point of acceptable determination performance. At this point, the determinator has obtained a P_{hc} of 0.5. In order to find the middle of the transition, a numerical analysis was performed on (6.9) to find the pairs of values of N_b and g that result in $P_{hc} = 0.5$. The results are plotted in Figure 25 with linear g against N_b. The range of values of N_b were from 10 to 10^4 with the idea that 10 presents the lowest amount of jamming gain that would be worthwhile while 10^4 represent an upper practical range. Figure 25 also shows that the calculated values approximately follow a straight line for which an empirical relation was determined to be

$$g = 9.61 \cdot \log(N_b) - 0.99. \tag{6.10}$$

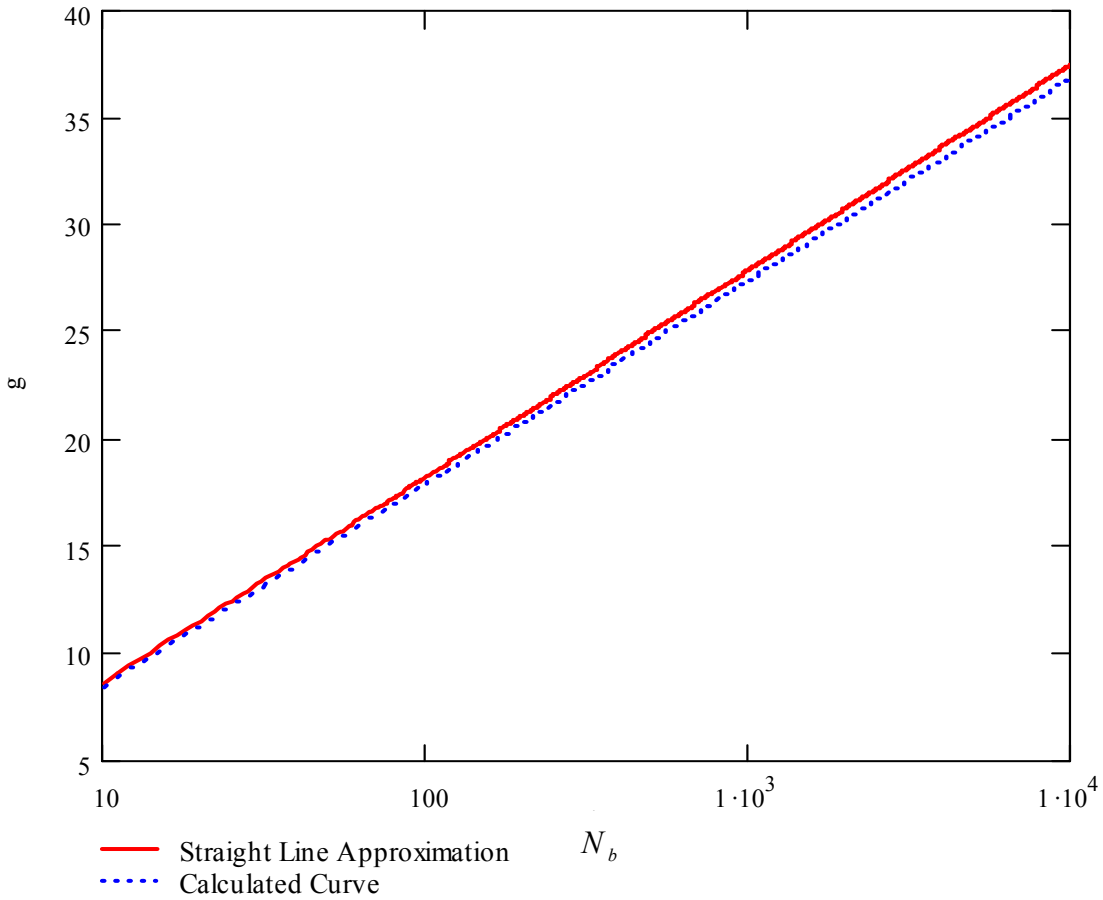

Figure 25. Numerically Computed Value of g and Straight Line Approximation for $P_{hc} = 0.5$ as a Function of N_b

By equating (6.8) to (6.10), the SNR for $P_{hc} = 0.5$ is found as

$$\left.\frac{E_{hf}}{N_0}\right|_{P_{hc}=0.5} = WT_h\left[9.61\cdot\log(N_b) - 0.99\right]. \tag{6.11}$$

In a slow frequency-hopping system E_{hf} must be replaced by $E_{sf}\cdot K$ where E_{sf} is the energy per symbol received by the jammer and K is the number of data symbols per hop. From (4.5)

$$K = \frac{R_s}{R_h}. \tag{6.12}$$

This SNR can be made a function of N_b only by using (6.1) so that

$$WT_h = \frac{W_{ss}}{N_b R_h}. \tag{6.13}$$

Equation (6.11), based on (6.12) and (6.13), is rewritten as

$$\left.\frac{E_{sf}}{N_0}\right|_{P_{hc}=0.5} = \frac{W_{ss}}{N_b R_s}\left[9.61\cdot\log(N_b) - 0.99\right], \tag{6.14}$$

or

$$\left.\frac{E_{bf}}{N_0}\right|_{P_{hc}=0.5} = \frac{W_{ss}\log_2(M)}{N_b R_b}\left[9.61\cdot\log(N_b) - 0.99\right]. \tag{6.15}$$

Referring to the SINCGARS system, the $W_{ss} = 58$ MHz and $R_h = 100$ hops/s. The value of $E_{sf}/N_0\big|_{P_{hc}=0.5}$ was calculated and then plotted in Figure 26 as a function of N_b for a number of values of M.

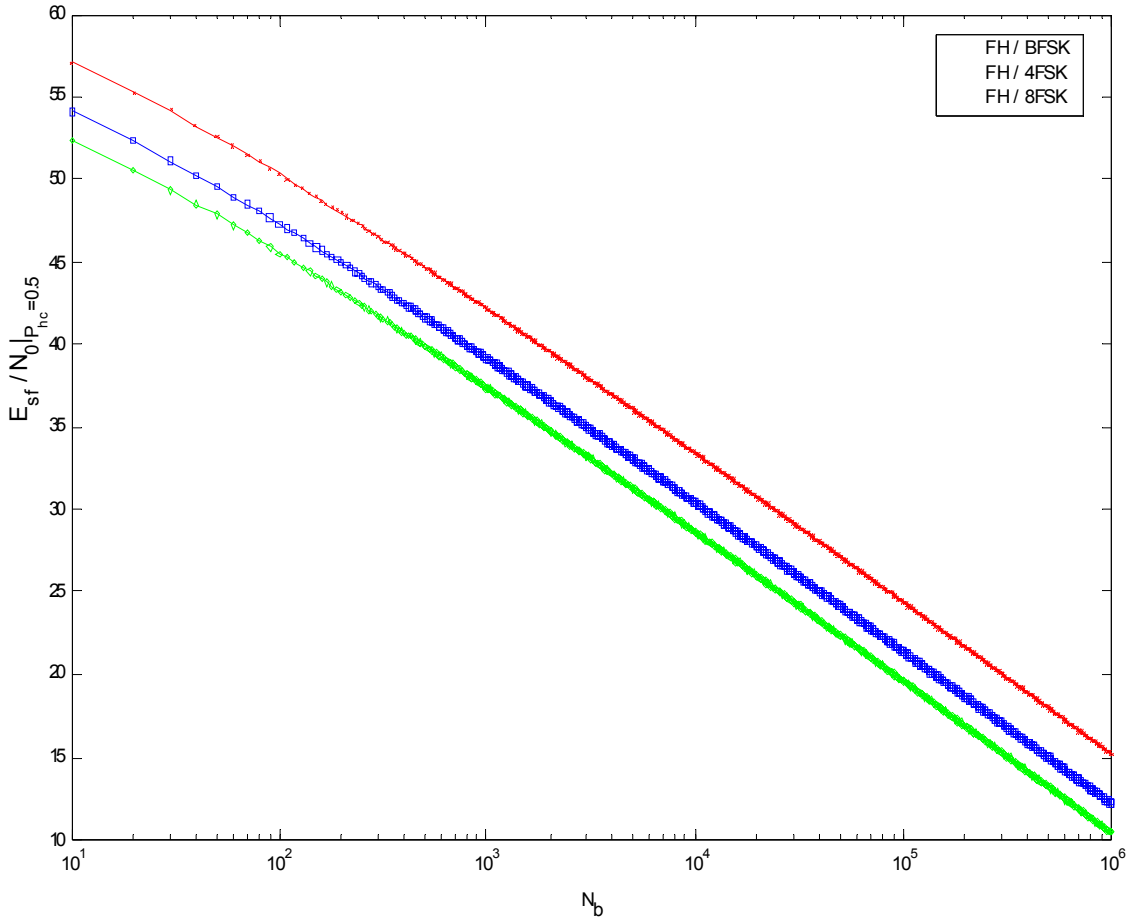

Figure 26. $E_{sf}/N_0\big|_{P_{hc}=0.5}$ as a Function of N_b for the SINCGARS Communication System

As expected intuitively, the jammer's required SNR increases as M is increased. However the required SNR decreases as N_b is increased, so the jammer will try to increase N_b as much as it can in order to achieve $P_{hc} = 0.5$ with less SNR. The jammer's choice of N_b involves a number of tradeoffs between jamming efficiency, determinator performance, and complexity.

Once the determinator has decided in which segment of width W the hop is located, all the available jamming power is concentrated into a jamming band, W_j, centered on this determined band. However, the determinator only knows that $K \cdot M$-ary tones exist somewhere in the width W. The determinator does not know which M frequencies the user is using. The jammer wants to jam the entire channel width W with optimum

jamming efficiency $W/(K/2)$. Therefore the maximum number of bins that the jammer needs to determine for the most efficient jamming is

$$N_{b|\max} = \frac{W_{ss}K}{2W} = \frac{NK}{2}. \tag{6.16}$$

For the case of SINCGARS $N = 2320$ and $K = \frac{R_S}{R_h} = k\frac{R_b}{R_h} = k\frac{16000}{100} = 160k,$ so (6.16) becomes

$$N_{b|\max} = 185600k. \tag{6.17}$$

The $AN/USQ-146$ jammer with the help of the variable filter bandwidths can create the above number of segments for $k = 1,2,3.$ For the above values of $N_{b|\max},$ the required $E_{sf}/N_0\big|_{P_{hc=0.5}}$ that the determinator needs to receive is shown in Figure 27.

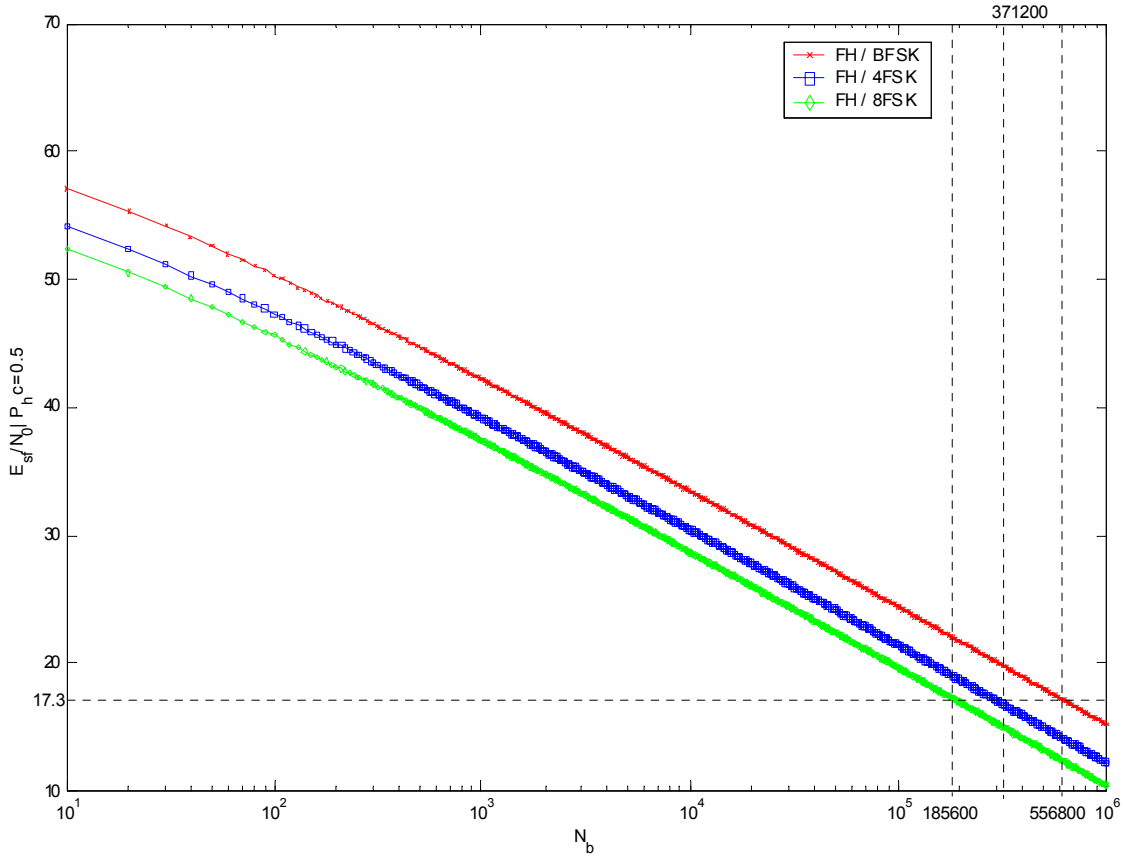

Figure 27. Required $E_{sf}/N_0\big|_{P_{hc=0.5}}$ for SINCGARS Case for Each FH/MFSK System

The figure shows that when the jammer changes the number of segments for the different orders of modulation for the constant $E_{sf}/N_0\big|_{P_{hc}=0.5}$. For the case of SINCGARS communication system $E_{sf}/N_0\big|_{P_{hc}=0.5} = 0.4$ dB.

The next section analyzes the link budget considerations that arise from the above conclusions and some numerical results are presented for the SINCGARS case.

C. LINK BUDGET CONSIDERATIONS

1. Transmitter/Jammer

It was seen that P_{hc} is dependent upon the SNR received by the determinator, which in turn is dependent upon the transmitted power P_t, the distance D_2, the transmitter's gain G_{tj} in the direction of the jammer, the bit rate R_b, and the receive sensitivity of the jammer R_{sen}.

The levels of E_{sf}/N_0 that would be affected by the various distances and gains can be obtained with a few simplifying assumptions. The transmitter usually transmits with the same gain in all directions on the battlefield. That is, the transmitter's pattern is omni directional ($G_{tj} = 1$). It is assumed that there is no multipath fading in the channel and the free space channel losses are given by the formula

$$L_c = \left(\frac{4\pi D_2 f}{c}\right)^2. \tag{6.18}$$

The SNR at the $AN/USQ-146$ jammer is given by

$$\frac{E_{sf}}{N_0} = \frac{\log_2(M)\cdot EIRP_t \cdot R_{sen}\cdot T_s}{L_c k R_b}, \tag{6.19}$$

where $EIRP_t$ is the effective radiated power of the transmitter, T_s is the system equivalent noise temperature, and *k* is the Boltzmann constant. The $EIRP_t$ is the product of the transmitted power with the gain of the transmitted antenna.

$$EIRP_t = P_t G_t. \tag{6.20}$$

The system equivalent noise temperature is

$$T_s = T_A + T_e, \tag{6.21}$$

where T_A is the effective noise temperature of the jammer's receive antenna and T_e is the equivalent noise temperature. For terrestrial communication $T_A = 290\ ^{\circ}\text{K}$ and

$$T_e = T_0(F-1), \tag{6.22}$$

where $T_0 = 290\ ^{\circ}\text{K},$ and F is the noise figure of the jammer. The $AN/USQ-146$ jammer has $F = 18$ dB. Replacing the above values in (6.22) gives $T_e = 18007.8\ ^{\circ}\text{K}$ and therefore $T_s = 18297.8\ ^{\circ}\text{K}$.

Rearranging the terms in (6.19), the SNR received by the determinator is

$$\frac{E_{sf}}{N_0} = \frac{\log_2(M) P_t G_t R_{sen} T_s}{\left(\frac{4\pi D_2 f}{c}\right)^2 k R_b}. \tag{6.23}$$

Equation (6.23) shows that the distance strongly influences the signal loss. For example, if the distance between the jammer and the receiver is doubled, the jammer must quadruple its output for the jamming to be effective.

The above observation forces the follower jammer to check if the distance D_2, which is determined by the boundary ellipse, influences the signal strength dramatically. If this is the case, the determinator and jamming transmitter is co-located in a smaller distance (D_2). For example, as noted in Figure 27, in order for the $AN/USQ-146$ jammer to be able to determine the hop frequency of a SINCGARS, the system needs at least $E_{sf}/N_0\big|_{P_{hc}=0.5} = 0.4$ dB.

From [8] the $EIRP_t$ of the SINCGARS transmitter is 0 dBW. The bit rate is 16000 bits/s. The transmitted frequencies f are in the range of 30-MHz to 88-MHz. From [1] the receive sensitivity of the $AN/USQ-146$ jammer is -95 dBm.

Keeping the distance D_2 as a variable, Figure 28 illustrates the relationship between E_{sf}/N_0 and distance D_2 for the maximum and minimum value of the frequency that a SINCGARS system can hop.

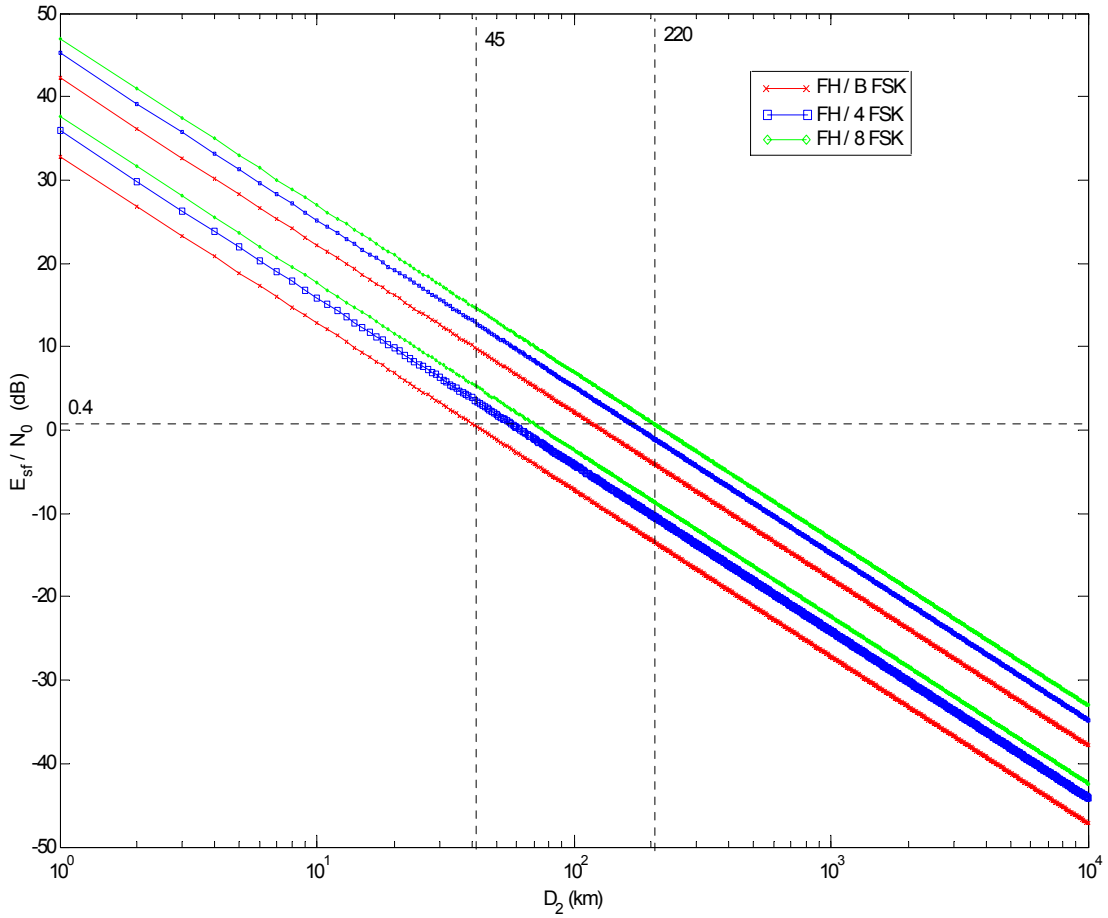

Figure 28. Received SNR by the Determinator in SINCGARS Case for Various D_2

The plot of E_{sf}/N_0 in Figure 28 states that the worst case is for FH/BFSK. In this case, when the hop frequency is achieving its maximum value, the determinator must be at a distance smaller than 45 km. This distance certifies that the determinator of the $AN/USQ-146$ jammer will receive any type of FH/MFSK system with a $E_{sf}/N_0 \geq 0.4$ dB, which is the value of the SNR that the determinator must receive in order to give a $P_{hc} = 0.5$.

In all the above, the determinator and the jammer transmitter is co-located in a boundary cycle with radius $D_2 = 45$ km. Comparing this to the value of $D_2 = 1500$ km, which was derived from Chapter V, one can conclude that in order to determine with great probability the right hop frequency the follower jammer must approach the transmitter at a distance 33 times smaller than the required distance, which was based on the value of the system's hop rate.

To clarify the influence that the above result has in the distance of the jammer from the area of interest, Figure 29 shows the previous and the new boundary surface of the jammer for $R_h = 100$ hops/s. The comparison in the figure indicates that the specifications of the determinator are the primary factors for the operational distance of the jammer in the case of the SINCGARS system.

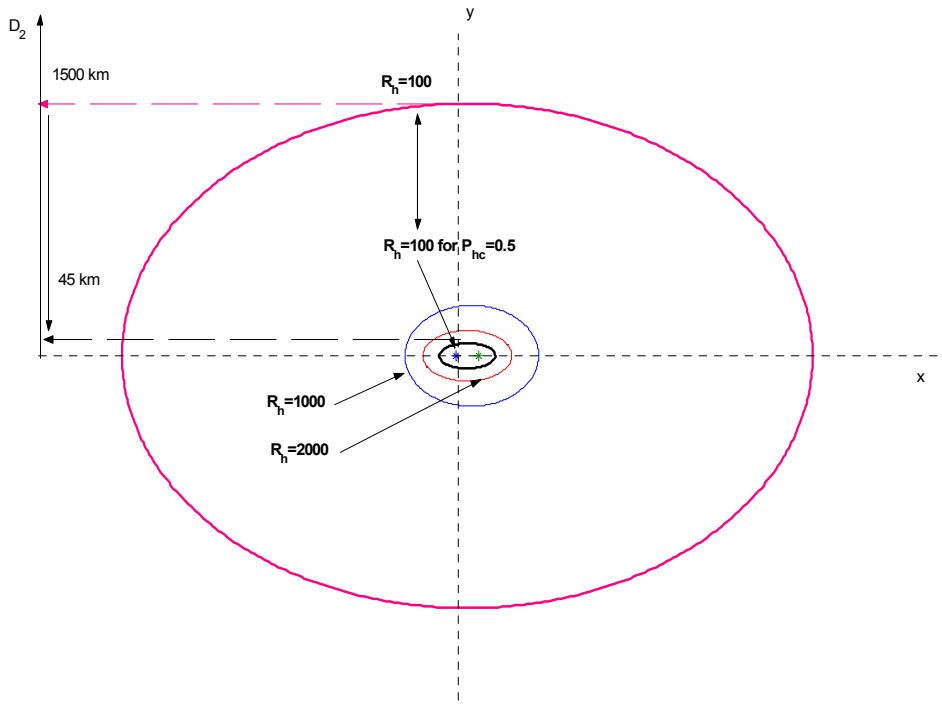

Figure 29. Comparison of Boundary Surface of the $AN/USQ-146$ Jammer for $R_h = 100$ hops/s Before and After the Determinator's Specifications

The above result is not valid for all types of FH systems. Due to the fact that Equations (6.15) and (6.23) do not depend on R_h but on the R_b, W_{ss}, and P_t of the communication system, for a FH system with $R_h \gg 2000$ hops/s, the specifications of the determinator may not change its boundary surface. For example, if a FH system has $R_h = 10000$ hops/s and all other characteristics are the same as the SINCGARS system, then the boundary surface of the jammer will not be influenced.

2. Jammer/Receiver

Up to this point only the restrictions of the distance D_2 have been examined. For the distance D_3, that is, the maximum effective jammer distance from the receiver, the upper limit must also be evaluated. For the $AN/USQ-146$ jammer, the value of the signal-to-noise ratio at the receiver input required to assure a specific bit error rate is given by

$$\left(\frac{P_I}{P_c}\right)_{\text{req(dB)}} \leq PG_{\text{rec(dB)}} - \left(\frac{E_b}{N_0}\right)_{\text{req(dB)}}, \tag{6.24}$$

where P_I is the total jammer power in W_{ss}, P_c is the average signal power in the W, E_b/N_0 corresponds to the specific BER for the modulation scheme, and $PG_{\text{rec(dB)}}$ is the receiver's processing gain. The worst case situation is when the inequality becomes an equality.

For the SINCGARS receiver, the processing gain is

$$PG_{\text{rec(dB)}} = 10\log\left(\frac{W_{ss}}{W}\right) = 10\log(N) = 33.7 \text{ dB}. \tag{6.25}$$

Assuming that the jammer wants to achieve four specific probabilities of bit error, for example 10^{-3}, 10^{-2}, 10^{-1} and 0.5, then based on Equation (4.11) the corresponding values of $(E_b/N_0)_{\text{req(dB)}}$ can be seen in Table 8.

P_b	$(E_b/N_0)_{\text{req(dB)}}$		
	$M=2$	$M=4$	$M=8$
10^{-3}	11	8.5	7.2
10^{-2}	9.22	7.21	6.21
10^{-1}	6.1	4.54	3.91
0.5	0	0	0

Table 8. Required Signal-to-Noise ratio Depending on the Desired P_b

For each case of P_b, taking the worst case for the jammer, which is when $M=8$, Equation (6.24) gives the results in Table 9.

P_b	10^{-3}	10^{-2}	10^{-1}	0.5
$(P_I/P_c)_{\text{req(dB)}}$	26.5	27.49	29.79	33.7

Table 9. Corresponding Values of $(P_I/P_c)_{\text{req(dB)}}$

From the basic theory of link budget analysis, the fraction (P_I/P_c) can be written as

$$\left(\frac{P_I}{P_c}\right)_{\text{req(dB)}} = \left(\frac{EIRP_j}{L_{cj}}\right)\left(\frac{EIRP_t}{L_{ct}}\right)^{-1}, \tag{6.26}$$

where L_{cj}, L_{ct} are the free space losses. The receiver antenna gains and miscellaneous losses (atmosphere, rain, pointing error) are assumed the same for both links and therefore cancel each other. Rearranging

$$\left(\frac{L_{cj}}{L_{ct}}\right) = \left(\frac{EIRP_j}{EIRP_t}\right)\left(\frac{P_I}{P_c}\right)^{-1}_{\text{req(dB)}}. \tag{6.27}$$

As noted in Chapter II, the $EIRP_j$ of the $AN/USQ-146$ jammer for the case of a system like SINCGARS is 30 dBW. From [8] the $EIRP_t$ of the SINCGARS transmitter is 0 dBW. So from (6.27) and the results on Table 9

$$\left(\frac{L_{cj}}{L_{ct}}\right)=\begin{cases}\left(\frac{10^3}{1}\right)\left(10^{2.65}\right)^{-1}=2.23 & \text{for } P_b=10^{-3}\\ \left(\frac{10^3}{1}\right)\left(10^{2.749}\right)^{-1}=1.78 & \text{for } P_b=10^{-2}\\ \left(\frac{10^3}{1}\right)\left(10^{2.979}\right)^{-1}=1.05 & \text{for } P_b=10^{-1}\\ \left(\frac{10^3}{1}\right)\left(10^{3.37}\right)^{-1}=0.43 & \text{for } P_b=0.5.\end{cases} \tag{6.28}$$

Based on Equation (6.18),

$$\left(\frac{D_3}{D_1}\right)=\sqrt{\left(\frac{L_{cj}}{L_{ct}}\right)}=\begin{cases}1.5 & \text{for } P_b=10^{-3}\\ 1.3 & \text{for } P_b=10^{-2}\\ 1.02 & \text{for } P_b=10^{-1}\\ 0.66 & \text{for } P_b=0.5.\end{cases} \tag{6.29}$$

The maximum distance at which the transmitter and the receiver of the SINCGARS system can establish reliable communication is $D_1=40$ km. In this case the maximum distance of the jammer from the receiver becomes

$$D_3=\begin{cases}60 \text{ km} & \text{for } P_b=10^{-3}\\ 52 \text{ km} & \text{for } P_b=10^{-2}\\ 40.8 \text{ km} & \text{for } P_b=10^{-1}\\ 26.4 \text{ km} & \text{for } P_b=0.5.\end{cases} \tag{6.30}$$

The above results specify the distances that the $AN/USQ-146$ jammer must have from the receiver in order to perform a probability of bit error close to 10^{-3}, 10^{-2}, 10^{-1} and 0.5 respectfully in any FH/MFSK system with $M=2,4$ or 8. The results of (6.30) indicate that for the case of $P_b=0.5$ the jammer approaches the receiver at a distance (D_3) closer than the distance between the transmitter and the receiver (D_2). However, this distance is considered to be secure enough for the jammer.

At this point both the maximum distance of the jammer from the transmitter and the maximum distance of the jammer from the receiver have been evaluated. In order to find the optimum position of the jammer two circles with a radius D_2 and D_3 respectively must be drawn. The first circle will have as a center the position of the transmitter and the second circle the position of the receiver. The intersection of the two circles is the area in which the jammer can operate with a probability of a correct determination that equals to 0.5 and a BER equal to 10^{-3}, 10^{-2}, 10^{-1} or 0.5.

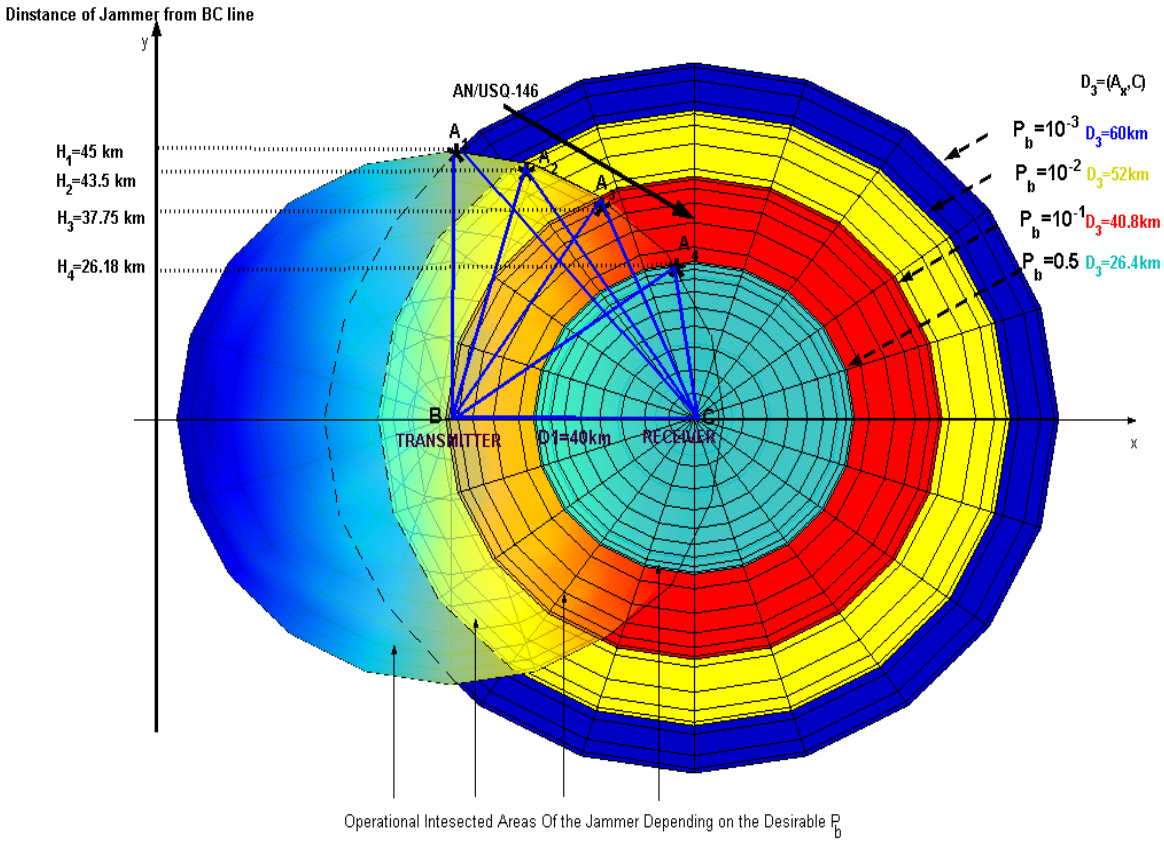

Figure 30. Optimum Position of $AN/USQ-146$ Jammer in a SINCGARS System

As Figure 30 indicates, the best position of the jammer in each of the four intersected operational areas is the positions, A_1, A_2, A_3 and A_4 respectfully. In these positions the jammer is at the furthest point from both the transmitter and the receiver. The y coordinates of the A_1, A_2, A_3 and A_4 points give the optimum height that the jammer can operate. Observing the values of H_1, H_2, H_3 and H_4 in the Figure 30 it becomes obvious

that in order for the jammer to achieve higher values of P_b it must approach the hostile communication system at a shorter distance. For the above example the jammer, in order to increase the probability of bit error from 10^{-3} to $0.5,$ must lower the height from $H_1 = 45$ km to $H_1 = 26.18$ km.

The jammer along with the transmitter and the receiver create a triangle with sides the distances D_1, D_2 and $D_3.$ Considering that the distance between the transmitter and the receiver is a variable, the other two sides of the triangle can be determined from the jammer based on the previous link budget analysis.

D. SUMMARY

Reviewing the main points of this chapter, it is important to emphasize the influence of the determinator on the performance of the $AN/USQ-146$ jammer in reactive jamming. From the above analysis, it was shown that the determinator of the $AN/USQ-146$ jammer can determine which segment contains the frequency hop of a FH system with $P_{hc} = 0.5.$ The restriction that the jammer has in order to achieve such a performance is that it must be at a proper distance from the transmitter. This restriction does not depend on the hopping rate of the system but on the bit rate, the received spread band, and the transmitted power of the system.

The next important factor is the output power of the jammer, which determines the distance of the jammer from the receiver. The output power of the $AN/USQ-146$ jammer varies based on the operational bandwidth and can be considered as sufficient enough on the modern battlefield.

Before starting to operate as a follower jammer the $AN/USQ-146$ jammer must estimate three distances: its boundary ellipse, the proper distance that the determinator requires, and its distance from the receiver. The first distance depends on the R_h, the second distance on the W_{ss}, R_b, and P_t of the FH system, and the third distance on the output power of the jammer and the BER that it wants to invoke in the system. Designating the shortest distance between the first two distances as distance $D_2,$ and the third as dis-

tance D_3, the jammer is confident about operating successfully as a follower jammer. The distance D_3 is influenced by the desired BER. Specifically for the case of the SINCGARS system, in order for the jammer to achieve $P_b = 0.5$ it must approach the receiver of the communication scheme in a distance shorter than the distance between the transmitter and the receiver.

The next chapter discusses the performance of the jammer in FH/MFSK systems using various types of jamming in reactive jamming mode. It is assumed that the jammer has taken into account all the above limitations and operates inside the proper geometrical zone.

THIS PAGE INTENTIONALLY LEFT BLANK

VII. PERFORMANCE OF THE AN/USQ-146 JAMMER IN VARIOUS METHODS OF REACTIVE JAMMING

This chapter investigates the performance of the $AN/USQ-146$ jammer in the repeat mode jamming. It is assumed that the jammer has considered all the limitations that were presented in the previous two chapters and operates inside the geometrical zone, which ensures the determinator's performance with a probability of a correct determination of $P_{hc} = 0.5$.

The three most important strategies that the $AN/USQ-146$ jammer uses when it operates as follower jammer are the *noise repeat jamming,* the *partial-band Gaussian noise repeat jamming,* and the *follower tone jamming*. The following sections analyze the performance of each of the three strategies, in an uncoded slow FH/MFSK system, and the results are compared with the results presented in Chapter IV in which the $AN/USQ-146$ was operating with the same strategies in the manual spot mode.

A. PERFORMANCE OF THE AN/USQ-146 JAMMER USING NOISE REPEAT JAMMING IN A FH/MFSK SYSTEM

Because of the differential geometrical delay, $\Delta T = \left(D_2 + D_3 - D_1\right)/c$ and the sampling delay T_w, the $AN/USQ-146$ jammer will jam only the final section, $T_h - \left(\Delta T + T_w\right)$ of the hop, provided $T_h - \left(\Delta T + T_w\right) > 0$.

Let the average total jamming power be P_I. This jamming power is transmitted for time T_h, and is spread over the jamming band W_j. Furthermore, the receiver integrates over T_h so that the effective jamming power, on those hops correctly determined, is reduced by the factor $\left[T_h - \left(\Delta T + T_w\right)\right]/T_h$. Thus the effective jamming noise power density as seen at the receiver is

$$J_{oe} = \frac{P_I}{W_j} \cdot \frac{T_h - \left(\Delta T + T_w\right)}{T_h}. \tag{7.1}$$

The signal-to-jammer ratio (SJR) at the legitimate receiver on the jammed hops is then

$$SJR_r = \frac{E_{st}}{J_{oe}}. \tag{7.2}$$

Also, $SNR_r = E_{st}/N_{or}$. Let the probability of symbol error as a function of SNR and SJR be P_s, which is given by (4.8). Then the total error probability is

$$P_{stot} = P_{hc} \cdot P_s\left(\frac{E_{st}}{J_{oe} + N_{or}}\right) + \left(1 - P_{hc}\right) \cdot P_s\left(\frac{E_{st}}{N_{or}}\right). \tag{7.3}$$

Combining (4.8) and (7.3) results in

$$\begin{aligned} P_{stot} = P_{hc} \cdot & \left(\sum_{n=1}^{M-1} \binom{M-1}{n} (-1)^{n+1} \frac{1}{n+1} e^{-\frac{n\log(M)}{n+1}\frac{E_{bt}}{J_{oe}+N_{or}}} \right) \\ & + \left(1 - P_{hc}\right) \cdot \left(\sum_{n=1}^{M-1} \binom{M-1}{n} (-1)^{n+1} \frac{1}{n+1} e^{-\frac{n\log(M)}{n+1}\frac{E_{bt}}{N_{or}}} \right). \end{aligned} \tag{7.4}$$

Considering that the jammer fulfills all the requirements for repeat jamming and following the same assumptions for the SNR of the channel as in the previous analysis, Equation (7.4) becomes

$$\begin{aligned} P_{stot} = P_{hc} \cdot & \left(\sum_{n=1}^{M-1} \binom{M-1}{n} (-1)^{n+1} \frac{1}{n+1} e^{-\frac{n\log(M)}{n+1}\frac{1}{\left(\frac{E_{bt}}{J_{oe}}\right)^{-1} + \left(10^{1.335}\right)^{-1}}} \right) \\ & + \left(1 - P_{hc}\right) \cdot \left(\sum_{n=1}^{M-1} \binom{M-1}{n} (-1)^{n+1} \frac{1}{n+1} e^{-\frac{n\log(M)}{n+1}\frac{1}{\left(10^{1.335}\right)^{-1}}} \right). \end{aligned} \tag{7.5}$$

The total probability of bit error is

$$P_{btot} = \frac{M}{2(M-1)}\left[P_{hc} \cdot \left(\sum_{n=1}^{M-1} \binom{M-1}{n} (-1)^{n+1} \frac{1}{n+1} e^{-\frac{n\log(M)}{n+1}\frac{1}{\left(\frac{E_{bt}}{J_{oe}}\right)^{-1}+\left(10^{1.335}\right)^{-1}}} \right) + \left(1-P_{hc}\right) \cdot \left(\sum_{n=1}^{M-1} \binom{M-1}{n} (-1)^{n+1} \frac{1}{n+1} e^{-\frac{n\log(M)}{n+1}\frac{1}{\left(10^{1.335}\right)^{-1}}} \right) \right]. \tag{7.6}$$

Based on the conclusions in Chapter VI, in order for the $AN/USQ-146$ to be able to jam a SINCGARS system with $P_{hc}=0.5,$ the received signal-to-noise ratio on the jammer's receiver must be equal to $E_{sf}/N_0\big|_{P_{hc}=0.5}=0.4$ dB.

Assuming that the jammer's distance from the transmitter (D_2) permits a value of $E_{sf}/N_0\big|_{P_{hc}=0.5}=0.4\,\text{dB},$ the (7.6) becomes

$$P_{btot} = \frac{M}{4(M-1)} \cdot \left[\sum_{n=1}^{M-1} \binom{M-1}{n} (-1)^{n+1} \frac{1}{n+1} e^{-\frac{n\log(M)}{n+1}\frac{1}{\left(\frac{E_{bt}}{J_{oe}}\right)^{-1}+\left(10^{1.335}\right)^{-1}}} + \sum_{n=1}^{M-1} \binom{M-1}{n} (-1)^{n+1} \frac{1}{n+1} e^{-\frac{n\log(M)}{n+1}\frac{1}{\left(10^{1.335}\right)^{-1}}} \right]. \tag{7.7}$$

The above equation has as a variable the signal-to-jamming ratio at the receiver of the communication system and estimates the probability of bit error that the $AN/USQ-146$ jammer causes in the SINCGARS system when it is operating in noise follower jamming technique.

The plot of Equation (7.7) for the cases of $M=2,4,8$ for the SINCGARS system is shown in Figure 31.

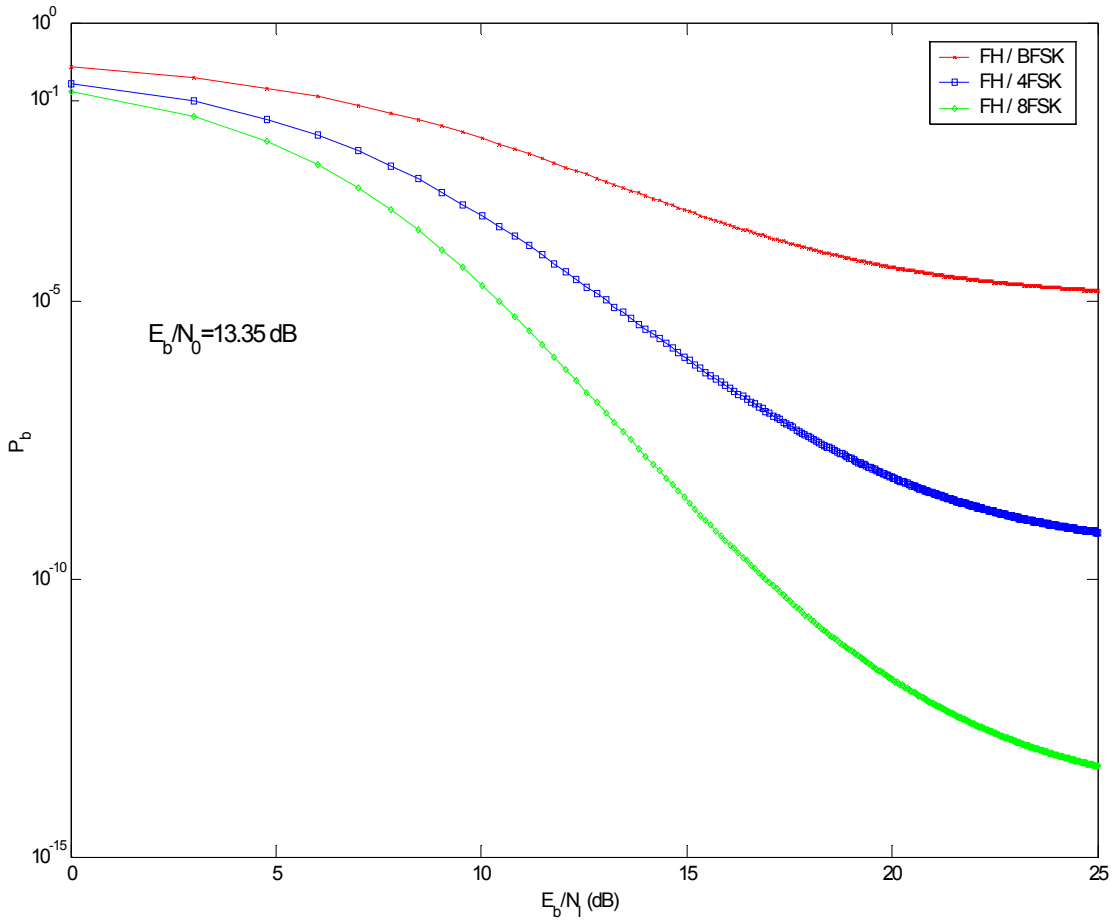

Figure 31. Effect of the $AN/USQ-146$ in Follower Noise Jamming on the Performance of a SINCGARS System in AWGN

Figure 31 indicates that the $AN/USQ-146$ jammer is very effective when it operates in noise repeat mode. As the modulation order (M) of the communication system increases, the performance of the jammer decreases, especially for large values of SJR.

This particular technique is the simplest follower jamming strategy that the $AN/USQ-146$ jammer can select to operate. In manual spot mode the corresponding technique is the barrage noise jamming. A comparison of these two cases can be seen in Figure 32.

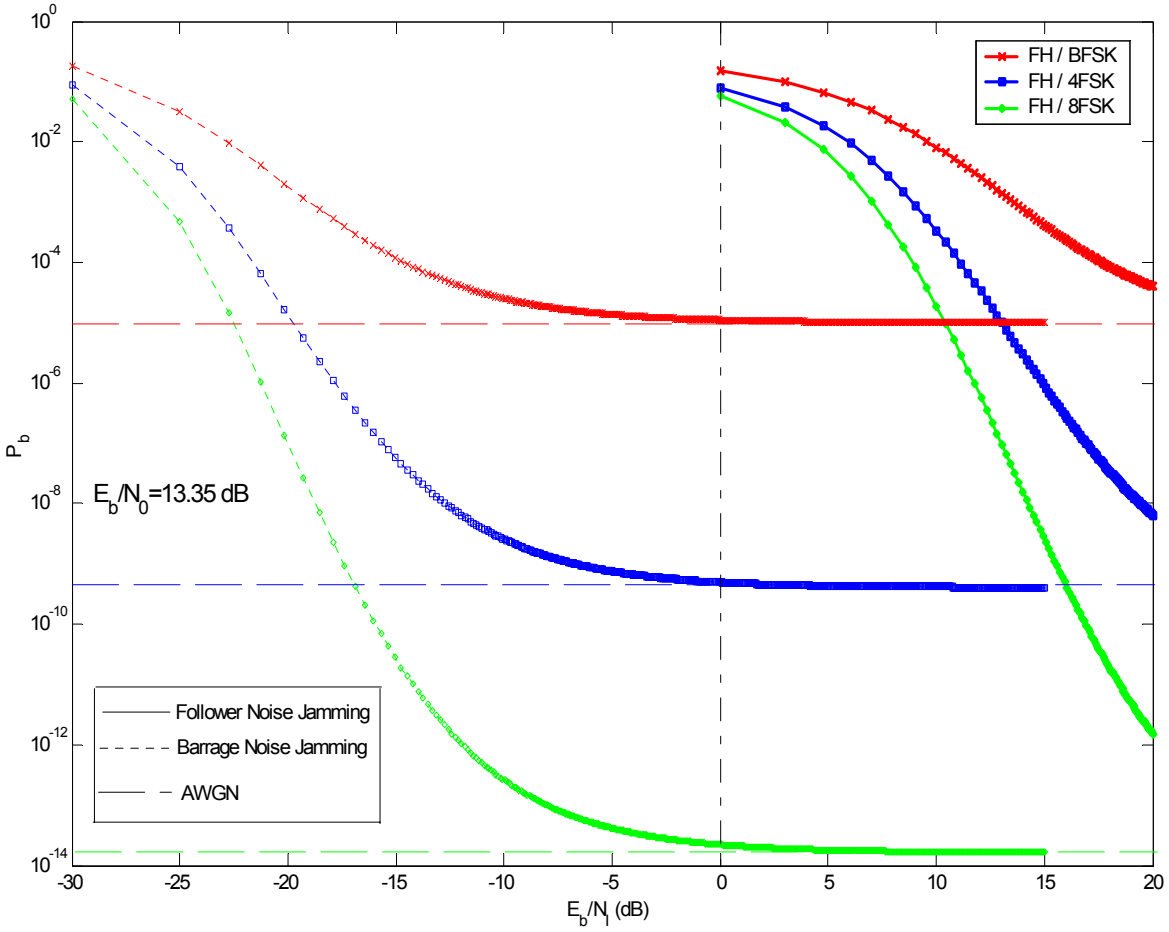

Figure 32. Comparison of the Effect of the $AN/USQ-146$ in Noise Follower and Barrage Noise Jamming Techniques on the Performance of a SINCGARS System in AWGN

Figure 32 is the combination of Figures 13 and 31. The study of Figure 32 verifies that the performance of the $AN/USQ-146$ jammer in repeat mode has increased dramatically. The most important observation is that the noise follower jammer achieves a probability of bit error in the range of 0.5 with 30 dB less energy than the barrage noise technique. As an example, for the case of the FH/4FSK, the jammer for $E_b/N_I = 0$ dB causes a $P_b \approx 0.5$. On the other hand, for the same level of interference, the P_b for barrage noise jamming is $P_b = 10^{-9}$.

The next section analyzes a more complicated but also more effective type of repeat jamming. This is the partial-band Gaussian noise follower jamming technique, which is investigated for two types of FH/MFSK communication modes.

B. PERFORMANCE OF THE AN/USQ-146 JAMMER USING FOLLOWER PARTIAL-BAND GAUSSIAN NOISE JAMMING IN A FH/MFSK SYSTEM

1. Introduction

The system model that the $AN/USQ-146$ jammer jams is a FH/MFSK system with N frequency slots. The transmitter, the receiver, and the channel are described in the following sections.

a. Transmitter/Receiver

Based on [9], during each signaling interval, the transmitter/receiver operates in one of the two modes, *conventional* or *unconventional.* The *conventional* mode is selected by the transmitter and the receiver pseudorandomly with a probability p_c. In this case, the transmitter transmits one of M tones of duration T, and $\log_2(M)$ bits are conveyed. The receiver consists of a dehopper followed by noncoherent match filters. The filter corresponding to the largest output is taken to be the transmitted symbol.

The *unconventional* mode is selected with probability $1-p_c$. In this case the transmitter randomly chooses one of the M tones and transmits it in one of the $r \le N$ frequency slots, where the set of r frequency slots are selected pseudorandomly. The M tones that are transmitted do not carry any information, but it is the presence or absence of energy in the r selected frequency slots that do convey information. In this case, $\log_2(r)$ information bits are transmitted.

The choice of r depends on the system tradeoffs (usually data rate, complexity, and throughput). A common assumption is to set $r = M$. The receiver consists of a bank of radiometers measuring the energy in the r frequency slots. The slot with the largest energy is chosen as the transmitted symbol. Figure 33 shows a time-frequency diagram of the described modes.

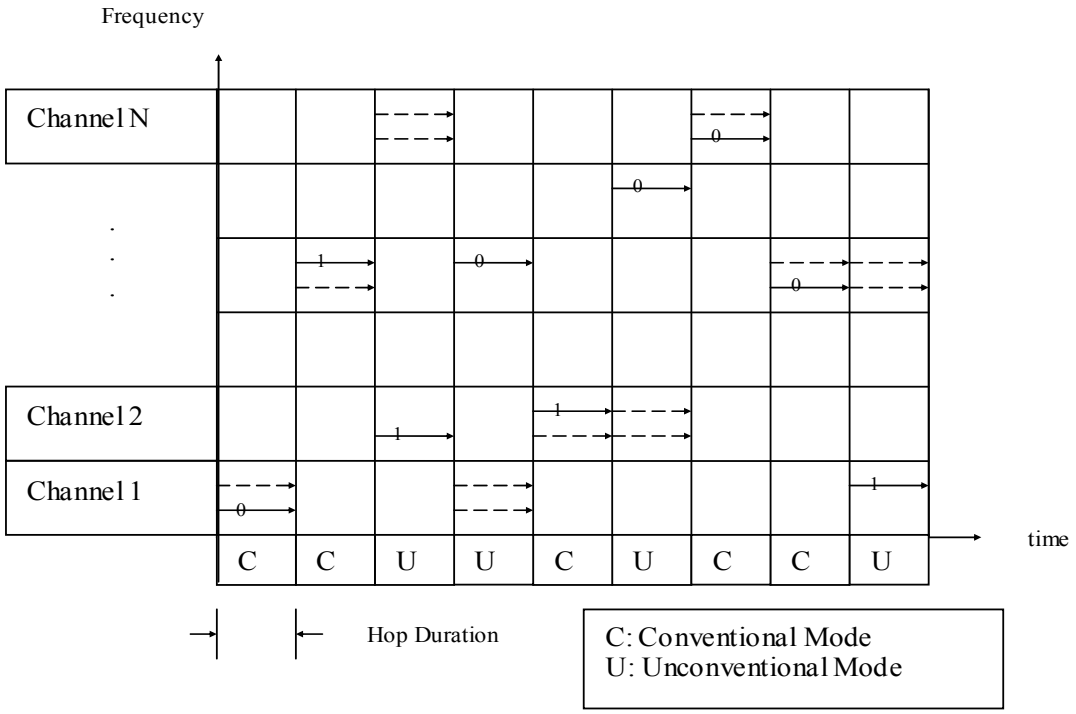

Figure 33. Time-Frequency Diagram of the Conventional-Unconventional Frequency Hopping System [After Ref. 9]

The above figure illustrates the case where $M = r = 2.$ The solid tones represent the transmitted sequence whereas the dash tones represent the binary compliment. Notice that in the unconventional mode two dashed tones are shown indicating that it does not matter which tones are chosen in that channel.

b. Channel

The $AN/USQ-146$ jammer interferes with the communication system in the repeat partial-band Gaussian noise jamming mode. As mentioned previously, W_{ss} is the total spread spectrum bandwidth, and P_I is the total power available to the follower jammer. The effective noise power spectral density is

$$N_I = \frac{P_I}{W_{ss}}. \tag{7.8}$$

The jammer concentrates all the available power on a fraction ρ of the spread spectrum bandwidth so

$$N_I^{'} = \frac{N_I}{\rho}, \tag{7.9}$$

where $\rho = s/N$, $s = 1,2,...,N.$ So Equation (7.9) can be rewritten as

$$N_I^{'} = \frac{N_I}{s} N. \tag{7.10}$$

Two modes of operation are also available to the $AN/USQ-146$ jammer, *conventional* and *unconventional.* The jammer chooses to operate in the *conventional* mode with probability p_j. In this case the jammer injects all its power in the transmitter's hop. The *unconventional* mode is chosen with a probability $1-p_j$. In this case, the jammer does not jam the transmitter's hop, but randomly jams a subset of the other $N-1$ frequency slots. Note that the jammer randomizes its decision based on its knowledge of the communication system.

It is obvious that in this channel the worst case for the jammer is when the transmitter is operating in the *unconventional* mode and the jammer selects the *conventional* mode. In this case, the jammer is helping the communicator by adding more energy into its frequency slot. This event occurs with a certain probability, and its effect improves the system's performance rather than degrades it.

2. Performance Evaluation

Let Z_c be a random variable that takes values in $\{0,1\}$ such that $Z_c = 0,$ which indicates that the transmitter/receiver are in conventional mode, and $Z_c = 1$ indicates the unconventional mode. Similarly,

$$Z_j = \begin{cases} 0 & \text{if the jammer is in conventional mode} \\ 1 & \text{if the jammer is in unconventional mode.} \end{cases} \tag{7.11}$$

Also let E_s be the event that an information symbol is in the error, and let P_b be the bit error rate. Then

$$P(E_s) = \sum_{i,j} P(E_s \mid Z_c = i, Z_j = j) \cdot P(Z_c = i, Z_j = j). \tag{7.12}$$

It is assumed that Z_j and Z_c are independent random variables. Thus,

$$P\left(Z_c = i, Z_j = j\right) = P\left(Z_c = i\right) \cdot P\left(Z_j = j\right), \tag{7.13}$$

where $P\left(Z_c = 0\right) = 1 - P\left(Z_c = 1\right) = p_c$ and $P\left(Z_j = 0\right) = 1 - P\left(Z_j = 1\right) = p_j$.

Consider first the case of both the communicator and jammer operating in conventional modes $\left(Z_c = Z_j = 0\right)$. Based on Equation (7.10), the Gaussian jamming noise density in the one slot jammed $\left(s = 1\right)$ is $N_I' = N \cdot N_I$, and the resulting error probability with non-coherent reception is the same as Equation (4.8) but with $N_o = N_I' + N_0$ or $N_o = N \cdot N_I + N_0$, so

$$P_s = \sum_{n=1}^{M-1} \binom{M-1}{n} (-1)^{n+1} \frac{1}{n+1} e^{-\frac{n \log_2(M)}{n+1} \frac{1}{\left(\frac{E_b}{N_0}\right)^{-1} + \left(\frac{E_b}{N_I}\right)^{-1} N}}. \tag{7.14}$$

Next consider the case of the conventional mode for the communicator and unconventional mode for the jammer, and vise versa. In these two cases, the error is caused only by the AWGN in the channel with result

$$P\left(E_s \mid Z_c = 0, Z_j = 1\right) = P\left(E_s \mid Z_c = 1, Z_j = 0\right) = \sum_{n=1}^{M-1} \binom{M-1}{n} (-1)^{n+1} \frac{1}{n+1} e^{-\frac{n \log(M)}{n+1} \frac{E_b}{N_0}}. \tag{7.15}$$

Finally consider the unconventional mode for both the communicator and jammer. In this case, the receiver uses an energy detector or a radiometer to decide on the hop used (representing the *M*-ary symbol). If the jammer signal $j(t)$ hops into one of these M frequency slots, the input to the radiometer is a stationary Gaussian process with double-sided power spectral density

$$\frac{N_I'}{2} = \frac{N_I}{2\rho} = \frac{N N_I}{2s}, \tag{7.16}$$

where s is the number of frequency slots jammed. In this case the output of the energy detector U is given by

$$U = \int_0^T j^2(t) dt. \tag{7.17}$$

It can be seen from [5] that the probability density function of U is given by

$$p(u)=\begin{cases}\dfrac{\left(N_I^{'}u\right)^{M-1}}{2^{2k-1}(M-1)!}e^{-\frac{N_e}{4s}}, & u>0\\ 0, & \text{otherwise.}\end{cases} \tag{7.18}$$

Obviously, the output of the energy detector when only the transmitted signal is present is $\Gamma_s = E_b \log_2(M)$.

Let $H^{(j)}$ be the event that the jammer hops into exactly j of the transmitter's set of M designated frequency slots. Note that j must be less than N since the jammer, in the nonconventional mode, does not jam the hop being used by the transmitter. Also, j must be at least 1; otherwise, the jammer does not transmit at all and the error probability will be zero.

The output of the radiometers affected by the jammer is a sequence of independent and identical distributed random variables $\{U_1, U_2, ..., U_j\}$. Then

$$P\left(E_s \mid Z_c=1, Z_j=1\right)=\sum_{j=1}^{\min(M-1,s)} P\left(E_s \mid Z_c=1, Z_j=1, H^{(j)}\right)\cdot P\left(H^{(j)}\right), \tag{7.19}$$

where

$$P\left(E_s \mid Z_c=1, Z_j=1, H^{(j)}\right)=1-f_j\left(\frac{E_b}{N_I^{'}}\right), \tag{7.20}$$

and as [9] shows

$$\begin{aligned} f_j\left(\frac{E_b}{N_I^{'}}\right) &= P\left\{\bigcap_{i=1}^{j} U_i < E_b \log_2(M)\right\} = \prod_{i=1}^{j} P\{U_i<\Gamma_s\} \\ &= \left[P\{U_i<\Gamma_s\}\right]^j = \left[1-P\{U_i>\Gamma_s\}\right]^j \\ &= \left[1-\frac{1}{2^M(M-1)!}\int_{\Gamma_s}^{\infty} p(u)du\right]^j \\ &= \left[1-e^{-\frac{\Gamma_s}{N_I^{'}}}\sum_{i=0}^{M-1}\frac{1}{i!}\left(\frac{\Gamma_s}{N_I^{'}}\right)i\right]^j . \end{aligned} \tag{7.21}$$

Also a simple combinational argument shows

$$P\left(H^{(j)}\right)=\frac{\binom{M-1}{j}\binom{N-M}{s-j}}{\binom{N-1}{s}}. \tag{7.22}$$

Therefore, the symbol error rate is given by

$$P\left(E_s\right)=\alpha\cdot p_c p_j+\beta\cdot\left(1-p_c\right)\left(1-p_j\right)+\gamma\cdot p_c\left(1-p_j\right)+\delta\cdot p_j\left(1-p_c\right), \tag{7.23}$$

where α is given by Equation (7.14), γ,δ are given by Equation (7.15) and

$$\beta=\sum_{j=1}^{\min(M-1,s)}\frac{\binom{M-1}{j}\binom{N-M}{s-j}}{\binom{N-1}{s}}\left[1-f_j\left(\frac{E_b}{N_I^{'}}\right)\right],\quad 1\le s\le N-1. \tag{7.24}$$

The bit error probability P_b is determined from the symbol error probability by

$$P_b=\frac{M}{2(M-1)}P\left(E_s\right). \tag{7.25}$$

In Equation (7.23) the only term that depend on s is β. The jammer then has to numerically choose s to maximize β and therefore maximize P_b for a fixed E_b/N_I. Assuming that N,s are very large numbers, the ratio N/s becomes finite. In this situation Stirling's approximation can be used to arrive at

$$\frac{\binom{N-M}{s-j}}{\binom{N-1}{s}}\approx\rho^j\left(1-\rho\right)^{M-1-j}, \tag{7.26}$$

where $\rho=s/N$. Using this approximation in Equation (7.24) yields

$$\beta=\sum_{j=1}^{\min(M-1,s)}\binom{M-1}{j}\rho^j\left(1-\rho\right)^{M-1-j}\left[1-f_j\left(\frac{E_b}{N_I^{'}}\right)\right]. \tag{7.27}$$

Rearranging the terms in (7.21) and assuming $s\gg M-1$, the above expression becomes

$$\beta = \sum_{j=1}^{\min(M-1,s)} \binom{M-1}{j} \rho^j (1-\rho)^{M-1-j} \left[1 - \left[1 - e^{-\frac{E_b}{N_I}\rho} \sum_{i=0}^{M-1} \frac{\left(\frac{E_b}{N_I}\rho\right)^i}{i!} \right]^j \right]$$

$$= \sum_{j=1}^{\min(M-1,s)} \binom{M-1}{j} \rho^j (1-\rho)^{M-1-j} - \sum_{j=1}^{\min(M-1,s)} \binom{M-1}{j} (1-\rho)^{M-1-j} \left\{ \rho \left[1 - e^{-\frac{E_b}{N_I}\rho} \sum_{i=0}^{M-1} \frac{\left(\frac{E_b}{N_I}\rho\right)^i}{i!} \right] \right\}^j . \quad (7.28)$$

Equation (7.28) can be simplified to

$$\beta = 1 - (1-\rho)^{M-1} - \left\{ \rho \left[1 - e^{-\frac{E_b}{N_I}\rho} \sum_{i=0}^{M-1} \frac{\left(\frac{E_b}{N_I}\rho\right)^i}{i!} \right] + (1-\rho) \right\}^{M-1} + (1-\rho)^{M-1}$$

$$= 1 - \left\{ \rho \left[1 - e^{-\frac{E_b}{N_I}\rho} \sum_{i=0}^{M-1} \frac{\left(\frac{E_b}{N_I}\rho\right)^i}{i!} \right] + (1-\rho) \right\}^{M-1} = 1 - \left\{ 1 - \rho \left[e^{-\frac{E_b}{N_I}\rho} \sum_{i=0}^{M-1} \frac{\left(\frac{E_b}{N_I}\rho\right)^i}{i!} \right] \right\}^{M-1} . \quad (7.29)$$

Reference [9] shows that the form of Equation (7.29) has a unique maximum with respect to ρ, which is

$$\rho = \begin{cases} 1, & \text{if } \frac{E_b}{N_I} \le \frac{B_M}{\log_2(M)} \\ \frac{B_M}{\log_2(M)} \left(\frac{E_b}{N_I}\right)^{-1}, & \text{if } \frac{E_b}{N_I} \ge \frac{B_M}{\log_2(M)}, \end{cases} \quad (7.30)$$

where B_M is the solution to

$$x \frac{\partial \left(e^{-x} \sum_{i=0}^{M-1} \frac{(x)^i}{i!} \right)}{\partial x} = -e^{-x} \sum_{i=0}^{M-1} \frac{(x)^i}{i!} . \quad (7.31)$$

The resulting form for β is

$$\beta = \begin{cases} 1 - \left(1 - e^{-\frac{E_b}{N_I}} \sum_{i=0}^{M-1} \frac{\left(\frac{E_b}{N_I} \right)^i}{i!} \right)^{M-1}, & \text{if } \frac{E_b}{N_I} \le \frac{B_M}{\log_2(M)} \\ 1 - \left(1 - \frac{B_M}{\log_2(M)} \left(\frac{E_b}{N_I} \right)^{-1} e^{\frac{B_M}{\log_2(M)}} \sum_{i=0}^{M-1} \frac{\left(\frac{B_M}{\log_2(M)} \right)^i}{i!} \right)^{M-1}, & \text{if } \frac{E_b}{N_I} \ge \frac{B_M}{\log_2(M)}. \end{cases} \tag{7.32}$$

Setting as

$$A_M = \frac{B_M}{\log_2(M)}, \tag{7.33}$$

the above equation becomes

$$\beta = \begin{cases} 1 - \left(1 - e^{-\frac{E_b}{N_I}} \sum_{i=0}^{M-1} \frac{\left(\frac{E_b}{N_I} \right)^i}{i!} \right)^{M-1}, & \text{if } \frac{E_b}{N_I} \le A_M \\ 1 - \left(1 - A_M \left(\frac{E_b}{N_I} \right)^{-1} e^{-A_M} \sum_{i=0}^{M-1} \frac{\left(A_M \right)^i}{i!} \right)^{M-1}, & \text{if } \frac{E_b}{N_I} \ge A_M. \end{cases} \tag{7.34}$$

In the next table, the values of A_M and $A_M e^{-A_M} \sum_{i=0}^{M-1} \frac{\left(A_M \right)^i}{i!}$, for $M = 2, 4, 8$ are listed.

M	A_M	$A_M e^{-A_M} \sum_{i=0}^{M-1} \frac{(A_M)^i}{i!}$
2	1.618	0.8399
4	1.473	0.9712
8	1.935	1.49

Table 10. Constants Used to Determine β

Statistical unclassified information for the $AN/USQ-146$ jammer indicates that the jammer prefers to choose its strategy p_j based on its knowledge of p_c. In this case, the solution to the problem is $\max_{p_j} \min_{p_c} P(p_j, p_c)$. The following theorem is proven in Reference [9].

Theorem:

$$\max_{p_j} \min_{p_c} P(p_j, p_c) = \min_{p_j} \max_{p_c} P(p_j, p_c) = \frac{\alpha\beta}{\alpha - \gamma + \beta}, \tag{7.35}$$

where

$$P(p_c, p_j) = \alpha \cdot p_c p_j + \beta \cdot (1 - p_c)(1 - p_j) + \gamma \cdot p_j (1 - p_c). \tag{7.36}$$

Rearranging the terms in Equation (7.23), the symbol error probability becomes

$$P(E_s) = (\alpha - 2\gamma) \cdot p_c p_j + \beta \cdot (1 - p_c)(1 - p_j) + \gamma. \tag{7.37}$$

The implementation of the previous theorem in Equation (7.37) gives

$$\max_{p_j} \min_{p_c} P(p_j, p_c) = \max_{p_j} \min_{p_c} P(E_s) = \frac{(\alpha - 2\gamma)\beta}{\alpha - 2\gamma + \beta} + \gamma. \tag{7.38}$$

Based on (7.25), the probability of the bit error is

$$\max_{p_j} \min_{p_c} P_b(p_j, p_c) = \frac{M}{2(M-1)} \cdot \left(\frac{(\alpha - 2\gamma)\beta}{\alpha - 2\gamma + \beta} + \gamma \right). \tag{7.39}$$

As proven in Chapter VI, the probability of correct determination $\left(P_{hc}\right)$ of the jammer when it is at the proper distance $\left(D_2\right)$ is 0.5. So the total probability of error in the case of repeat partial-band jamming is

$$\begin{aligned} P_{btot} &= P_{hc}P_b + \left(1-P_{hc}\right)\frac{M}{2(M-1)}\gamma \\ &= \frac{1}{2}P_b + \frac{1}{2}\frac{M}{2(M-1)}\gamma \\ &= \frac{M}{4(M-1)}\cdot\left(\frac{(\alpha-2\gamma)\beta}{\alpha-2\gamma+\beta}+2\gamma\right). \end{aligned} \tag{7.40}$$

As mentioned before, a is given by Equation (7.14), β for the worst case ρ is given by Equation (7.34), and γ is replaced by Equation (7.15).

The parameters that Equation (7.40) depends on are the signal-to-jammer noise ratio E_b/N_I, the signal-to-noise ratio of the channel E_b/N_0, the modulation order of the communication system M, and the number of hop bins N.

In Figure 34, the probability of bit error that the $AN/USQ-146$ jammer causes is plotted, in a FH/MFSK system when it operates as a follower partial-band noise jammer with the maximum probability for the conventional mode and the minimum for the unconventional mode. The communication system is the SINCGARS $\left(N=2320\right)$, the signal-to-noise ratio is $E_b/N_0 = 13.35$ dB, and the horizontal axis is the E_b/N_I.

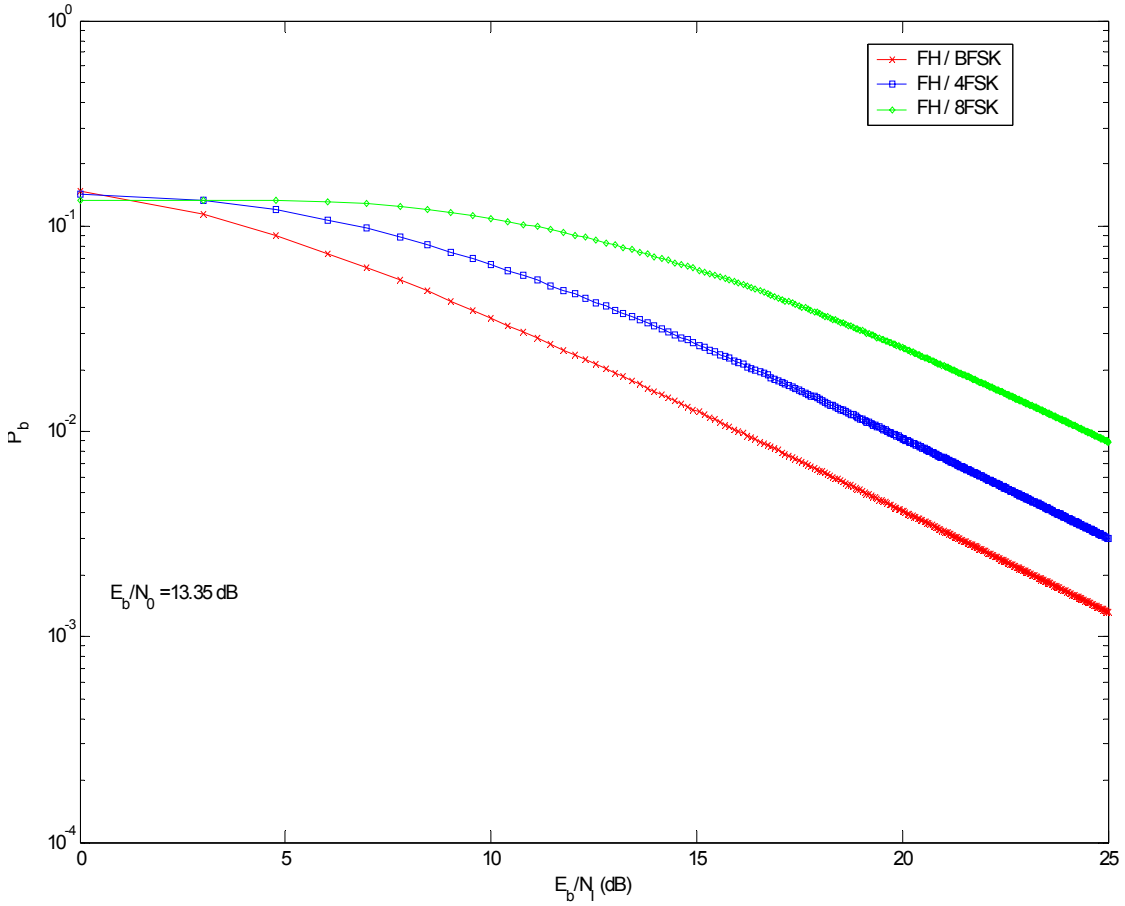

Figure 34. Effect of the $AN/USQ-146$ in Repeat Partial-Band Jamming on the Performance of a SINCGARS System in AWGN

Observing the above figure, it is apparent that whenever the jammer can maximize p_j based on the knowledge of p_c, its ability to interfere in a communication system by using repeat partial-band jamming improves. The problem for the jammer is determining the communicator's operational mode. Each time the jammer cannot accurately conclude the mode of operation of the system, it causes no error to the communication. That is, the AWGN becomes the only source of interference to the system. The unclassified sources that were used for this thesis do not refer to the way that the jammer decides the operational mode that it will use. When the jammer decides correctly, the probability of the bit error is given in Equation (7.40). On the other hand, when the jammer does not decide correctly, the probability of error is negligible.

Based on the above conclusions, a good strategy for the jammer is to use the follower partial-band jamming technique only when it is sure about the operational mode of the communicator. Otherwise jamming with the noise follower jamming technique is better.

Comparing the above two types of jamming, it is clear that the follower partial-band jamming is more effective than the noise follower jamming. In addition, the follower partial-band jammer is also more effective than the PBJ in manual spot jamming. The problem appears when the jammer fails to decide correctly. In this case, the jammer does not influence the communication system.

As Figure 35 verifies, the only type of jamming that is competitive with the follower PBJ, until this point, is the multitone manual spot jamming. For small values of signal-to-interference noise ratio, the manual spot multitone jamming appears to perform better than the repeat PBJ. On the other hand, as the signal power increases the performance of the repeat partial-band, jamming improves its effectiveness, particularly for the case of $M = 8$.

The disadvantage of the multitone manual spot jamming, as mentioned in Chapter IV is the lack of any sufficient information about the actual hop frequency. The operator is based only on statistical data that are provided by the jammer's software in order to specify the spread bandwidth. This information can only give the jammer a speculation of what the proper transmitted power of the jamming tones is.

Balancing the advantages and disadvantages of the two most powerful types of jamming that have been investigated until now, it is valid to say that the follower PBJ is more preferable for the interference of a FH system. This conclusion is based on the fact that the jammer in the repeat mode can guarantee a probability of correct determination of the frequency hop close to 0.5. On the other hand, in manual spot jamming, the probability of correct determination of the spread bandwidth, and not the frequency hop, is a parameter that is based only on the observation of the operator during a specific period of time.

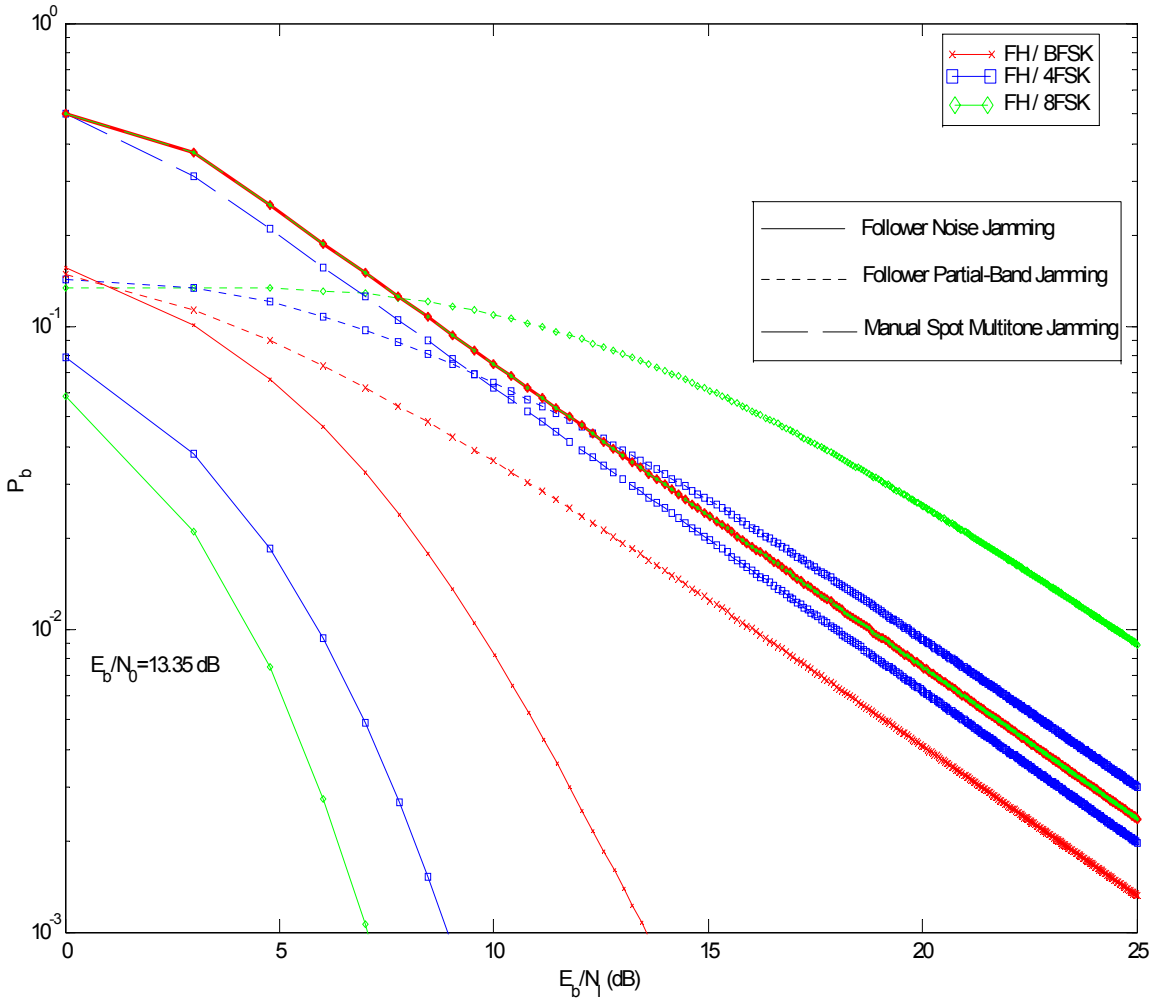

Figure 35. Comparison of the Effect of the $AN/USQ-146$ Jammer in Follower Partial-Band, Follower Noise and Multitone Manual Spot Jamming on the Performance of a SINCGARS System in AWGN

The next section investigates the last and most effective jamming technique of the $AN/USQ-146$ jammer. This is the *optimal follower tone jamming*, with the jammer allowed to transmit one or two tones in the frequency channel, depending on the mode of transmission.

C. PERFORMANCE OF THE AN/USQ-146 JAMMER USING OPTIMAL FOLLOWER TONE-JAMMING IN A FH/MFSK SYSTEM

This section discusses the effect of the $AN/USQ-146$ jammer when it operates as a follower multitone jammer. The analysis below concludes that the optimum follower tone jammer strategy is to transmit either one or two tones in a frequency channel, depending on the mode of transmission.

1. Introduction

The communication system is again a slow FH/MFSK system with N frequency channels available for hopping. Each channel can be considered as a group of M tones. That is, the communicator has $N \cdot M$ available tones. In the slow frequency hopping more than one *M*-ary symbol are transmitted prior to each frequency hop.

a. Transmitter/Receiver

As stated in the previous section, for each signaling interval, the transmitter/receiver operates in one of two modes: *conventional* or *unconventional.*

In the *conventional* mode, the transmitter transmits one of M tones within the corresponding channel (i.e., within one of the N channels). The receiver consists of a dehopper followed by M noncoherent matched filters. The filter corresponding to the largest output is taken to be the transmitted symbol.

In the *unconventional* mode, the transmitter randomly chooses one of the M tones and transmits it to one of M channels, where the M channels are selected pseudorandomly. Notice that the M tones do not carry any information, but it is the presence or absence of energy in the M channels that conveys information. The receiver looks at the whole of each M channel and consists of an energy detector, which may be a compressive receiver or a bank of M independent radiometers. The channel with the largest energy is chosen as the transmitted symbol. Next follows a description of this channel.

b. Channel

In this case the source of interference for the channel is the transmission of q tones by the $AN/USQ-146$ jammer. The power of each tone is large enough to dominate a communicator's tone. Based on [1] and [10], the $AN/USQ-146$ jammer can inject multiple tones per channel if it chooses. Due to this capability, the jammer has two modes of operation: *conventional* and *unconventional*.

In the *conventional* mode, the jammer injects a single tone in the transmitters channel and transmits the other $q-1$ tones in $s \le q-1$ distinct and randomly chosen channels. In the *unconventional* mode, the jammer does not jam the transmitter's channel but randomly distributes its q tones over the other $s-1$ distinct channels so that each channel has at most one interfering tone.

In the above general description of the channel and in the performance evaluation that follows, the number of the output tones by the jammer q is considered to be unknown. When the analysis leads to a general result, the variable q will be replaced by the actual number of tones that the $AN/USQ-146$ jammer can produce.

2. Performance Evaluation

The output power of the multitone jammer is P_J, and it transmits a tone with just enough power to exceed that of the transmitter's power. If the communicator's power at the receiver is P_c, then

$$q = \frac{P_J}{P_c}. \tag{7.41}$$

Based on Equations (4.36), (7.8) and the fact that the power at the receiver is

$$P_c = E_b R_b, \tag{7.42}$$

Equation (7.41) becomes

$$q = \frac{W_{ss} N_J}{E_b R_b} = \frac{(M+1)\cdot N \cdot N_J}{\log_2(M) E_b},$$

$$q = \frac{(M+1)\cdot N}{\log_2(M)\frac{E_b}{N_I}}. \tag{7.43}$$

Following the same steps as in the partial-band follower jamming, the Z_c random variable indicates whether the transmitter/receiver operates in conventional or unconventional mode. Mathematically this corresponds

$$Z_c = \begin{cases} 0 & \text{if the transmitter and receiver is in conventional mode} \\ 1 & \text{if the transmitter and receiver is in unconventional mode.} \end{cases}$$

Similarly,

$$Z_j = \begin{cases} 0 & \text{if the jammer is in conventional mode} \\ 1 & \text{if the jammer is in unconventional mode.} \end{cases}$$

Again, E_s is the event that an information symbol is in error. Then

$$P(E_s) = \sum_{i,j} P(E_s \mid Z_c = i, Z_j = j)\cdot P(Z_c = i, Z_j = j).$$

The transmitter/receiver selects to operate in the conventional mode with the probability p_c and the jammer with a probability p_j. Then $P(Z_c = 0) = 1 - P(Z_c = 1) = p_c$, $P(Z_j = 0) = 1 - P(Z_j = 1) = p_j$, and

$$P(E_s \mid Z_c = 0, Z_j = 0) = 1. \tag{7.44}$$

Next consider the case of the conventional mode for the communicator and unconventional mode for the jammer. In this case the error is caused only by the AWGN in the channel, so

$$P(E_s \mid Z_c = 0, Z_j = 1) = \sum_{n=1}^{M-1} \binom{M-1}{n} (-1)^{n+1} \frac{1}{n+1} e^{-\frac{n\log(M)}{n+1}\frac{E_b}{N_0}}. \tag{7.45}$$

As mentioned in $[10]$, an optimal conventional jammer will follow the transmitter's tone by injecting one tone in the complimentary channel and randomly distributes the remaining $q-1$ tones among $\left\lfloor \frac{q-1}{2} \right\rfloor$ channels with exactly two tones per channel. In

this case $P\left(E_s \mid Z_c = 1, Z_j = 0\right) \neq P\left(E_s \mid Z_c = 0, Z_j = 1\right)$, since the two tones, with a finite probability, can coincide with one of the transmitter's unconventional channels.

The two tones are optimal and more tones would be a waste of the jammer's energy. Equivalently, the jammer can use one tone with slightly more than twice the power of the communicator's tone. Since the mathematical model gives the same results whether the jammer uses either of these methods, the next analysis assumes that the jammer sends two tones in the remaining $\lfloor (q-1)/2 \rfloor$ channels.

Let $Ph(q) = P\left(E_s \mid Z_c = 1, Z_j = 1\right)$. In addition, as Reference $[10]$ indicates, $Ph(q)$ is the probability that the jammer hits at least one of the $M-1$ remaining signaling channels.

$$Ph(q) = \begin{cases} 1 - \prod_{i=1}^{q} \left(1 - \dfrac{M-1}{N-i}\right) & \text{if } q \leq N - M + 1 \\ 1 & \text{if } q > N - M + 1. \end{cases} \tag{7.46}$$

The condition $q \leq N - M + 1$ is equivalent to $\dfrac{E_b}{N_I} \geq \dfrac{(M+1)\cdot N}{\log_2(M)(N-M+1)}$. That means

$$Ph(q) = \begin{cases} 1 - \prod_{i=1}^{q} \left(1 - \dfrac{M-1}{N-i}\right) & \text{if } \dfrac{E_b}{N_I} \geq \dfrac{(M+1)\cdot N}{\log_2(M)(N-M+1)} \\ 1 & \text{if } \dfrac{E_b}{N_I} < \dfrac{(M+1)\cdot N}{\log_2(M)(N-M+1)}. \end{cases} \tag{7.47}$$

Also

$$P\left(E_s \mid Z_c = 1, Z_j = 0\right) = Ph\left(\left\lfloor \frac{q-1}{2} \right\rfloor\right). \tag{7.48}$$

Based on (7.44), (7.45), (7.46), and (7.48) the symbol error rate is given by

$$\begin{aligned} P(E_s) = {} & p_c p_j + Ph(q)\cdot(1-p_c)(1-p_j) + Ph\left(\left\lfloor \frac{q-1}{2} \right\rfloor\right)\cdot p_j(1-p_c) \\ & + \sum_{n=1}^{M-1} \binom{M-1}{n} (-1)^{n+1} \frac{1}{n+1} e^{-\frac{n\log(M)}{n+1}\frac{E_b}{N_0}} p_c(1-p_j). \end{aligned} \tag{7.49}$$

The corresponding bit error probability (P_b) is then,

$$P_b = \frac{M}{2(M-1)}\left[\begin{array}{l} p_c p_j + Ph(q)\cdot(1-p_c)(1-p_j) + Ph\left(\left[\frac{q-1}{2}\right]\right)\cdot p_j(1-p_c) \\ +\sum_{n=1}^{M-1}\binom{M-1}{n}(-1)^{n+1}\frac{1}{n+1}e^{-\frac{n\log(M)}{n+1}\frac{E_b}{N_0}} p_c(1-p_j) \end{array}\right]. \quad (7.50)$$

Equation (7.50) is in the same form as Equation (7.23). This time

$\alpha = 1$, $\beta = Ph(q)$, $\gamma = Ph\left(\left[\frac{q-1}{2}\right]\right)$, and $\delta = \sum_{n=1}^{M-1}\binom{M-1}{n}(-1)^{n+1}\frac{1}{n+1}e^{-\frac{n\log(M)}{n+1}\frac{E_b}{N_0}}$. Based on the theorem in Section $VII.B.2$,

$$\max_{p_j}\min_{p_c} P_b(p_j, p_c) = \frac{M}{2(M-1)}\cdot\frac{a\beta}{\alpha-\gamma+\beta}. \quad (7.51)$$

As proven in Chapter VI, the probability of the correct determination (P_{hc}) of the jammer when it is in the proper distance (D_2) is 0.5. The total probability of error in the case of follower tone jamming is

$$\begin{aligned} P_{btot} &= P_{hc}P_b + (1-P_{hc})\frac{M}{2(M-1)}\delta \\ &= \frac{1}{2}P_b + \frac{1}{2}\frac{M}{2(M-1)}\delta \\ &= \frac{M}{4(M-1)}\cdot\left(\frac{\alpha\beta}{\alpha-\gamma+\beta}+\delta\right). \end{aligned} \quad (7.52)$$

The parameters that Equation (7.52) depends on are the signal-to-jammer noise ratio E_b/N_I, the signal-to-noise ratio of the channel E_b/N_0, the modulation order of the communication system M, and the number of hop bins N. Figure 36 presents the plot of (7.52) with respect to E_b/N_I.

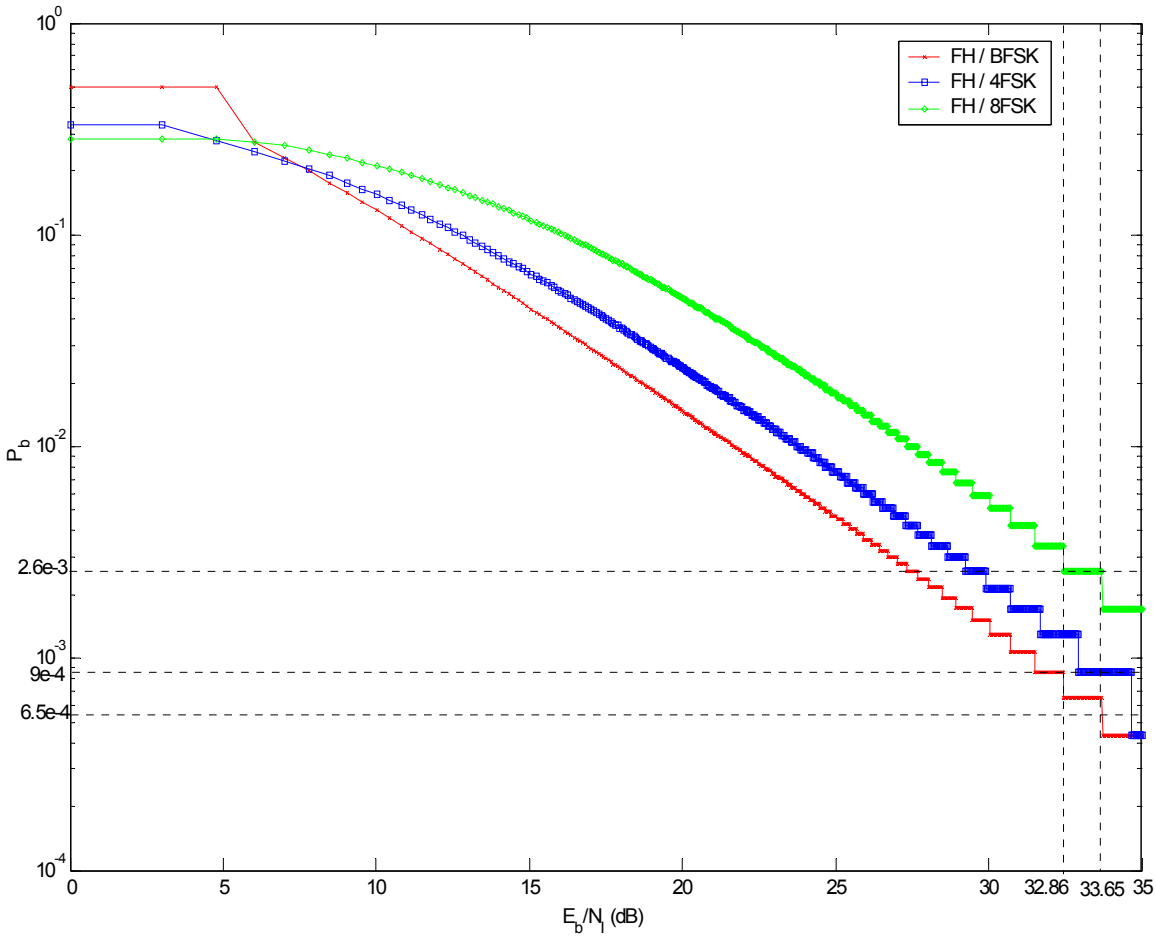

Figure 36. Effect of the $AN/USQ-146$ Jammer in Follower Multitone Jamming on the Performance of a SINCGARS System in AWGN

The above figure indicates that, as mentioned in the case of the multitone manual spot jamming, the performance of the communication system becomes inversely proportional to the modulation order. This phenomenon occurs due to the influence of Equation (7.47) in Equation (7.52). As the signal-to-interference noise ratio increases, Equation (7.47) becomes equal to its upper branch. The upper branch represents the probability that the jammer hits at least one of the $M-1$ remaining signaling channels when both the $AN/USQ-146$ jammer and communication system operate in the unconventional mode. It is also obvious that as M increases, the probability that the jammer will hit one of the $M-1$ channels increases.

The three equivalent output tones of the $AN/USQ-146$ jammer in follower multitone jamming produce a signal-to-interference jamming ratio that depends on the modulation order M. A rearrangement of the terms in Equation (7.43) gives

$$\frac{E_b}{N_I} = \frac{(M+1)\cdot N}{\log_2(M)q}. \tag{7.53}$$

Setting $N = 2320$ and $q = 3$, Table 11, indicates the produced E_b/N_I for all the cases of M.

M	$\frac{E_b}{N_I}(\text{dB})$
2	33.65
4	32.86
8	33.65

Table 11. Produced E_b/N_I from the $AN/USQ-146$ Jammer in Follower Multitone Jamming Technique

As Figure 36 indicates for the above values of E_b/N_I, the $AN/USQ-146$ jammer achieves a probability of bit error between 6.5×10^{-4} and 2.3×10^{-3}.

For the same values of E_b/N_I that the above table lists, the follower PBJ technique produces a bit error near 10^{-5}. That is, the follower multitone jamming technique improves the jammer performance to nearly 20 dB. In addition, compared to the multitone manual spot jamming, there is an improvement of 10 to 15 dB.

However, the follower multitone jamming technique can achieve a bit error rate in the range of 0.5 $(E_b/N_I = 0 \text{ dB})$, if the jammer can increases its output power per jamming tone. Based on Equation (7.53), the necessary increase of the output jamming power is shown in the next table.

M	Necessary Increase of Output Power Per Jamming Tone for $P_b = 0.5$
2	38.42 dB
4	37.63 dB
8	38.42 dB

Table 12. Necessary Increase of the Follower Multitone Output Power Per Jamming Tone for $P_b = 0.5$

Based on the conclusions in the previous section, the plot of Equation (7.52) must be compared with the two most prevailed performances of the jammer. That is, the follower PBJ and in multitone manual spot jamming. Figure 37 illustrates the performance of the $AN/USQ-146$ jammer in a SINCGARS system using the above three most effective techniques.

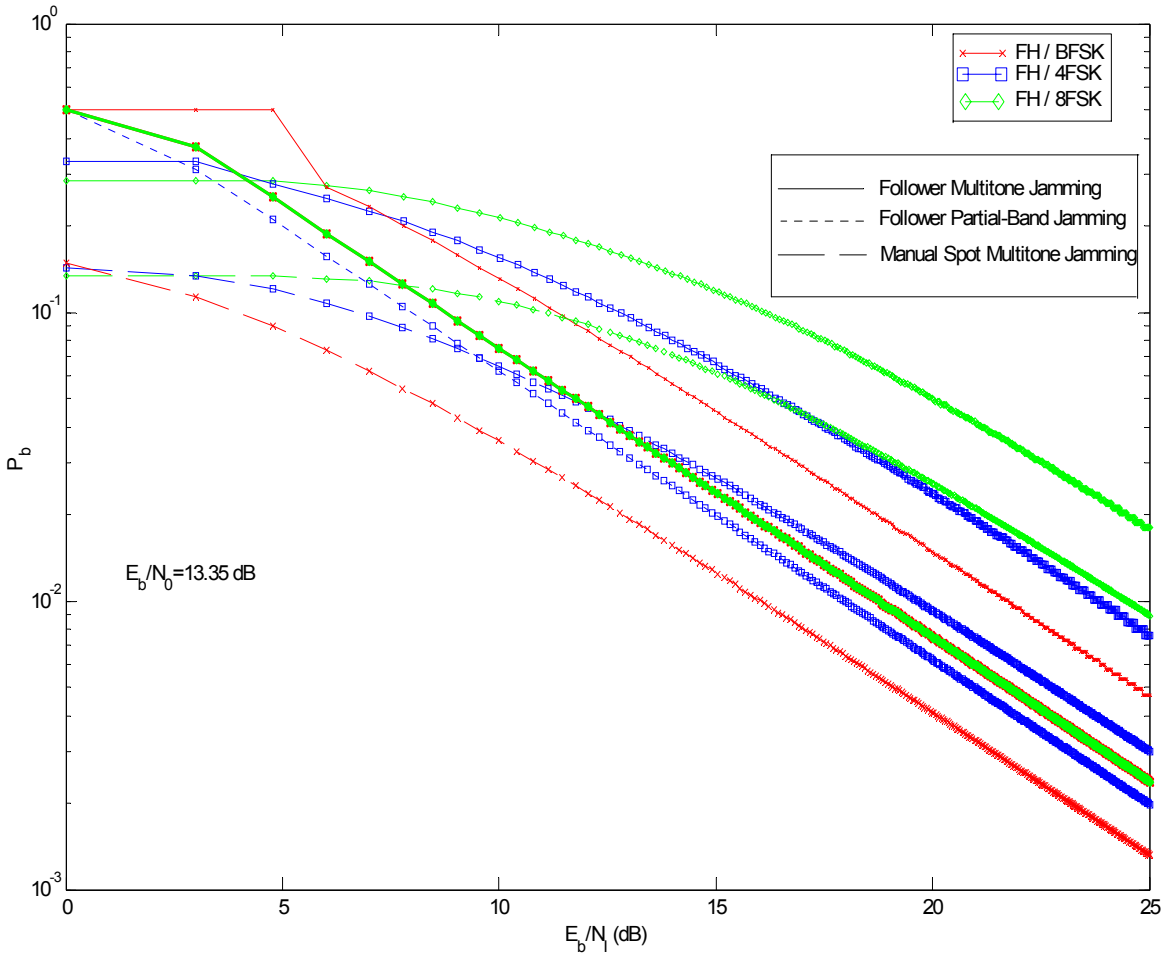

Figure 37. Comparison of the Effect of the $AN/USQ-146$ Jammer in Follower Multitone, Follower Partial-Band and Multitone Manual Spot Jamming on the Performance of a SINCGARS System in AWGN

The above figure shows the superiority of the follower multitone technique against the two other techniques. For small values of E_b/N_I the performances of the manual mode and follower multitone are similar enough, but as the signal-to-jamming ratio increases the follower multitone technique presents a $8-10$ dB greater degradation in the hostile communication system regardless of the modulation order. On the other hand, the performance of the follower partial-band jamming for small values of E_b/N_I is clearly worse than the two other techniques. However as the E_b/N_I increases, the repeat partial-band jamming improves its performance against the manual spot multitone jam-

ming. Specifically, for values of signal-to-interference noise ratio greater than 10 dB, the follower PBJ performs $5-10$ dB better than the manual spot multitone technique.

At this point is important to emphasize that the manual spot multitone jamming technique achieves the specific performance under certain conditions, which were analyzed in this chapter. As a result, most of the times the follower PBJ is preferable to manual spot multitone jamming.

D. SUMMARY

Based on the above results, it can be concluded that the best jamming technique that the $AN/USQ-146$ jammer must follow when it is interested in a FH/MFSK system is the follower multitone jamming. This result was expected since in this specific mode of operation, the jammer is using its output power and the determinator's decision most efficiently.

The second most effective technique is the repeat partial-band noise jamming. Even though the results of the multitone manual spot jamming are better for small values of SJR, the fact that its performance is influenced by many external factors, such as the operator's experience and the observation time of the system by the jammer, make the repeat partial-band noise jamming a more preferable jamming strategy.

This chapter concludes the theoretical analysis for the $AN/USQ-146$ jammer, and the sub-sequential step is verifying the outgoing results from this analysis through a simulation environment.

Chapter VIII introduces the creation of two simulation environments. The first one is a FH system identical to the SINCGARS communication system, which will verify the results in Chapters IV and VII. The second simulation environment is the IEEE 802.11*a* *wireless local area network* (WLAN) system, which is used to investigate the capabilities of the manual spot jamming mode of the $AN/USQ-146$ jammer in a non-FH system. The simulation environments were created by using a relatively new software called SystemView.

VIII. SIMULATION RESULTS OF THE AN/USQ-146 JAMMER PERFORMANCE IN TWO TYPES OF COMMUNICATION SYSTEMS

The purpose of this chapter is to present simulation results for the $AN/USQ-146$ jammer operating on two types of communication systems. The first communication system is the SINCGARS frequency hopping communication system. In this environment, the jammer is simulated to perform in manual spot mode and in repeat mode for all types of jamming. For every case, the probability of bit error due to jamming is measured, and a comparison with the corresponding theoretical result is presented.

The second communication system is the IEEE 802.11*a* Standard WLAN system. This commercial communication system has an *orthogonal frequency division multiplexing* (OFDM) scheme. The purpose of this simulation is to investigate the performance of the $AN/USQ-146$ jammer in a non-FH commercial system. In this case, since the system does not hop frequencies, the jammer is simulated only in manual spot jamming mode.

All the simulations were created with the help of a relatively new software package, which is called SystemView.

A. SIMULATION OF THE AN/USQ-146 JAMMER PERFORMANCE IN A SINCGARS COMMUNICATION SYSTEM

This section describes the simulation of the SINCGARS communication system as performed in SystemView by Elanix. This simulation scheme is used as a platform upon which each type of jamming is represented by adding the appropriate blocks (tokens). These tokens reflect the specifications and the operational characteristics of the $AN/USQ-146$ jammer for every type of interference.

1. SINCGARS Simulation Model

The overall block diagram of the SINCGARS communication system is shown in Figure 38.

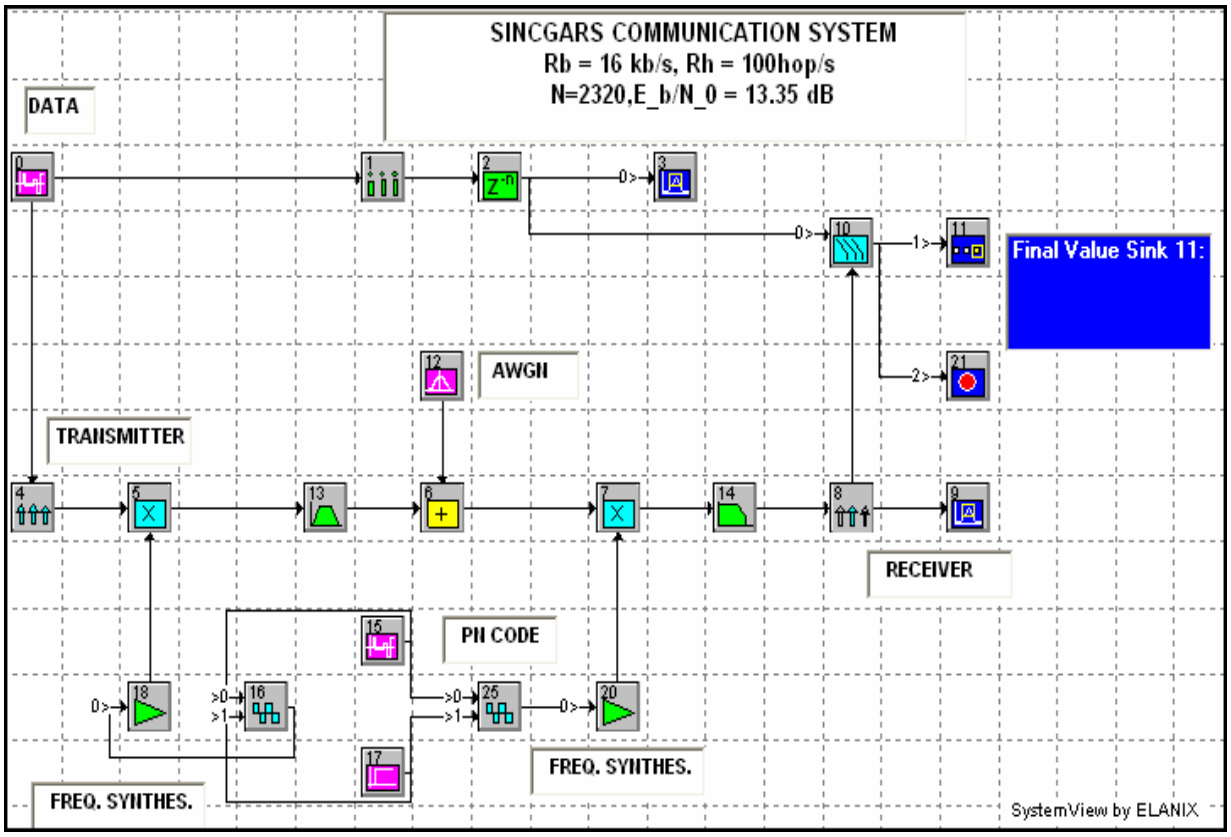

Figure 38. SINCGARS Simulation Scheme

The 16 kbps data source (token 0) is first modulated in the MFSK modulator (token 4). The modulated signal with bandwidth $W = 25$ kHz is multiplied by the output of the frequency synthesizer (token 16). The frequency synthesizer consists of a numerical controlled oscillator (token 16) and a PN code (token 15). The PN code produces the 2320 frequencies of the FH system with a rate $R_h = 100$ hops/s. Token 13 represents the spread bandwidth of the SINCGARS system, which is $W_{ss} = 88\text{ MHz} - 30\text{ MHz} = 58\text{ MHz}$.

As assumed in the theoretical analysis, the noise of the channel is modeled as AWGN with signal-to-noise ratio equal to $E_b/N_0 = 13.35$ dB. Token 6 represents the additive Gaussian noise in the channel.

Considering perfect synchronization, the frequency synthesizer (token 20) at the receiver is driven by the same PN code (token 15) as it is used in the transmitter. The multiplication in token 7 succeeds the perfect dehopping of the signal. The dehopped signal is completely filtered out by the bandpass filter (token 14), and it passes through the MFSK demodulator (token 8) to extract the data. Finally token 10 compares the transmitted data with the received data and extracts the probability of the bit error of the system. The modulation order of the system and the symbol rate are parameters that can be adjusted by the tokens 4 and 10. The number of samples that will pass from the system, the sample rate, the variable token and the number of system loops can be arranged from the system time specifications of the software. Before presenting the influence of the $AN/USQ-146$ jammer model in different types of jamming, it is important to examine the above simulation under the effect of the AWGN only in order to verify that the SINCGARS model behaves as the theory predicts.

2. SINCGARS Model in AWGN

The simulation model of the SINCGARS system in AWGN is illustrated in Figure 38. Enabling token 12 as a variable token, the system is running for ten different, continuously decreasing values of noise power (N_o), which correspond to ten different, continuously increasing values of E_b/N_0. The simulation model was executed for the cases of $M = 2, 4$ and 8.

In order to verify that the above simulation model is a FH system with 2320 possible hops with a rate of 100 hops/s, an oscilloscope is connected at the output of token 13. The output result on the oscilloscope window after 23.2 seconds can be seen in Figure 39.

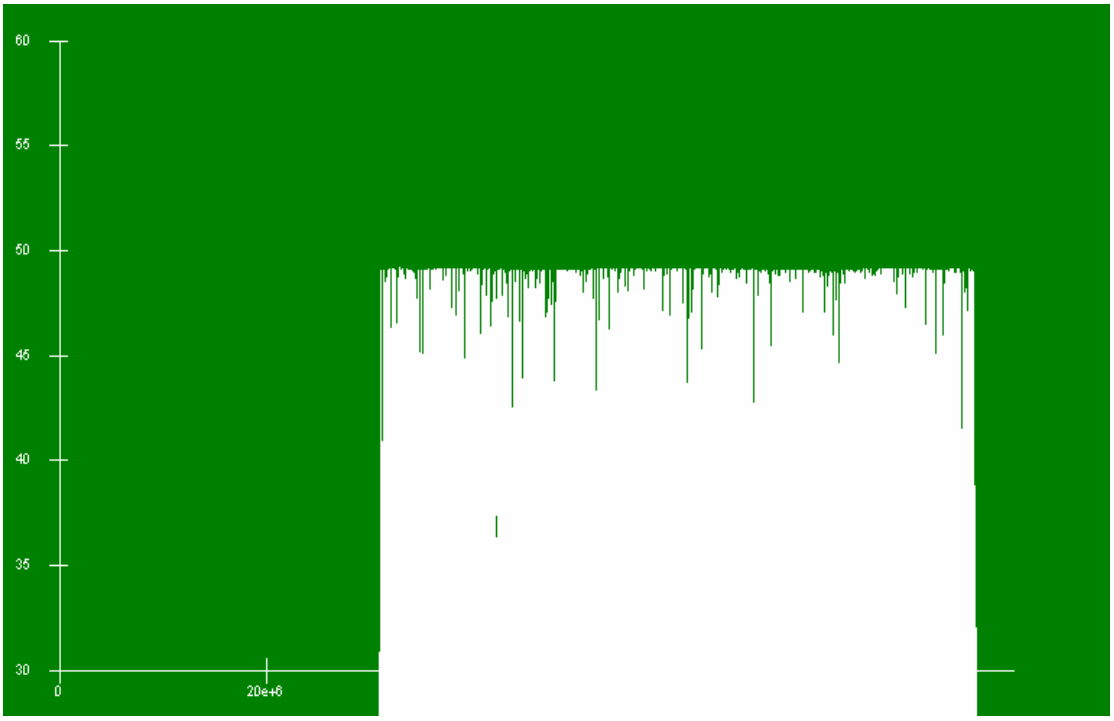

Figure 39. 2320 Hop Bins in the Spread-Spectrum Bandwidth of SINCGARS

When observing the above figure, it is apparent that the communication system is a FH system with $N = 2320,$ its spread bandwidth is $W_{ss} = 58$ MHz and its hop rate is $R_h = 100$ hops/s. After the above verification, the simulation is executed.

Figure 40 presents the simulated probabilities of bit error for the BFSK, 4FSK and 8FSK cases, together with the corresponding theoretical results from Figure 10. The results in Figure 40 verify that the simulation model behaves in AWGN as the theory predicts with small variations for small values of E_b/N_0.

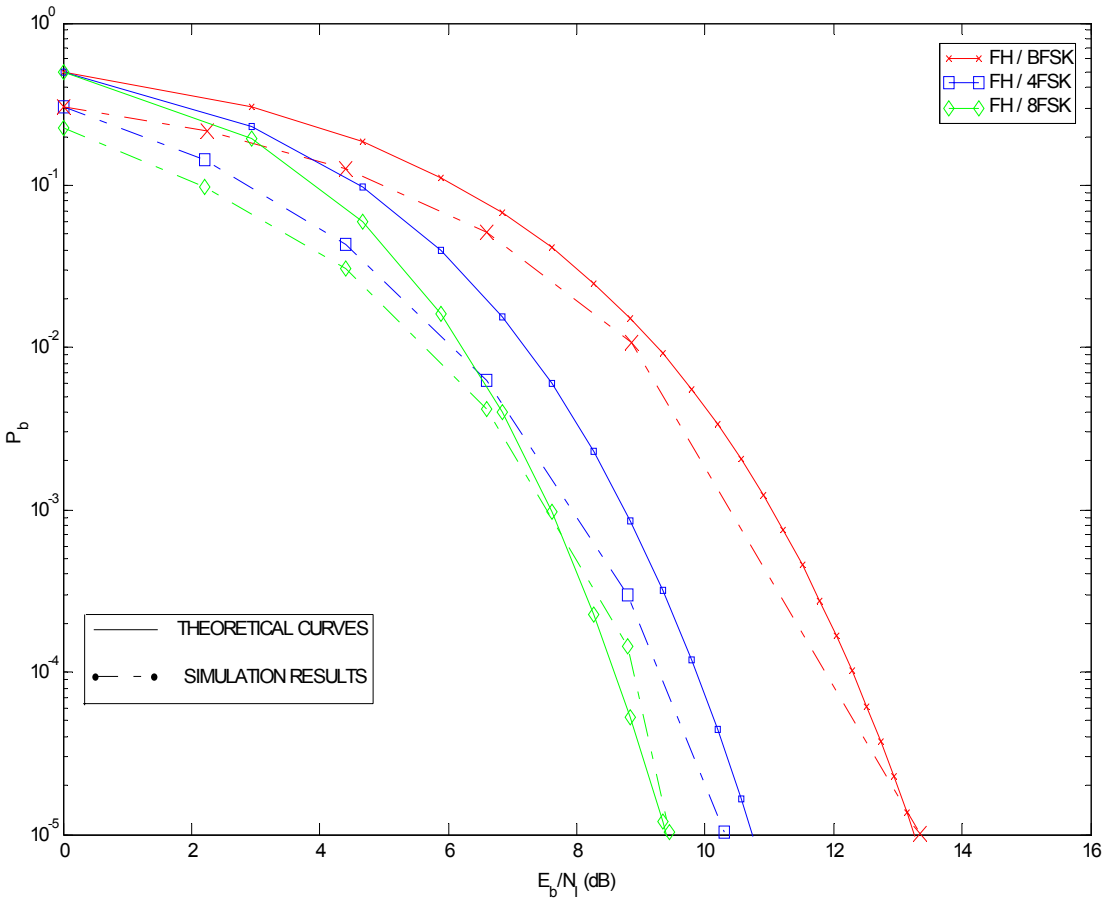

Figure 40. Simulation of SINCGARS Performance in AWGN as Compared to Theoretical Curves

The next step is to create the model of the $AN/USQ-146$ jammer in barrage noise jamming and observe its performance in the SINCGARS model.

3. SINCGARS Model under the Influence of the AN/USQ-146 in Barrage Noise Jamming

The source of interference that the $AN/USQ-146$ jammer uses in barrage noise jamming is an AWGN with $N_I = P_I/W_{ss}$. This interference is added in the channel to the thermal noise.

Figure 41 illustrates the above, in which token 23 represents the noise source of the jammer and token 24 restricts the interference inside the operational bandwidth of the SINCGARS system.

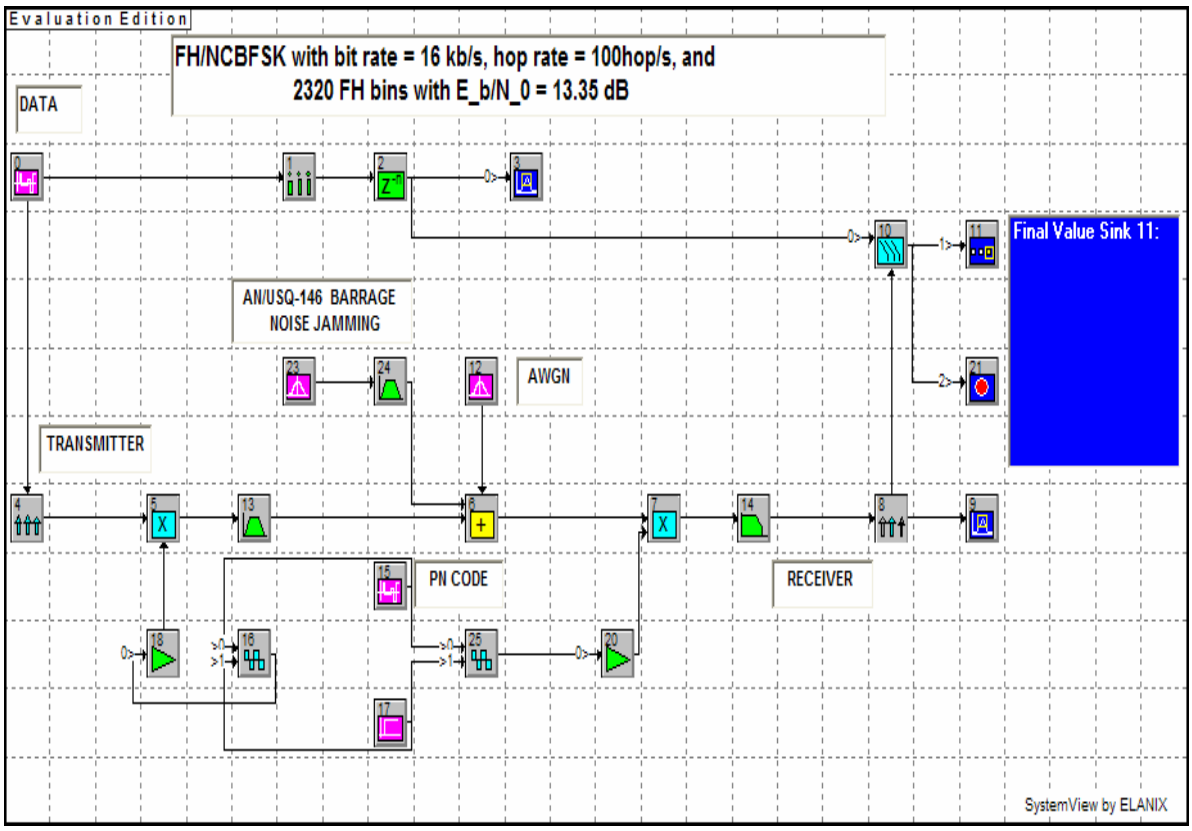

Figure 41. Barrage Noise Jamming Model of the $AN/USQ-146$ Jammer in the SINCGARS System

The noise of the channel is considered to be constant with $E_b/N_0 = 13.35$ dB. The parameter that varies in this simulation is the noise power of the jammer (token 23).

In Figure 42, with the help of the SystemView's oscilloscope, the influence of the BNJ on the communication system can be observed. The upper part of the figure illustrates the instantaneous frequency of the SINCGARS system together with the noise signal. In the lower part, the barrage noise jamming influence has been added.

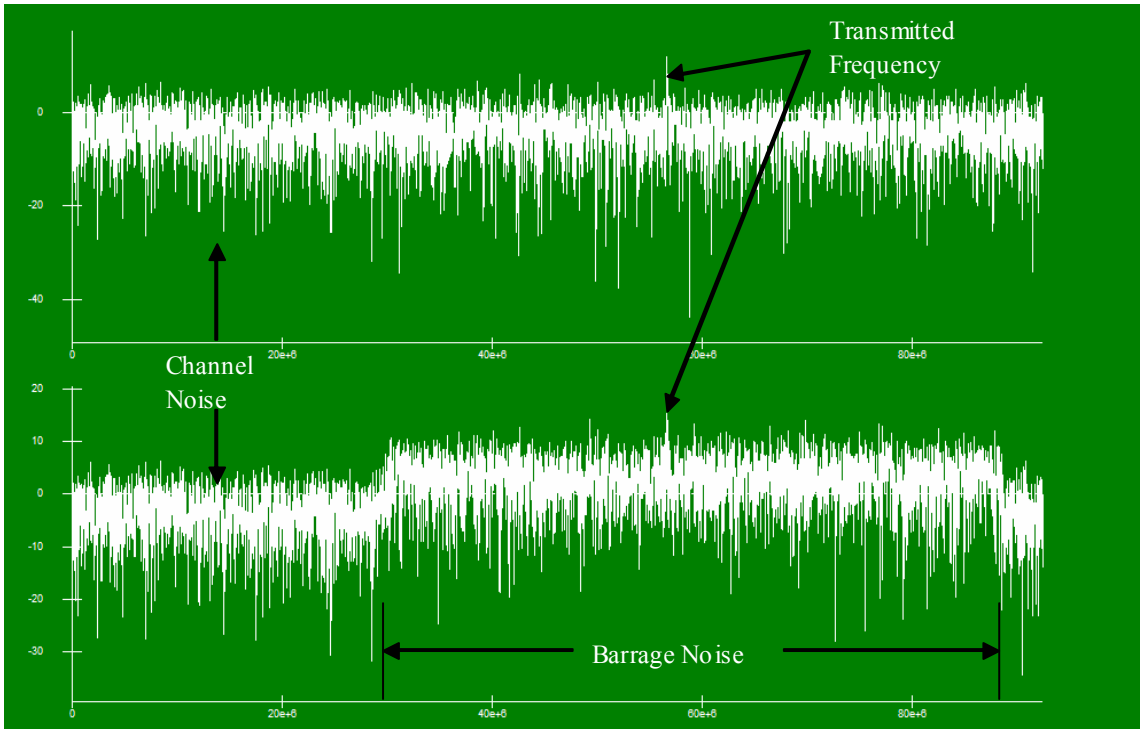

Figure 42. Influence of the $AN/USQ-146$ Jammer in Barrage Noise Jamming Mode over the SINCGARS System

As mentioned in the beginning of this chapter, the SystemView program estimates the probability of error by comparing the transmitted bit with the received one. The newest version of SystemView has the capability of transmitting in each loop at the most 2^{31} samples. That means that the lowest theoretical P_b that this software can calculate is in the range of 10^{-9}. If the error is less than 10^{-9}, the system sets $P_b = 0$.

The results of the simulation for $M = 2, 4$ and 8 are presented together with the theoretical curve in Figure 43.

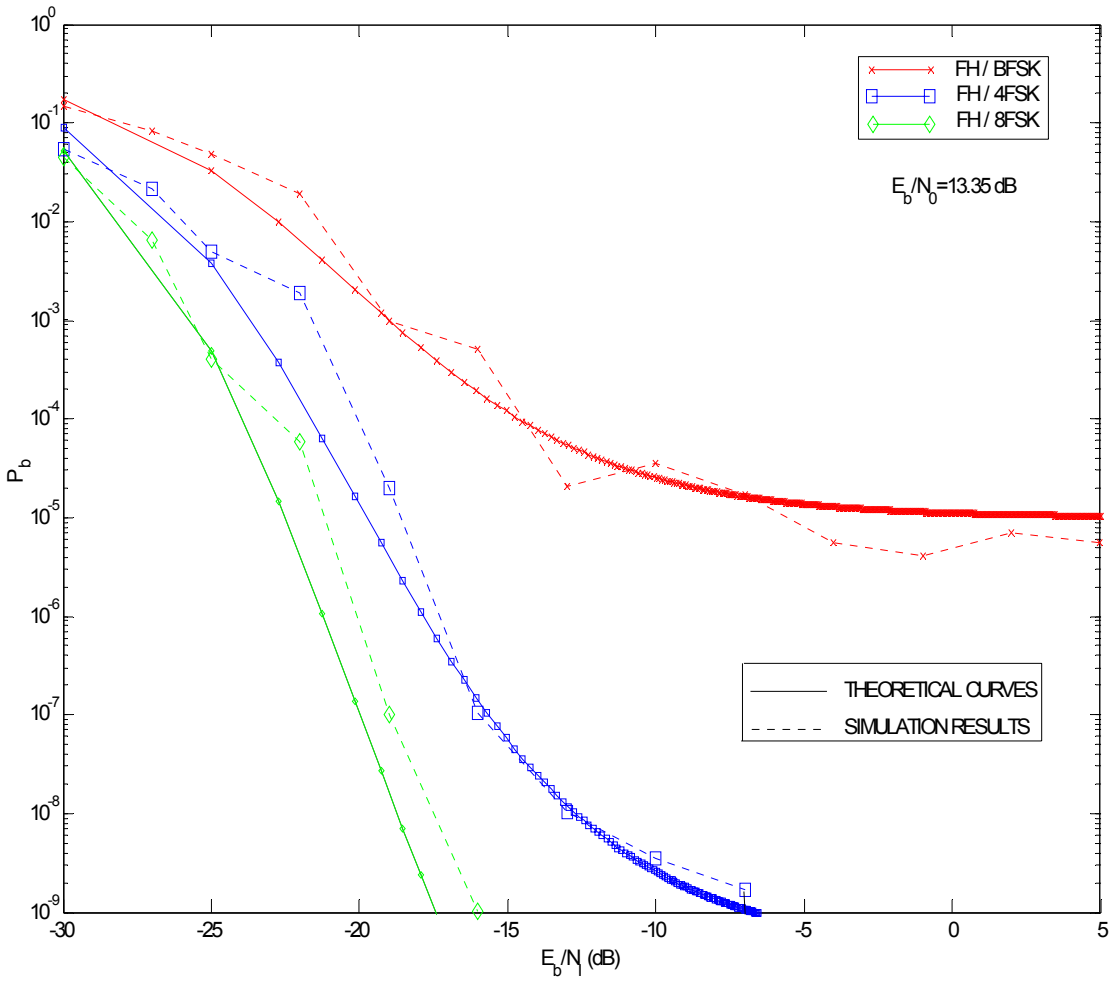

Figure 43. Simulation Results of the Effect of the $AN/USQ-146$ in Barrage Noise Jamming on the Performance of a SINCGARS System in AWGN as Compared to Theoretical Curves

The results in Figure 43 verify that the simulation model behaves in BNJ as the theory predicts with small variations for small values of E_b/N_0. Due to restrictions of the software, the simulation could not produce results for the cases of $M=4$ and $M=8$ when $P_b < 10^{-9}$.

4. SINCGARS Model under the Influence of the AN/USQ-146 in Worst Case Partial-Band Noise Jamming

The simulation model in partial-band case is the same as in the BNJ model. The only difference exists in the token 24 which determines the part of the bandwidth that

will be jammed. As mentioned in the theoretical analysis, the jammer calculates the worst fraction of jammed bandwidth (ρ_{wc}) each time from Equation (4.32) before it jams. For the SINCGARS case, the only variable in Equation (4.32) is the E_b/N_I.

Even though the signal-to-interference power can be set as a variable, ρ_{wc} cannot, since in the SystemView library there is no option for variable bandwidth filter. So the only possible procedure is to make one calculation with a given configuration for ρ_{wc}, save the results, and then change the value of E_b/N_I, the value of the filter bandwidth (token 24) and the noise power accordingly for the next run, and so on.

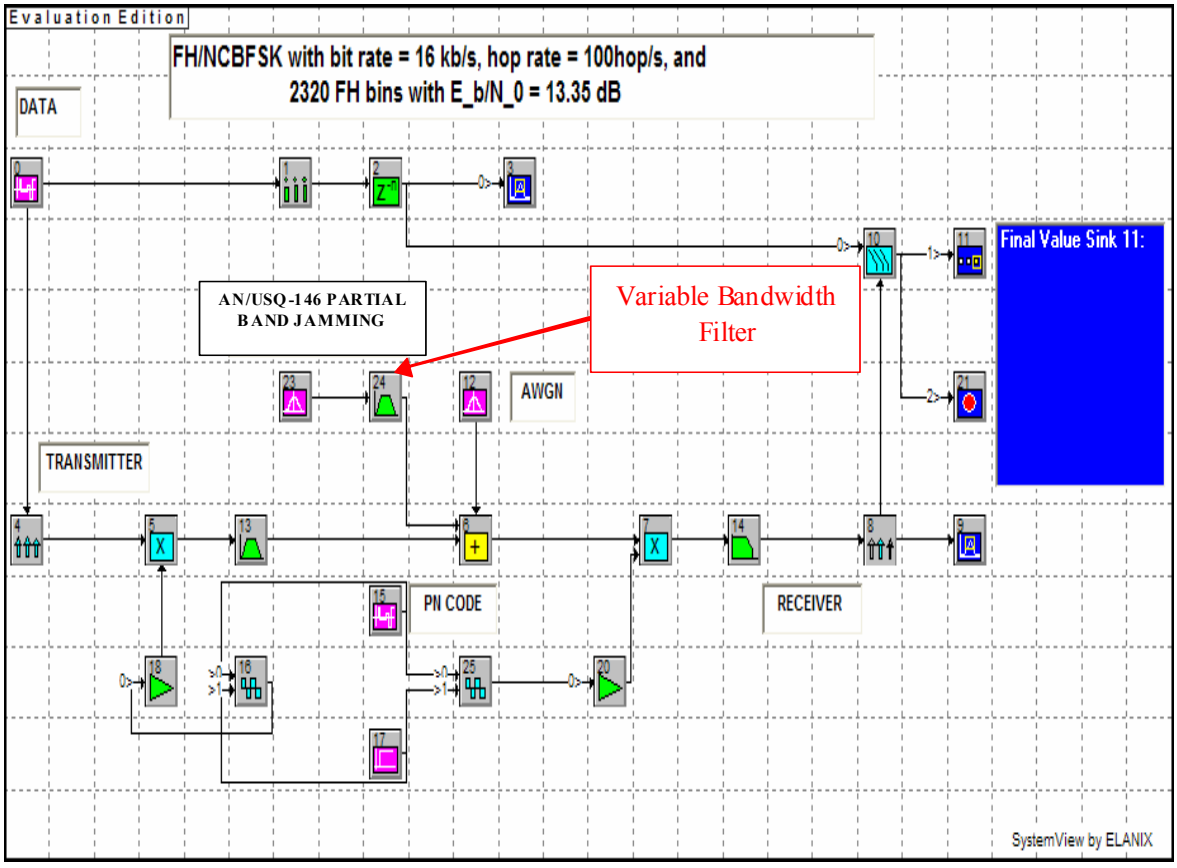

Figure 44. Partial-Band Noise Jamming Model of the $AN/USQ-146$ Jammer over a SINCGARS System

In Figure 45, with the help of the SystemView's oscilloscope, the influence of the jammer in the worst case PBJ in the communication system for a particular value of ρ_{wc} can be observed. The upper part of the figure illustrates the instantaneous frequency of

the SINCGARS system together with the noise signal. In the lower part, the partial-band noise jamming influence has been added.

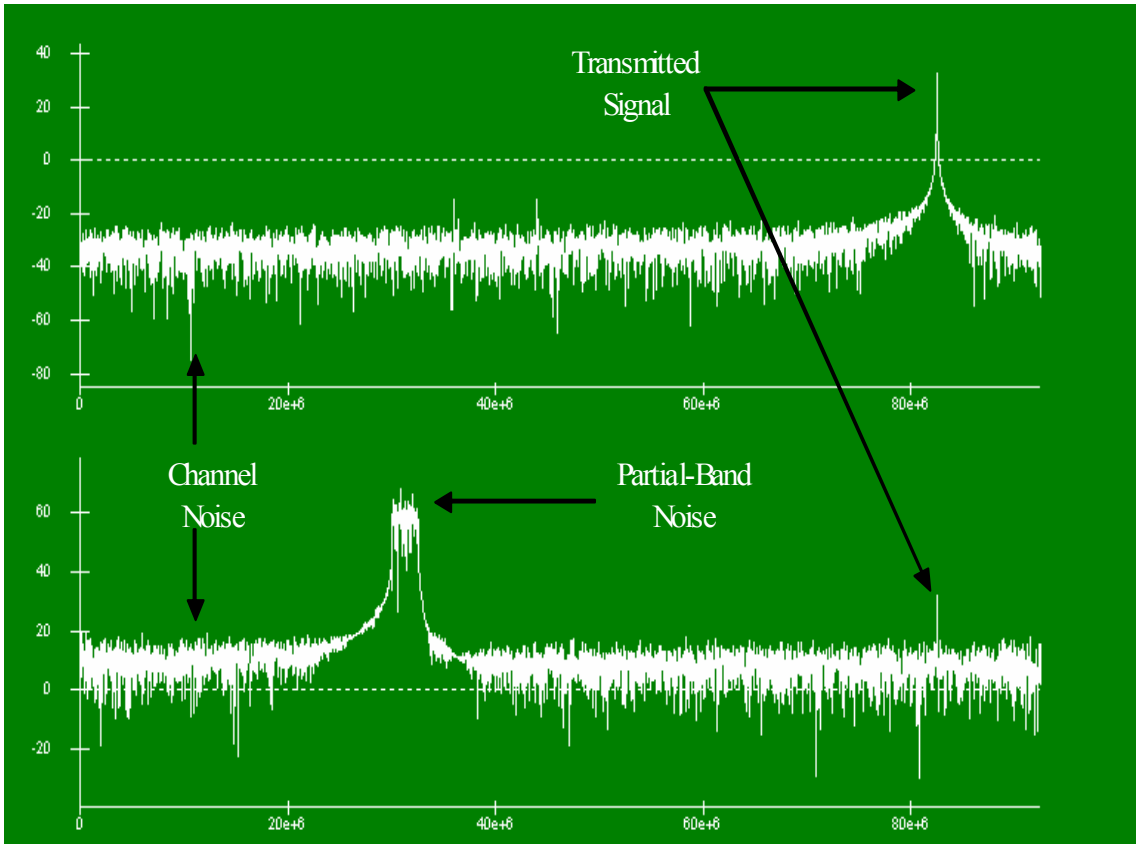

Figure 45. Influence of the $AN/USQ-146$ Jammer in Partial-Band Mode over the SINCGARS System

At the specific instant that the above picture was taken, the jammer noise did not share the same bandwidth region with the signal, but when it did, an error occurred. The results of the above simulation for $M = 2,\ 4,\ 8$ together with the theoretical results are shown in Figure 46.

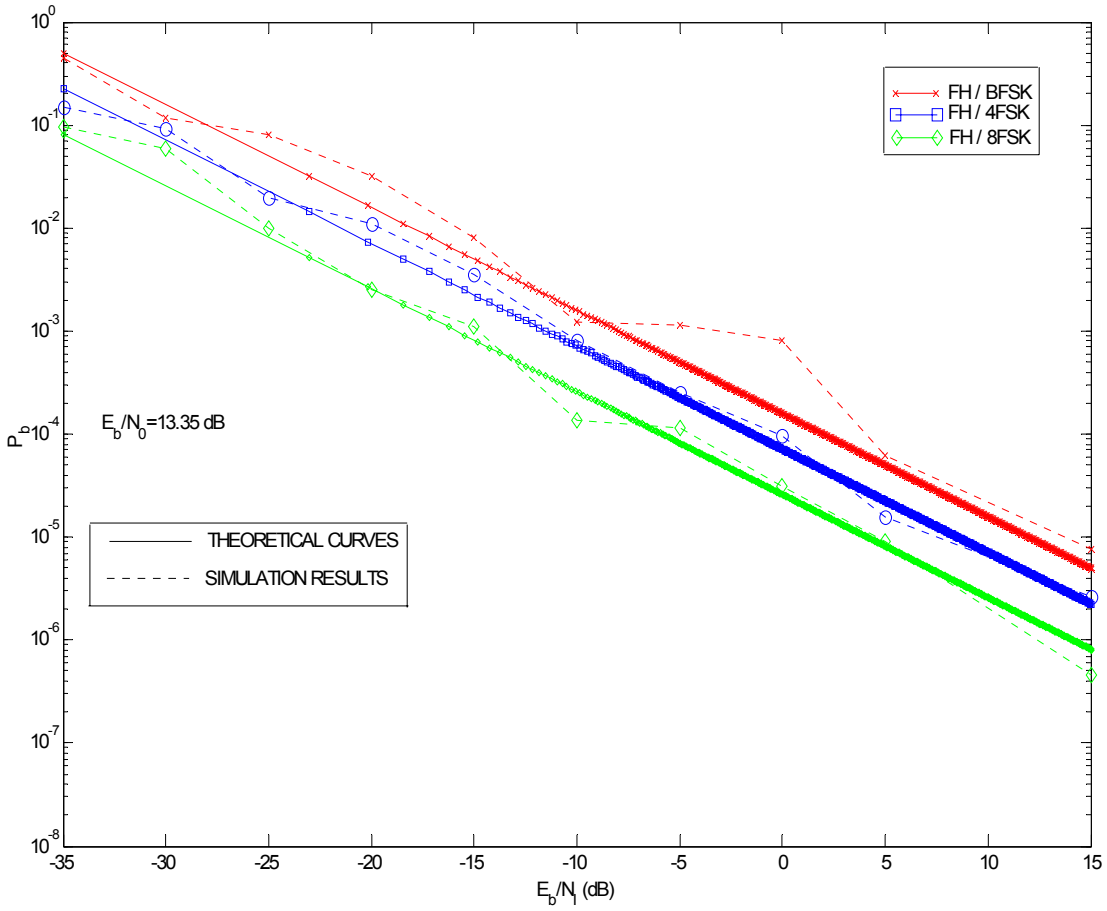

Figure 46. Simulation Results of the Effect of the $AN/USQ-146$ in Worst Case Partial-Band Jamming on the Performance of a SINCGARS System in AWGN as Compared to Theoretical Curves

The results in Figure 46 verify that the simulation model behaves in PBJ as the theory predicts with small variations. The next step is to create the model of the $AN/USQ-146$ jammer in multitone noise jamming and observe its performance in the SINCGARS model.

5. SINCGARS Model under the Influence of the AN/USQ-146 in Multi-tone Noise Jamming

The simulation of the $AN/USQ-146$ jammer interference in multitone jamming can be achieved by using one of the existing channel models in the SystemView library, which is called *narrow band interferer* (NBI).

This specific token generates unmodulated tones over a prescribed range. The desired signal $x(t)$ after the influence of the NBI becomes

$$y(t) = x(t) + \sum_{k=1}^{q} A_k \sin(2\pi f_k t + \varphi_k), \tag{8.1}$$

where q is the number of jamming tones. As mentioned in Chapter IV, for the case of the $AN/USQ-146$ jammer $q = 2$. The phase φ_k of each NBI is distributed between 0 and 2π. The amplitude A_k of each NBI is distributed between specific values that the user can set. A_k is also the variable in this specific simulation model. The frequency f_k of each NBI is chosen randomly over the communication bandwidth.

Figure 47 represents the simulation model for the multitone manual spot jamming case in which token 29 represents the influence of the $AN/USQ-146$ jammer.

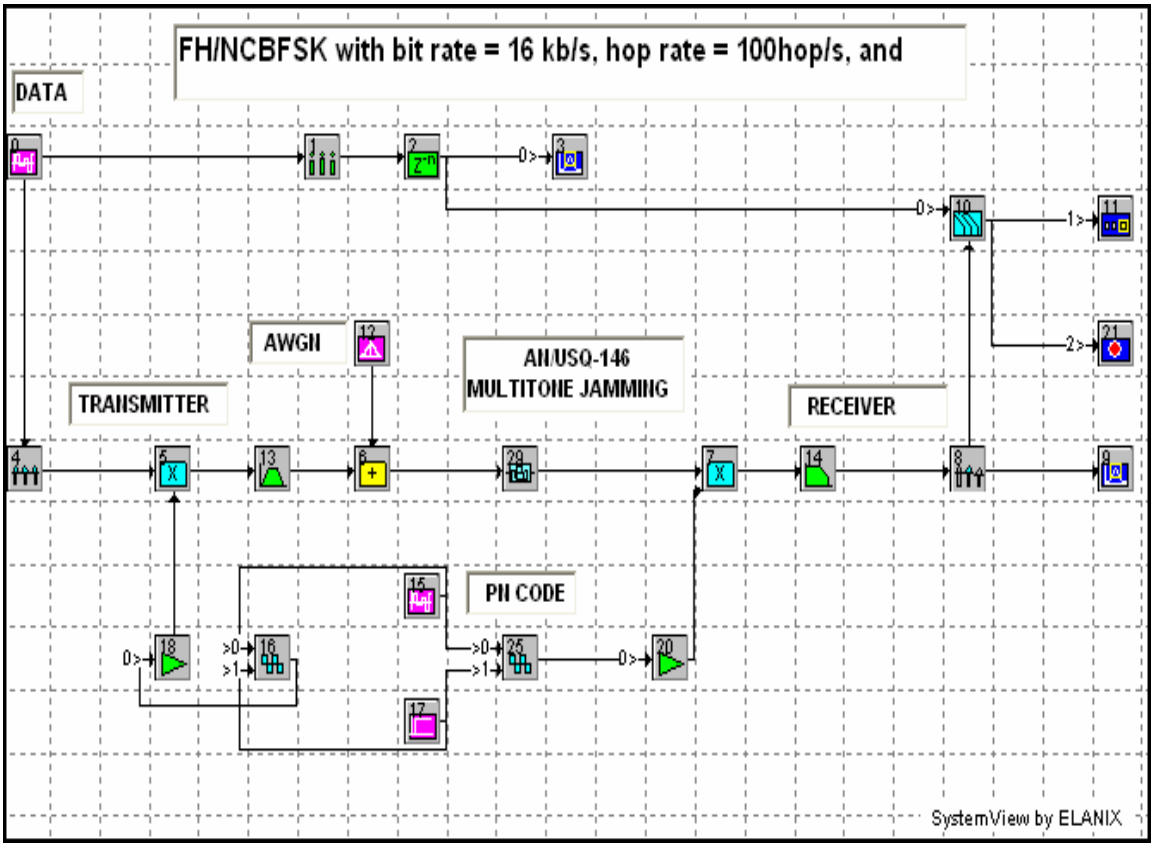

Figure 47. Multitone Jamming Model of $AN/USQ-146$ Jammer in the SINCGARS System

In Figures 48 and 49, with the help of the SystemView's oscilloscope, the influence of the jammer in multitone jamming can be observed. In the first figure, the signal tone is operating in a bandwidth away from the jamming tones. In the second figure, the signal tone has been hopped close and between the two jamming tones.

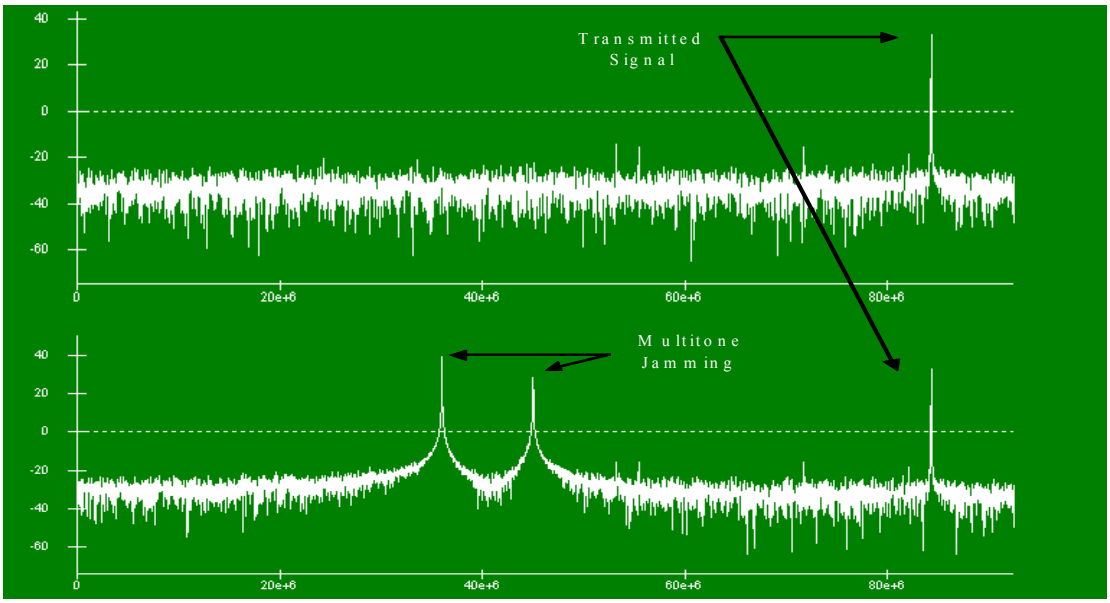

Figure 48. Influence of the $AN/USQ-146$ Jammer in Multitone Mode over a SINCGARS System

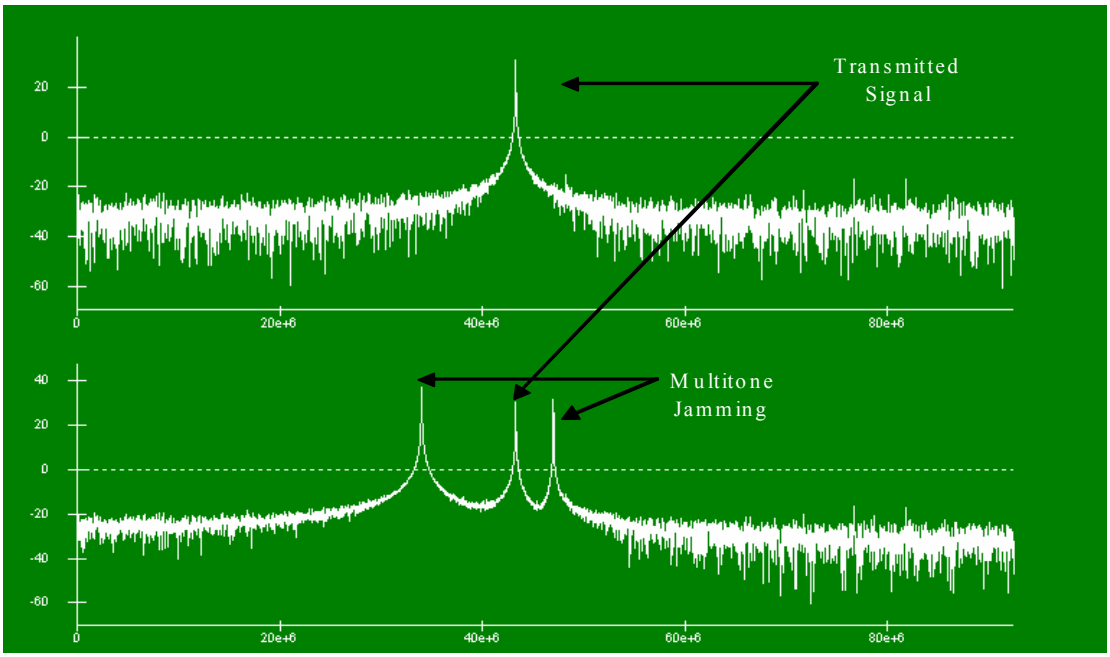

Figure 49. Influence of the $AN/USQ-146$ Jammer in Multitone Mode over a SINCGARS System in Another Hop

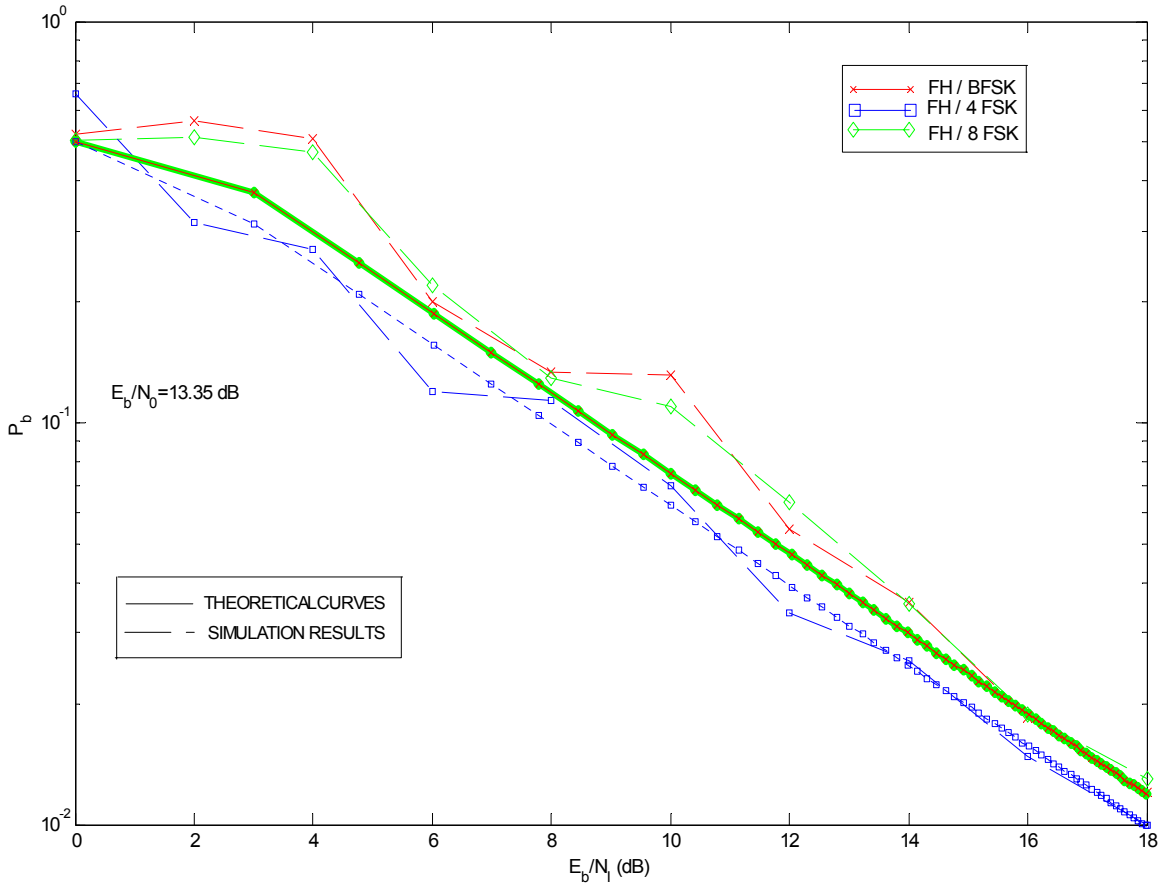

Figure 50. Simulation Results of the Effect of the $AN/USQ-146$ in Manual Spot Multitone Jamming $(q=2)$ on the Performance of a SINCGARS System in AWGN as Compared to Theoretical Curves

The results of the above simulation for $M=2,4,8$ together with the theoretical results are shown in Figure 50. It is obvious that the simulation model behaves in multitone jamming as the theory predicts with small variations. As mentioned in the theoretical analysis, the $AN/USQ-146$ jammer in multitone jamming behaves better when the order of modulation is increasing. The simulation results agree with the above conclusion when the jammer has perfect knowledge of all the basic characteristics of the communication system, except of course, for the hop pattern.

The above simulation model concludes the investigation of the manual spot jamming mode of the $AN/USQ-146$ jammer. As can be observed for all the cases of this mode of operation, the simulation models behaved as the theory predicted.

The next three sections investigate the behavior of the model in repeat jamming. Keeping the same communication model, which corresponds to the SINCGARS system, and making the proper modifications in the channel, the following sections simulate the noise, partial and multitone repeat jamming cases and compare the simulation results with the corresponding theoretical results. For all three cases it is assumed that the $AN/USQ-146$ jammer fulfills all the requirements of a repeat jammer.

6. SINCGARS Model under the Influence of the AN/USQ-146 in Repeat Noise Jamming

This section introduces the simulation model of the $AN/USQ-146$ jammer in repeat jamming. This simulation model is more complicated that the previous models due to the fact that the jammer has knowledge of the system's hop pattern with a probability 0.5.

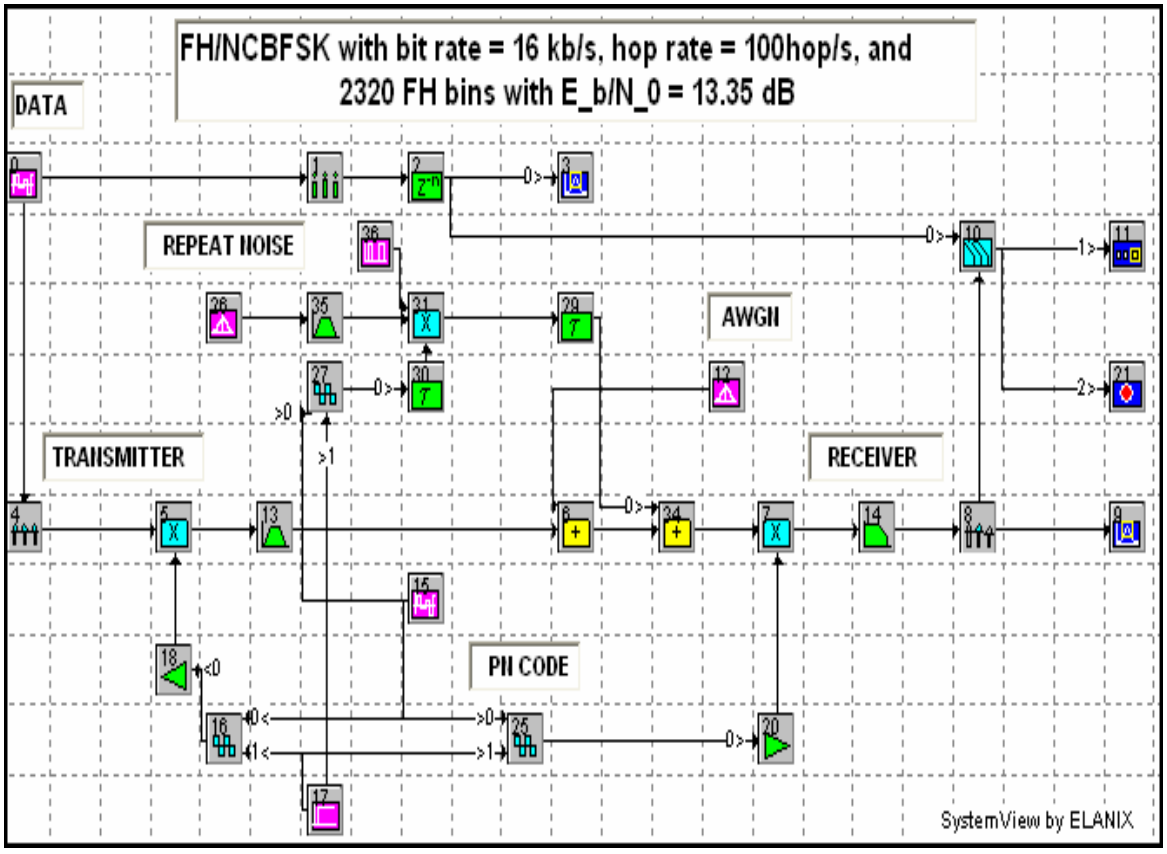

Figure 51. Noise Repeat Model of the $AN/USQ-146$ Jammer over a SINCGARS System

The determinator of the jammer is simulated by one oscillator (token 27), which is driven by the same PN code that the communication system uses (token 15). As can be see in Figure 51, in order to simulate the fact that the determinator of the $AN/USQ-146$ jammer has a probability of correctly determining the hop frequency equal to 0.5, a pulse train is multiplied by the output signal of the jammer (token 36). The pulse train has an equal number of ones and zeros with the result of the existence of the jammer noise interference on the correct hop frequency with a probability equal to 0.5. Token 29 represents the time delay of the jamming interference due to the distance between the jammer and the receiver, and token 30 represents the processing time of the jammer's determinator.

With the help of the SystemView's oscilloscope, the effect of the repeat jammer in the transmitted signal can be observed. The upper part of Figure 52 presents the case in which the jammer has not yet determined the transmitted frequency and the signal has no other interference than the channel noise.

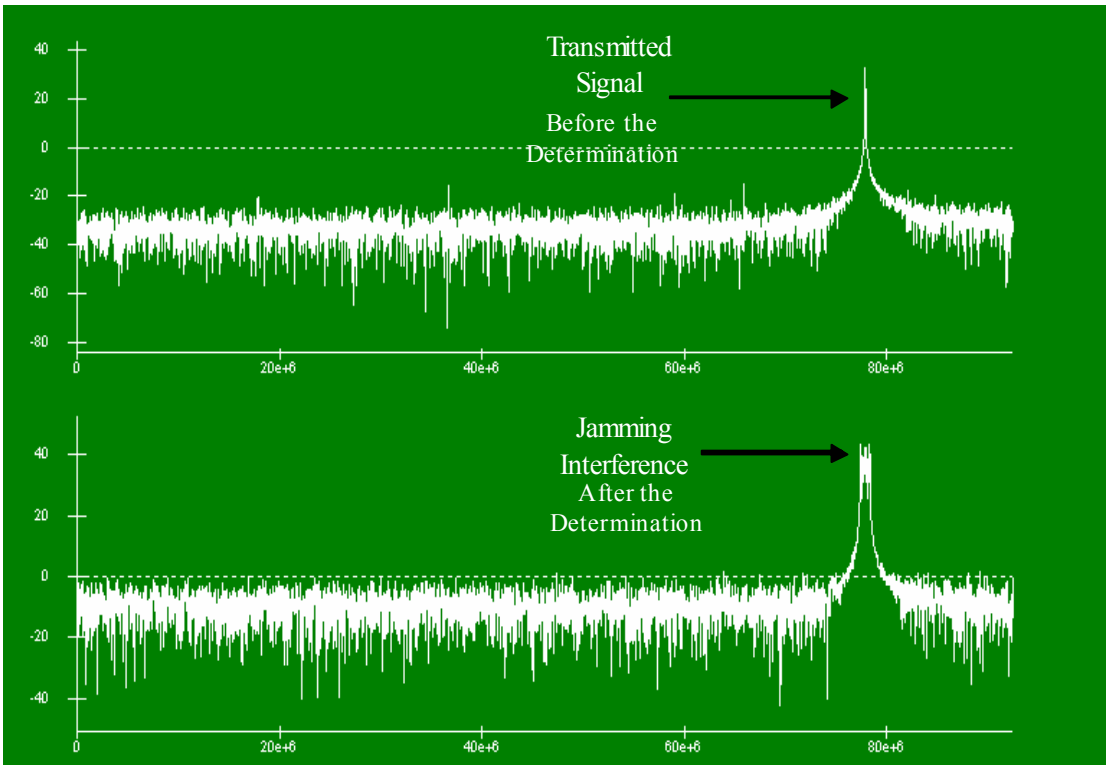

Figure 52. Influence of the $AN/USQ-146$ Jammer in Noise Repeat Jamming before and after the Determination of the Transmitted Frequency

The lower part of Figure 52 presents the case in which the jammer has determined the transmitted frequency and all the noise power of the jammer is centered on the hop frequency. The results of the above simulation for $M = 2, 4, 8$ together with the theoretical results are shown in Figure 53.

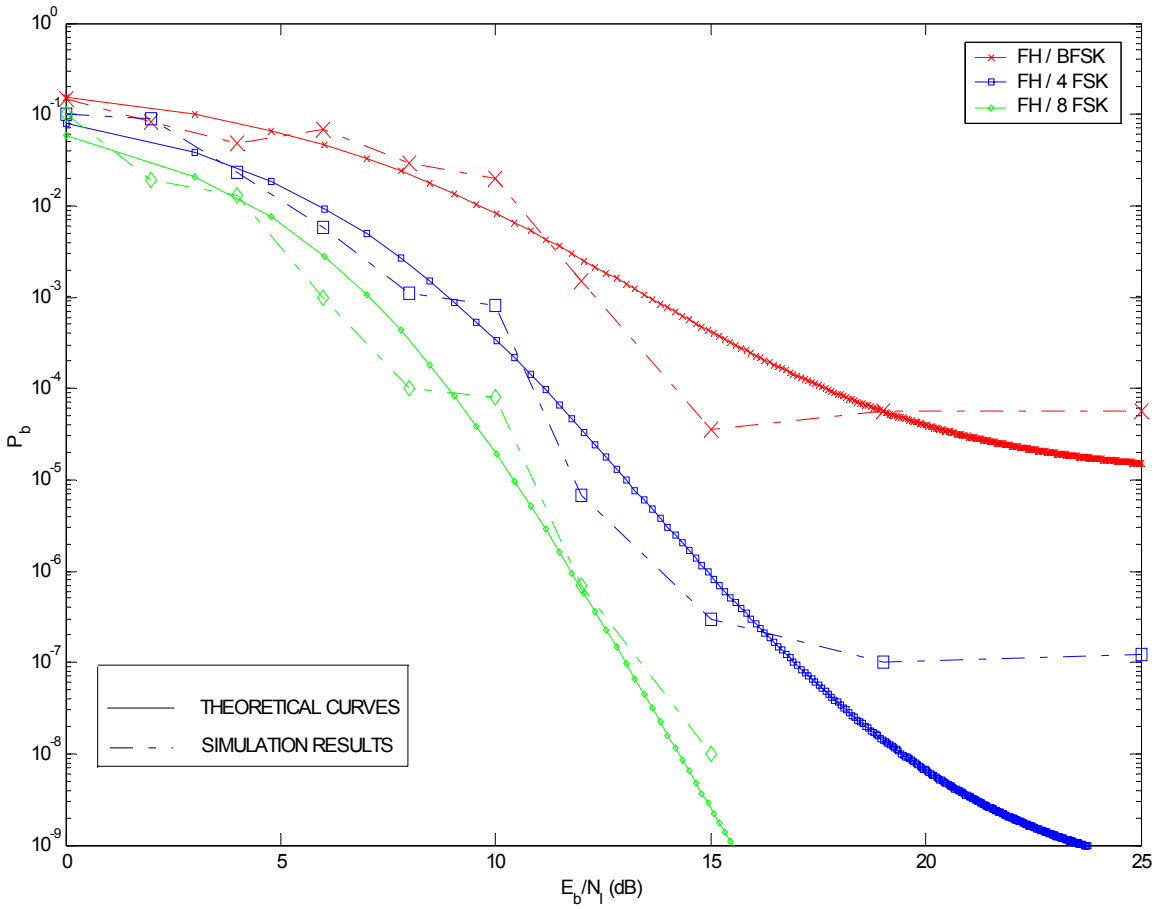

Figure 53. Simulation Results of the Effect of the $AN/USQ-146$ in Repeat Noise Jamming on the Performance of a SINCGARS System in AWGN as Compared to Theoretical Curves

The results in Figure 53 verify that the simulation model behaves in repeat noise jamming as the theory predicts with small variations. As mentioned at the beginning of this chapter, due to software limitations, the simulation model was able to extract useful numerical results only for the probability of bit error greater than or equal to 10^{-9}. This is the reason the probability of error curve in the FH/8 FSK case produced eight numerical simulation results and not ten, as in the other two cases.

The next section examines the model of the $AN/USQ-146$ jammer in repeat partial-band noise jamming and observes its performance in the SINCGARS model.

7. SINCGARS Model under the Influence of the AN/USQ-146 in Repeat Partial-Band Noise Jamming

As discussed in Chapter VII, in repeat partial-band jamming both the communication system and the $AN/USQ-146$ jammer have two choices of operational mode. These are the *conventional* and *unconventional* modes of operation.

As it indicated in the theoretical analysis, the two modes of operation result in four cases. These cases are

- When both the communication system and the jammer are in the conventional mode,
- When both the communication system and the jammer are in the unconventional mode,
- When the system operates in conventional mode and the jammer in the unconventional mode,
- When the system operates in unconventional mode and the jammer in the conventional mode.

The random combination of all the above cases increases the complexity of the simulation model dramatically, as can be seen in Figure 54. The specific model can be described in two parts. The first part is referred to as the upper part of the model and simulates the conventional mode of the system and the jammer. The second part describes the lower structure of the model and represents the unconventional operational mode of the system and the jammer. The combination of the two above cases is achieved with the help of pseudorandom sources that select the operational mode of the system and the jammer randomly.

The upper part of the simulation consists of the conventional transmitter (tokens 4 and 16), the conventional receiver (tokens 8 and 20), and the channel with its AWGN (token 12). The $AN/USQ-146$ jammer operates in conventional mode and consist of tokens 67, 35, 27, 29, 30 and 36.

The lower part of the simulation consist of the unconventional transmitter (tokens $85, 86, 88, 89, 102, 113$), the unconventional receiver (tokens $112, 116, 117, 118$), and the AWGN channel (token 53, the same as token 12). The $AN/USQ-146$ jammer operates in unconventional mode and consist of tokens $61, 67, 77$ and 80.

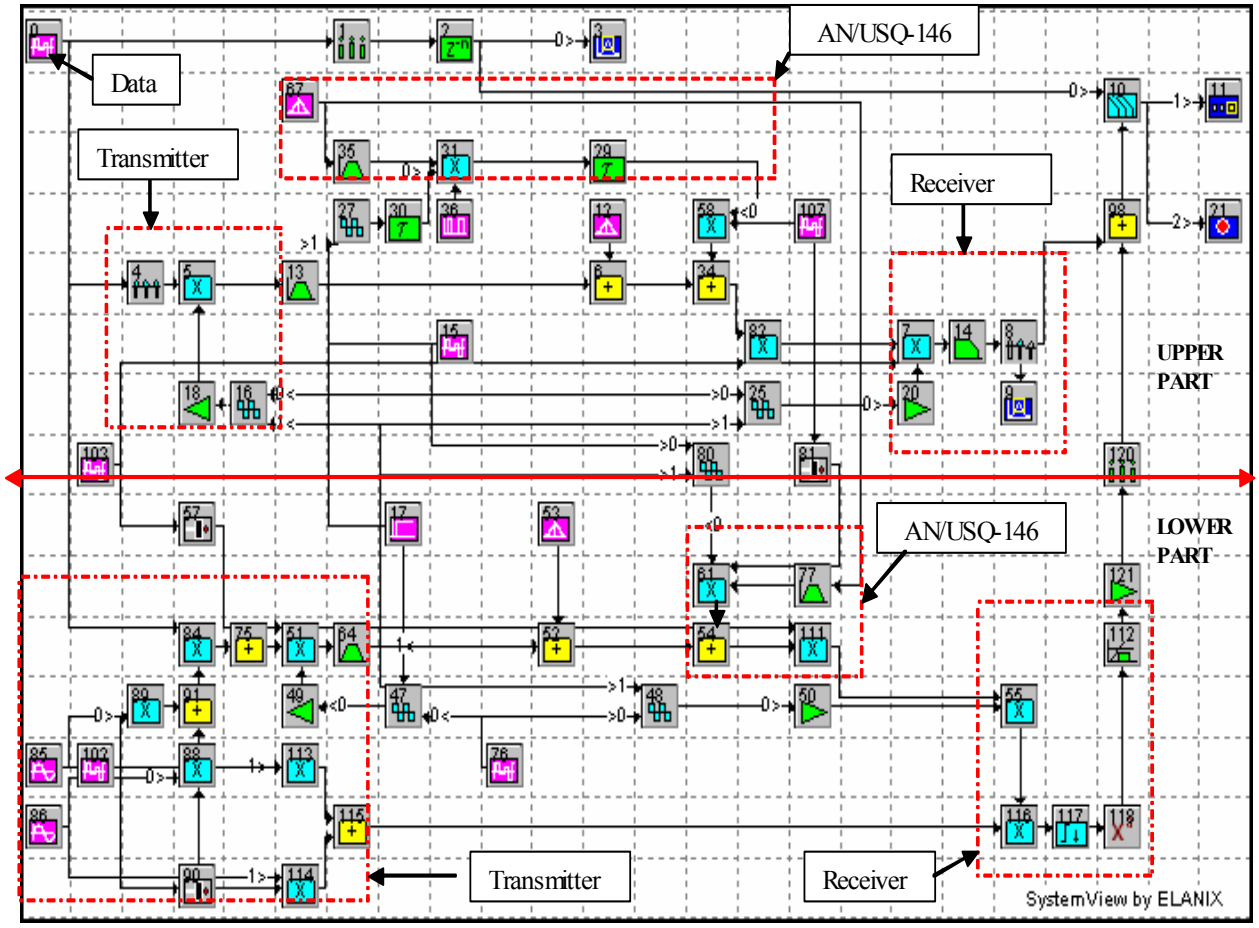

Figure 54. Partial-Band Repeat Model of the $AN/USQ-146$ Jammer over a SINCGARS System for $M = 2$

As Chapter IV demonstrated, in the unconventional mode, the FH/MFSK transmitter randomly chooses one of the M tones (tokens $85, 86$) and transmits it to one of the $r \le N$ frequency slots (token 76), where the set of r frequency slots are selected pseudorandomly (token 76). The transmitted M tones do not carry any information, but the presence or absence of energy in the r selected frequency slots conveys the information.

In this case, $\log_2(r)$ information bits are transmitted. A common assumption is to set $r = M$. The receiver consists of a bank of radiometers (token 117,118) measuring the energy in the in the r frequency slots. The slot with the largest energy is chosen as the transmitted symbol. In Figure 54, the case of $M = 2$ is presented. For the cases of $M = 4$ and $M = 8$, the number of sinusoid sources increases to 4 and 8 respectively.

Finally the random selection of the operational mode of the communication system and the jammer is controlled by two different random sources of ones and zeros (tokens 103, 107).

In the following figures, with the help of the SystemView's oscilloscope, the four cases that exist in the above system can be observed. In Figure 55, both SINCGARS and the $AN/USQ-146$ jammer operate in conventional mode. By comparing the upper and lower part of the figure, it is clear that the jammer has detected the hop frequency and jams the signal.

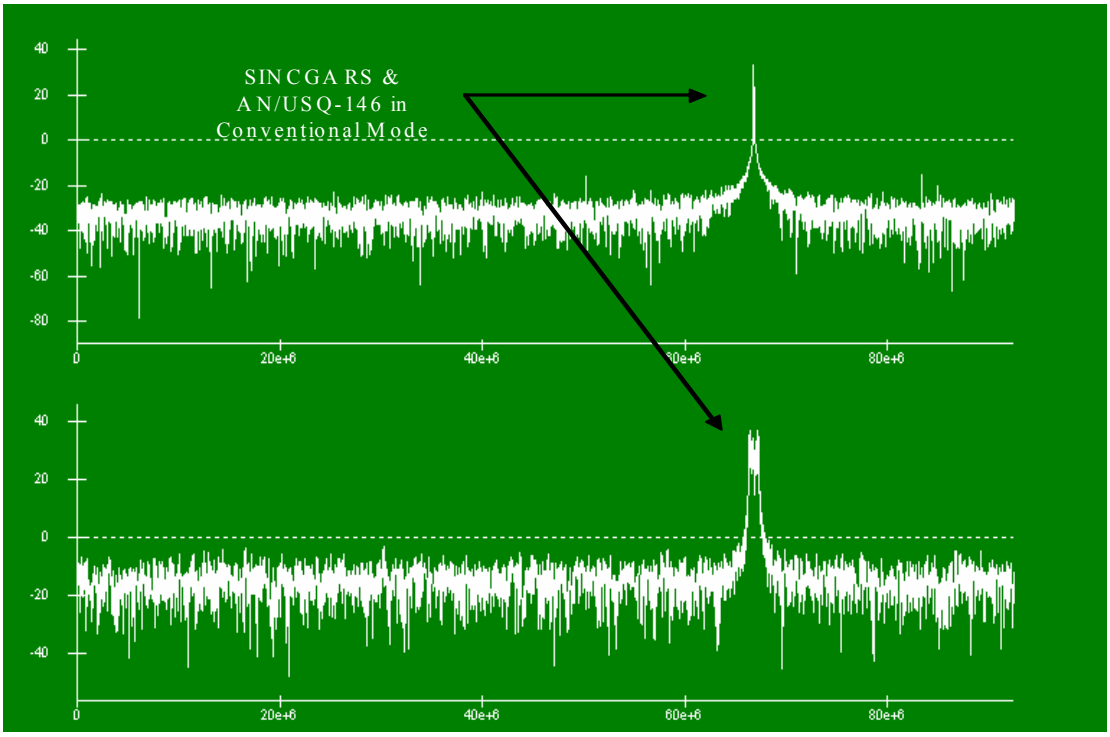

Figure 55. SINCGARS and the $AN/USQ-146$ Jammer in Conventional Mode

Figure 56 shows the case in which the communication system operates in conventional mode and the jammer in unconventional mode of operation. It is obvious that the jammer causes no degradation in the system's performance.

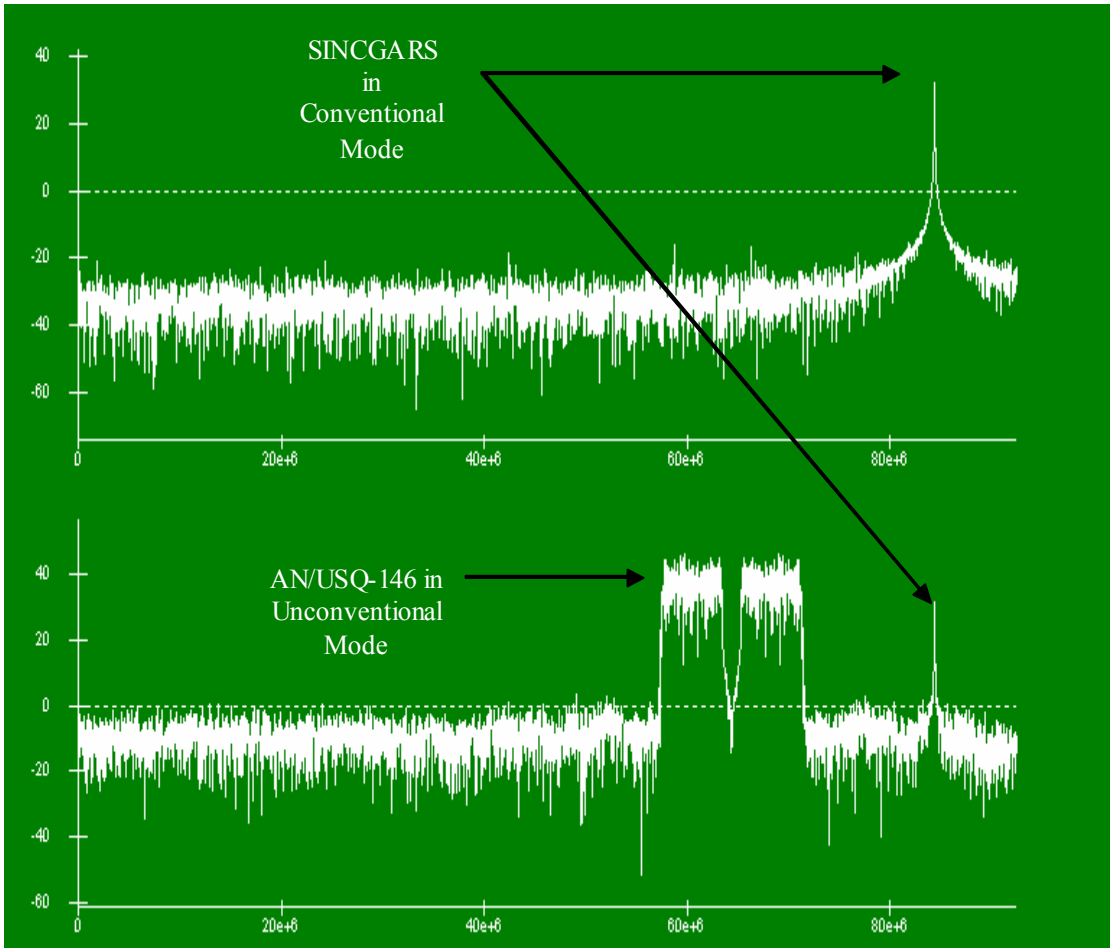

Figure 56. SINCGARS in Conventional Mode and the $AN/USQ-146$ Jammer in Unconventional Mode

Figure 57 shows the case in which the communication system operates in unconventional mode and the jammer in conventional mode of operation. It becomes apparent that the jammer has no effect on the system's performance most of the time.

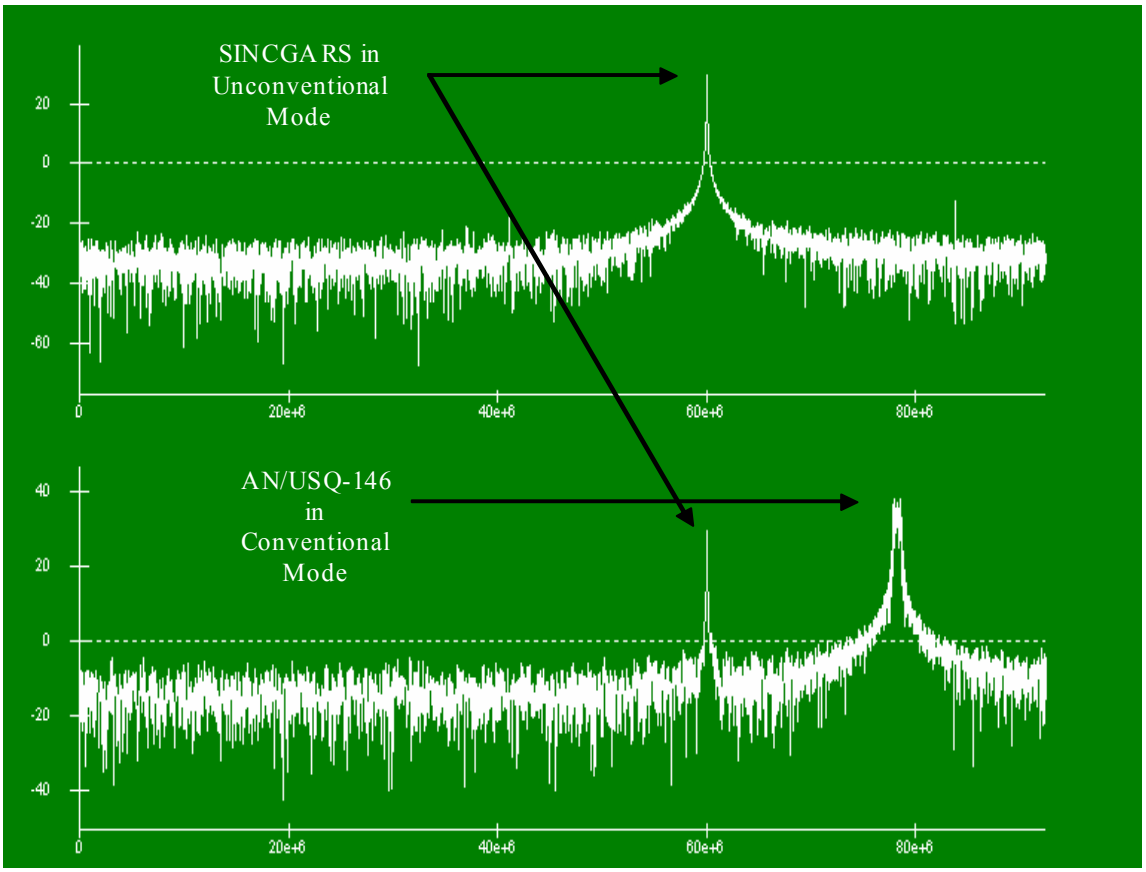

Figure 57. SINCGARS in Unconventional Mode and the $AN/USQ-146$ Jammer in Conventional Mode

Finally Figures 58 and 59 present the case in which both the SINCGARS and the $AN/USQ-146$ jammer operate in unconventional mode. As the theory describes, the jammer randomly selects a part of the transmitted bandwidth and transmits its power. As a result, this sometimes causes the signal to be jammed by the jamming power (Figure 58) and causes the signal to remain unaffected from the jammer's efficiency at other times (Figure 59).

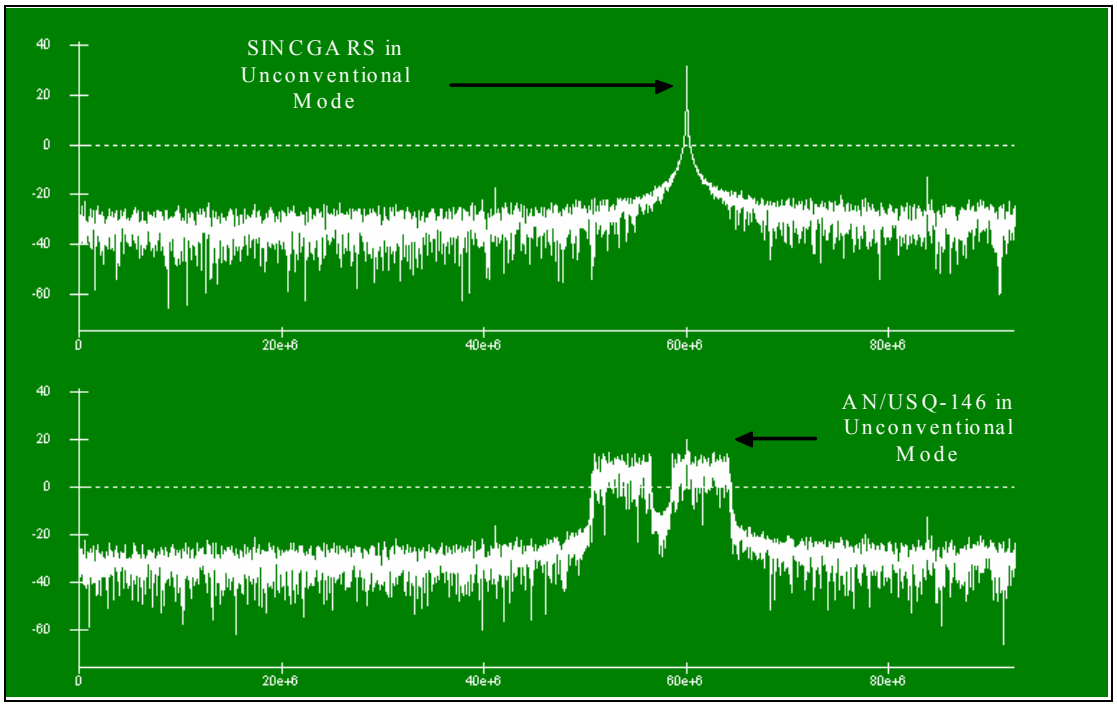

Figure 58. The SINCGARS and the $AN/USQ-146$ Jammer in Unconventional Mode When the Jammer Affect the Communication System

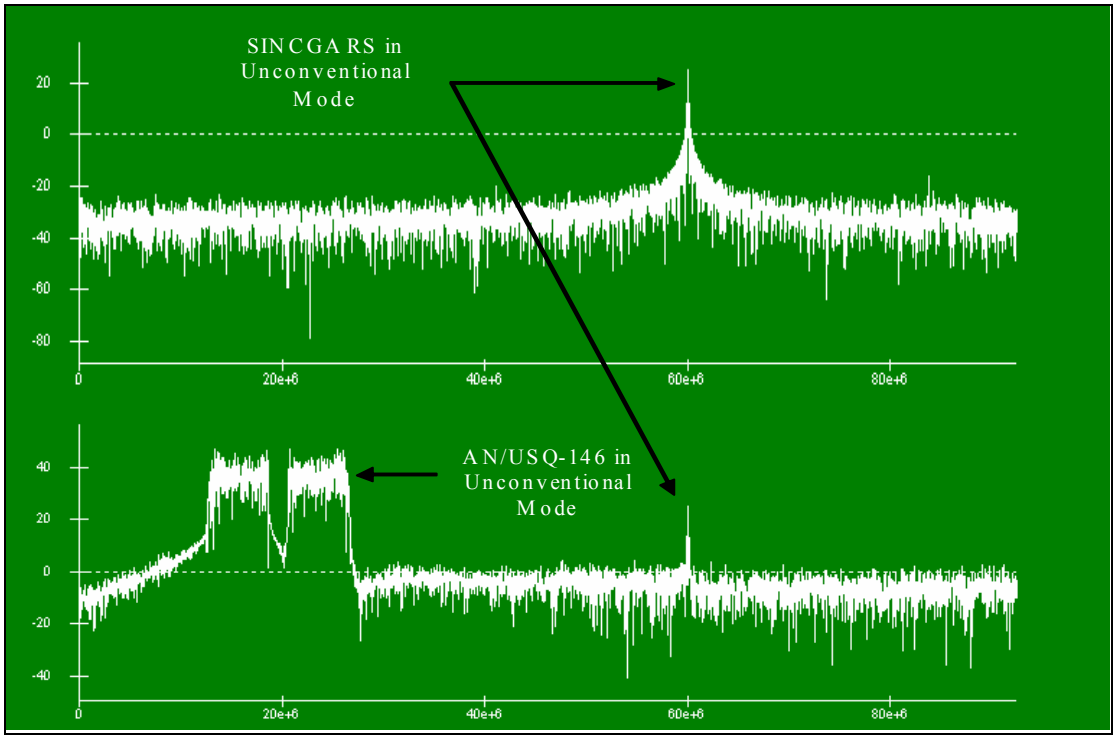

Figure 59. The SINCGARS and the $AN/USQ-146$ Jammer in Unconventional Mode When the Jammer Does Not Affects the Communication System

The results of the above simulation for $M = 2, 4, 8$ together with the theoretical results are shown in Figure 60. It can be seen that the simulation model behave in follower PBJ as the theory predicts with small variations.

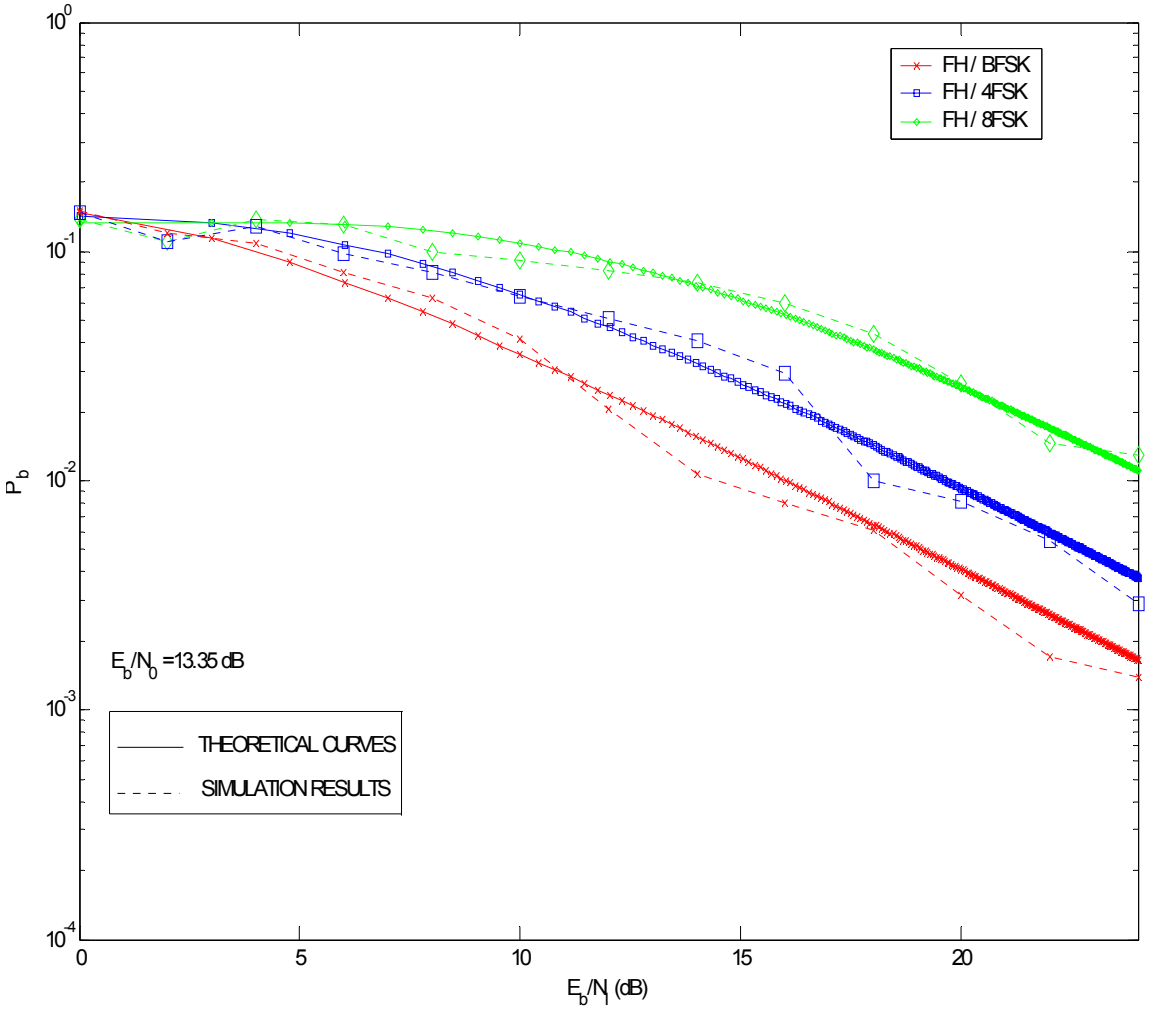

Figure 60. Simulation Results of the Effect of the $AN/USQ-146$ in Repeat Partial-Band Jamming on the Performance of a SINCGARS System in AWGN as Compared to Theoretical Curves

The next section investigates the influence of the $AN/USQ-146$ jammer in repeat multitone noise jamming. This is the last and most important jamming strategy of the specific jammer since the theoretical analysis concluded that the repeat multitone noise jamming causes the largest degradation in a FH/MFSK system.

8. SINCGARS Model under the Influence of the AN/USQ-146 in Repeat Multitone Noise Jamming

As mentioned in Chapter VII, for this case, the source of interference for the channel is the transmission of q tones by the $AN/USQ-146$ jammer. The power of each tone is large enough to dominate a communicator's tone. Based on [1] and [10], the $AN/USQ-146$ jammer can choose to inject multiple tones per channel. Due to this capability the jammer can operate in two modes: *conventional* and *unconventional*.

In the *conventional* mode the jammer injects a single tone in the transmitter's channel and transmits the other $q-1$ tones in $s \le q-1$ distinct and randomly chosen channels. In the *unconventional* mode the jammer does not jam the transmitter's channel, but randomly distributes its q tones over the other $N-1$ distinct channels such that each channel has at most one interfering tone.

Since the communication system also has two modes of operation, the simulation model is a combination of four cases. These cases are

- When both the communication system and the jammer are in the conventional mode,
- When both the communication system and the jammer are in the unconventional mode,
- When the system operates in conventional mode and the jammer in the unconventional mode,
- When the system operates in unconventional mode and the jammer in the conventional mode.

The random combination of all the above cases increases the complexity of the simulation model dramatically, as can be seen in Figure 61. The specific model can be described in two parts. The first one is referred to as the upper part of the model and simulates the conventional mode of the system and the jammer. The second part describes the lower structure of the model and represents the unconventional operational mode of the system and the jammer. The combination of the two above cases is achieved with the help of pseudorandom sources that select the operational mode of the system and the jammer randomly.

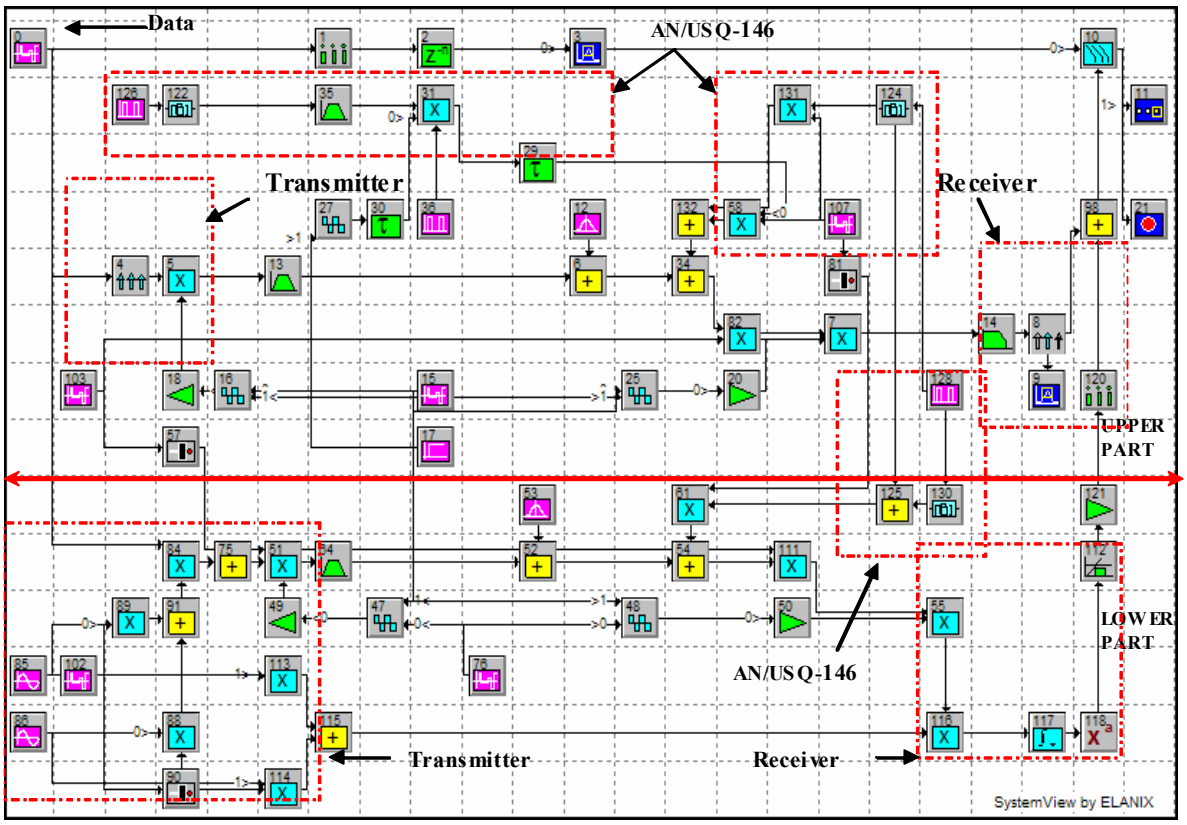

Figure 61. Follower Tone Jamming Model of the $AN/USQ-146$ Jammer over the SINCGARS System for $M = 2$

The upper part of the simulation consists of the conventional transmitter (tokens 4 and 16), the conventional receiver (tokens 8 and 120), and the channel with its AWGN (token 12). The $AN/USQ-146$ jammer operates in conventional mode and consist of tokens $27, 29, 30, 31, 35, 122, 124$ and 126. As can be observed in this case, the source of interference is simulated by the NBI token, which was presented in the simulation model for the multitone manual spot jamming. In this case, the jammer transmits a single tone in the transmitter's channel (token 22) and transmits the other two tones in two distinct and randomly chosen channel (token 24).

The lower part of the simulation consist of the unconventional transmitter (tokens $85, 86, 88, 89, 102$ and 113), the unconventional receiver (tokens $112, 116, 117$ and 118), and the channel with its AWGN (token 53, the same as token 12). Figure 61 presents the case for $M = 2$. For the cases of $M = 4, 8$ the number of sinusoid sources increase to

4 and 8 respectively. In the lower part of the model the $AN/USQ-146$ jammer operates in unconventional mode and consists of tokens 124, 125 and 130. In this case the jammer does not jam the transmitter's channel but randomly distributes its three tones over three distinct channels. Finally, the random selection of the operational mode of the communication system and the jammer is controlled by two different random sources of ones and zeros (tokens 103 and 107).

In a series of four figures, with the help of the SystemView's oscilloscope, the four cases that exist in the above system can be observed. In Figure 62, both the SINCGARS and the $AN/USQ-146$ jammer operate in conventional mode. By comparing the upper and lower part of the figure, it is clear that the jammer has detected the hop frequency and jams the signal with one tone. The other two tones are transmitted randomly in the remaining channels.

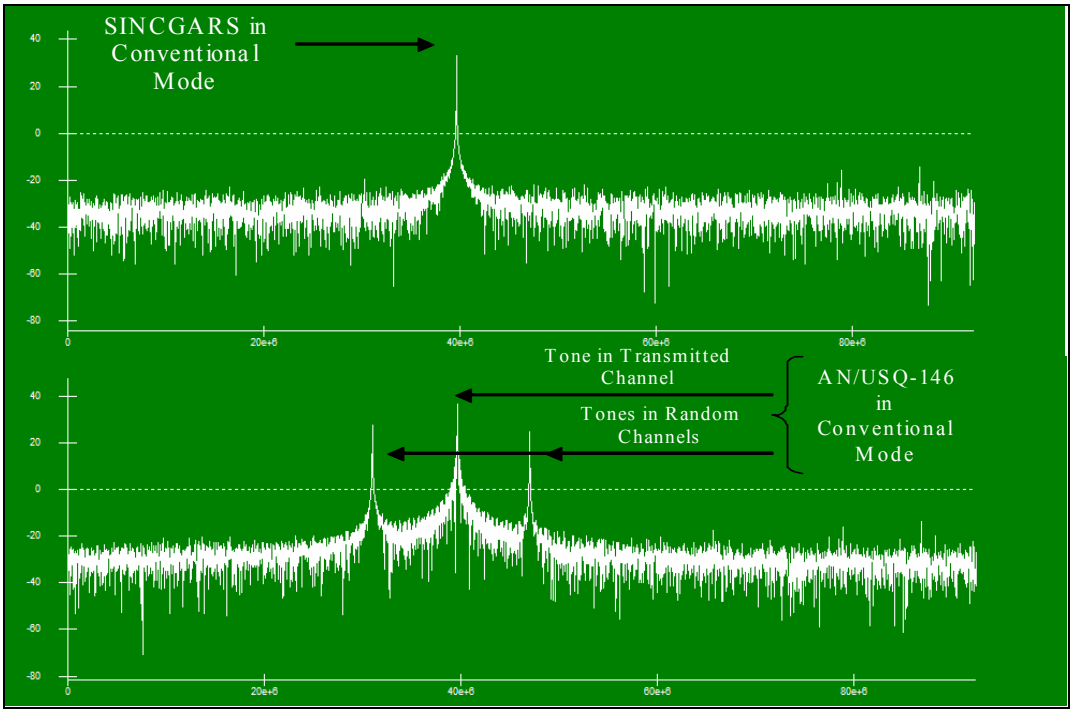

Figure 62. SINCGARS and the $AN/USQ-146$ Jammer in Conventional Mode

Figure 63 indicates the case in which the communication system operates in conventional mode and the jammer in the unconventional mode of operation. It is obvious that the jammer causes no degradation in the system's performance.

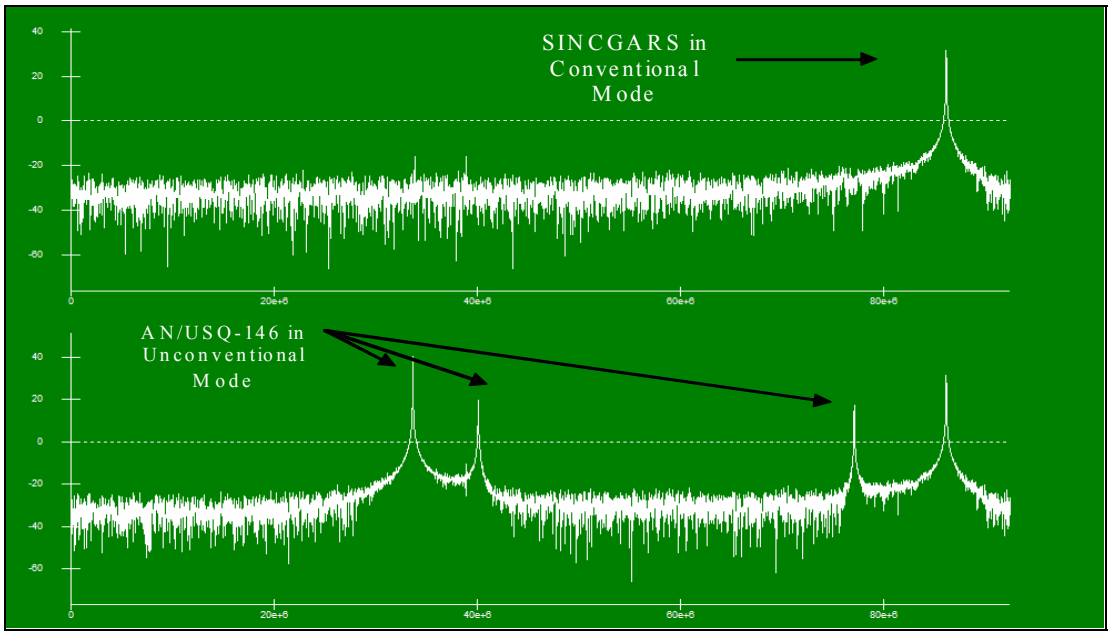

Figure 63. SINCGARS in Conventional Mode and the $AN/USQ-146$ Jammer in Unconventional Mode

Figure 64 shows the case in which the communication system operates in unconventional mode and the jammer in conventional mode. Due to the fact that the two tones, with finite probability, can coincide with one of the transmitter's unconventional channels, the error probability is nonzero.

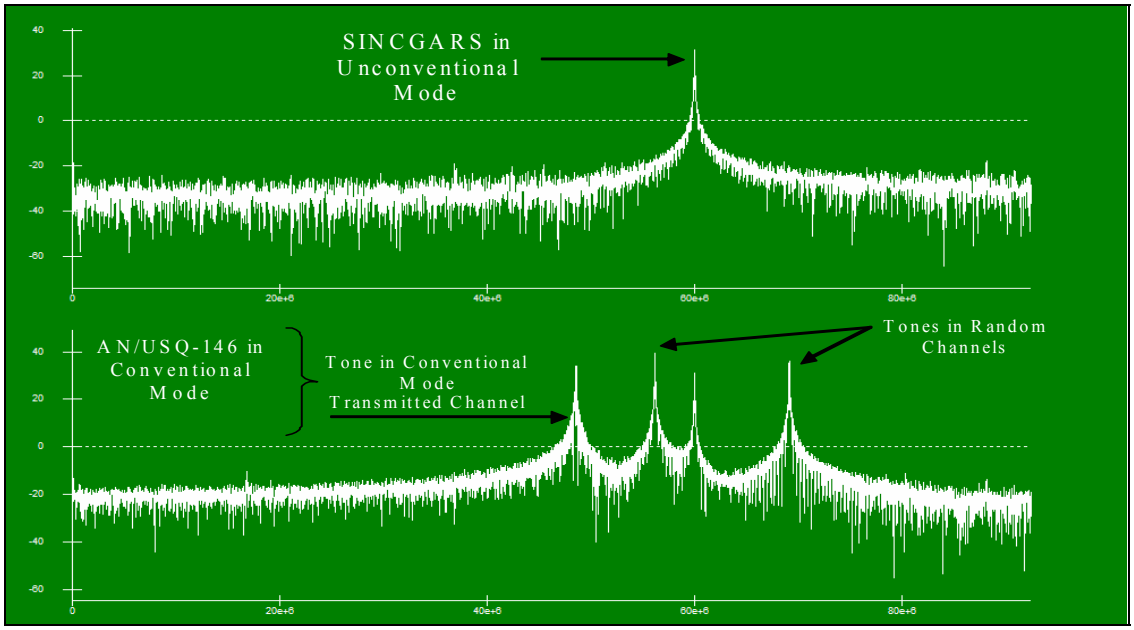

Figure 64. SINCGARS in Unconventional Mode and the $AN/USQ-146$ Jammer in Conventional Mode

Finally, Figure 65 presents the case in which both the SINCGARS and the $AN/USQ-146$ jammer operate in unconventional mode. As the theory predicts, the jammer randomly selects three channels and transmits the jammer's tones.

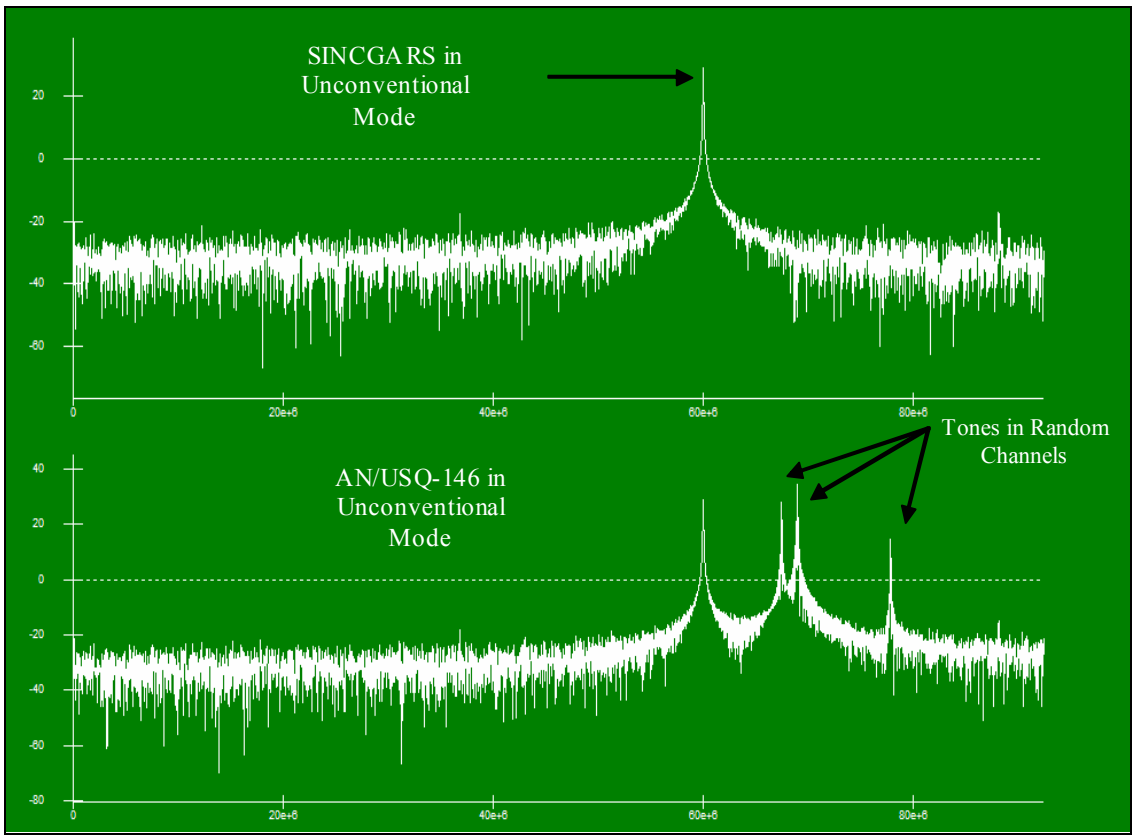

Figure 65. SINCGARS and the $AN/USQ-146$ Jammer in Unconventional Mode

The results of the above simulation for $M = 2, 4$ and 8 together with the theoretical results are shown in Figure 66. It becomes obvious that the simulation model behaves in follower multitone jamming as the theory predicts with small variations. Figure 66 also verifies that, as mentioned in the theoretical analysis, the performance of the communication system becomes inversely proportional to the modulation order.

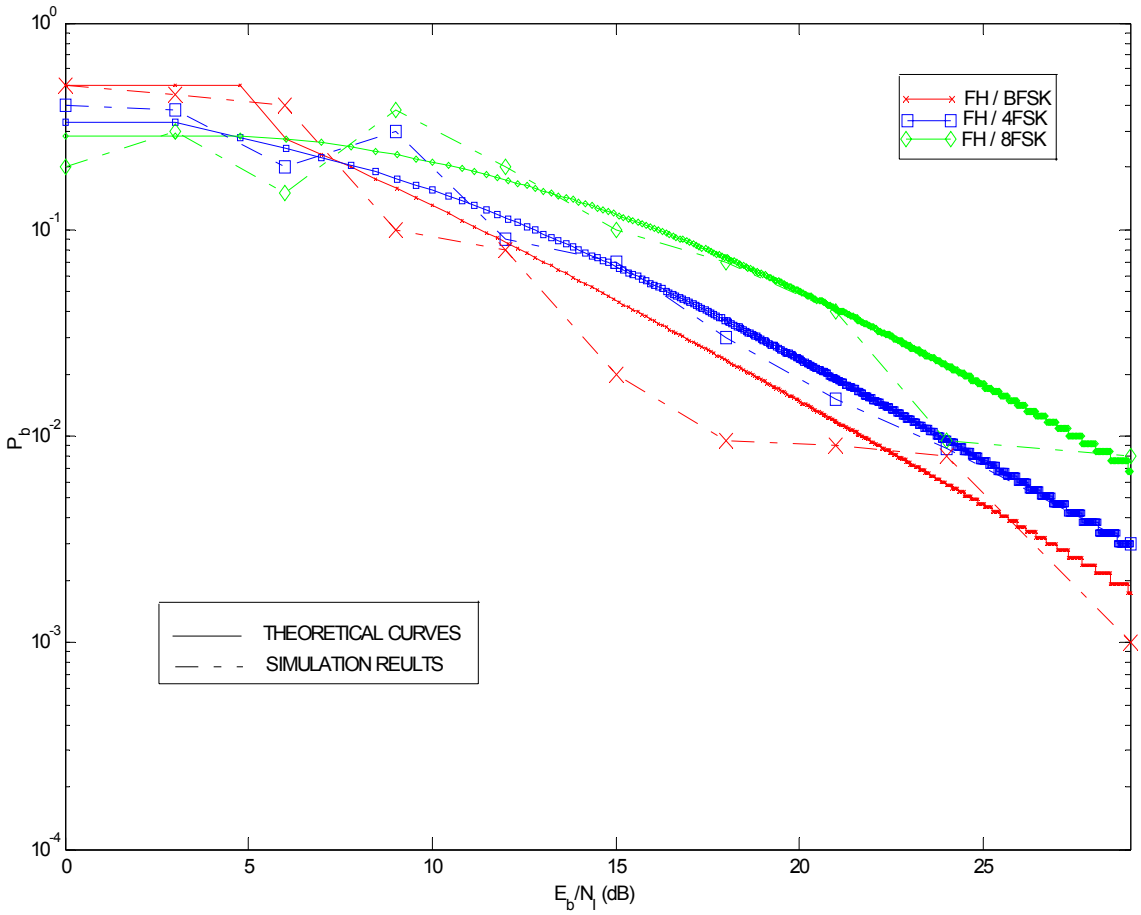

Figure 66. Simulation Results of the Effect of the $AN/USQ-146$ in Repeat Multitone Jamming $(q=2)$ on the Performance of a SINCGARS System in AWGN as Compared to Theoretical Curves

This completes the simulation modeling of all the operational modes of the $AN/USQ-146$ jammer in a FH/MFSK system. Figures 40, 43, 46, 50, 53, 60 and 66 prove that the simulation models behave as the theoretical analysis predicted in Chapters IV and VII.

Regarding a probabilistic performance, verifying the theoretical results from the simulation models that were introduced in Chapter VIII guarantees that the $AN/USQ-146$ jammer performs optimally in a FH/MFSK system when the jammer's operator selects the follower multitone jamming mode. If the jammer does not have the capability to work in this mode, the next most efficient strategy is the repeat partial-band jamming. On the

other hand, in the case when the jammer cannot operate in repeat mode the most effective mode for the degradation of a slow FH/MFSK system is the manual spot multitone jamming technique. This technique can cause a significant error in a slow FH/MFSK system when the jammer has complete knowledge of the signal structure.

The next section investigates, with the help of the SystemView software, the influence of the $AN/USQ-146$ jammer in the IEEE 802.11*a* Standard WLAN system. The purpose of this simulation is to present the performance of the $AN/USQ-146$ jammer in a non-FH commercial system. This section can be considered as a pioneer step to a future work with the main objective of employing military jammers against new commercial technologies.

B. SIMULATION OF THE AN/USQ-146 JAMMER PERFORMANCE IN A IEEE 802.11A COMMUNICATION SYSTEM

Before analyzing the simulation model of the 802.11*a* system under the influence of the $AN/USQ-146$ jammer, the assumptions that were made must first be indicated in order for the following results to be understood.

The IEEE 802.11*a* Standard is designed to operate in the 5-GHz frequency range with an available bandwidth of 300 MHz. As mentioned in Chapter II, the $AN/USQ-146$ jammer can operate in the 1.5 to 2500-MHz frequency ranges. On the other hand, based on Reference [11], the new model of the $AN/USQ-146$ jammer (Rubicon II) can perform at frequencies up to 8.4 GHz. The assumption that was made for the following simulation models is that the power specifications of Rubicon II and the $AN/USQ-146$ jammer, for the manual spot jamming mode, are exactly the same. The above assumption is based only on [11] since the manufacturer considers the detailed operational characteristics of the Rubicon II to be classified.

The next section presents a description of the basic characteristics of the 802.11*a*. This description was used as a guideline in the structure of the simulation model.

1. IEEE 802.11a Basic Characteristics

The 802.11*a* standard, which supports data rates of up to 54 Mbps, is the Fast Ethernet analog to the 802.11*b*, which supports data rates of up to 11 Mbps. Like Ethernet and Fast Ethernet, 802.11*b* and 802.11*a* use an identical MAC (Media Access Control). However, while Fast Ethernet uses the same (except that it is faster) physical-layer encoding scheme as Ethernet, the 802.11*a* uses an entirely different encoding scheme, called *Orthogonal Frequency Division Multiplexing* (OFDM).

Based on the IEEE standard (Reference [12]), the 802.11*a* system is designed to operate in the 5-GHz frequency range. Specifically, the FCC has allocated 300 MHz of spectrum for unlicensed operation in the 5-GHz block, 200 MHz of which is at 5150 MHz to 5350 MHz, with the other 100 MHz at 5725 MHz to 5825 MHz. The spectrum is split into three working domains. The first 100 MHz in the lower section is restricted to a maximum power output of 50 mW. The second 100 MHz has a more generous 250 mW power budget, while the top 100 MHz is delegated for outdoor applications, with a maximum of 1 W power output. This specific portion of bandwidth can be interfered by the $AN/USQ-146$ jammer (Rubicon II).

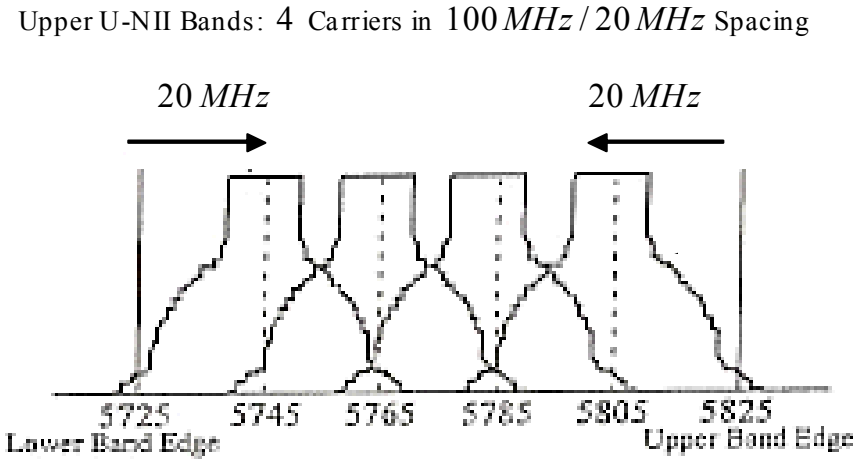

Figure 67. Four Independent Clear Channels in the Upper 100 MHz of the 5-GHz Spectrum [From Ref. 14]

The 802.11*a* standard gains some of its performance from the higher frequencies at which it operates. The laws of information theory tie frequency, radiated power and distance together in an inverse relationship. Thus, moving up to the 5-GHz spectrum from 2.5-GHz (802.11*b*) leads to shorter distances, given the same radiated power and encoding scheme. In addition, the encoding mechanism used to convert data into analog radio waves can encode one or more bits per radio cycle (Hertz). By rotating and manipulating the radio signal, vendors can encode more information in the same time slice. To ensure that the remote host can decode these more complex radio signals, more power must be used at the source to compensate for signal distortion and fade. The 802.11*a* technology overcomes some of the distance loss by increasing the EIRP to the maximum 1 W.

However, power alone is not enough to maintain the 802.11*b*-like distances in an 802.11*a* environment. To compensate, vendors specified and designed a new physical-layer encoding technology that departs from the traditional direct-sequence technology being deployed today. This technology is called COFDM (coded OFDM). COFDM works by breaking one high-speed data carrier into several lower-speed subcarriers, which are then transmitted in parallel. Each high-speed carrier is 20 MHz wide, as Figure 67 shows, and is broken up into 52 subchannels, each approximately 300 kHz wide. COFDM uses 48 of these subchannels for data, while the remaining four are used for error correction. COFDM delivers higher data rates and a high degree of multipath reflection recovery, owing to its encoding scheme and error correction.

2. IEEE 802.11a Simulation Model

The structure of IEEE 802.11*a* model is based on Reference [13]. The suite of the modulation parameters valid for the 802.11*a* system is given in Table 13. In this model, the $54\text{Mbps} - 64\text{QAM}$ $(R = 3/4)$ option is presented.

Data rate (Mbits/s)	Modulation	Coding rate (R)	Coded bits per subcarrier (N_{BPSC})	Coded bits per OFDM symbol (N_{CBPS})	Data bits per OFDM symbol (N_{DBPS})
6	BPSK	1/2	1	48	24
9	BPSK	3/4	1	48	36
12	QPSK	1/2	2	96	48
18	QPSK	3/4	2	96	72
24	16-QAM	1/2	4	192	96
36	16-QAM	3/4	4	192	144
48	64-QAM	2/3	6	288	192
54	64-QAM	3/4	6	288	216

Table 13. 802.11*a* Modulation Parameters [From Ref. 13]

The overall block diagram is shown in Figure 68. The 54 Mbps data source (token 10) is first sampled at once per bit (token 11). Token 12 is the [131,171] constraint length 7 convolutional encoder. The data rate out of the encoder is 108 Mbps. Token 55 follows this, which performs the puncturing operation. The net effect is that for every three bits into the convolutional encoder there are four bits out of the puncture token. Thus the rate is now 72 Mbps. The data is then interleaved in token 27. The bit-to-symbol token 14 and the QMAP token 15 combine to produce the proper baseband I and Q signals. The symbol rate is 12 Msymb/s.

Then it follows the procedure of the packet structure. The General Demultiplexer (token 18) splits the data symbols into the appropriate segments for use by the General Multiplexer (token 19). Token 19 assembles the packet for the I signal, and it has 13 segments in order to create the 48 data subcarriers per symbol. A similar discussion applies for the Q signal. The sync data is controlled by a 7-stage PN source (token 16). The total is 64 carriers required by the OFDM symbol modulator. The final I and Q signals are then sent to the OFDM modulator (token 5).

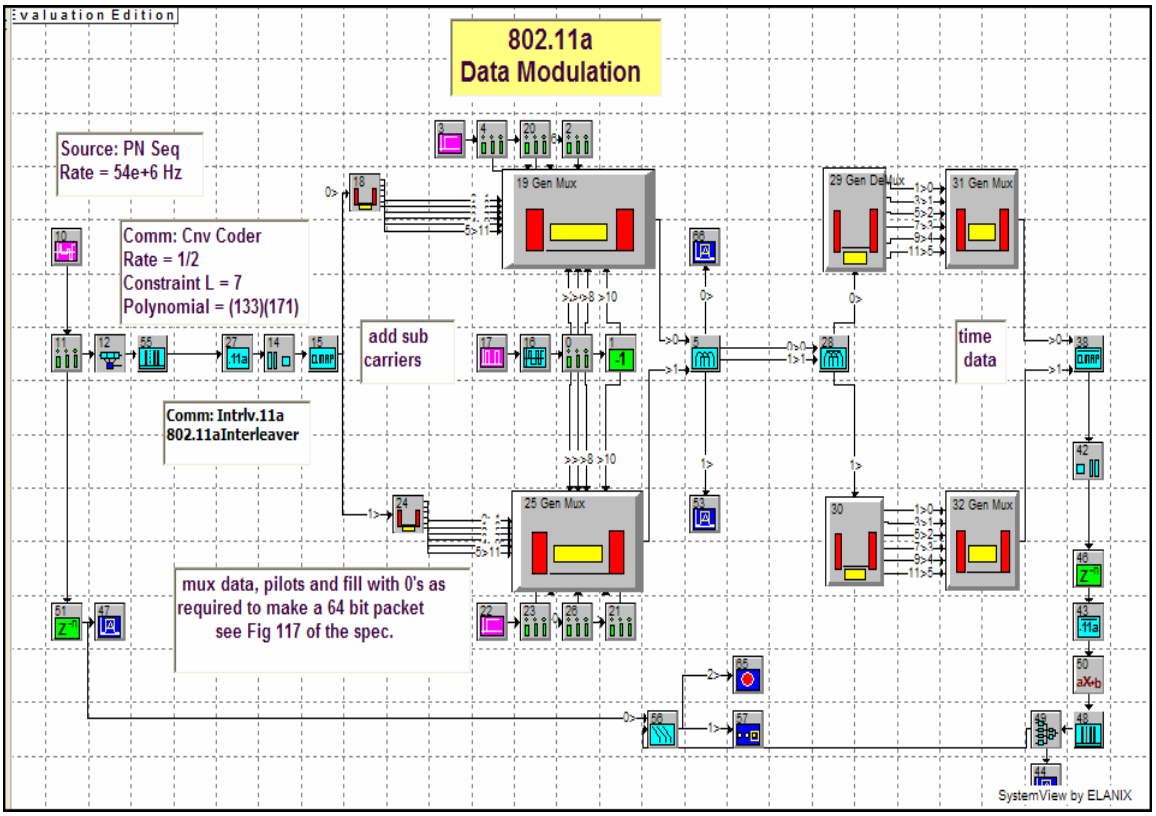

Figure 68. IEEE 802.11*a* Simulation Model

The steps just described for the modulation process are applied in reverse order to recover the original data. In the demodulation process, it is important to emphasize the fact that token 49, which represents the convolutional decoder, operates in soft decision mode. For the hard decision case, the SystemView by Elanix does not produce the correct results. This malfunction in the simulation is caused by the punctured and de-punctured tokens $(55, 48)$. The de-punctured code for every punctured bit adds a zero-bit resulting in the incorrect hard decoding decision from the convolutional decoder (token 49).

On the other hand, the theoretical analysis of the performance of the IEEE 802.11*a*, 64QAM $(R = 3/4)$ in *soft decision decoding* (SDD) is extremely complicated, and there are no any publications referring to the performance of the above communication scheme under the influence of barrage, partial-band or multitone jamming. Only for the case of the IEEE 802.11*a*, 64QAM $(R = 3/4)$ in AWGN it is feasible to compare the simulation results with the theoretical results that were presented in Reference [14].

Before investigating the influence of the $AN/USQ-146$ jammer (Rubicon II) model in different types of manual spot jamming, it is important to observe the above simulation under the effect of the AWGN only in order to verify that the IEEE 802.11*a* model behaves as the theoretical analysis of Reference [14] predicts.

3. IEEE 802.11a Model in AWGN

The simulation model of the IEEE 802.11*a* in AWGN is illustrated in Figure 69. Enabling token 65 as a variable token, the system is executing for ten different, continuously decreasing values of noise power (N_o), which correspond to ten different, continuously increasing, values of E_b/N_0.

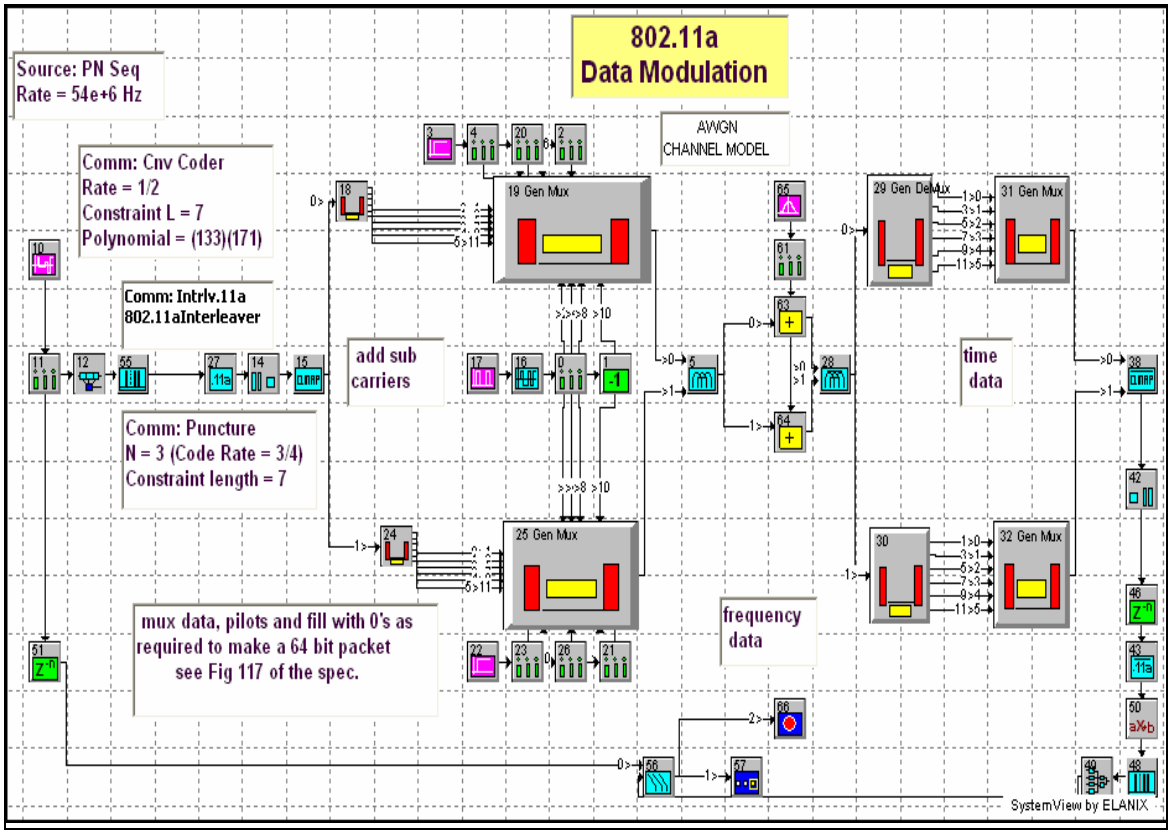

Figure 69. IEEE 802.11*a* Simulation Model in AWGN Channel

In Figure 70, with the help of the SystemView's oscilloscope, one of the four channels of Figure 67 can be observed in detail. The upper part of the figure illustrates the signal spectrum of the 802.11*a* system without noise. In the lower part the influence of the channel noise has been added.

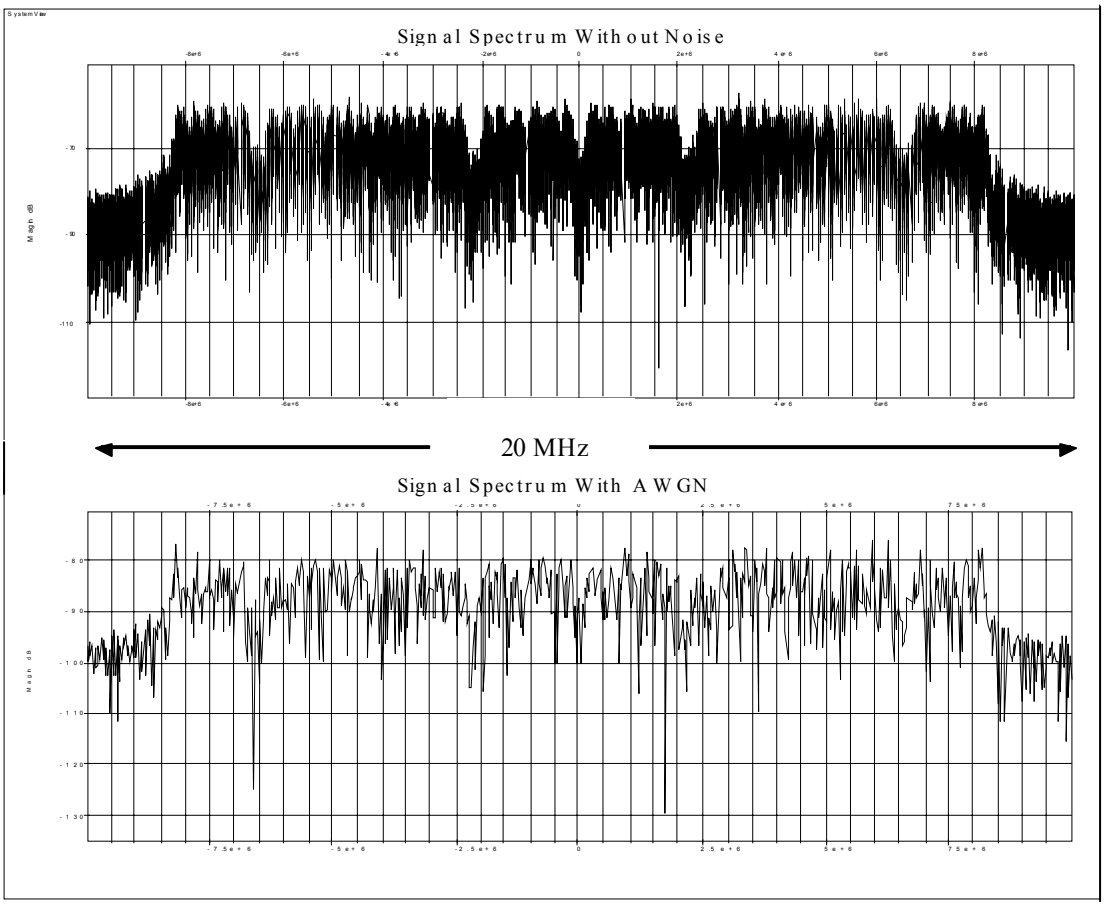

Figure 70. Influence of AWGN in the 802.11*a* 's Signal Spectrum

It is obvious that the AWGN influences the shape of the signal's spectrum. Figure 71 presents the simulated probability of bit error together with the corresponding theoretical results from Reference [14].

The results in Figure 71 verify that the simulation model behaves in the AWGN as the theory predicts with small variations for values of E_b/N_0 between 0 and 9 dB. In this range, the theoretical curve of the probability of bit error is equal to 1. In the simula-

tion model, and also in a real word system, the value of $P_b = 1$ is impossible, so these variations are considered legitimate.

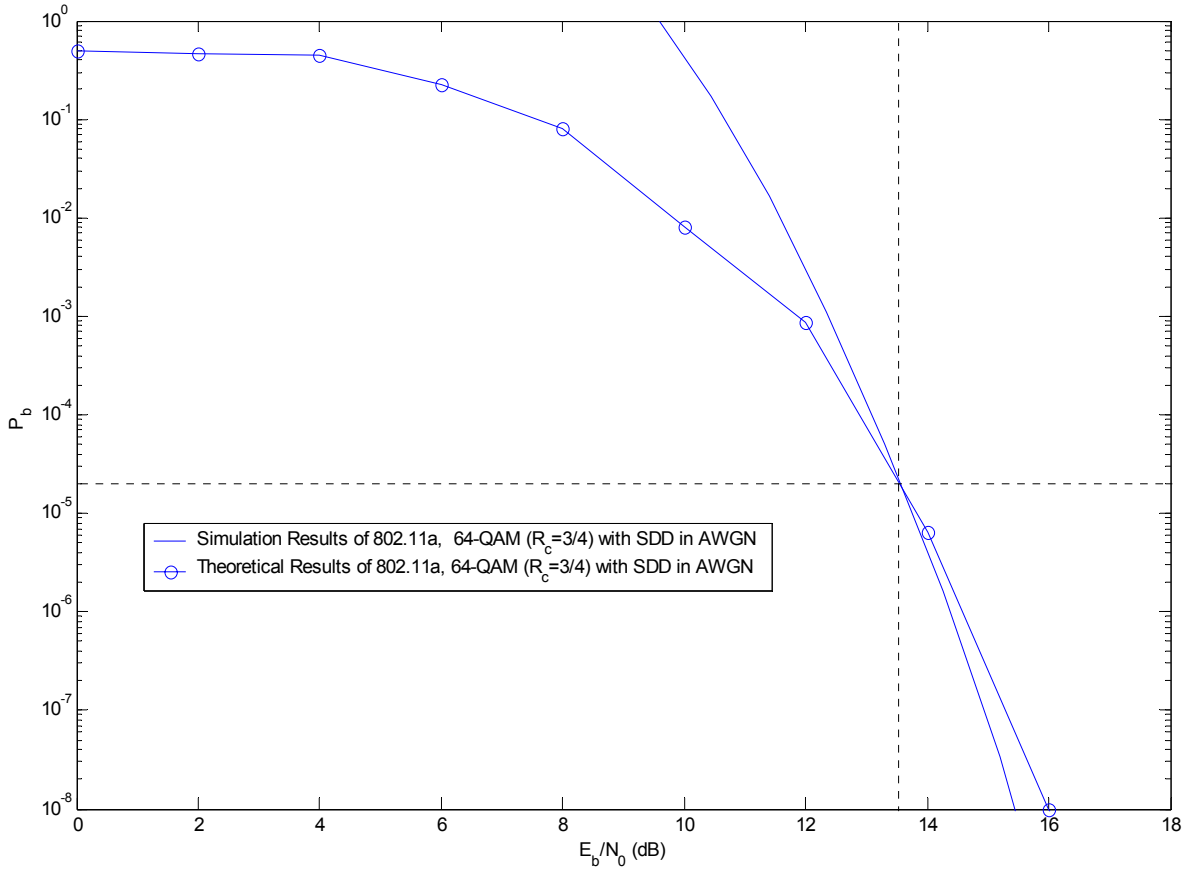

Figure 71. Performance of the $802.11a$, $64-\text{QAM}$ $\left(R_c = 3/4\right)$ with Soft Decision Decoding in AWGN as Compared to Theoretical Curve

The next step is to specify the signal-to-noise ratio $\left(E_b/N_0\right)$ of the channel, add the interference of the $AN/USQ-146$ jammer (Rubicon II) in barrage noise jamming and observe its performance.

4. IEEE 802.11a Model under the Influence of the AN/USQ-146 in Barrage Noise Jamming

The source of interference that the $AN/USQ-146$ jammer (Rubicon II) uses in barrage noise jamming is an AWGN with $N_I = P_I/W_{802.11a}$. This interference is added in

the channel together with the thermal noise of the channel. Based on the assumptions made at the beginning of this section, the output power of the $AN/USQ-146$ is the same as the output power of the Rubicon II. In addition, the description of the $802.11a$ in Section $VIII,B,1$ shows that the bandwidth of each high-speed carrier is $W_{802.11a} = 20$ MHz. On the other hand, in the case of the SINCGARS system, the jammed bandwidth is $W_{ss} = 58$ MHz. That means that the $AN/USQ-146$ can produce a jamming power over the $802.11a$ system, 2.9 times more than that in the SINCGARS case. That is,

$$N_{I_{802.11a}} = 2.9 N_{I_{SINCGARS}} . \tag{8.2}$$

Equation (8.2) increases the $AN/USQ-146$ model's output power density by a factor of 2.9 compared to the noise PSD values that were used in the SINCGARS model.

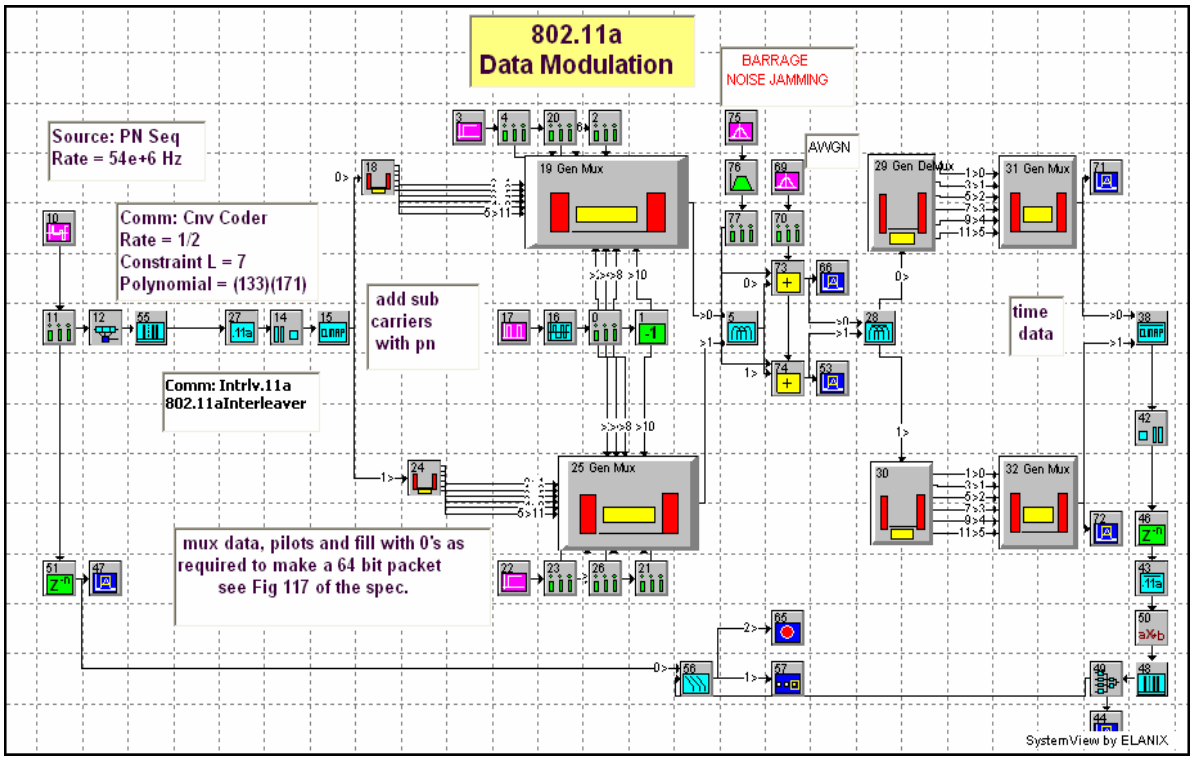

Figure 72. Barrage Noise Jamming Model of the $AN/USQ-146$ (Rubicon II) Jammer over an $802.11a$, $64-\text{QAM}$ $(R_c = 3/4)$ with Soft Decision Decoding

Figure 72 presents the simulation model for the barrage noise jamming of the $802.11a$. The $AN/USQ-146$ in this case consists of tokens 75 and 76. Token 75 represents the noise source and token 76 restricts the output noise power in the bandwidth of

$W_{802.11a}$. As in the previous cases, the AWGN channel (token 69) has a constant value of $E_b/N_0 = 13.35$ dB, which entails a probability of bit error, in the $802.11a$ system, close to 10^{-5}. The jammer is expected to increase the probability of bit error of the system between the range of 0.5 and 10^{-5}. The produced BER curve of the above simulation model can be observed in Figure 73.

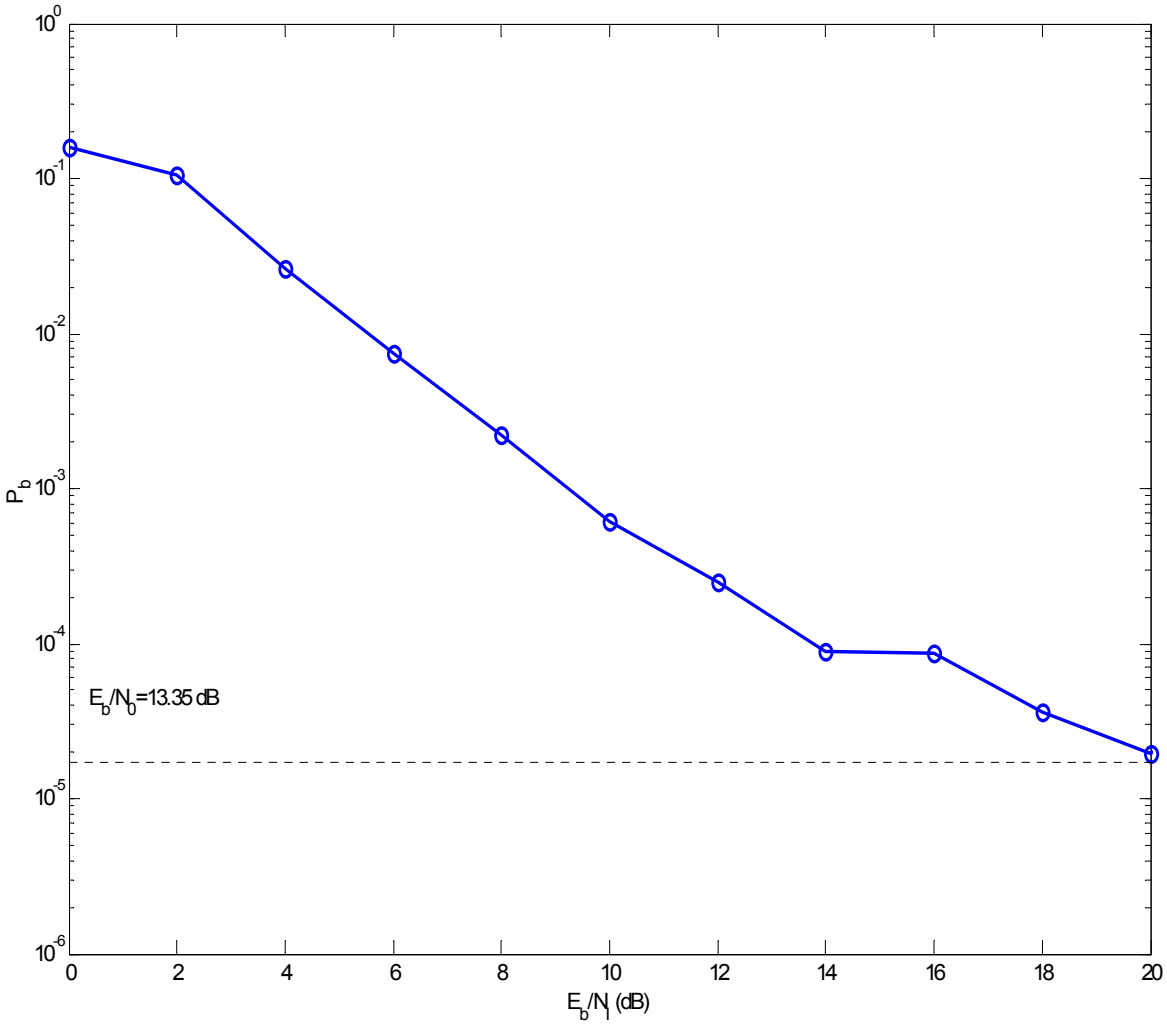

Figure 73. Simulation Results of the Effect of the $AN/USQ-146$ (Rubicon II) in Barrage Noise Jamming on the Performance of an $802.11a$, $64-\text{QAM}$ $(R_c = 3/4)$ with Soft Decision Decoding System in the AWGN

Figure 73 indicates that the $AN/USQ-146$ (Rubicon II) jammer has a satisfactory influence over the $802.11a$ standard when the jamming power becomes equal to the

signal's power $(E_b/N_I \approx 0 \text{ dB})$. For larger values of signal-to-interference noise ratio, a severe decrease in the produced probability of bit error appears. In the range of $0 \text{ dB} \le E_b/N_I < 2 \text{ dB}$, the barrage noise jammer causes an error in the $802.11a$ system, which is 20 dB greater than the error produced by the AWGN. However, the probability of bit error cannot be considered efficient enough. Furthermore, for $E_b/N_I \approx 20$ dB, the BER curve approaches the error floor of 10^{-5}.

The following section investigates the performance of the jammer in partial-band noise jamming for various values of ρ and with the same level of AWGN.

5. IEEE 802.11a Model under the Influence of the AN/USQ-146 in Partial-Band Noise Jamming

The simulation model in the partial-band case is the same as in the BNJ model. The only difference exists in the values of the tokens 75 and 76, which determine the part of the bandwidth that will be jammed and the corresponding output noise PSD.

Table 14 presents the values of $\rho = W_{jammed}/W_{802.11a}$ that will be examined in the model of Figure 74, together with the corresponding values of the jammed bandwidth (token 75) and the jamming noise power N_I (token 76).

ρ	W_{jammed}	Increase in N_I
0.5	10 MHz	$2 \cdot N_I$
0.4	8 MHz	$2.5 \cdot N_I$
0.3	6 MHz	$3.33 \cdot N_I$
0.2	4 MHz	$5 \cdot N_I$
0.1	2 MHz	$10 \cdot N_I$

Table 14. Values of Parameter ρ in Partial-Band Jamming Simulation Model

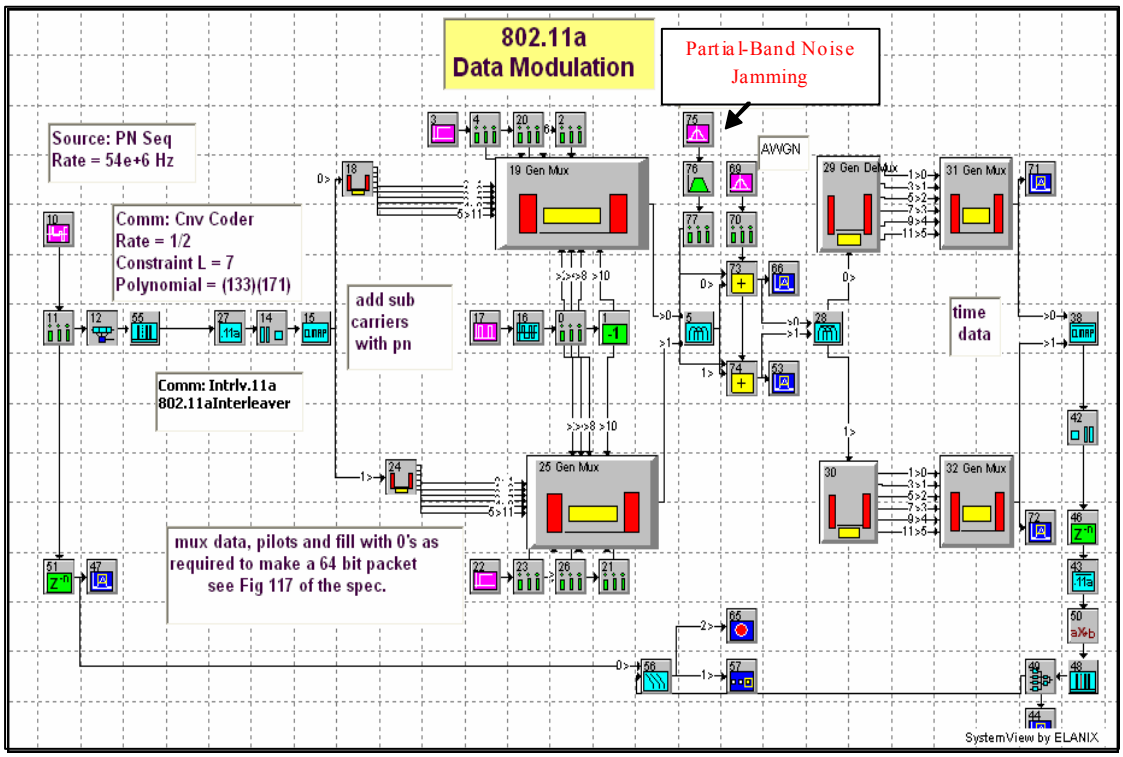

Figure 74. Partial-Band Noise Jamming Model of the $AN/USQ-146$ (Rubicon II) Jammer over an 802.11a, $64-$QAM $(R_c = 3/4)$ with Soft Decision Decoding

For each one of the above values of ρ, the SystemView produced the corresponding probability of bit error curve. Figure 75, for comparison reasons, presents the overlaid plots of BER for all the cases of ρ.

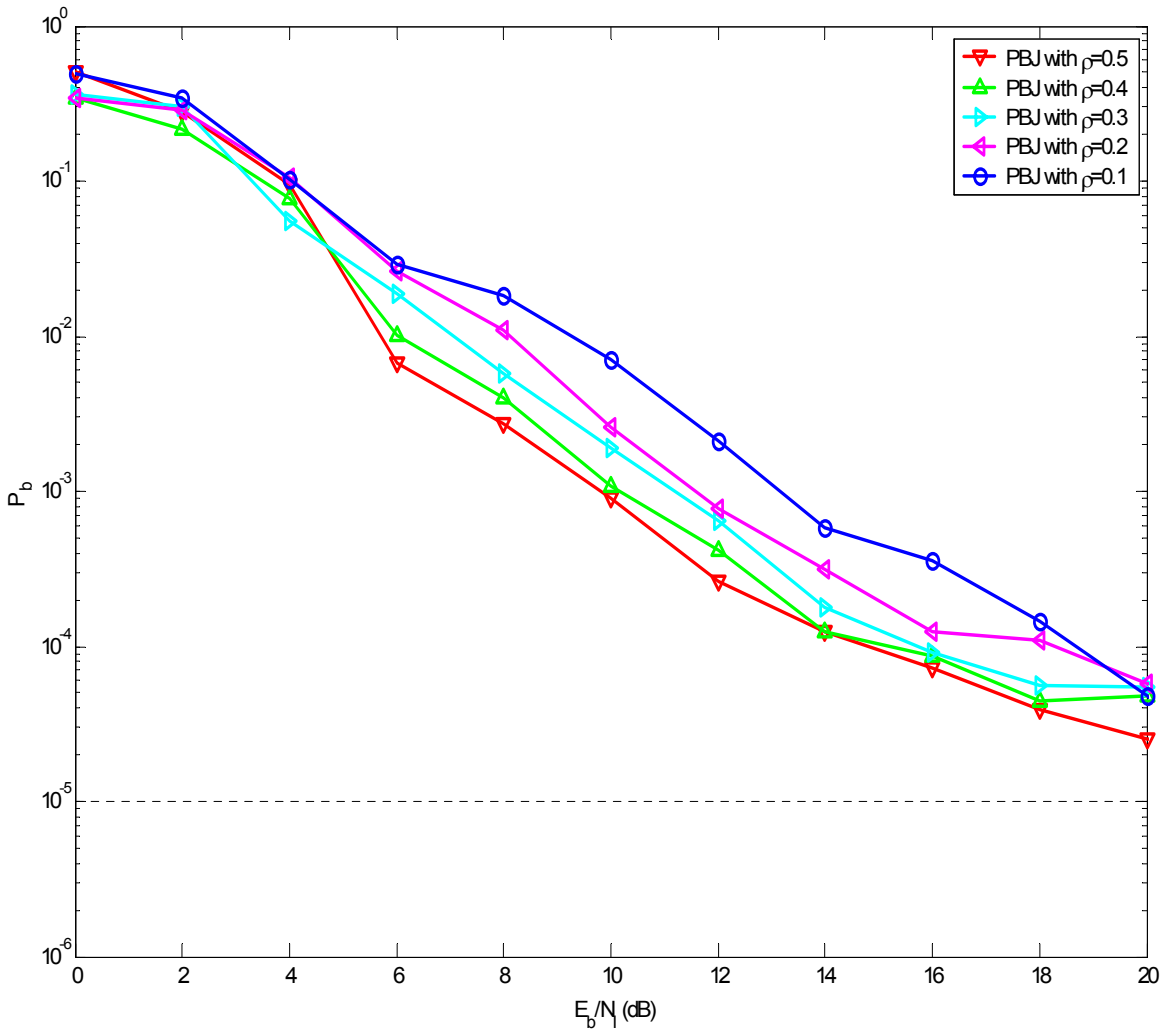

Figure 75. Simulation Results of the Effect of the $AN/USQ-146$ (Rubicon II) in Partial-Band Jamming for Various ρ on the Performance of an $802.11a$, $64-\text{QAM}$ $(R_c = 3/4)$ with Soft Decision Decoding System in AWGN

The examination of Figure 75 leads to the conclusion that the $AN/USQ-146$ (Rubicon II) jammer improves its performance over an $802.11a$, $64-\text{QAM}$ $(R_c = 3/4)$ with SDD system as the value of ρ becomes smaller. Due to the fact that all the BER curves cross close to the point $P_b = 10^{-1}$ when $E_b/N_I = 4$ dB, the improvement of the jammer's performance becomes more obvious for values of E_b/N_I greater than 4 dB. Additionally for SJR between 0 and 4 dB, the effect of the jamming signal is severe for every ρ.

As the signal-to-jamming ratio increases, the probability of error curves for all ρ have the tendency to meet the same value of P_b. This value is in the range of 10^{-5}, which is the error produced due to the AWGN.

In Figure 76, the results from Figures 73 and 75 have been overlaid in order to compare the performance of the $AN/USQ-146$ (Rubicon II) jammer in PBJ and BNJ.

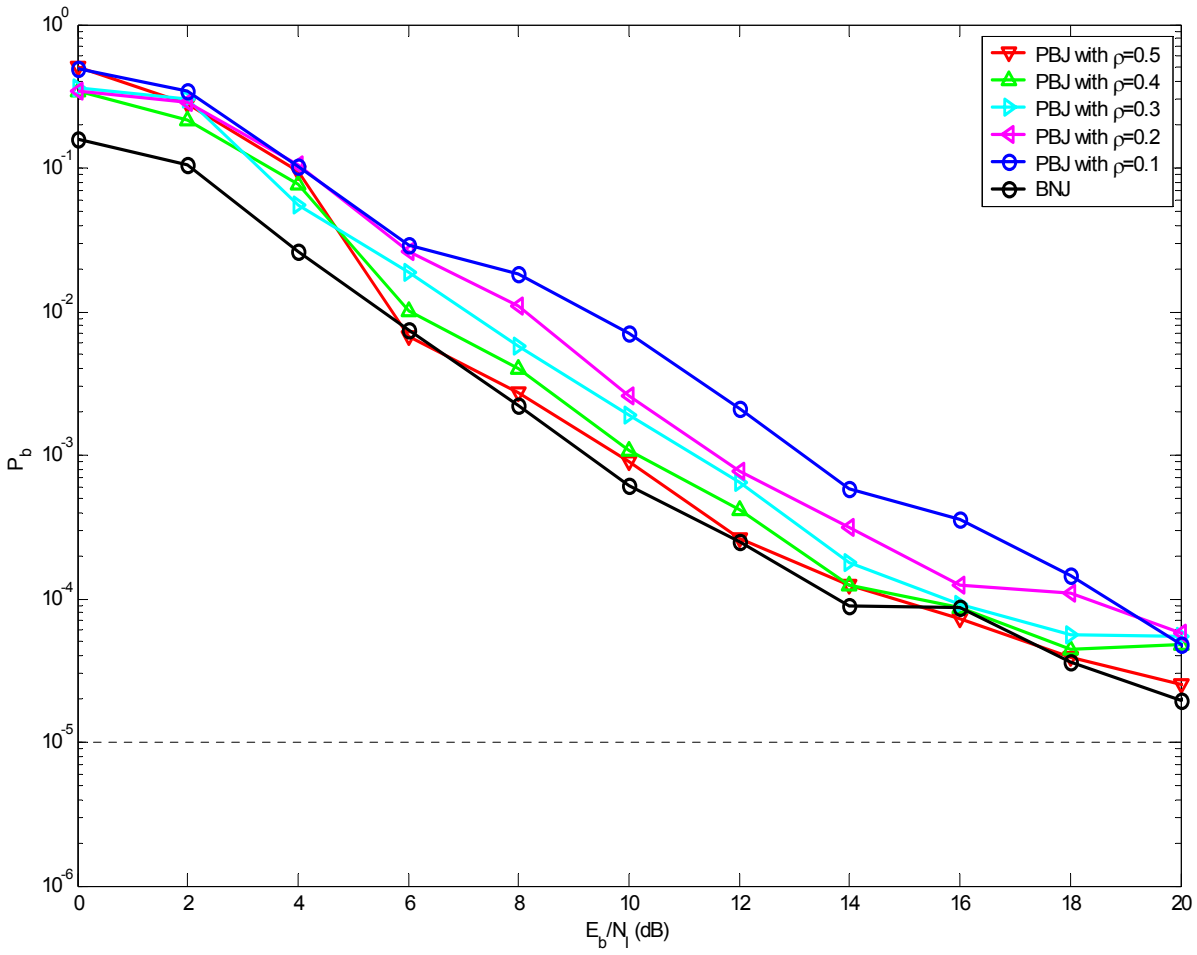

Figure 76. Comparison of the Effect of the $AN/USQ-146$ (Rubicon II) Jammer in Barrage and Partial-Band Noise Jamming over an $802.11a$, $64-\text{QAM}$ $(R_c = 3/4)$ with Soft Decision Decoding System

Consequently, comparing the simulation results of the two above jamming strategies shows that the $AN/USQ-146$ (Rubicon II) jammer performs better over an

$802.11a,\ 64-\text{QAM}\ (R_c = 3/4)$ system when it operates in the PBJ. In addition, as the fraction of the jammed bandwidth (ρ) decreases, the jamming efficiency increases. Especially for the case of $\rho = 0.1,$ the PBJ technique is almost 5 dB superior that the BNJ.

The next section presents the last simulation model of the $802.11a,\ 64-\text{QAM}$ $(R_c = 3/4)$ with SDD system under the influence of the $AN/USQ-146$ (Rubicon II) jammer. In this case, the jammer is simulated to operate with the manual spot multitone jamming technique.

6. IEEE 802.11a Model under the Influence of the AN/USQ-146 in Multitone Noise Jamming

As the description of the $802.11a$ illustrated, the basic concept of the OFDM technology is to transmit high-speed serial data at a much lower rate in parallel on N subcarriers that are orthogonally spaced.

Consequently, a single broadband data-stream is represented by many narrowband data-streams. The orthogonality of the subcarriers allows the frequency guard-band, required for the FH/MFSK, to be removed. In the presence of highly frequency-selective fading, the channel has a narrow coherence bandwidth due to multipath echoes and this modulation scheme provides frequency diversity in these circumstances. In effect, the frequency selective fade for a single carrier has been replaced by uncorrelated flat fades for the OFDM system. Based on $[15],$ this, in itself, is not an advantage, but by using forward error-correction (FEC) coding and interleaving in the time and frequency-domains, advantage can be taken of the uncorrelated fades to improve the bit error rate.

In some respects, the generation of errors due to highly frequency selective fading and tone jamming are similar. As a result, based on the fact that the primary purpose of the structure of the OFDM is to resist fading or tone jamming, it is expected that the $AN/USQ-146$ (Rubicon II) jammer in multitone jamming will not be as effective as it was in the previous two cases.

As mentioned in Chapter II, the jammer is capable of simultaneously transmitting two tones over the hostile signal. Figure 77 shows that the OFDM channel consist of two signals, the I and the Q. In order to implement the I and the Q signal of the two jamming tones (tokens 79 and 80), the produced tones pass through the IQ-Mixer (tokens 77 and 81) and then are added to the corresponding channels. The IQ-Mixer token produces the *inphase* and *quadrature* version of an input signal.

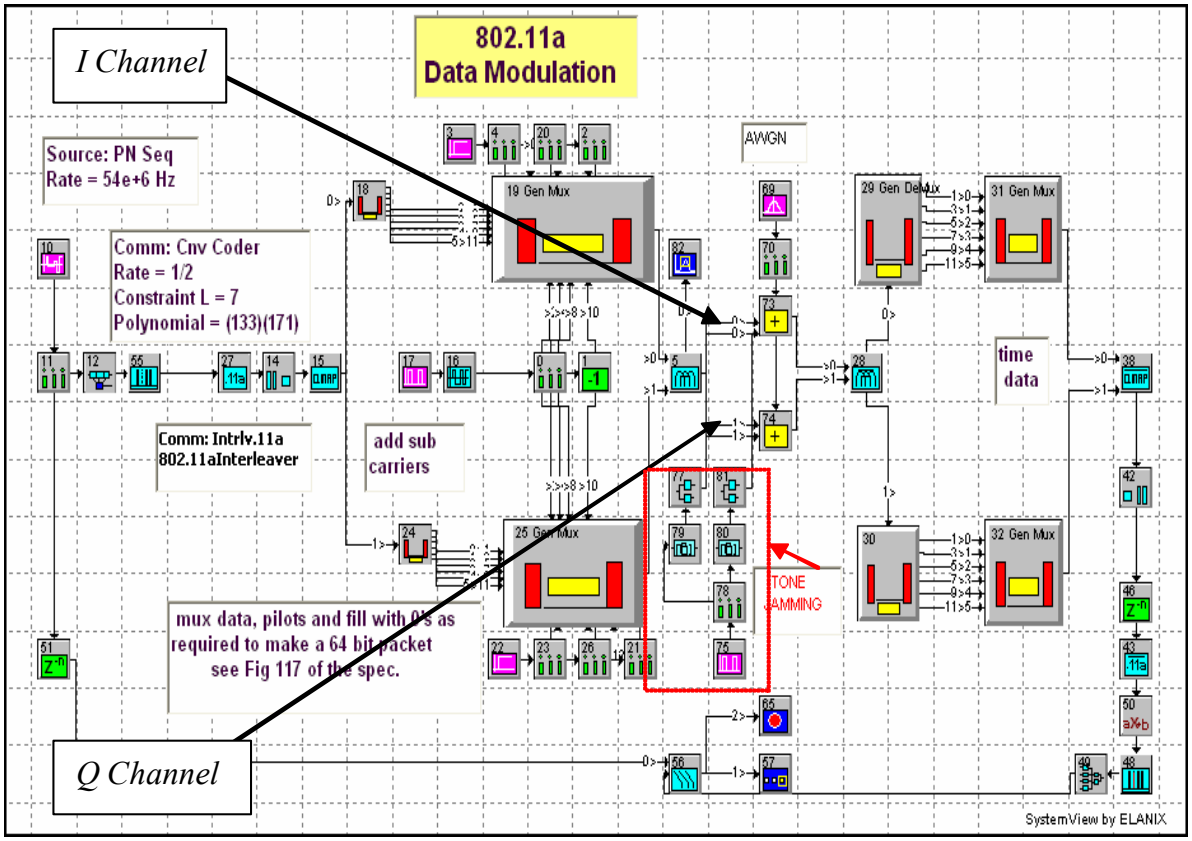

Figure 77. Multitone Jamming Model of the $AN/USQ-146$ (Rubicon II) Jammer in 802.11a, $64-\text{QAM}$ $(R_c = 3/4)$ with Soft Decision Decoding

For reasons of comparison and in order to verify that the simulation model behaves as the theory predicts, two strategies are investigated concerning the center frequencies of the jamming tones. In the first strategy, the produced two jamming tones are perfectly aligned with two of the subchannel frequencies of the transmitted signal. In the second strategy, the frequencies of the simulated jamming signals are chosen to fall midway between the adjacent subchannels tones of the OFDM signal.

Keeping the signal-to-noise-ratio equal to 13.35 dB (token 69) and setting the tones power as a variable, the above simulation model was executed for thirteen continuously decreasing values of the tone jamming power $(-4 \text{ dB} \le E_b/N_I \le 22 \text{ dB})$ for the above strategies. The received BER curves are seen in Figure 78.

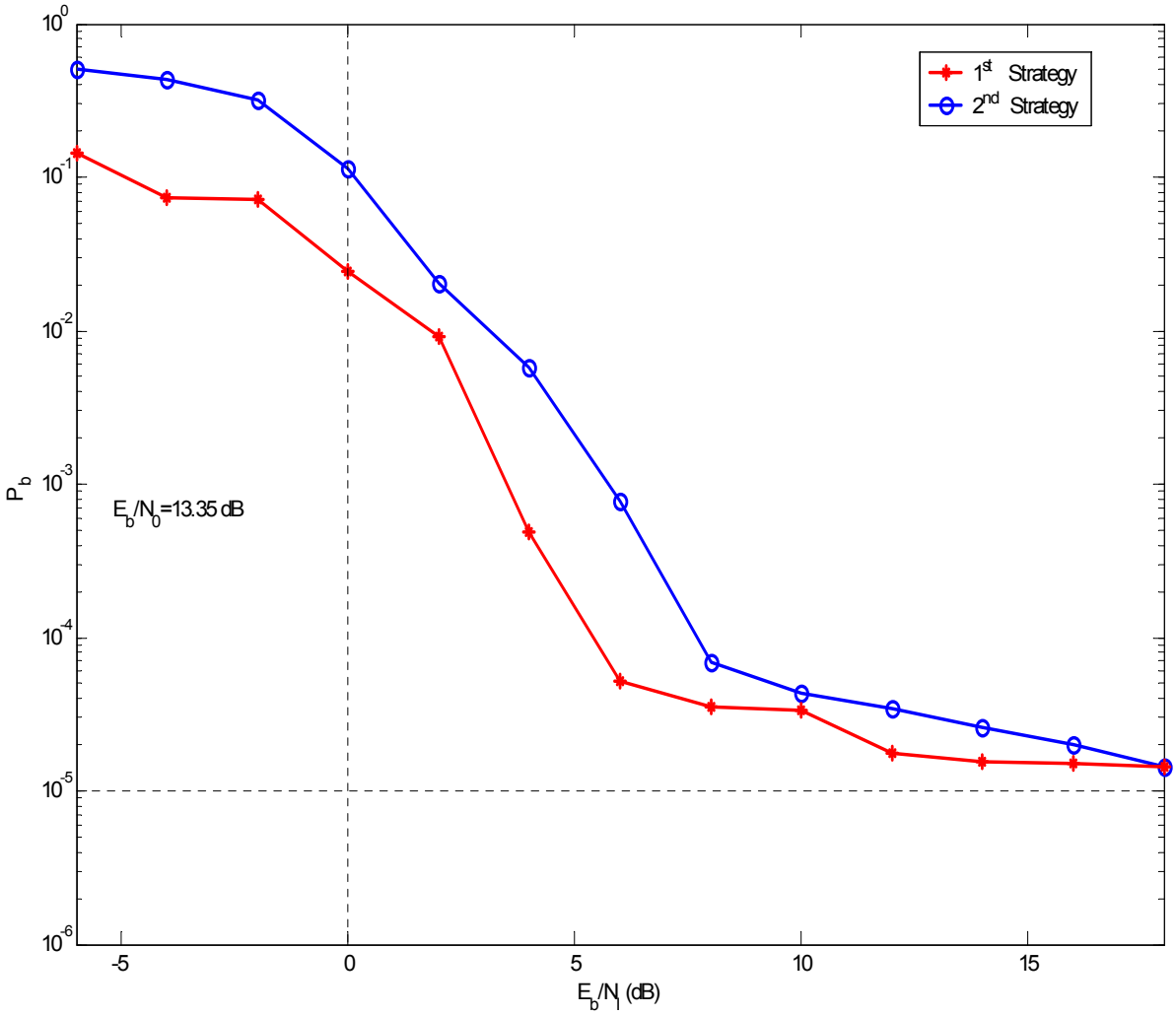

Figure 78. Simulation Results of the Effect of the $AN/USQ-146$ (Rubicon II) in Two Strategies of Multitone Jamming $(q=2)$ on the Performance of an 802.11a, $64-\text{QAM}$ $(R_c = 3/4)$ with Soft Decision Decoding System in AWGN

The results in Figure 78 indicate that the best multitone jamming strategy is the second. In this strategy the jamming tones were chosen to fall midway between adjacent

subchannel tones. Based on $[15]$, when the frequency of the jamming signal is perfectly aligned with one of the subchannel frequencies of the transmitted signal only data on the carrier is affected by the jamming signal when the received signal is processed using the FFT algorithm. Furthermore, once the jamming power significantly exceeds the power of the hostile signal, the probability of an error on that subcarrier saturates.

However, when the frequencies of the jamming signals lie midway between two subchannel frequencies, spectral leakage in the spectrum of the jamming signal impacts the other frequency components of the received signal when the received signal is processed using the FFT algorithm. In this case, the jamming power has a significant effect on the average bit error rate as the increased magnitude of the spectral leakage components of the jamming signal affect more of the hostile signal components.

In Figure 79, the bit error curves of the barrage noise, partial-band noise for $\rho = 0.1$ and the second strategy of multitone jamming have been overlaid in order to ascertain which jamming method is the most effective on the $802.11a$, $64-\text{QAM}\ (R_c = 3/4)$ system.

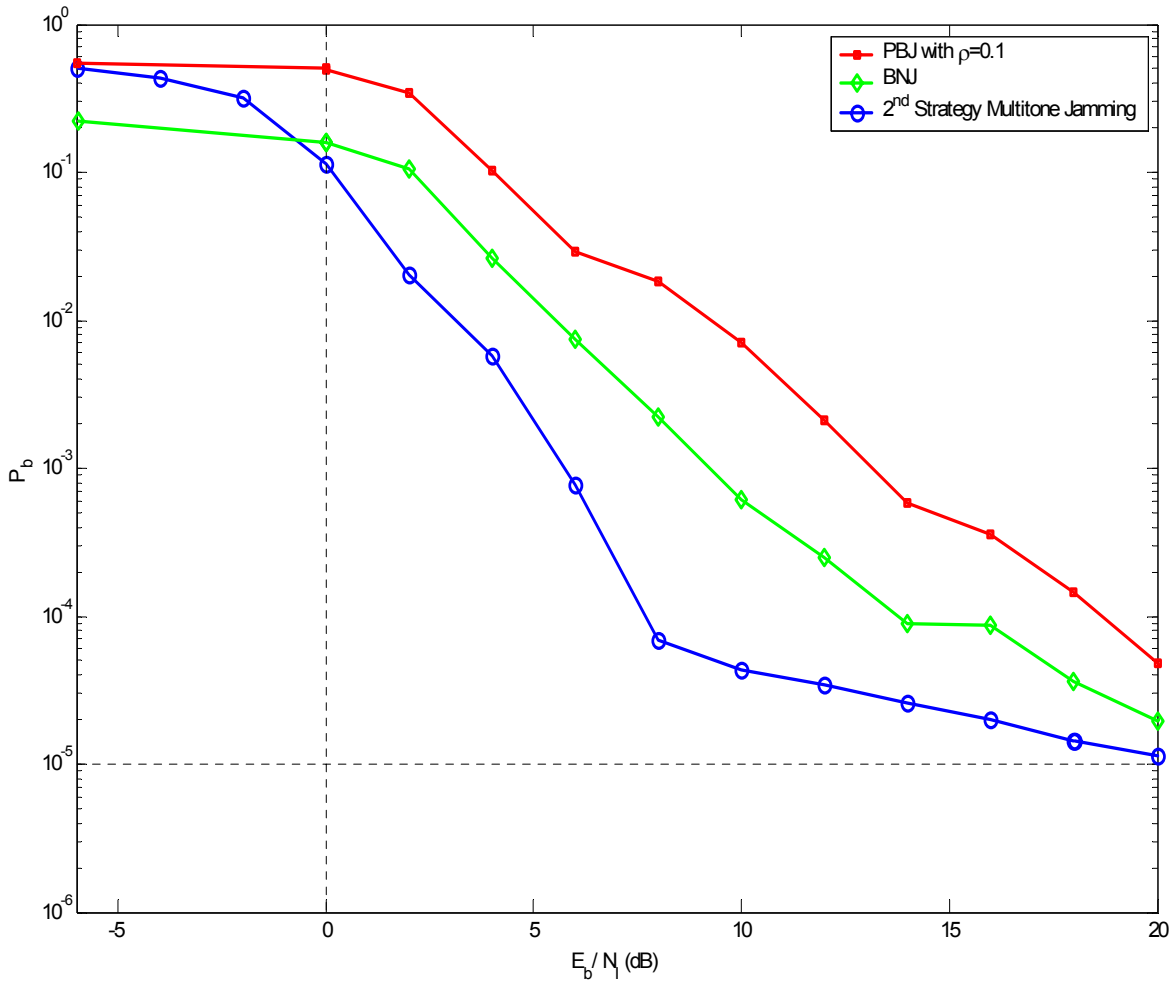

Figure 79. Comparison of the Effect of the $AN/USQ-146$ (Rubicon II) Jammer in Barrage Noise, Partial-Band Noise with $\rho = 0.1$ and 2^{nd} Strategy of Multitone Jamming over an $802.11a$, $64-\text{QAM}$ $(R_c = 3/4)$ with Soft Decision Decoding System

The probabilistic comparison of the three types of jamming shows that the effect of all the jamming strategies on the bit error rate of the $802.11a$, $64-\text{QAM}$ $(R_c = 3/4)$ with SDD system is significant at signal-to-jamming ratios lower than 0 dB. However, for $E_b/N_I > 0$ dB the partial-band jamming presents the best performance of all the jamming strategies. On the other hand, it is observed that the effect of the multitone jamming is insignificant and as the SJR increases it becomes even worse than the barrage noise jamming. This occurred due to the rapid slope that the multitone jamming bit error rate curve presents for values of $E_b/N_I > 0$ dB. As mentioned early in this section, this

severe decrease of the multitone jamming performance was expected and represents the resistance of the OFDM system in fading and tone jamming.

Consequently, the selection of the most effective jamming strategy of the $AN/USQ-146$ (Rubicon II) jammer over the $802.11a$, $64-\text{QAM}\ (R_c = 3/4)$ with SDD, is the partial-band jamming with $\rho = 0.1$.

C. SUMMARY

This chapter presented the implementation of the simulation models of the $AN/USQ-146$ jammer over two advanced communication systems. The first part of the chapter examined the simulation model of the SINGARS communication system. The second part investigated the simulation model of the IEEE $802.11a$ standard WLAN system in various jamming strategies of the $AN/USQ-146$.

The purpose of the implementation of the SINGARS simulation model in various methods of jamming was dual. Firstly, verifying the theoretical results of Chapter IV and VII was needed, and secondly it was necessary to create a simulation environment in which the performance of the $AN/USQ-146$ jammer and other similar jammers could be investigated.

Both of the above purposes were achieved. The simulation results in Section A verified that the most effective jamming strategy that the $AN/USQ-146$ jammer must select in order to deny the SINCGARS military communication systems is the repeat multitone jamming. As the theory predicted and simulation results proved, the next most advanced jamming strategy is the follower partial-band jamming together with the manual spot multitone jamming. For all the above simulation models, it was considered that the jammer had full knowledge of the hostile system except for its hopping pattern.

The second part of this chapter presented the simulation model of the $AN/USQ-146$ (Rubicon II) jammer over the IEEE $802.11a$ standard WLAN system. Specifically the $64-\text{QAM}\ (R_c = 3/4)$ with soft decision decoding scheme was chosen since this modulation option produces the highest data rate $(54\ \text{Mbps})$. As mentioned in

the description of the $802.11a$ standard, the specific system uses Orthogonal Frequency Division Multiplexing (OFDM) as a modulation technique and not a FH technology. This is the reason that the $AN/USQ-146$ (Rubicon II) jammer was simulated only for the manual spot mode jamming strategies.

The simulation results showed that the most effective jamming strategy that the $AN/USQ-146$ (Rubicon II) jammer must follow over the $802.11a$, $64-\text{QAM}\,(R_c = 3/4)$ with soft decision decoding system is the partial-band jamming. In the PBJ, the best results are obtained when 10% of the transmission spectrum is corrupted by the $AN/USQ-146$ (Rubicon II) jammer.

THIS PAGE INTENTIONALLY LEFT BLANK

IX. CONCLUSIONS AND FUTURE WORK

The goal of this thesis was to evaluate the performance and capabilities of one of the most advanced devices that detects, analyzes and denies enemy signals: the Rockwell Collins $AN/USQ-146$ transportable communication jammer.

The results of the theoretical analysis and the simulation modeling of the specific jammer, in all types of jamming over uncoded slow FH/MFSK military communication systems and new advanced commercial wireless standards, can be used as guidelines for selecting the most effective jamming strategies depending on the type of hostile waveform. The simulation models have a general scope of applicability much larger than the special case of the $AN/USQ-146$ jammer. The same models with the appropriate changes can be used to evaluate other types of jammers over different communication schemes.

The main points and conclusions of the investigation of the $AN/USQ-146$ jammer's performance are summarized by chapter together with suggestions for future work.

A. CONCLUSIONS

In Chapter II, a general description of the $AN/USQ-146$ jammer was provided. The specific jammer operates in the 1.5-MHz to 2500-MHz frequency ranges. It has two mode of operation: the manual spot mode and the reactive mode.

In Chapter III, the importance of investigating effective jamming techniques for the interference of FH communication systems was introduced.

In Chapter IV, the performance of the $AN/USQ-146$ jammer in the manual spot mode against the SINCGARS communication system was presented. The jamming techniques that were analyzed are barrage noise jamming, partial band noise jamming and multitone jamming. The interference of the first two types of jamming cannot be considered efficient enough on the modern battlefield, since the effect of the jamming signal on the bit error rate is significant $\left(P_b \approx 0.5\right)$ only when the jamming power becomes 1000

times greater than the signal power $(E_b/N_I = -30 \text{ dB})$. On the other hand, the manual spot multitone jamming technique proved to be the most effective type of manual spot jamming with a capability of creating severe damage in a FH/MFSK system for $E_b/N_I = 0$ dB.

In Chapters V and VI, the fundamental limitations of the $AN/USQ-146$ jammer in reactive mode and the link budget considerations of the transmitter-jammer and jammer-receiver geometriese were analyzed. It was shown that the operational characteristics of the specific jammer give the authority to the operator of the $AN/USQ-146$ to function in the reactive mode with no practical limitations. On the other hand, the link budget analysis revealed that the receive sensitivity and the output transmitted power of the jammer are the basic factors that determine its optimum position relative to the hostile communication system.

In Chapter VII, the performance of the $AN/USQ-146$ jammer in repeat mode against the SINCGARS communication system was analyzed. In this specific mode of operation, the jammer can select the following three strategies: (1) the noise repeat jamming, (2) repeat partial-band jamming, or (3) follower-tone jamming. In the theoretical analysis of the follower partial-band jamming and the follower multitone jamming, the author considered the fact that the communication system and the jammer can select to operate either in the conventional mode or the unconventional mode. All three reactive jamming strategies of the $AN/USQ-146$ jammer proved to be efficient enough over the SINCGARS system with the follower multitone jamming technique being the most effective.

In conclusion, the probabilistic comparison of all types of jamming in manual spot, and repeat modes showed that the most effective jamming strategy over an uncoded slow FH/MFSK system is follower multitone jamming.

In Chapter VIII, the simulation models of the $AN/USQ-146$ jammer over two communication systems were developed with the use of the SystemView software by Elanix.

Firstly, the advanced military FH/MFSK system called SINGARS was implemented. Each model was composed of two main parts. The first part represented the SINCGARS communication system and the second part represented the simulation of the $AN/USQ-146$ jammer for every type of jamming in manual spot and repeat mode. In all cases the simulation results verified the conclusions that were derived from the theoretical analyses in Chapters IV and VII.

The second part of Chapter VIII investigated the performance of the new model of the $AN/USQ-146$ jammer (Rubicon II) over the IEEE $802.11a$, $64-\text{QAM}$ ($R_c = 3/4$) with soft decision decoding WLAN commercial system. The simulation results indicated that the $AN/USQ-146$ (Rubicon II) jammer must select the partial-band jamming with $\rho = 0.1$ technique.

Consequently, as expected, the jammer's best strategy varies with respect to the modulation technique that the hostile communication system uses. As the theoretical analysis and the simulation results indicated, the $AN/USQ-146$ jammer achieves its best performance over a FH/MFSK system when it selects the repeat multitone jamming strategy. However, when the hostile communication system is the $802.11a$, WLAN system, the partial-band jamming strategy with the smallest possible fraction of jammed bandwidth (ρ) is the best solution.

B. FUTURE WORK

The basic purpose of this thesis was investigating the performance of the $AN/USQ-146$ jammer against a FH/MFSK military system and the IEEE $802.11a$ WLAN commercial system.

The basic assumptions that were made for the FH/MFSK communication system are listed below:

- The hostile communication system uses an uncoded slow FH/MFSK modulation scheme.
- The communication channel is an AWGN channel and is being jammed at every instance by a single $AN/USQ-146$ jammer.

- The jammer fulfills all the requirements derived from Chapters V and VI when it operates in reactive mode.

The basic assumptions that were made for the IEEE 802.11*a* WLAN commercial system are:

- The IEEE 802.11*a* WLAN commercial system uses the $64-\text{QAM}\,(R_c = 3/4)$ with soft decision decoding option.
- The operational characteristics of Rubicon II and the $AN/USQ-146$ jammer for the manual spot jamming mode are exactly the same.

Based on the above assumptions, there are four major areas that can be identified for future work. First, it would be interesting to observe how the performance of the $AN/USQ-146$ jammer changes in a coded slow FH/MFSK system. Secondly, investigating a more complicated channel model as the fading channel would model the operational environment of the jammer more accurately. Thirdly, following the modern spirit of joint forces, it would be very interesting to examine the performance of a combination of jamming strategies by using two or more $AN/USQ-146$ jammers at different distances and locations from the communication scheme. Finally, the theoretical analysis of the IEEE 802.11*a* standard WLAN system with SDD in barrage noise, partial-band and tone jamming, and their comparison with the corresponding simulation results in Chapter VIII, would also be an interesting topic for further research.

LIST OF REFERENCES

[1] Rockwell Collins, *VME Enhanced CCW System Equipment Specification*, Rockwell Collins, 400 Collins Road, NE, 2001.

[2] Roger L. Peterson, *Introduction to Spread Spectrum Communications*, Prentice Hall PTR, Upper Saddle River, New Jersey, 2000.

[3] George T. Katsoulis, "ECCM potential of a noncoherent FH/MFSK communications system under worst case hostile ECM an fading channels," MSEE Thesis, Naval Postgraduate School, Monterey, CA, March1997.

[4] Barry E. Fealstead, *Follower Jammer Considerations for Frequency Hopped Spread Spectrum*, Communication Research Centre, Upper Ottawa Canada, 1998.

[5] Don J. Torrieti, *Principles of Secure Communication Systems*, Artech House, 610 Washington Street, Dedham, MA, September 1985.

[6] H. Urkowitz, **"**Energy detection of unknown deterministic signals," *IEEE Trans. on Communications*, vol. 55, pp. 523 – 531, April 1967.

[7] Rodger E. Ziemer and Roger L. Peterson, *Digital Communications and Spread Spectrum Systems*, Macmillan, New York, 1985.

[8] U.S. Marine Corps, *TALK II-SINCGARS* Air Land Application Center, Quantico, VA, May 1996.

[9] Amer A. Hassan, Wayne E. Stark and John E. Hershey, "Frequency-Hopped Spread Spectrum in the Presence of a Follower Partial-Band Jammer," *IEEE Trans. on Communications*, vol. 41, no. 7, July 1993.

[10] Amer A. Hassan, Wayne E. Stark and John E. Hershey, "Error Rate for Optimal Follower Tone-Jamming*," IEEE Trans. on Communications,* vol. 44, no. 5, May 1996.

[11] Rockwell Collins, *Communications Jamming for Digital Battlespace Dominance*, Rockwell Collins, 400 Collins Road, NE, April 2002.

[12] Institute of Electrical and Electronics Engineers, *802.11a, Wireless LAN Medium Access Control (MAC) and Physical Layer (PHY) Specifications: High-Speed Physical Layer Extension in the 5 GHz Band,* 16 September 1999.

[13] Maurice L. Schiff, 802.11*a System Simulation Using SystemView by Elanix,* Application Note, Elanix, Inc, Westlake Village, CA, November 2002.

[14] Clark Robertson, Notes for EC4580 (Coding and Information), Naval Postgraduate School, Monterey, CA, 2001 (unpublished).

[15] R.F. Ormondroyd, E. Al-Susa, "Impact of Multipath Fading and Partial-Band Interference on the Performance of a COFDM/CDMA Modulation Scheme for Robust Wireless Communications," Military Communications Conference, MILCOM '98, Proceedings, IEEE, vol. 2, pp. 673 – 678, 18 – 21 October 1998.

INITIAL DISTRIBUTION LIST

1. Defense Technical Information Center
   Ft. Belvoir, Virginia

2. Dudley Knox Library
   Naval Postgraduate School
   Monterey, California

3. Chairman, Code EC/Po
   Department of Electrical and Computing Engineering
   Naval Postgraduate School
   Monterey, California

4. Chairman, Code IS/Bo
   Department of Information Sciences
   Naval Postgraduate School
   Monterey, California

5. Professor Tri T. Ha, Code EC/Ha
   Department of Electrical and Computing Engineering
   Naval Postgraduate School
   Monterey, California

6. Professor David C. Jenn, Code EC/Jn
   Department of Electrical and Computing Engineering
   Naval Postgraduate School
   Monterey, California

7. Embassy of Greece, Naval Attaché
   Washington, DC

8. Aristeidis Dalakos
   Kerasias 37, Ag. Dimitrios,
   Athens, GREECE
   TK: 17342